

Explanations exist; they have existed for all time; there is always a well-known solution to every human problem — neat, plausible, and wrong.

H. L. Mencken

University of Alberta

Molecular and phenotypic characterization of *Cecr2* mouse models: implications
for the role of mesenchymal/epithelial regulation in neural tube and renal
development

by

Nicholas Andrew Fairbridge

A thesis submitted to the Faculty of Graduate Studies and Research
in partial fulfillment of the requirements for the degree of

Doctor of Philosophy
in
Molecular Biology and Genetics

Biological Sciences

©Nicholas Andrew Fairbridge
Spring 2013
Edmonton, Alberta

Permission is hereby granted to the University of Alberta Libraries to reproduce single copies of this thesis and to lend or sell such copies for private, scholarly or scientific research purposes only. Where the thesis is converted to, or otherwise made available in digital form, the University of Alberta will advise potential users of the thesis of these terms.

The author reserves all other publication and other rights in association with the copyright in the thesis and, except as herein before provided, neither the thesis nor any substantial portion thereof may be printed or otherwise reproduced in any material form whatsoever without the author's prior written permission.

This thesis is dedicated to the memory of R.C. (Jack) von Borstel, who gave a young student bench space, stacks of textbooks, and the wealth of his time.

Abstract

Embryogenesis is a crucial process during mammalian development that relies on a wide variety of genetic and epigenetic regulatory factors. Chromatin remodeling complexes are one such epigenetic means to control gene transcription through alteration of DNA-histone packaging. The developmental roles of chromatin remodelling protein CECR2 are determined through the characterization of *Cecr2* mouse mutations. To this end, a new *Cecr2*^{tm1.1Henc} deletion allele is presented.

Phenotypic examination of the *Cecr2*^{tm1.1Henc} mutation, alongside the founding *Cecr2*^{Gt45Bic} allele, expands the *Cecr2*-associated mutant defects to include the neurulation-associated defects of midline facial clefts, encephaloceles, reduced adult brain weight, and caudal vertebrae malformations in addition to the prevalent exencephaly. The *Cecr2* mutations on a FVB/N genetic background further develops a series of congenital abnormalities of the kidney and urinary tract. The expression of *Cecr2* during renal development is in the condensing metanephric mesenchyme and the transient comma-shaped and S-shaped body epithelium of the developing nephrons. Similarities amongst the affected organ systems suggest an underlying defect in mesenchymal-epithelial transitions.

Cecr2^{Gt45Bic} homozygous mutants at the time of neurulation show a variety of transcriptional changes in both the BALB/c and FVB/N strains. Amongst the altered genes is an abundance of mesenchymal and epithelial transcription factors and developmental regulators. The affected transcripts cluster into enriched regions on chromosome 6A, 6F-G and chromosome 12B, which may indicate direct targets of CECR2 remodeling. The molecular and developmental roles of the candidate genes suggest CECR2 regulates a mesenchymal-associated gene network, whose misregulation results in the formation of cranial neural tube defects.

This dissertation would not have been possible without the guidance and support of a great many colleges and friends. First and foremost I would like to thank my supervisor Dr. Heather Mcdermid for her constant support and patience. Drs. Rachel Wevrick and David Pilgrim also were invaluable in refining both my thesis and the very way I think about science.

Thanks go to Troy Locke, Matt  a Bujold, and Dr. Kirst King-Jones for technical and experimental design support. The animal care facilities and personnel of the BSAS and HSLAS kept our mice healthy and happy, and I must thank the mice themselves, as the work could not have been done without their contributions. Special thanks go to my labmates and fellow students. Whether it was late into the night, unbearably early morning, across campus, or just across the hall for cake, I was never alone in my pursuits. I am grateful to AHFMR and NSERC for their financial support and investments.

I am indebted to the 25th MedVents for keeping me sane and distracted when distractions were needed. I must also acknowledge the support and care from my family and friends. Finally, I must thank my wife Marilyn for her unwavering support and passionate ambition that inspires me to be more than I am.

Table of Contents

1:	Introduction	1
1.1:	Animal models of neural tube defects	1
1.2:	Process of neural tube closure	5
1.3:	Epigenetic factors in neural tube closure	16
1.4:	CECR2 is associated with epigenetic regulation of euchromatin and is necessary for neural tube closure	19
1.5:	Advances in chromatin remodeling research	20
1.5.1:	DNA compaction and chromatin remodeling	21
1.5.2:	Chromatin remodeling ATPases	22
1.5.3:	The imitation-switch (ISWI) subfamily	22
1.5.4:	Developmental roles of ISWIs	25
1.5.5:	BAZ-like ISWI partners control transcriptional targeting	26
1.6:	Directed questions and research	26
1.6.1:	Does CECR2 regulate transcription of the planar cell polarity pathway during neural tube closure?	27
1.6.1.1:	Overview of planar cell polarity	27
1.6.1.2:	Proposed research into the transcriptional regulation of planar cell polarity genes by CECR2	28
1.6.2:	Does CECR2 target clusters of genes within defined chromosomal regions?	28
1.6.2.1:	Overview of BAZ-like chromosomal targeting	28
1.6.2.2:	Proposed chromosomal enrichment research	29
1.6.3:	Do <i>Cecr2</i> mutations produce additional subtle developmental defects?	29
1.6.3.1:	<i>Cecr2</i> expression is seen in many non-neural tissues	29
1.6.3.2:	Overview of renal development	32
1.6.3.3:	Proposed phenotypic characterization and research	36
1.7:	Summary	37
2:	Materials and methods	38
2.1:	Generation and genotyping of <i>Cecr2</i> mutant mice	38
2.2:	Necropsy and organ collection	38
2.3:	Micro-CT rendering	39
2.4:	Ovary cyst analysis	39
2.5:	Urine and blood analysis	39
2.6:	Embryo collection	39
2.7:	Embedding and histology	40
2.8:	Stereociliary analyses	40
2.9:	RNA extraction for quantification	40
2.10:	Gene expression profiling: microarray	40
2.11:	Gene expression profiling: quantitative real-time PCR	41
2.12:	<i>In situ</i> hybridization	42
2.13:	Apoptosis TUNEL analysis	42
2.14:	Statistical significance	42

Table of Contents

3:	Results	43
3.1:	Generation of the <i>Cecr2^{tm1.1Hemc}</i> allele	43
3.2:	Testing whether a disruption of <i>Cecr2</i> influences transcript expression during cranial neural closure	46
3.2.1:	<i>Cecr2^{Gt34Bic}</i> BALB/c and <i>Cecr2^{Gt34Bic}</i> FVB/N microarray analyses found a set of generally low fold-change, but significant, candidate transcripts	47
3.2.2:	Microarray and qRT-PCR analyses did not support a disruption in the relative expression of planar cell polarity transcripts during neural closure of <i>Cecr2^{tm1.1Hemc}</i> BALB/c homozygous embryos	55
3.2.3:	Microarray analyses identified a number of candidate transcripts with roles in neural tube closure	58
3.3:	<i>Cecr2</i> microarray analyses revealed three regions showing chromosomal enrichment of transcripts that may identify direct target regions of CECR2 remodeling	58
3.4:	Testing the hypothesis that the <i>Cecr2^{Gt34Bic}</i> mutants manifest multi-system congenital defects	63
3.4.1:	<i>Cecr2^{Gt34Bic}</i> BALB/c non-exencephalic homozygous and heterozygous adult animals possessed caudal vertebrae defects	63
3.4.2:	<i>Cecr2^{Gt34Bic}</i> non-exencephalic homozygous adult animals from both strains showed reduced brain weight compared to wildtype littermates	68
3.4.3:	<i>Cecr2^{Gt34Bic}</i> adult males of both strains developed smaller testes with reduced weight compared to wildtype males	69
3.4.4:	Rare cases of hemorrhagic ovarian cysts developed in <i>Cecr2^{Gt34Bic}</i> FVB/N homozygous females	72
3.4.5:	Congenital abnormalities of the kidney and urinary tract were found within <i>Cecr2^{Gt34Bic}</i> FVB/N homozygous animals	75
3.5:	Testing the hypothesis that a <i>Cecr2^{tm1.1Hemc}</i> deletion allele would show increased severity and range of <i>Cecr2</i> -mutant aberrant phenotypes	77
3.5.1:	<i>Cecr2^{tm1.1Hemc}</i> BALB/c embryos showed an increased penetrance of exencephaly compared to the <i>Cecr2^{Gt34Bic}</i> BALB/c line	77
3.5.2:	The <i>Cecr2^{tm1.1Hemc}</i> FVB/N homozygous embryos partially overcame FVB/N strain resistance modifiers and manifested both the neural tube defects exencephaly and midline facial clefts	78
3.5.3:	Inner ear analyses confirmed the stereocilia alignment defects were present in a <i>Cecr2^{tm1.1Hemc}</i> BALB/c mutant background	81

Table of Contents

3.5.4:	Congenital abnormalities of the kidney and urinary tract were seen in <i>Cecr2</i> ^{tm1.1Hemc} FVB/N homozygotes and recapitulated <i>Cecr2</i> ^{Gt34Bic} FVB/N defects	92
3.5.5:	<i>Cecr2</i> ^{tm1.1Hemc} FVB/N homozygous neonates possessed extensive renal apoptosis	95
3.5.6:	<i>Cecr2</i> ^{tm1.1Hemc} FVB/N homozygous adults had hyperkalemia, but all other renal markers are within normal ranges	95
3.6:	Testing whether CECR2 targets a core set of conserved transcripts during its roles in multiple developmental systems	102
3.6.1:	Candidate gene mouse mutations allowed for the review and comparison of candidates based on associated developmental defects	102
3.6.2:	<i>Cecr2</i> expression was limited to the mesonephric tubules, metanephric mesenchyme and newly formed epithelium of comma-shaped and S-shaped bodies during renal development	107
3.6.3:	<i>Cecr2</i> ^{Gt34Bic} FVB/N microarray analysis revealed a number of candidate transcripts showing changes during neurulation, which also were known to be involved in renal development	107
3.6.4:	QRT-PCR of <i>Cecr2</i> ^{tm1.1Hemc} FVB/N homozygous metanephric kidneys did not confirm the same transcript disruptions as found during neurulation	112
3.6.5:	Metanephric tissue assessment by <i>in situ</i> hybridization supported the qRT-PCR results	113
3.6.6:	Mesonephric tissue assessments by <i>in situ</i> hybridization did not reveal a loss of tissue identity	114
4:	Discussion	116
4.1:	Re-evaluating the molecular function of CECR2	116
4.2:	Planar cell polarity gene transcription is not affected by CECR2 remodeling during neurulation	118
4.2.1:	Proposed future directions of PCP-related CECR2 research	119
4.3:	CECR2-affected transcripts cluster to broad localized chromosomal regions during neurulation	121
4.3.1:	Comparing CECR2 to BPTF chromosomal targets	123
4.3.2:	Proposed future directions of CECR2 chromosomal targeting research	125
4.4:	CECR2 affects the transcription of genes during neurulation with known roles in open neural tube defects	126
4.4.1:	A proposed role for <i>Cecr2</i> in neural closure	127
4.4.2:	Proposed future directions of CECR2 neurulation research	128

Table of Contents

4.5:	<i>Cecr2</i> mutations manifest congenital abnormalities of the kidney and urinary tract, but whether the same candidates identified during neurulation are targeted in renal organogenesis remains unclear	133
4.5.1:	A proposed role for <i>Cecr2</i> in renal development	135
4.5.2:	Proposed future directions to determine whether the targets of CECR2 are consistent throughout development	136
4.5.3:	Proposed future directions of CECR2 CAKUT research	138
4.6:	Re-exploring <i>Cecr2</i> as a Cat Eye Syndrome gene candidate	140
4.7:	Concluding Remarks	141
	Bibliography	142
	Appendix 1	161
	Appendix 2	167
	Appendix 3	175
	Appendix 4	197

List of Figures or Illustrations

Figure 1	Primary and secondary neurulation processes	2
Figure 2	Convergent extension processes	6
Figure 3	Overview of planar cell polarity signaling	8
Figure 4	Neural hinge point formation	10
Figure 5	Neuroepithelial fusion and lumen formation	12
Figure 6	Defects of primary neural tube closure	14
Figure 7	Epigenetic regulation of transcription	17
Figure 8	General structure and variation of mammalian ISWI complexes	24
Figure 9	Theiler stages of mouse development	30
Figure 10	Renal initiation and nephrogenesis	33
Figure 11	Diagram of <i>Cecr2^{tm1.1Hemc}</i> conditional deletion gene structure and genotyping	44
Figure 12	Cranial and caudal-vertebrae skeletal defects developed in <i>Cecr2^{Gt45Bic}</i> BALB/c homozygotes	64
Figure 13	Rare cancerous ovarian cysts were found in <i>Cecr2^{Gt45Bic}</i> FVB/N homozygous females	70
Figure 14	Congenital abnormalities of the kidney and urinary tract manifested in <i>Cecr2^{Gt45Bic}</i> FVB/N homozygotes	73
Figure 15	<i>Cecr2^{tm1.1Hemc}</i> FVB/N homozygous pups developed exencephaly and midline facial clefts	79
Figure 16	<i>Cecr2^{tm1.1Hemc}</i> BALB/c homozygous and heterozygous embryos developed stereocilia polarity defects	82
Figure 17	<i>Cecr2^{tm1.1Hemc}</i> BALB/c homozygous and heterozygous stereocilia displayed an increase in angle variation	85
Figure 18	<i>Cecr2^{tm1.1Hemc}</i> FVB/N homozygous embryos recapitulated the CAKUT phenotypes	87
Figure 19	The neonatal renal cortex displayed abnormal apoptosis in <i>Cecr2^{tm1.1Hemc}</i> FVB/N homozygotes	90
Figure 20	<i>Cecr2</i> expression persisted throughout pro-, meso- and metanephric development	103
Figure 21	<i>In situ</i> hybridizations of <i>Cecr2^{tm1.1Hemc}</i> FVB/N homozygous metanephric renal markers did not indicate a change in tissue morphology	108
Figure 22	<i>In situ</i> hybridizations of <i>Cecr2^{tm1.1Hemc}</i> FVB/N homozygous mesonephric renal markers indicated minimal change in tissue morphology	110

List of Tables

Table 1	Significant transcripts shared between strains as predicted by the microarrays	49
Table 2	Gene ontology clusters of highest stringency candidates	51
Table 3	PCP qRT-PCR of <i>Cecr2^{tm1.1Hemc}</i> BALB/c cranial tissue versus wildtype BALB/c	57
Table 4	QRT-PCR of <i>Cecr2^{tm1.1Hemc}</i> BALB/c homozygous cranial tissue versus wildtype BALB/c	59
Table 5	Chi-squared analyses for chromosomal regions enriched in significant transcripts	60
Table 6	Chromosome 6 qRT-PCR of <i>Cecr2^{Gt45Bic}</i> homozygotes versus wildtype	61
Table 7	Organ weight comparisons of <i>Cecr2^{Gt45Bic}</i> homozygotes and wildtypes of both strains	67
Table 8	Urine analysis of <i>Cecr2^{tm1.1Hemc}</i> FVB/N homozygotes surviving to adulthood	93
Table 9	Blood chemistry of <i>Cecr2^{tm1.1Hemc}</i> FVB/N homozygotes surviving to adulthood	94
Table 10	Candidate transcripts with gene mutations showing phenotypes similar to <i>Cecr2</i> mutations	96
Table 11	TS24 renal <i>Cecr2^{tm1.1Hemc}</i> FVB/N qRT-PCR versus wildtype FVB/N	106

List of Symbols, Nomenclature, or Abbreviations	
ACF	ATP-dependent chromatin assembly and remodelling factor
Alx	aristaless-like homeobox
Anxa	annexin
ATP	Adenosine triphosphate
B-gal	β -galactosidase
BAZ-like	bromodomain-adjacent zinc finger
Bmp	bone morphogenic protein
Bptf	bromodomain PHD-finger transcription factor
CAKUT	congenital anomalies of the kidney and urinary track
anti-Cam	anti-cytokeratin
Cart	cartilage homeoprotein
Cdk5rap	CDK5 regulatory subunit associated protein
cDNA	complementary DNA
Cecr	cat eye syndrome chromosome region, candidate
Celsr	cadherin, EGF LAG seven-pass G-type receptor
CERF	CECR2-containing remodelling factor
CES	cat eye syndrome
Chd1	chromatin helicase DNA binding protein 1
ChIP	chromatin immunoprecipitation
Chr	chromosome
CHRAc	chromatin accessibility complex
Cited	Cbp/p300-interacting transactivator with Glu/Asp-rich carboxy-terminal domain
Clec	C-type lectin domain family
CO ₂	carbon dioxide
Csb	Cockayne syndrome group B
Csn	casein kappa
Dach	dachshund
dCHIP	DNA-chip analyzer
Ddm1	deficient in DNA methylation 1
DDT	DNA binding homeobox and different transcription factor
DEL	deletion
Dkk	dickkopf homolog
Dlg	discs large homologue gene trap
Dlx	distal-less homeobox
DNA	Deoxyribonucleic acid
dpc	days post coitum
Dvl	dishevelled
EcR	ecdysone receptor
EMT	epithelial-mesenchymal transition
Eph	ephrin
ES	embryonic stemcell
EST	expressed sequence tag
Eya	eyes absent
Fat	FAT tumor suppressor homologue
Fgfr	fibroblast growth factor receptor
Fjx	four jointed box
FoxC	forkhead box C

List of Symbols, Nomenclature, or Abbreviations	
g	grams
Gap	growth associated protein
gcRMA	gc-rich robust multiarray averaging
Gdnf	glial cell line derived neurotrophic factor
Gfra	glial cell line derived neurotrophic factor family receptor alpha
Gli	GLI-kruppel family member
Gtf2ird	general transcription factor II I repeat domain-containing
H	histone
Hox	homeobox
IHC	inner hair cell
INO80	inositol requiring 80
ISWI	Imitation Switch
Itfg	integrin alpha FG-GAP repeat containing
Jag	jagged
Klhdc	klech domain containing
L	litre
Lacz	lactose Z
Ldhb	lactate dehydrogenase B
Lhx	LIM homeobox
Lix	limb expression
Luzp	leucine zipper protein
Mdfi	myod family inhibitor
Mdm	transformed mouse 3T3 cell double minute
MET	mesenchymal-epithelial transition
mg	milligrams
MGI	mouse genome informatics
Micro-CT	micro computer-assisted tomography
MM	metanephric mesenchyme
mmol	millimoles
MOE	mouse expression
mRNA	messenger ribonucleic acid
Mks	meckel syndrome
n	sample number
N	generation number
Ncam	neural cell adhesion molecule
Ncapd	non-SMC condensin I complex subunit D
Ndn	necdin
Nfia	nuclear factor I/A
ng	nanograms
NoRC	nucleolar remodelling complex
NTD	neural tube defects
Nudt	nudix-type
NURF	nucleosome remodelling factor
OHC	outer hair cell
Pax	paired box gene
PCP	planar cell polarity
PCR	polymerase chain reaction

List of Symbols, Nomenclature, or Abbreviations	
Pds	precocious dissociation of the sisters
Pecam	platelet/endothelial cell adhesion molecule
PHD	plant homeo domain
Prkaca	protein kinase cAMP dependent catalytic alpha
Prrx	paired related homeobox
Ptprf	protein tyrosine phosphatase receptor type
qRT-PCR	quantitative real-time PCR
RACE	rapid amplification of cDNA ends
RAD54	radiation 54
Ret	ret proto-oncogene
Rhox	reproductive homeobox
Robo	roundabout homolog
rRNA	ribosomal ribonucleic acid
RSF	remodelling and spacing factor
SANT	SWI-SNF and ADA transcriptional co-repressor N-CoR and TFIIB
Scrib	scribbled homolog
SEM	scanning electron microscope
Sema	semaphorin
Shh	sonic hedgehog
Six	sine oculis-related homeobox
Ski	sloan-kettering institute proto-oncogene
Slit	slit homolog
Smad	MAD homolog
SMARC	swi/snf related, matrix associated, actin dependent regulator of chromatin
SNF	sucrose non-fermenting
Snf2h	sucrose non-fermenting-homologue
Snf2l	sucrose non-fermenting-like
Sox	sry-box containing gene
SWI	failure in switching
Sypl	synaptophysin-like
Tcf	transcription factor
Tgfb	transforming growth factor beta
TS	theiler stage
Tshz	teashirt zinc finger family member
TUNEL	terminal deoxynucleotidyl transferase dUTP nick end labeled
UB	ureteric bud
ul	microlitres
Unc	uncoordinated locomotion
UTR	untranslated region
Vangl	vang-like
WICH	WSTF-ISWI chromatin remodelling complex
WINAC	WSTF including nucleosome assembly complex
Wnt	wingless/integrated
WSTF	williams syndrome transcription factor
Wt	wilms tumor

List of Symbols, Nomenclature, or Abbreviations	
X-gal	5-bromo-4-chloro-indolyl- β -D-galactopyranoside
Zeb	zinc finger E-box binding homeobox
Zfp	zinc finger protein

1: Introduction

It is estimated that at least 5% of pregnancies in Canada carry congenital abnormalities (Kohut and Rusen, 2002). These developmental defects account for one quarter of all neonatal and postnatal infant deaths. Even when non-lethal, congenital malformations can significantly impact quality of life, and impart substantial medical care costs. Neural tube defects make up a prominent subcategory of congenital defects, which affect the embryonic structures that develop into the spinal cord and brain. Neural tube defects are severe birth anomalies where failures in neural closure result in stillbirth or neonatal death if affecting the brain (anencephaly/exencephaly), or moderate to severe mobility issues if limited to the sacral spine (spina bifida). Non-syndromic incidences of neural tube defects show multifactorial inheritance and environmental influences with a recurrence risk of 2-3% in subsequent pregnancies (Hall and Solehdin, 1999).

Significant advancement in the prevention of neural tube defects came from nutritional studies showing that folic acid supplementation could reduce the risk of neural tube defects by ~50-75% (Centers for Disease Control and Prevention, 1991). Folic acid supplementation and fortification programs were implemented in numerous countries and have proven a successful measure in the prevention or reduction of congenital defects (De Wals et al., 2007). Despite yearly multi-million dollar investments in such programs with an estimated 40:1 cost-savings ratio in the hundreds of millions (US) (Grosse et al., 2005), there is not a clear understanding of how folic acid reduces the risk of neural tube defects. There further appears to be a subset of ~25-50% of neural tube defects cases that are insensitive to folate supplementation.

Studies attempting to link human genetic defects or variant alleles to neural tube defects have shown only limited success, and the few candidate alleles generated this way cannot explain the variety or frequency of human neural tube defects (Greene et al., 2009). The process of human neural closure finishes by 28 days following conception, often before the mother is aware of the pregnancy. The limitation of human samples, multifactorial complicating variables, and inability to manipulate the embryos during development leads to an interest in tractable animal models for study.

1.1: Animal models of neural tube defects

The process of neural tube closure in humans follows an elevation, folding, and fusion process termed primary neurulation (Figure 1) (reviewed by Harris and Juriloff, 1999; Copp et al., 2003; De Marco et al., 2006). Defects in primary neurulation result in neural tubes open to the external environment that can develop into anencephaly/exencephaly, spina bifida, or severe and fully open cases of craniorachischisis. A second neurulation process, referred to as secondary neurulation, progresses in the post-anal, caudal neural tube as defined by an internal epithelialization and cavitation mechanism to form a secondary neural tube that fuses to the primary tube (Figure 1). Birds and mammals retain the use of secondary neurulation, but it is limited to caudal neural tube formation

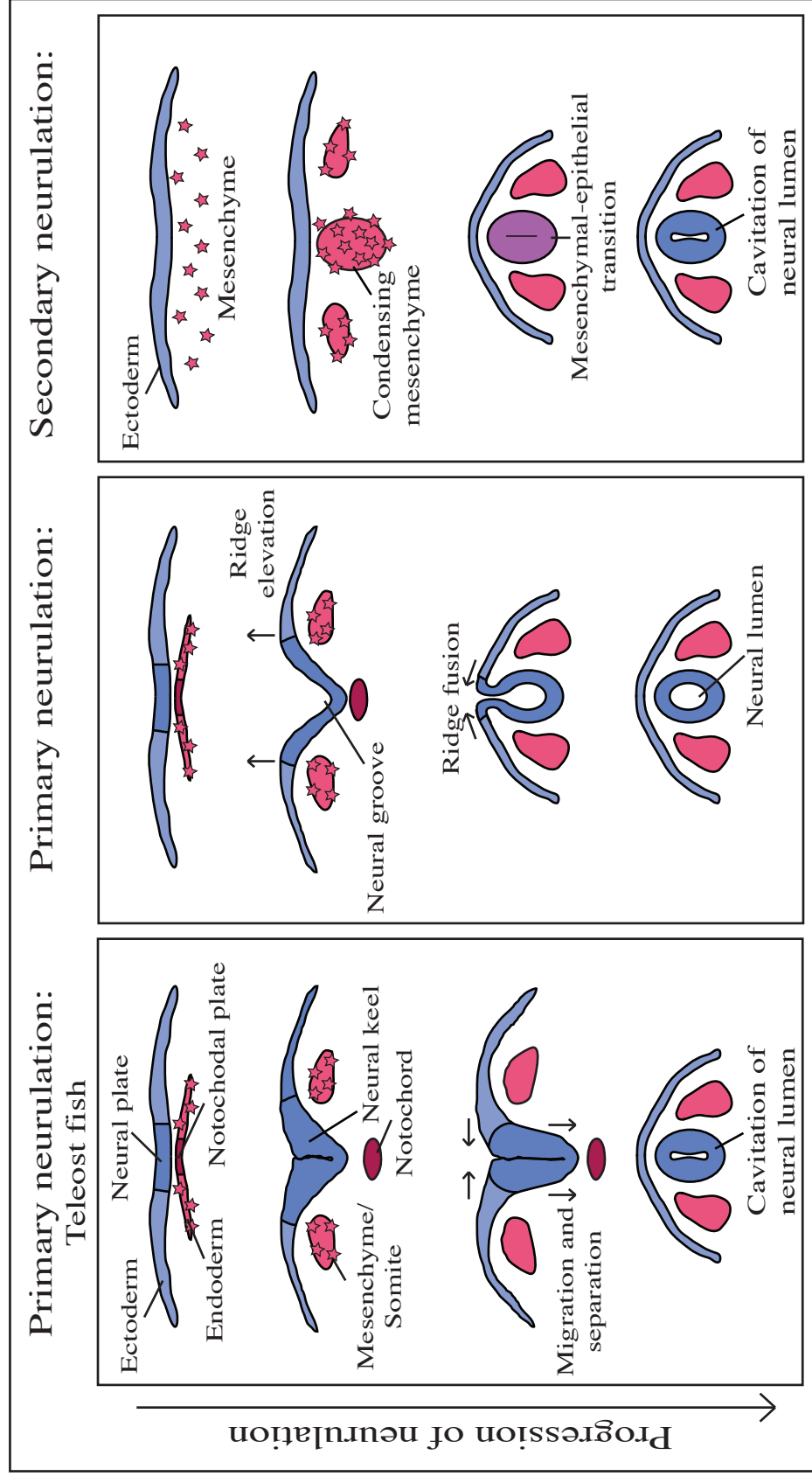


Figure 1:
Primary and secondary neurulation processes

Primary neurulation processes involve the formation of an internal epithelial neural lumen from external neuroepithelial tissue. At least two major methods of primary neural tube formation are found amongst vertebrates. Teleost fish form a neural plate from the outer ectoderm similar to avian and mammalian initialization. The underlying mesenchymal cells condense into the forming somites and notochord, a transient signaling structure which specifies the ventral neural regions. Teleost fish develop a thickened and folded ridge of the neuroepithelium called the neural keel. This mass of epithelialized tissue migrates into the embryonic body until the outer ectoderm can fuse and separate it into a distinct neural mass. This internalized keel of epithelia then cavitates and opens into the neural tube. Birds and mammals do not form a neural keel. They instead rely on the elevation, folding, and fusion of the neural ridges to form an open tube which is then internalized. Secondary neurulation initiates in the mesenchyme, and does not directly involve the ectoderm. A mass of mesenchymal tissue condenses and undergoes a mesenchymal-epithelial transition. The newly epithelialized mass then cavitates to form a hollow secondary neural tube. In many vertebrates, the post-anal neural tube is formed through the process of secondary neurulation. This secondary tube fuses to the primary neural tube to form a continuous neural lumen.

(Schoenwolf, 1983). The process of primary neurulation appears in many vertebrate phylogenetic groups and is proposed to be the ancestral vertebrate neurulation process (Handrigan, 2003). However, the morphology and mechanics of primary neurulation does differ between groups. Fish and lower vertebrates were once considered to undergo only secondary neurulation, although this has been overturned and the neural keel is now thought to represent primary neurulation processes (Figure 1) (Lowery and Sive, 2004).

Teleost fish such as zebrafish are a viable means of studying neurulation processes. The zebrafish is amenable to forward genetics and large-scale mutation screens that could generate candidate genes involved in neurulation processes. The forming neural tube is easily viewed in the external zebrafish egg and can be visualized and followed throughout development. Morpholino-based oligonucleotides are useful in knocking-down gene expression (Nasevicius and Ekker, 2000); however, reverse genetic tools are generally not as proficient at targeted mutations as they are in the laboratory mouse. Perhaps because of the misperceptions of teleost neurulation processes as being secondary or ‘primitive’ mechanisms, there has not been a thorough re-testing of neurulation gene candidates or pathways specifically in the zebrafish model. Many of the same molecular pathways may be used or co-opted from teleost to mammalian neural closure, but the morphology and process of formation is not the same (Figure 1).

Chicken embryos appear to use the same primary neurulation processes as in mammals (Hughes, 1955), but the laying of eggs allows for increased manipulation and viewing of the embryo without the need to sacrifice the mother. This makes the chick very applicable for morphological or gene expression studies when examining the process of primary neurulation. Procedures such as *in ovo* electroporation (Agarwala et al., 2001) allow molecular manipulation and testing of gene regulatory pathways during the chick neural development. Unfortunately, there are not as many genetic tools available in chicken in terms of gene-knockouts, as have been established in the rat or mouse systems.

Laboratory rodents offer a variety of molecular tools, cell lines, and germline mutations. Due to viviparous placental development, the mouse embryos are less accessible than the available egg-laying models. Slower generation time and smaller litter size makes the mouse less feasible for forward genetic screens. Fortunately, over two hundred and forty mouse mutations are established and identified as causing neural tube defects (Harris and Juriloff, 2010; Copp and Greene, 2009). The combination of gene-knockout studies along with an extensive history of neurulation studies done in mice provides both context and details of the pathways and processes involved in primary neural closure. Primary neurulation in the mouse relies on the processes of planar cell polarity and convergent extension, the regulation of cellular fate and embryo axis formation, apoptosis/proliferation control in the neuroepithelium and underlying mesenchyme, as well as the formation of apical constriction and hinge points in the forming neural tube (De Marco et al., 2006).

1.2: Process of neural tube closure

Initiation of neural closure begins with the specification of the neuroepithelium at the neural plate (Figure 1). The border of the neural plate is defined by a variety of WNT, BMP, and growth factor signals, while the forming notochord provides SHH floorplate specification (Patthey and Gunhaga, 2011; Jeong and Epstein, 2003). Throughout the early specification events, cells are also being recruited to the forming neural tube through planar polarity and convergent extension (Figure 2). The process of polarizing planar cells regulates the alignment of cells within an epithelial layer (Lawrence et al., 1975). The polarization and migration of cells controls the process of convergent extension (Figure 2). Polarized cells of the neuroepithelium intercalate during early neural development, and this process lengthens the embryo while raising the forming neural ridges. Convergent extension follows the establishment of planar polarity, which relies on non-canonical WNT signaling and FAT/DCHS cell-cell polarity signals (Figure 3).

The neural ridges further require the support of underlying mesenchyme to gain the mass and height necessary for neural fold fusion. Cellular growth, replication, and proper cell specification drive these early processes. The neural folds then differentiate along a dorsal-ventral axis according to positional cues (Figure 4). Fate mapping of cells along this axis is set up by morphogens, including the bone morphogenic proteins (BMP), sonic hedgehog (SHH) and the wingless/integrated (WNT) pathways (Timmer et al., 2002). The early neural tube is a complex mosaic of cells expressing various *Pax*, *Sox*, *Dlx* genes, as well as a number of other transcription factor families influencing final cellular identity. The determination of cellular fate is critical for brain and spinal development. In the context of neural closure, these factors are associated with the production of hinge points that help to bring neural folds together. Apical constriction of the filamentous actin bends the neural fold at the ventral midline and the dorsolateral hinge points (Figure 4) (De Marco et al., 2006).

After the rising folds come together, fusion proceeds through cell-cell interactions to form the neural tube lumen (Figure 5). The process involves adhesion molecules such as neural cell adhesion molecule (NCAM) and N-CADHERIN, which facilitate separation of neural tube from surface ectoderm (Moase and Trasler, 1991; Bronner-Fraser et al., 1992). The family of Eph tyrosine kinase receptors regulates fusion events (Holmberg et al., 2000).

Defects in neural tube formation can be categorized into one of the four generalized neurulation processes (Figure 6). Planar polarity and convergent extension defects leave the embryo too broad and with short neural folds (Figure 6). An apoptotic loss or delay of mesenchyme proliferation during neural folding can cause neural tube defects (Figure 6) (Berk et al., 1997; Beverdam et al., 2001). Hinge point defects can arise either from the misspecification of the hinge region or through the direct disruption of cytoskeletal proteins driving apical constriction. Even when cells receive the proper positional and sensory inputs, they can fail to form hinges if they lack the means to produce the necessary mechanical processes (Figure 6) (Lee et al., 2007; Haigo et al., 2003). Failure of

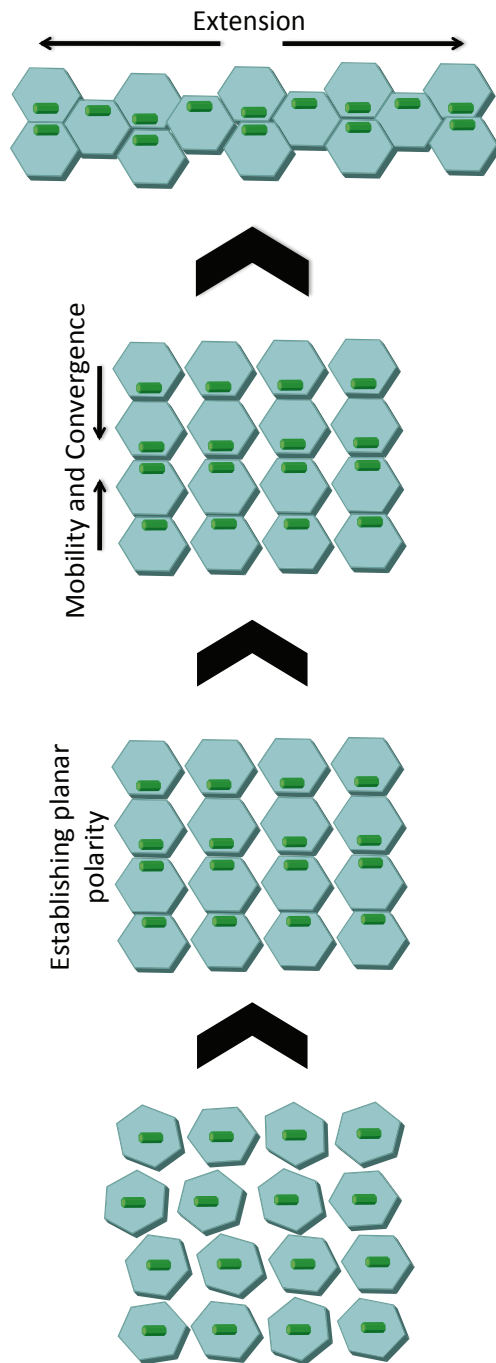


Figure 2:
Convergent extension processes

The developing embryo uses convergent extension to restructure cells during organogenesis. Mobile cells (shown in green) converge along one axis and extend through intercalation along a perpendicular axis. Convergent extension relies on planar cell polarity to orient the initial axis of convergence (demonstrated by the asymmetric position of the primary cilia).

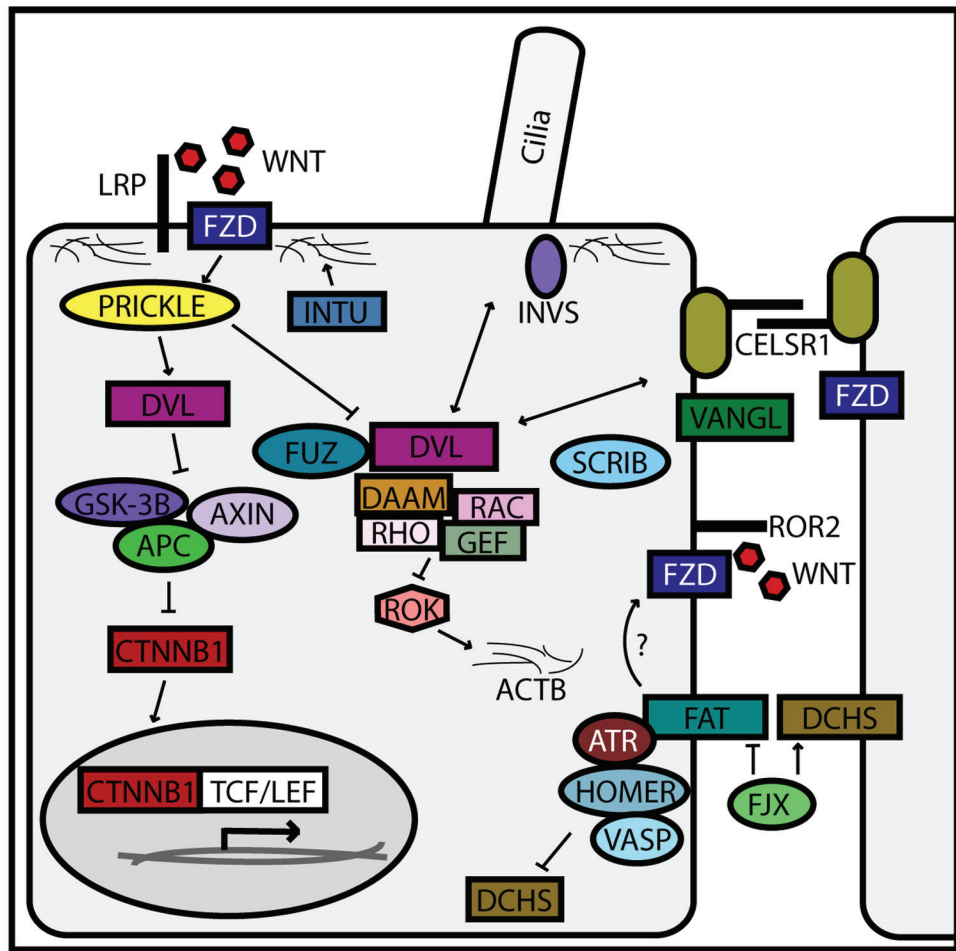


Figure 3:
Overview of planar cell polarity signaling

The organization and signaling of planar polarity within cells is regulated through the combined input of multiple cell surface receptors. The canonical WNT signaling pathway (top left) begins with WNT/FZD signaling through PRICKLE and results with transcriptional changes of CTNNB1/TCF/LEF targets. Often referred to as the non-canonical WNT pathways (upper right), the core PCP pathway signals through a combination of FZD, CELSR1, and VANGL. Although also utilizing DVL, the output of the non-canonical pathway is ACTB reorganization and direct polarization of cellular structures (cilia) and PCP effectors. FAT/DCHS signaling (bottom right) appears to run in parallel in the polarization of some cells, although there may be cross-talk with the non-canonical PCP pathway. Modified from Goodrich (2008) and Gray et al. (2011).

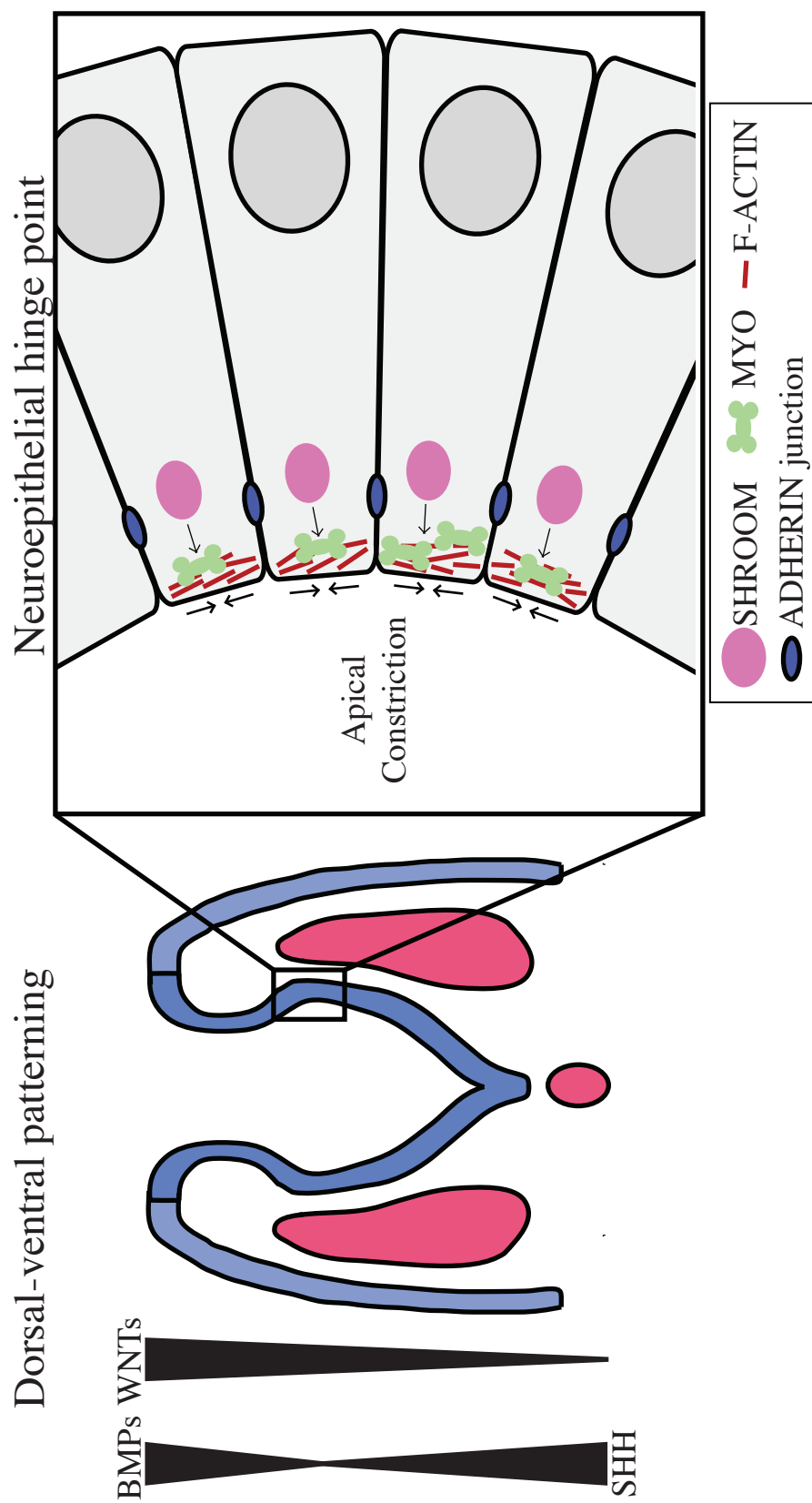


Figure 4:
Neural hinge point formation

The formation of lateral hinge points allows forming neural ridges to bend and come together. The bends are established by apical constrictions within the epithelia, and their location is regulated by dorsal-ventral specification of the forming neural tube. Dorsally secreted BMPs and WNTs help to identify and set a dorsal fate, while SHH is secreted from the notochord and floor plate to establish the ventral neural tube. Apical constriction (inset) relies on the recruitment and regulation of F-actin along the apical edge of the epithelial cells. SHROOM proteins initiate the F-actin localization, while myosin proteins drive the constriction of the F-actin. Modified from Lee (2012).

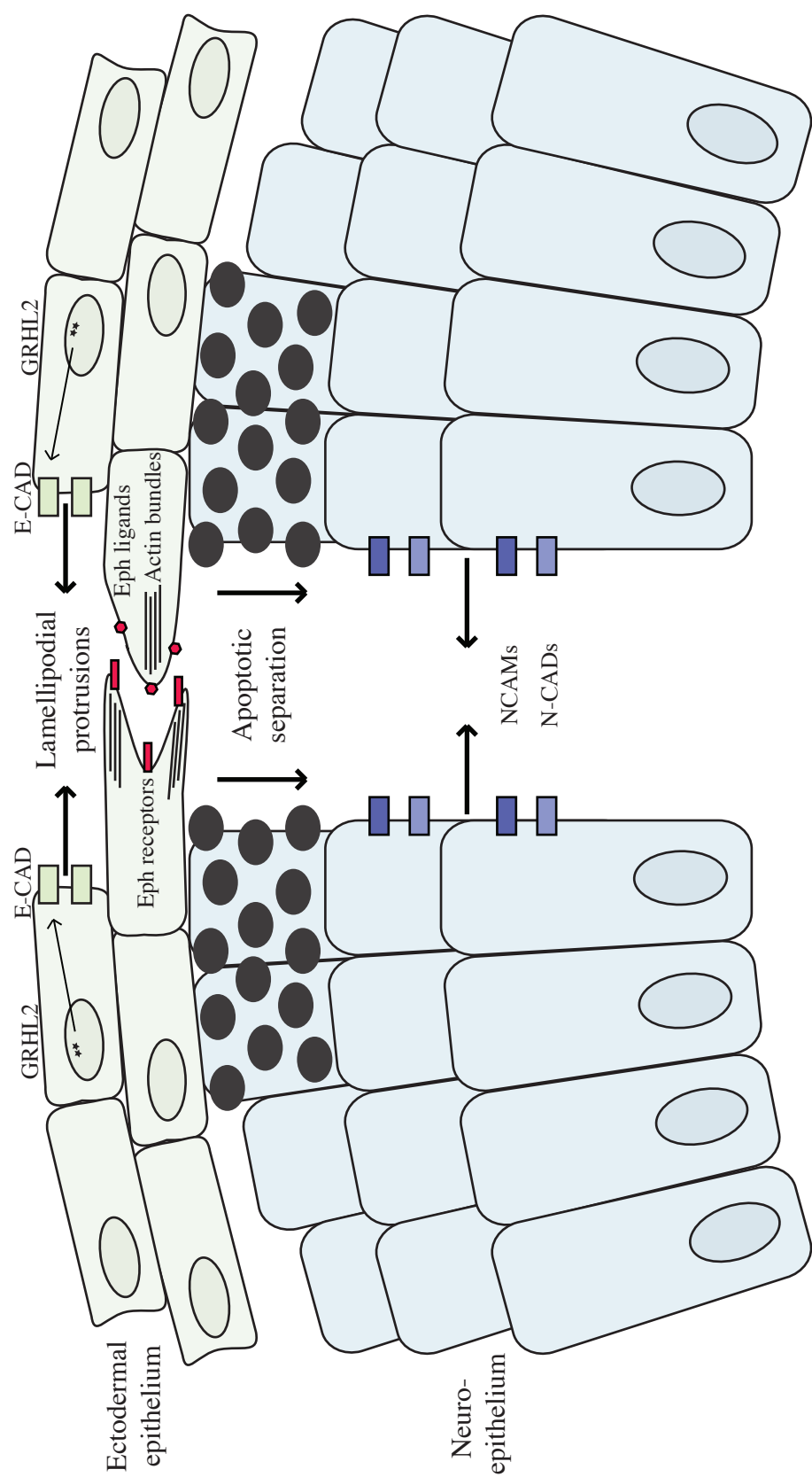


Figure 5:
Neuroepithelial fusion and lumen formation

Neural fusion events rely on cellular adhesion. The overlying ectodermal cells extend lamellipodia across the midline gap to initiate contact. Cell-cell signaling through Eph ligands and Eph receptors regulate the early interdigitation of the lamellipodia. As the edges come together, epithelial cadherins (E-CAD) establish stronger adhesion of the cells. E-CAD production relies on GRHL2 transcription factor activity. Neural cell adhesion molecules (NCAM), and neural cadherins (N-CAD) are thought to facilitate adhesion of the neuroepithelium; however, loss of these factors do not cause open neural tube defects. The epithelial layers then use apoptosis to remodel and separate the neuroepithelial cells from the outer ectoderm.

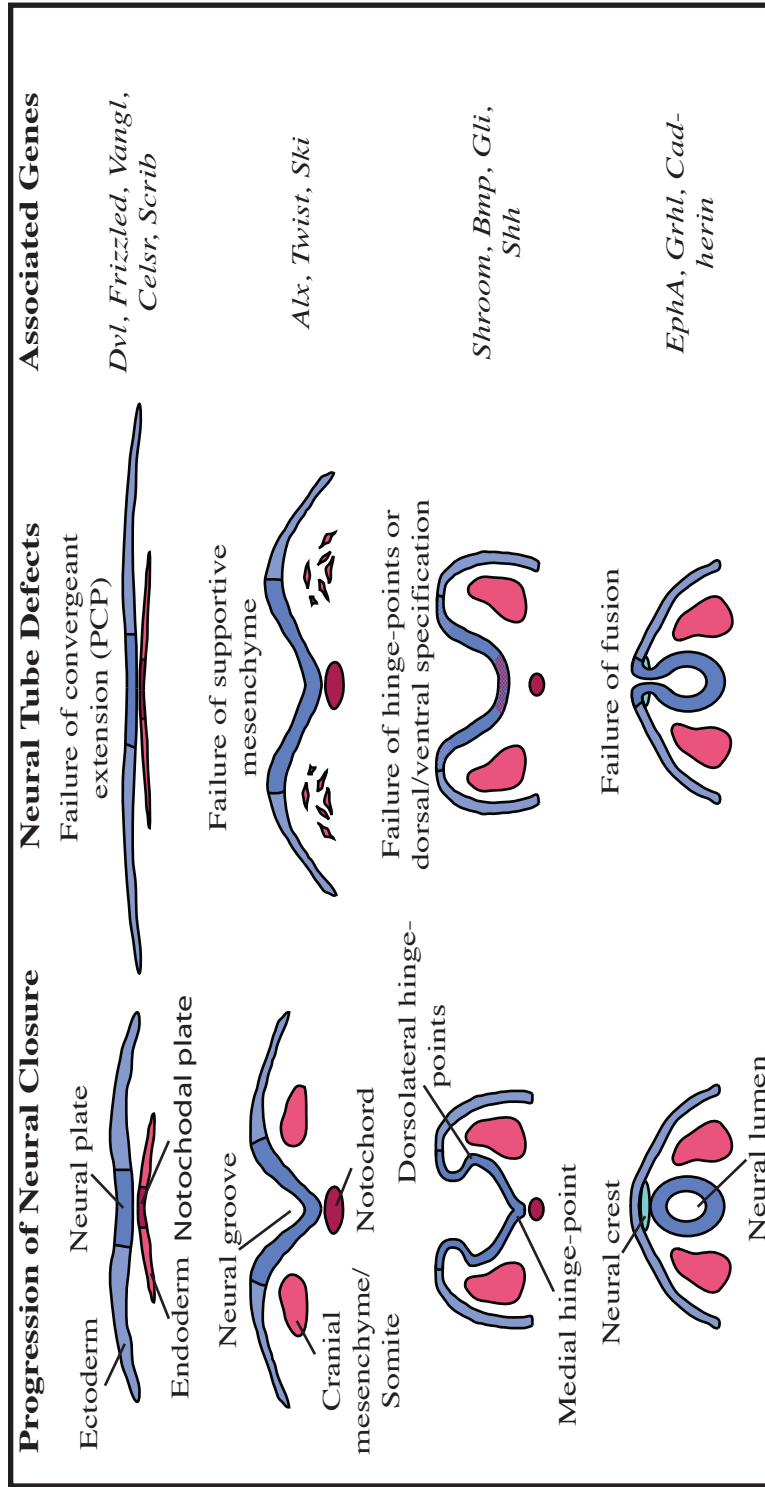


Figure 6:
Defects of primary neural tube closure

Primary neurulation begins with the specification of the notochord and neural plate. At this and later stages, planar cell polarity (PCP) signaling influences the convergent extension (CE) of migrating and intercalating cells into the forming ridges. Failures in PCP and CE processes result in wider neural ridges without the mass or height necessary to come together. The elevation of the neural ridges forms through the combined effects of neuroepithelial growth and the midpoint hinge constriction with support from the underlying paraxial mesenchyme. Loss of the paraxial mesenchyme is thought to hinder closure through a loss of the mechanical support. The formation of dorso-lateral hinge-points are necessary for cranial neural closure, which can be disrupted through either a mechanical disruption of apical constriction or through a loss of cellular identity and specification of the dorsal/ventral neural tube. The final fusion of neural ridges relies on cell-to-cell adhesion and signaling to both distinguish and separate ectoderm from the neural lumen. Gene families whose function or gene mutations are associated with the various classifications are included to the right of each section. Modified from Harris and Juriloff, (1999); Copp et al. (2003); De Marco et al. (2006).

fusion mechanisms can lead to the neural tube remaining open even after the other processes bring the neural ridges together (Figure 6) (De Marco et al., 2006).

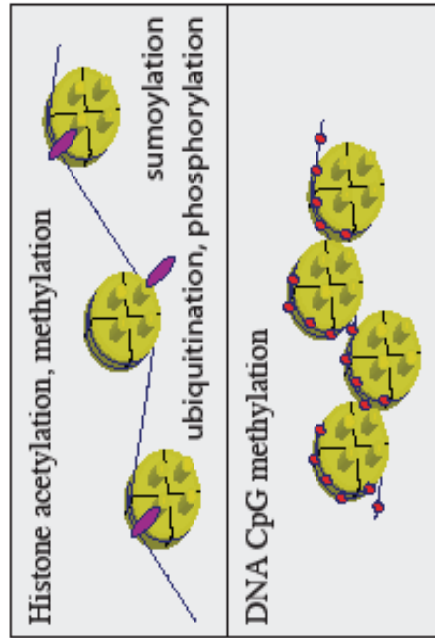
1.3: Epigenetic factors in neural tube closure

A number of external factors are associated with an increased risk of neural tube defects. Maternal exposure to cigarette smoke (Suarez et al., 2011), toxins (Marasas et al., 2004) or teratogenic drug effects (Buehler et al., 1994), are associated with increased risk. Maternal medical conditions such as diabetes (Eriksson et al., 2003) or obesity (Hendricks et al., 2001) can influence the risk of fetal neural tube defects, as can maternal diets with increased glycemic load (Yazdy et al., 2010), and deficiencies in vitamins such as B12 or folate (Smithells et al., 1976; Kirke et al., 1993). These factors may work directly to inhibit cellular or developmental processes, but some may act through changes in gene expression brought on by changes in epigenetic regulators. Folate supplementation can alter regulation of DNA methylation (Pufulete et al., 2005) and restore histone modifications associated with neural tube defects (Fleming and Copp, 1998; Ichi et al., 2010). Environmental and nutritional factors can change the output of chromatin remodeling processes. The field has not identified which epigenetic chromatin remodeling enzymes are affected by dietary folate, but has uncovered a few remodeling proteins involved in the regulation of neurulation.

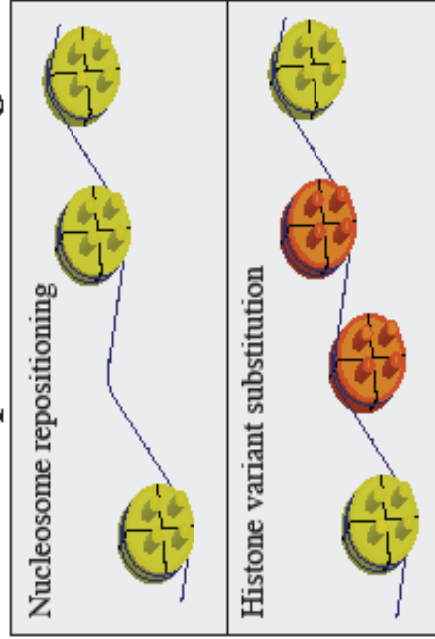
Epigenetics is the study of changes in gene expression or chromatin regulation that do not change the DNA sequence, but provides an additional means to regulate how genes are expressed (Egger et al., 2004). The control of epigenetic regulation works through a series of covalent and ATP-dependent chromatin remodeling factors that alter the DNA/histone packaging (Figure 7). The changes brought on by covalent modifications or nucleosome repositioning can alter binding sites or block access to target sites. The identification and understanding of epigenetic processes offers new opportunities for the diagnosis and treatment of complex clinical disorders, and this has led to a growing interest in the role of epigenetic regulation in the control of neurulation (Greene et al., 2011).

Of the 240 mouse mutations associated with neural tube defects (Harris and Juriloff, 2010), there are a few within chromatin remodeling enzymes. BRG1 contains the catalytic domain responsible for shifting nucleosomes (Bultman et al., 2000). BRG1 is active in numerous remodeling complexes, and mutations in *Brg1* show a failure in cranial neural closure (Bultman et al., 2000). SRG3, also known as BRG1-associated factor 155, participates in BRG1 complexes and provides histone-binding domains to target the complex (Sif et al., 2001; He et al., 2008). Mutation of *Srg3* shows a failure in neural closure at the midbrain-hindbrain junction (Kim et al., 2001). The CECR2-containing remodeling complex (CERF) made up of SNF2L and CECR2 shows functional similarities to the BRG1/SRG3 complexes (Banting et al., 2005), in that it remodels nucleosome positions through the same catalytic domain contained within the SNF2L member. CECR2 may have similar function to SRG3, as both contain histone-binding

Covalent modifications



ATP-dependent remodeling



Combinatorial epigenetic regulation of transcription

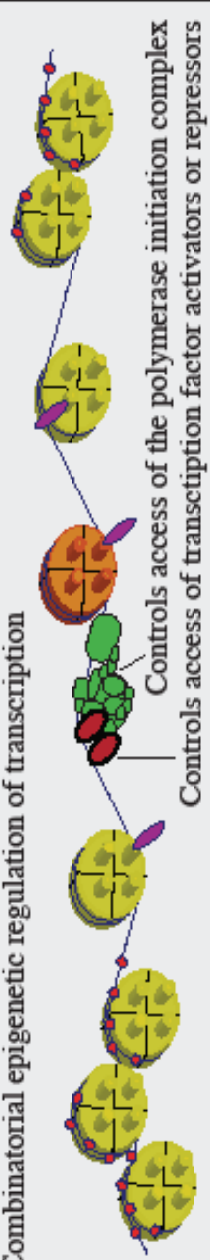


Figure 7:
Epigenetic regulation of transcription

Epigenetic chromatin remodeling works to change the position and interaction of DNA within nucleosomes. Nucleosomes (depicted in yellow) are octomers of histone proteins around which DNA is bound. The tails of the histones (depicted as yellow cylindrical projections) stick out from the nucleosome bead and are key regulatory sites for covalent modification. Epigenetic modification of the histones (acetylation represented by a purple moiety) or DNA (methylation depicted as red hexagon) alters how tightly the nucleosomes pack together. Such covalent changes can alter the shape of binding sites within the DNA sequence or histone tails, and can serve to recruit or block other regulatory factors. ATP-dependent chromatin remodeling complexes use an ATP-driven helicase to twist and interrupt the DNA/histone association. This allows nucleosomes to be shifted, or removed, from targeted sites of ATP-dependent remodeling. Histone variants (shown in orange) can serve a similar function to covalent modifications, but rely on ATP-dependent complexes to fully disrupt and replace the proteins. Transcriptional activation requires both physical space to load onto the DNA, and access to a variety of DNA regulatory sites. Accessibility of the initiation complex (depicted in green) and transcription activators/repressors (depicted in red) are reliant on the combined activity of chromatin remodeling processes. The changes are dynamic, but they are also stable, and this stability through generations is what makes these changes epigenetic regulators of transcription.

domains predicted to target their respective complexes (He et al., 2008). The mutation of *Cecr2* results in a failure of cranial neural tube closure (Banting et al., 2005).

Understanding how chromatin remodeling controls gene regulation and the developmental processes of neurulation may generate additional gene candidates useful to screen and diagnose human neural tube defects. It may eventually lead to an integrated environmental-to-genetic model, which could explain the mechanism of how environmental and maternal nutritional factors impact epigenetic regulation, and how this influences neural tube defects. The following thesis explores the role of CECR2 in epigenetic gene regulation and its role in embryonic development.

1.4: CECR2 is associated with epigenetic regulation of euchromatin and is necessary for neural tube closure

Tate et al. (1998) initiated the study of an epigenetic role for Cat Eye syndrome chromosome region, candidate 2 (CECR2) when it was discovered amongst a screen for novel chromosome-associated proteins. Mouse embryonic stem cell lines were examined that carried tagged constructs fusing gene products to the colourimetric reporter protein Beta-Galactosidase. The CECR2 fusion protein was restricted to the nucleus, where it appeared as discrete spots enriched in euchromatin and excluded from regions of heterochromatin (Tate et al., 1998). At the time of the Tate et al. (1998) study, CECR2 remained unnamed and unclassified with no identified homologues or family structure.

Interest in CECR2 resurfaced when the protein was once again identified in association with chromatin structure in Banting et al. (2005). A CECR2-containing Remodeling Factor (CERF) complex was discovered, which included CECR2 and a chromatin remodeling protein sucrose non-fermenting 2-like (SNF2L). SNF2L belongs to an imitation switch (ISWI) subfamily of ATP-dependent chromatin remodeling factors within a larger SWI/SNF family (Martens and Winston, 2003; Tang et al., 2010). Discovery of CERF further suggested that CECR2 was both physically associated with euchromatin binding (Tate et al., 1998) and functionally associated with the epigenetic remodeling or regulation of the chromatin (Banting et al., 2005).

Banting et al. (2005) provided domain analysis of CECR2 and identified an N-terminal DDT domain thought to bind the ISWI proteins (Fyodorov et al., 2002; Doerks et al., 2001). They found the first third of CECR2 contained a nuclear localization signal, an AT-hook and a bromodomain. AT-hooks bind the minor groove of AT-rich regions, with target regions predicted as (ATAA)_n or AA(A/T)T (Huth et al., 1997; Reeves, 2000). Bromodomains are predicted to bind acetylated histones, targeting the CERF complex to modified nucleosome regions (reviewed by Denis et al., 2010). Despite the relatively large size of the CECR2 protein at 1453 amino acids, within the last two-thirds of the protein the only structural domain identified contains a large proline-rich region following the bromodomain. Proline-rich regions within the SWI/SNF protein family were thought to act as transcriptional activators and protein binding sites (Williamson,

1994). Beyond the sequence analysis, there remained only a limited understanding of how the CECR2 protein functions *in vivo*. Banting et al. (2005) confirmed the human CECR2 protein binds and could be pulled down with the SNF2L protein when over-expressed in a human embryonic kidney cell line. They also established that this pair could influence nucleosome position in an *in vitro* assay (Banting et al., 2005). However, the general assay could not establish what specific functions or chromatin target regions may be selected by CECR2 *in vivo*.

Banting et al. (2005) explored the *in vivo* developmental roles of CECR2 by generating the *Cecr2*^{Gt45Bic} mouse line. The *Cecr2*^{Gt45Bic} BALB/c homozygous mice exhibited perinatal lethality resulting from exencephaly and a failure of cranial neural tube closure. The *Cecr2*^{Gt45Bic} homozygous exencephalic penetrance appeared to be strain dependent, as did the two other reported phenotypes of open eyelids and kinked tails (Banting et al., 2005). These studies suggested CECR2 epigenetic remodeling of the euchromatin was necessary for the development of the neural tube, but dependent on unidentified strain modifiers. Banting et al. (2005) did not propose a mechanism by which remodeling may occur, or how it could result in the reported developmental defects.

The CECR2 field also has unresolved discrepancies regarding the molecular and biological roles for CECR2. Articles by Liu et al. (2002) and Liu and McKeehan (2002), interpreted CECR2 to be involved in mitochondrial apoptotic pathways and vesicular trafficking. This is inconsistent with CECR2 subcellular localization (Tate et al., 1998) and the remodeling function indicated by Banting et al. (2005). The proposal is also inconsistent with the known functions of ISWI complexes as reviewed by Martens and Winston (2003). CECR2 is predicted act as a nuclear ISWI subunit whose function would be consistent with other BAZ-like ISWI subunits in its ability to regulate nucleosome position (Banting et al., 2005; Ito et al., 1997; Landry et al., 2008; Tsukiyama and Wu, 1995).

As both an epigenetic regulator and neural tube defect associated gene, understanding CECR2 function and processes may offer insights into how epigenetic remodeling may influence NTD manifestation. Identifying the pathways affected by CECR2 epigenetic regulation may identify other genes as candidates involved in neural tube closure. The broad expression of *Cecr2* may further show a role for epigenetic developmental regulation in multiple organs, and thus the mechanisms identified may be applicable to other congenital defects. This thesis focuses on the effects of mouse *Cecr2* loss during development and does not address directly the protein structure or remodeling activities of the CECR2 protein. Nonetheless, this author suggests it is CECR2's role as a chromatin remodeler that will provide important context toward understanding both the experiments undertaken and the conclusions drawn from this work.

1.5: Advances in chromatin remodeling research

The application and understanding of chromatin remodeling processes in the context of developmental biology remains in its relative infancy. The characterization, and even the discovery, of additional remodeling complexes is

an ongoing process. Predictions of CECR2 function can be generated through comparing other BAZ-like proteins, how they interact with ATP-dependent chromatin remodeling complexes, and their impact on embryonic development.

1.5.1: DNA compaction and chromatin remodeling

The basic molecular function of chromatin remodeling proteins is to regulate the chromatin state through the alteration of nucleosome position and composition (Figure 7) (Winston and Carlson, 1992; Cairns et al., 1996; He et al., 2008). Composed of a central octamer of histones H2A, H2B, H3 and H4, the nucleosome is entwined with 146 bp of DNA wrapped roughly 1.7 times around the core (Luger et al., 1997). The nucleoprotein structure can be further stabilized through the addition of the linker histone H1 to reversibly clamp the DNA to the nucleosome octamer (Wolffe and Hayes, 1999).

The dynamic nature of chromatin is influenced by nucleosome interactions, and the mechanical processes regulating the nucleosomes are controlled by chromatin remodeling complexes. Covalent remodeling encompasses the various modifications made to histone tails such as acetylation, methylation, phosphorylation and ubiquitination. The addition or removal of moieties along the N-terminal histone tail can directly influence the binding of DNA by changing the steric topology or charge. Such changes can present unique binding sites or markers for further protein interactions that alter the chromatin structure. Markers laid down by covalent remodeling recruit the second sub-category of adenosine triphosphate (ATP)-dependent, non-covalent, chromatin remodeling (Zawadzki et al., 2009). The rotational position for a particular DNA binding site determines whether it faces out from the nucleosome and is exposed to the nuclear environment, or is orientated into the nucleosome surface where it remains inaccessible to binding factors (Hebert and Roest Crolius, 2010). The translational position of a nucleosome determines where along a strand of DNA the nucleosome sits as well as the relative distance between nucleosomes (Mavrich et al., 2008). ATP-dependent mechanisms affect the topological and positional interaction of the DNA on the histone primarily through torsion and mechanical displacement.

Within the promoters of active genes, the combination of covalent and ATP-dependent remodeling forms open regions through the positioning of nucleosomes (Mavrich et al., 2008, Hebert and Roest Crolius, 2010). Alternatively, repressed gene states can be preserved through the placement of nucleosomes to block sites otherwise recognized by transcription factors (Belikov et al., 2000). Nucleosome remodeling mechanisms are propagated over large areas of chromatin to form the transcriptionally active euchromatin or the condensed regions of heterochromatin. A nucleosome region contains epigenetic information necessary for the maintenance of gene transcription and, at times, the conservation of cellular identity; both of which must be maintained through cell lineages after multiple rounds of replication (Lowary and Widom, 1997; McNairn and Gilbert, 2003).

1.5.2: Chromatin remodeling ATPases

ATP-dependent chromatin remodeling complexes share a core family of sucrose non-fermenting-like (SNF-like) helicase proteins. These remodeling proteins were first reported in yeast where, when mutated, they interrupt chromatin structure and transcription in screens showing a failure in switching (SWI) of mating type, or as an inability to utilize sucrose as sucrose non-fermenting (SNF) (Neugeborn and Carlson, 1984; Stern et al., 1984). Unfortunately, the field has been unable to coordinate the use of one name, and refers to this class of proteins as SWI/SNF.

The classification of ATP-dependent chromatin remodelers now includes a variety of subfamilies (reviewed by Martens and Winston, 2003; Tang et al., 2010). All of the ATP-dependent remodeling complexes possess the core SNF2-like ATPase and helicase-like domain. Chromatin-binding domains are present either within the core ATPase protein or as part of a co-factor. Both bromodomains and the SANT domain are thought to bind N-terminal histone tails and facilitate the targeting and stability of the remodeling complex (Zeng and Zhou, 2002; Boyer et al., 2002, Boyer et al., 2004).

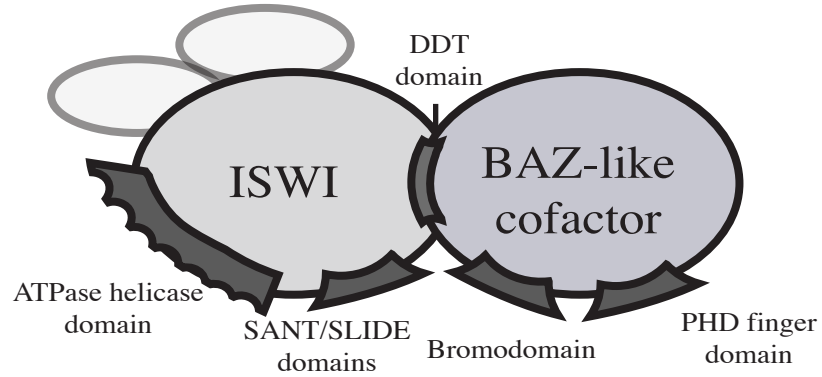
1.5.3: The imitation-switch (ISWI) subfamily

The ISWI subfamily possesses fewer subunit components than other chromatin remodeling subfamilies (Figure 8), but retains the same *in vitro* ability to reposition nucleosomes (Elfring et al., 1994). ISWI ATPases are identified by the presence of a SANT domain and a novel DNA-binding SLIDE domain in addition to the core ATPase/helicase (Grune et al., 2003). The ISWI ATPase proteins also lack a bromodomain, which is necessary for function of the complex. ISWI bromodomains are gained through association with bromodomain-adjacent zinc finger (BAZ) or BAZ-like subunits. Each of the two mammalian ISWI proteins binds with CECR2, forming similar but perhaps biologically distinct functional complexes (Banting et al., 2005; Thompson et al., 2012). The mammalian ISWI proteins are SNF2H and SNF2L.

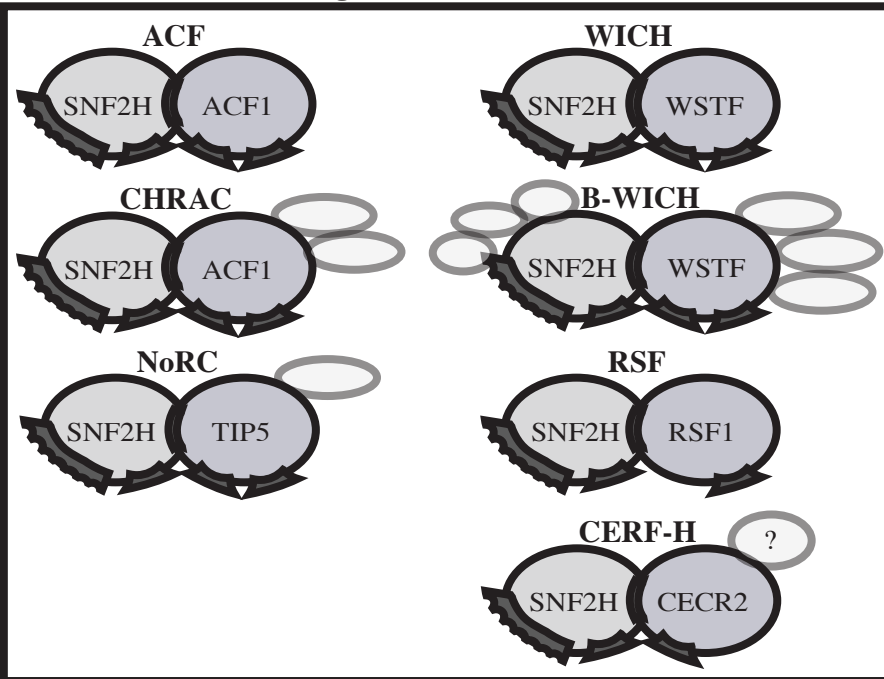
The list of identified ISWI complexes originates from work in multiple eukaryotic species including yeast, fruit fly, mice and humans. The mammalian SNF2H exists in a variety of complexes (Figure 8). The SNF2L homologue resides in two characterized complexes (Figure 8). Recent studies involving the human SNF2-like family have attempted to unify the various names under a common convention: SWI/SNF related, matrix associated, actin dependent regulator of chromatin (SMARC) followed by a subfamily designation and number. Many mouse studies have since adopted this naming system, although there is not universal adherence to the SMARC nomenclature. In its current format, the SMARC convention does not properly designate or identify the subfamilies present. Two genes originally named SNF2-like (SNF2L) and SNF2-homologue (SNF2H) represent the mammalian ISWI subfamily. The SMARC designations are SMARCA1 (SNF2L) and SMARCA5 (SNF2H) for these related genes. The SMARC system does not convey that SMARCA1 and SMARCA5 are likely gene duplications with functional and structural similarities, and distinct

A) ISWI Structure

Fewer co-factors than SWI/SNF



B) ISWI: SNF2H Binding



C) ISWI: SNF2L Binding



Figure 8:
General structure and variation of mammalian ISWI complexes

(A) The ISWI subfamily is defined by the ATPase/helicase containing catalytic subunit of the SWI/SNF family. ISWI proteins also share a novel SANT/SLIDE domain thought to bind DNA or histone-tails. Bromodomain-adjacent-to-zinc-finger (BAZ)-like cofactors form a family of proteins containing a bromodomain and a PHD domain zinc-finger domains. BAZ-like cofactors bind ISWI proteins through a DDT domain. (B) SNF2H containing ISWI complexes appear the most diversified, with a variety of cofactors specifying the targeting or function of the complexes formed. The SNF2H complexes are ATP-dependent chromatin assembly and remodeling factor (ACF) (Bochar et al., 2000; LeRoy et al., 2000), chromatin accessibility complex (CHRAC) (Poot et al., 2000), WSTF-ISWI chromatin remodeling complex (WICH) (Bozhenok et al., 2002), nucleolar remodeling complex (NoRC) (Strohner et al., 2001), remodeling and spacing factor (RSF) (LeRoy et al., 1998), SNF2H-cohesin (Hakimi et al., 2002), and a novel SNF2H-CECR2 complex not fully characterized (Thompson et al., 2012). (C) There have been only two SNF2L containing ISWI cofactors identified. The nucleosome remodeling factor (NURF) complex was identified in *Drosophila* (Tsukiyama and Wu, 1995), and the mammalian NURF was later confirmed as the first SNF2L containing remodeling complex (Barack et al., 2003). The second SNF2L complex was designated CECR2-containing remodeling factor (CERF) with CECR2 as the only currently identified co-factor (Banting et al., 2005).

from the other SMARCA members. In this thesis, ISWI members will be referred to by their original names rather than the SMARCA conventions.

1.5.4: Developmental roles of ISWIs

ISWI complexes affect transcription, but as a family they do not all evoke transcriptional changes in the same manner. Mammalian NoRC activity represses sites of rRNA transcription to form condensed heterochromatin-like structure through the recruitment of various methylase proteins (Santoro et al., 2002; Strohner et al., 2004). The mammalian WICH and ACF complexes appear primarily in repair pathways (Yoshimura et al., 2009) or the replication of heterochromatin (Bozhenok et al., 2002; Collins et al., 2002), while the binding of additional components converts WICH to WINAC where it can mediate transcription with the vitamin D receptor (Kitagawa et al., 2003). Thus, only a subset of the ISWI complexes directly regulates transcripts.

The *Drosophila* NURF complex works in association with the GAGA factor, a transcription factor and transcriptional activator, to reverse gene silencing and activate GAGA factor targets (Deuring et al., 2000). *Ultrabithorax* and *Engrailed* have been identified as GAGA/NURF targets (Badenhorst et al., 2002), a role that is conserved in the SNF2L-mediated regulation of mammalian *Engrailed* (Barack et al., 2003). The *Drosophila* NURF301 component of the NURF complex acts as a primary co-factor for EcR, a nuclear receptor that mediates ecdysteroid signaling by regulating downstream genes in response to the steroid hormone ecdysone (Badenhorst et al., 2005). In addition, NURF mediates access to armadillo/catenin target gene activation during canonical Wnt signaling (Song et al., 2009).

Drosophila null mutants of both sexes without the ISWI core ATPase die by the pupal stage. The mutant males possess a highly aberrant polytene X-chromosome structure (Deuring et al., 2000). The ISWI proteins are linked to specific interactions with the GAGA transcription factor and the regulation of *Engrailed* and *Ultrabithorax*, but Deuring et al. (2000) could not determine how the loss of ISWI resulted in aberrant polytene structure of the entire male X-chromosome. The loss of *Snf2h* in mice results in the death or arrest of cells within the trophectoderm and inner cell mass (Stopka and Skoultschi, 2003). This early developmental disruption causes embryonic death shortly after implantation. The mouse mutation of *Snf2l* is not embryonic lethal, and shows only a mild neural overgrowth phenotype in adult animals (Yip et al., 2012). In the case of *Snf2l* mutation, *Snf2h* is thought to partially compensate (Picketts, personal communication 2009). *Snf2l* is suspected of being involved in human X-linked mental retardation (Lazzaro et al., 2008), and is thought to regulate development of the ovary through regulation of the steroidogenic acute regulatory gene (Lazzaro et al., 2006). *Snf2h* and *Snf2l* are expressed during early embryogenesis and organogenesis of the brain, gonads, lungs, kidneys and gut (Lazzaro and Picketts, 2001). The expression of *Snf2h* is dominant in proliferating cell populations and *Snf2l* becomes upregulated in terminally differentiated cells.

1.5.5: BAZ-like ISWI partners control transcriptional targeting

With *in vitro* studies, the addition of the associated co-factors to the core ATPase/bromodomain complex not only improved specificity and rate of remodeling, but within CHRAC/ISWI complexes the addition of certain components could reverse the direction of nucleosome movements (Eberharter et al., 2001). As other components bind to an ISWI, they can influence whether the ATPase forms structured nucleosome spacing or disorder (Ito et al., 1997; Tsukiyama and Wu, 1995). Remodeling complexes sharing the same ATPase core protein can show a wide variety of functions specified by the non-catalytic subunits unique to each complex (He et al., 2008). Thus the study of subunits which determine target selection will be crucial to understanding how a given ISWI complex regulates transcription and development.

The mouse non-catalytic bromodomain-containing subunits of the ISWI complexes belongs to a novel family named bromodomain-adjacent zinc finger (BAZ) or BAZ-like members that includes ACF1, NURF301, BAZ2A, WSTF, and CECR2 (Jones et al., 2000; Banting et al., 2005; Thompson et al., 2012). The ISWI cofactors often include PHD fingers, DDT domains, and bromodomains. PHD fingers are thought to bind tri-methylated tails of histones; bromodomains binds acetylated histone tails; while the DDT domains were originally annotated as DNA binding domains, but are necessary for binding to the ISWI component (Fyodorov et al., 2002; Doerks et al., 2001).

The non-catalytic BAZ-like cofactor of the mouse NURF complex is the bromodomain PHD finger transcription factor (BPTF). It appears predominantly developmental in nature with a dynamic expression during organogenesis of the testis, spleen, brain and kidney. Loss of the mammalian BPTF results in the misregulation of transcription markers for visceral endoderm and the primitive streak, supporting the phenotypic assessment that homozygous *Bptf* mutant animals appear developmentally arrested at primitive streak formation (Landry et al., 2008). The BPTF/SNF2L (NURF) complex regulates SMAD components, suggesting BPTF remodeling directly works on the promoter regions of SMAD-regulated genes to recruit or restrict SMAD transcription factors (Landry et al., 2008).

As the only other SNF2L-binding BAZ-like component currently identified, BPTF is the closest functional analogue to CECR2. The dichotomy of NURF and CERF, or BPTF versus CECR2, could allow the direct testing of the hypothesis put forward by He et al. (2008), that the non-catalytic BAZ-like components define the biological activity of the complex. Extrapolating from He et al. (2008), CECR2/CERF would be expected to show different targets than those of BPTF, but the molecular means by which it invokes target changes, through SNF2-remodelling, may be similar to BPTF/NURF.

1.6: Directed questions and research

Research into the epigenetic control exerted by mammalian remodeling complexes on developmental regulation is aided by the availability of mouse models harboring mutations of the remodeling proteins (Banting et al., 2005;

Bultman et al., 2000; Landry et al., 2008; Reyes et al., 1998; Stopka and Skoultschi, 2003). The presented research explores the developmental defects and transcriptional disruption caused by mutations of the BAZ-like chromatin remodeling protein CECR2 in mice. Orthologs to *Cecr2* appear throughout the animal kingdom from Ecdysozoa to Mammalia (Keuling et al., 2007). This project focuses on the effects of CECR2 regulation during primary neural tube closure. The work employs mouse models as the embryos undergo primary neurulation and *Cecr2* germline mutations are available (Banting et al., 2005).

The overall goal is to understand how CECR2 influences embryonic development through transcriptional gene regulation. There are two complementary technical approaches. The first follows transcriptional changes affected by the mutation or loss of CECR2. QRT-PCR analysis facilitates directed inquiries, while microarray comparisons allow for data mining of new candidates. The second approach is a thorough investigation and characterization of the aberrant phenotypes associated with *Cecr2* mouse mutations. The associated defects may provide further insight into the developmental processes that require CECR2 remodeling. The focus is on what gene pathways or developmental processes CECR2 remodeling regulates. The discovery of *Cecr2* mutant inner ear defects presented in Dawe et al. (2011) suggests the planar cell polarity pathway may be targeted.

1.6.1: Does CECR2 regulate transcription of the planar cell polarity pathway during neural tube closure?

1.6.1.1: Overview of planar cell polarity

Dawe et al. (2011) speculated that CECR2 regulates the planar cell polarity (PCP) pathway during early development. This was based primarily on phenotypic similarities between *Cecr2*^{Gr45Bic} BALB/c mice and the characteristic defects associated with PCP mutations (Dawe et al., 2011; De Marco et al., 2006). Although open neural tubes, open eyelids, and stereocilia defects are present in both *Cecr2* and PCP mutations, phenotypic similarities on their own can not definitively identify CECR2 as a PCP regulator. As ISWI/BAZ remodelers are known to control gene transcription during development (Badenhorst et al., 2005; Barack et al., 2003; Deuring et al., 2000; Kitagawa et al., 2003; Landry et al., 2008; Song et al., 2009), I predict that CECR2 remodeling affects the transcription of PCP genes during neural tube closure.

The signaling and regulation of planar cell polarity processes is a complex network initiated through multiple cellular receptors including FRZD, CELSR1, VANGLs, and the FATs (Figure 3). The core proteins of the primary planar polarity signaling pathway involves FZD and VANGL2/CELSR1 transmembrane signaling through SCRIB, PRICKLE, INVERSIN, and DVL family members (De Marco et al., 2006). Occasionally, downstream effector proteins INTU, FUZ, and FRZB are included (Wallingford, 2006; Gray et al., 2009). The output of the pathway results in actin and cytoskeletal reorganization to reorient the primary cilia or other effector molecules to a particular pole. Some members of

the WNT family are included and the overall PCP pathway can be referred to as the noncanonical WNT signaling pathway. However, other than WNT5 and WNT11, the majority of WNTs have not been found to regulate planar polarity and convergent extension processes in vertebrates and they have not been found to participate in *Drosophila* PCP (Gordon and Nusse, 2006). The other pathway known to regulate general planar polarity of cells is through FAT, DACHS, and FJX (Matakatsu and Blair, 2004). Polarity is established through asymmetric assembly of surface complexes and sensed through cell-cell interactions (Matakatsu and Blair, 2004). The FAT/PCP pathway acts in parallel to the FZD/PCP pathway (Casal et al., 2006), but can be downstream of canonical WNT regulation (Matakatsu and Blair, 2004).

The mutations of various FZD/PCP components have been associated with NTDs in mice where the loss of convergent extension leads to craniorachischisis, spina bifida, and some cases of exencephaly (Kibar et al., 2001; Hamblet et al., 2002; Wang et al., 2002; Kibar et al., 2007; Qian et al., 2007). FZD/PCP mouse mutations have also been associated with misaligned stereocilia and cochlear defects (Kelly and Chen, 2007), polycystic kidney disorders (Fischer et al., 2006), and kinked or curly tails (Hamblet et al., 2002; Kibar et al., 2001). FAT/PCP signaling has not been associated with open neural tubes defects, but mutants can manifest developmental defects associated with other planar polarity or convergent extension processes, such as polycystic kidney disorder (Saburi et al., 2008).

1.6.1.2: Proposed research into the transcriptional regulation of planar cell polarity genes by CECR2

Microarray analyses of *Cecr2* homozygotes during neurulation will provide an indication of what transcriptional pathways or genes are misregulated due to a loss of CECR2. Expected changes may be involved in PCP-related processes, although other known genes or pathways involved in neural closure should also be considered. Potential candidates can be drawn from the over 240 genes known to cause neural tube defects when mutated in mice (Harris and Juriloff, 2010; Copp and Greene, 2009). Although current microarray chip technologies do not possess full coverage of all mouse genes, the microarray analysis can be complemented by qRT-PCR to test PCP and associated genes absent from the arrays.

1.6.2: Does CECR2 target clusters of genes within defined chromosomal regions?

1.6.2.1: Overview of BAZ-like chromosomal targeting

Landry et al. (2008) provide extensive microarray data of *Bptf*-dependent transcripts. The microarray data display a striking overrepresentation of upregulated homeobox transcription factors among the datasets; suggesting BPTF/NURF may regulate homeobox transcription factors during early development. The datasets (Landry et al., 2008) further suggest a clustering of targets within

discrete chromosomal locations. BPTF/NURF appear to affect the regulation of broad chromosomal regions and I interpret this to be the first functional insight of how ISWI complexes regulate chromosomal regions and the genes within. *Bptf* appears to regulate regional changes in transcription, and is not necessarily limited to single-gene targeted activation.

What Landry et al. (2008) did not address is how the broad chromosome regional effects related to specific regulation of their candidates such as the SMAD components. It has also not been established how BPTF recognizes targets or regions; whether it targets a specific sequence or a more transient histone modification. How such chromosomal regional effects might be defined, constrained, or propagated is not understood (Landry et al., 2008). If CECR2 were also found to affect broad, but discrete, chromosomal locations, then the trend would suggest an overall method by which BAZ-like/ISWI complexes affect transcription.

1.6.2.2: Proposed chromosomal enrichment research

It is not yet known specifically how ISWI complexes locate or act upon their DNA/histone targets. *Cecr2* disruption may cause regionalized expression changes in multiple genes clustered within chromosomal hotspots similar to the results of Landry et al. (2008) in *Bptf* BAZ-like mutations. Consistent with the predictions of He et al. (2008), I further hypothesize that the specific targeted locations will differ from those found by Landry et al. (2008).

The suggested microarray experiments will generate a dataset also applicable to testing the chromosomal enrichment hypothesis. Chi-Squared analysis can estimate an overabundance or scarcity of affected transcripts within each of the mouse chromosomes. The chromosomes can then be broken out into smaller units to test for localized regions of enrichment or scarcity. Expression changes of genes from within enriched regions should be tested by qRT-PCR to confirm the effect is biological and repeatable. Localized clusters can then be compared to those found by Landry et al. (2008) to look for sites of similarity.

1.6.3: Do *Cecr2* mutations produce additional subtle developmental defects?

1.6.3.1: *Cecr2* expression is seen in many non-neural tissues

CECR2 appears in a variety of mouse developmental stages (Figure 9). Banting et al. (2005) determined that the CECR2 fusion protein was expressed in many developing tissues beyond the neural tube, including the forming limbs, eyes, nasal epithelium, a strip of intercostal muscle, and mammary buds. These structures were not reported to show phenotypic defects at the time of the study. Further expression analysis of *Cecr2*^{Gr45Bic} homozygous and heterozygous embryos found expression in the neural tube and weaker expression in many mesenchymal embryonic tissues (Dawe et al., 2011). No expression was detected in the heart, coelomic structures, or extraembryonic membranes (Dawe et al., 2011). Following neural closure, the general embryonic expression changed to expression in a specific subset of developing tissues. The neural tube expression remained in

Theiler stages

Mouse

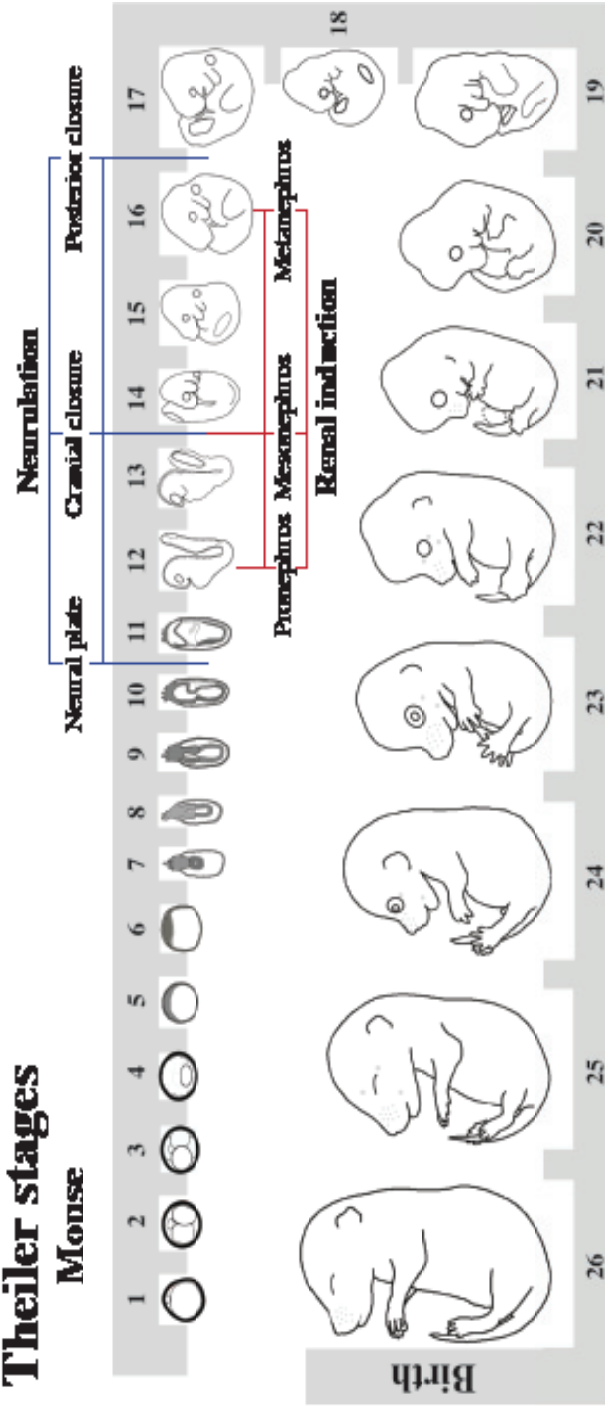


Figure 9:
Theiler stages of mouse development

Theiler staging separates mouse development into a numerical system based on the appearance of external morphological characteristics. Stage 1 starts with the one cell egg, and follows through to birth after stage 26. Neurulation spans stages 11-16. The neural plate appears in stage 11, and the neural ridges form and raise between stages 11 to 13. Stage 14 is defined by the first cranial closure site and fusion of the cranial neural tube. Closure proceeds through stage 15 and the posterior neuropore finishes by stage 16. During this time, renal induction is ongoing. The pronephros appears partway through stage 12, mesonephric tissue at the beginning of stage 14, and the ureteric bud invades the metanephric mesenchyme of the metanephric kidney partway through stage 16. Modified from EMAP eMouse Atlas Project (<http://www.emouseatlas.org>).

the spinal cord, forming brain, and telencephalon. From Theiler stage (TS) 15 to 23, the forming limbs displayed strong expression in the regions of chondrocyte condensation and tendon specification (Mann, personal communication 2009). From TS16 through to neonatal development, the CECR2 fusion protein is detected in the eye, including the forming optic cup, the lens nuclei, retina, and mesenchyme of the forming eyelid (Dawe, personal communication 2010; Niri, personal communication 2010). Prior to and continuing into TS24, there is staining in the nasal epithelium, mammary buds, intercostal muscle, dorsal ganglia, and within the skin follicles (Dawe, Mann, Niri, and McDermid, personal communications 2010). Staining was also found in the forming cochlear duct adjacent to the stereocilia of TS26 embryos (Dawe et al., 2011).

The extensive staining in regions not reported to show defects raises the question of whether subtle defects are present, but not yet found. Of particular interest is whether the *Cecr2* homozygous mutants manifest polycystic kidney disorders. Planar cell polarity defects are predicted to be affected by CECR2 remodeling during neurulation. CECR2 may further be necessary for PCP processes in the developing renal system as numerous PCP-associated defects are associated with cystic kidney disorders (Fischer et al., 2006; Saburi et al., 2008). Finding similar disorders would strengthen the association between CECR2 and planar cell polarity or convergent extension processes.

1.6.3.2: Overview of renal development

Kidney and urinary track abnormalities are common human birth defects (reviewed by Hahn, 2010; Nakanishi and Yoshikawa, 2003) and a growing number of mouse mutational models allow manipulation and identification of the molecular and developmental processes involved (reviewed by Pope et al., 1999; Susztak et al., 2008). Collectively termed congenital anomalies of the kidney and urinary track (CAKUT), these defects manifest as early as Wolffian duct development and can result in kidney agenesis, smaller or dysplastic kidneys, duplex kidneys, obstructed ureters and chronic renal failure in infants (Hahn, 2010; Nakanishi and Yoshikawa, 2003; Stahl et al., 2005). Polycystic kidney disorders typically arise from a failure of polarity and convergent extension processes, which leaves the kidney tubule too wide (Fischer et al., 2006; Saburi et al., 2008). These broad tubules are prone to forming cysts throughout the collection ducts as they are unable to withstand the pressure of filtration.

The nephrogenic cord arises during TS12-13 from the intermediate plate mesoderm, first forming a simplified pronephron transiently at the cranial end (Figure 10.A) (Dressler, 2006; Pohl et al., 2000). Intermediate mesenchyme differentiates into the intermediate mesonephric tubules by TS14-15 (Qiao et al., 1995), with functional primitive glomeruli actively filtering and processing amniotic fluids. The interplay between Wolffian duct and mesenchyme continues caudally as new regions of mesenchyme condense into the metanephric mesenchyme (MM), which by the end of TS15 induces Wolffian duct to form the ureteric bud (UB) (Majumdar et al., 2003). Subsequent invasion of the UB into the MM mass initiates tubule branching by TS19 and induces a coordinated

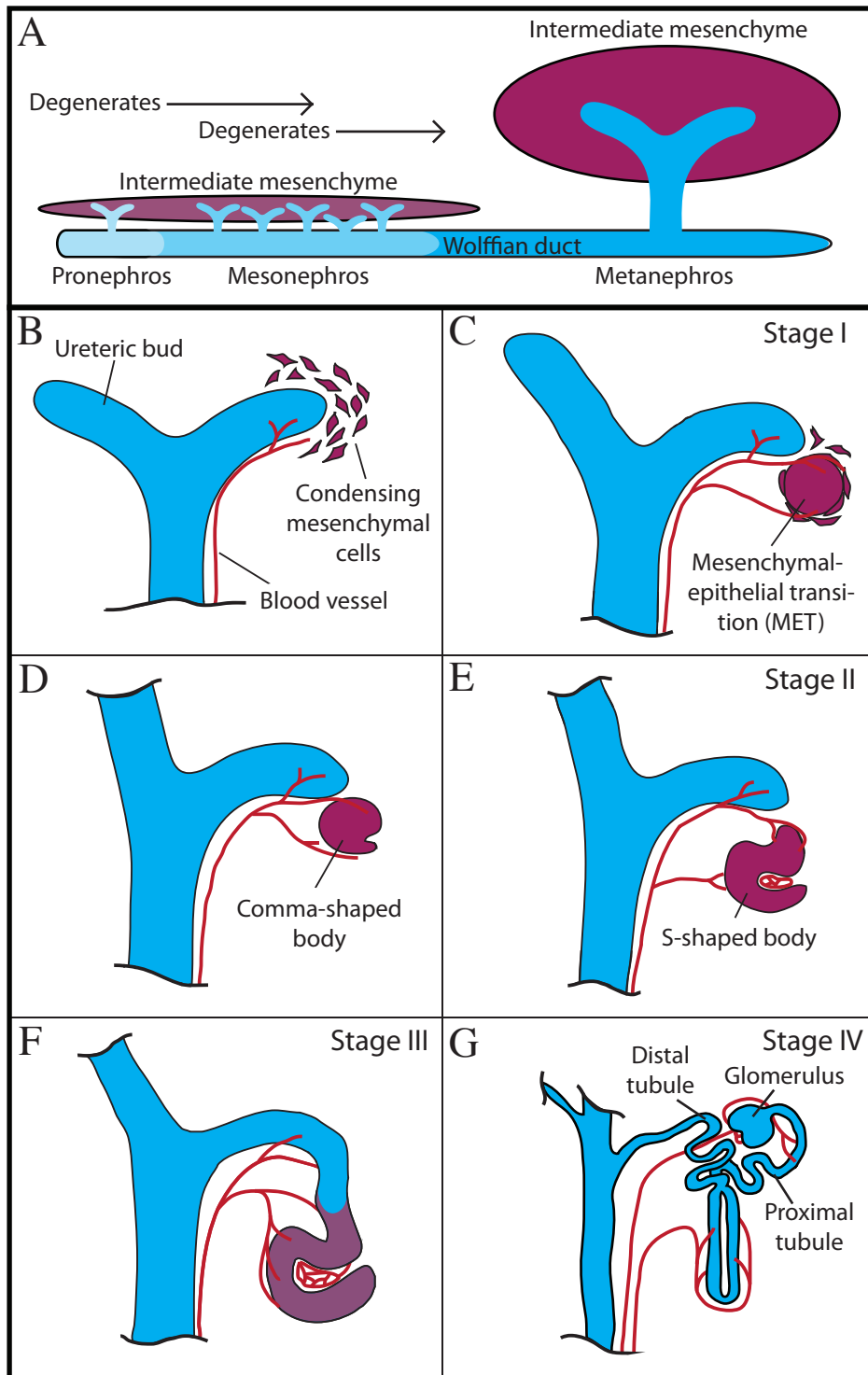


Figure 10:
Renal initiation and nephrogenesis

(A) The developing renal system in mice forms from three waves of nephrogenesis. A single pronephron forms at the proximal end of the forming Wolffian duct through a condensation and mesenchymal-epithelial transition of the intermediate mesenchyme in Theiler stage 12. The pronephros eventually degrades as the mesonephric ducts form caudally through the same intermediate mesenchyme to epithelium transitions by Theiler stage 13. The mesonephros also degrades as the metanephric kidney begins with the ureteric bud invading the metanephric mesenchyme by Theiler stage 15. (B-G) The metanephric mesenchyme condenses and forms into the early nephrons, which fuse to the ureteric bud collection tubes. The mesenchyme capping the leading branch aggregates into nephrogenic mesenchyme to initiate nephrogenesis (B). The nephrogenic mesenchyme undergoes a mesenchymal-epithelial transition (C) into a comma-shaped body as a Stage I nephron (D). Stage II nephrogenesis denotes the lengthening of the comma-shaped body into a S-shaped body of epithelial cells (E). The S-shaped body, derived from nephrogenic mesenchyme, fuses to the collecting duct, derived from the ureteric bud, to form the Stage III nephron (F). The mature Stage IV nephron grows and undergoes convergent extension processes to form the Loop of Henle as well as regionalized proximal and distal tubule sections (G). These structures integrate with the capillary system to form the functional filtration structure (glomerulus). The ureteric branches later mature into collecting ducts. Failures in planar polarity and convergent extension processes leave the ureteric collecting ducts and the nephron tubules too broad and short. Broad tubules are prone to forming cysts under the pressure of the urine. Modified from Hahn, (2010); Lipschutz, (1998); Wellik et al., (2002).

maturation of the two tissues. Interplay between the leading branches of the tubules and the condensing metanephric mesenchyme leads to the differentiation of early comma-shaped and later into S-shaped bodies from the metanephric mesenchyme at TS21. S-shaped bodies differentiate and integrate with podocytes and capillaries to form glomeruli, and undergo fusion to the ureteri bud branches that have matured into the collecting tubules. The early nephrogenic process follows a mesenchymal-epithelial transition (MET) (Plisov et al., 2000).

Metanephric-secreted GDNF and its ureteric bud receptor RET initiate the development of the kidney (Dressler, 2006; Pohl et al., 2000). RET and its co-receptor GFRA1 activates an intracellular cascade controlling bud growth and branching (Jain, 2009). The initial *Gdnf* signal can be influenced by a number of mesenchymal factors, either directly controlling *Gdnf* expression or affecting the positioning, differentiation, and state of the mesenchyme tissue. Such factors include transcription factor FOXC1 and SLIT2/ROBO2 signaling, which restrict expression of *Gdnf* (Grieshammer et al., 2004; Kume et al., 2000). Loss of *Foxc1/Slit2/Robo2* repression leads to an expansion of the nephrogenic mesenchyme inducing factors *Eya1* and *Gdnf* within the metanephric mesenchyme (Grieshammer et al., 2004; Kume et al., 2000). In turn, this leads to numerous *Ret*/UB induction sites that develop into additional ureters to form duplex or multiplex kidneys. Initiation and differentiation of the *Gdnf*/MM tissue has been found to rely on *Pax2*, *Eya1*, *Six1*, and the *Hox11* family where disruptions of these genes cause a loss of *Gdnf*/MM signaling and a failure to initiate *Ret*/UB branching (reviewed by Hahn, 2010; Lipschutz, 1998; Wellik et al., 2002). If no ureteric bud forms, not only do ureters fail to develop, but also the loss leads to complete agenesis of the metanephric kidney (Hahn, 2010).

Nephron development begins with mesenchymal aggregation and differentiation prompted by the invading ureteric branch (Figure 10.A). *Eya1*, *Cited2* and *Six2* mark a region of cap mesenchyme with *Gdnf* expression throughout the cap and nephrogenic interstitium. A loss of the UB results in no kidney being produced, while a reduction in the branching and invasion potential of the ureteric branches results in fewer regions of nephron development and ultimately reduced kidney mass (Hahn, 2010; Pope et al., 1999; Susztak et al., 2008).

Stage I nephron development begins as the pretubular mesenchymal aggregate undergoes a mesenchymal-epithelial transition (Figure 10.B-C) into the renal vesicle then marked by *Wnt4*, *Jag1*, *Bmp2*, and *Dkk1* expression (Hahn, 2010; Pope et al., 1999; Susztak et al., 2008). As the vesicle matures it elongates into a comma-shaped body (Figure 10.D) and later a S-shaped body, which signifies a stage II nephron (Figure 10.E). The S-shaped body continues to lengthen and differentiates into a *Wt1* expressing terminal capillary corpuscle at the tip of the proximal section as the distal portion of the tubule fuses into a continuous lumen with the ureteric tip (Figure 10.F). The intermediate stage III nephron further lengthens and integrates with the vasculature system to form the final stage IV nephron with all the structural morphology of a functioning nephron (Figure 10.G). Planar cell polarity defects manifest during Stage I-IV nephrons as

short, widened tubules bulged into cysts, as the tubule lengthening is dependent of convergent extension processes (Hahn, 2010; Pope et al., 1999; Susztak et al., 2008). Other PCP phenotypes include abnormal glomerular morphology or reduced glomeruli number (Hahn, 2010; Pope et al., 1999; Susztak et al., 2008).

The process of nephron development repeats in expansive waves as the ureteric tips continue to branch into the outer nephrogenic interstitium. Following distal tubule fusion, the epithelial lumen of the ureteric branches matures into the collecting ducts. The renal pelvis and ureter form out of the expanded ureteric duct, both surrounded by smooth muscle marked by *Tshz3* expression (Caubit et al., 2008; Jenkins et al., 2010). Ureter defects, such as those caused by the mutation of *Tshz3*, include swelling of the ureter (hydroureter) or destructive swelling of the renal pelvis (hydronephrosis) (Caubit et al., 2008; Jenkins et al., 2010). Surrounding and supporting the collecting ducts and Loops of Henle are the stromal cells of the cortical and medullar interstitium marked by *Tcf21*, and *Alx1* expression (Hatini et al., 1996; Mendelsohn et al., 1999). Stromal cell abnormalities result in smaller kidneys with less branching as the stromal cells both physically support renal development as well as coordinate development through numerous secreted growth factors (Hatini et al., 1996; Mendelsohn et al., 1999). Arterial and venous vasculature is interspersed throughout the renal tissue. Blood vessels are identified histologically by morphology or by the presence of red blood cells, if present, and vascular markers such as *Pecam1*.

1.6.3.3: Proposed phenotypic characterization and research

There are many structures expressing *Cecr2* that may have subtle defects in the mutants. As this approach is exploratory in nature, I will present an extensive phenotypic characterization of *Cecr2* mutations from the early embryo through to adulthood on both the FVB/N and BALB/c strains. This project generates and characterizes a novel *Cecr2^{tm1.1Hemc}* deletion allele in addition to the original *Cecr2^{Gt45Bic}* gene-trap allele generated by Banting et al. (2005). I hypothesize that the deletion allele will show an increased penetrance of neural tube defects, and that either allele will harbour additional subtle defects. This assessment is based in part upon the nature of the gene-trap mutation, which is thought to retain some CECR2 function. The phenotypic characterization of the *Cecr2* mutation presented by Banting et al. (2005) was limited to discovering the source of embryonic lethality and did not analyze the effects on later stages of development or adulthood.

This thesis work will cover the discovery and characterization of a variety of additional *Cecr2* homozygous phenotypes. Additional consideration is given to a set of congenital abnormalities of the kidney and urinary tract in *Cecr2^{Gt45Bic}* and *Cecr2^{tm1.1Hemc}* homozygous embryos in the FVB/N strain background. I will determine whether these defects are PCP-like defects. As part of that characterization, expression analysis and phenotypic assessments establish where CECR2 is present throughout nephrogenesis. Key marker genes necessary for mesonephric and metanephric development are to be probed by *in situ* hybridization to assay for shifts in a variety of regulators.

1.7: Summary

The study of CECR2 chromatin remodeling sits at an intriguing crossroads between the fields of early developmental regulation, organogenesis and cellular differentiation, and the field of histone modification regulation. Histone remodelling is thought to add another layer of complexity to the regulation and control of developmental processes. The prominent hypothesis of the field is that the alteration of histone position and composition by ATPase chromatin remodelling results in changing the accessibility of transcriptional machinery, ultimately changing gene expression (Barack et al., 2003; He et al., 2008; Landry et al., 2008; Song et al., 2009). Due to the complexity of the system, this hypothesis has yet to be confirmed with a transcriptional reporter assay.

The CERF complex, composed of CECR2 and SNF2L or SNF2H, is the most recent addition to the family of ISWI histone remodelling proteins (Banting et al., 2005; Thompson et al., 2012). Mice carrying mutations in any of the CERF components show a range of developmental defects (Stopka and Skoultschi, 2003; Banting et al., 2005; Yip et al., 2012), although it is the CECR2 subunit that is predicted to be the key determinant for target selection (He et al., 2008). CECR2 activity is necessary for proper neural closure, and shows expression throughout a number of developing organs (Banting et al., 2005). The field has not identified precisely how the *Cecr2*, *Snf2l* or *Snf2h* mutations result in such mutations; however, studies thus far appear consistent with the hypothesis that these genes work together to regulate the expression of developmentally regulated genes (Lazzaro and Picketts, 2001; Stopka and Skoultschi, 2003; Yip et al., 2012).

The primary goal of the presented work is to establish what pathways or processes CECR2 regulates during primary neurulation. The work begins with the question of whether CECR2 is influencing the regulation of the planar cell polarity pathway, but will also explore alternate processes involved in neurulation. The developmental and transcriptional consequences of CECR2 loss is further characterized in a new mouse germline deletion mutation of *Cecr2* in addition to the gene-trap allele (Banting et al., 2005). Microarray analyses of embryos undergoing neurulation provide a broad assessment of what transcriptional changes result from *Cecr2* mutation. Directed qRT-PCR of transcriptional changes will confirm whether it is PCP-like misregulation that may result in the manifestation of neural tube defects in *Cecr2* mice, or generate new candidates to explore. The microarray databases further allow for the assessment of whether CECR2 appears to target or affect clustered regions in a manner similar to another reported BAZ-like protein. Indications of targeting may suggest a common mechanism for BAZ-like remodeling and the resulting transcriptional changes. Phenotypic assessment of the mutants complements the molecular data through the identification and characterization of the processes defective in *Cecr2* homozygous embryos. The following work will establish whether *Cecr2* mutation results in the transcriptional misregulation of key developmental genes during neurulation.

2: Materials and methods

2.1: Generation and genotyping of *Cecr2* mutant mice

The novel *Cecr2*^{tm1.1Hemc} allele was generated through LoxP-Cre deletion of exon 1. LoxP sites were engineered flanking exon 1, including 1 kbp upstream (InGenious Targeting Laboratory). The region contained both the ATG start codon, half of the DDT domain predicted to bind to Snf2l, and possible regulatory elements. Chimeric animals heterozygous for the altered *Cecr2* exon 1 (iTL BA1 (C57BL/6 x 129/SvEv)) were obtained and bred to BALB/c-Tg(CMV-cre)1Cgn/J mice (Jackson Laboratories) in order to obtain germline deletion of *Cecr2* exon 1. The deletion was distinguished from both LoxP-flanked or wildtype *Cecr2* through a multiplex PCR genotype reaction with primers InGeniousLox1 (TTAGAATAGGTGAGGGAGGAG), InGeniousSDL2 (GTAGCGCCTATTTGTATTGGTCA), and CECR2_DEL3R (AATGGTGGCGAAATCAACTC). Genotyping to confirm the loss of Cre after deletion used primers CREIMR0042 (CTAGGCCACAGAATTGAAAGATCT), CREIMR0043 (GTAGGTGGAAATTCTAGCATCATCC), CREIMR0567 (ACCAGCCAGCTATCAACTCG), and CREIMR0568 (TTACATTGGTCCAGCCACC). Cre was confirmed to be lost in the breeder lines after the first backcross. QRT-PCR samples were collected from heterozygous crosses between the fourth and fifth generation onto BALB/c. *Cecr2*^{tm1.1Hemc} heterozygous mice were crossed onto an FVB/N background. The heterozygotes were crossed and analyzed after three FVB/N backcrosses.

Cecr2^{Gt45Bic} FVB/N adults were housed and bred as a homozygous line with separate wildtype FVB/N breeding pairs generating control embryos. The *Cecr2*^{tm1.1Hemc} FVB/N, *Cecr2*^{tm1.1Hemc} BALB/c, and *Cecr2*^{Gt45Bic} BALB/c lines were all housed separately as heterozygous lines due to neonatal lethality. Most experiments relied on heterozygous crosses for the generation of homozygous mutant embryos. In rare cases, a fertile homozygous *Cecr2*^{Gt45Bic} BALB/c male was used in plug testing for embryo collection.

Mice were housed under a daily cycle of 14-hour light/10-hour dark and fed Laboratory Rodent Diet 5001 (LabDiet). Breeders were fed Mouse Diet 9F 5020 (LabDiet) to provide higher fat content. The Animal Care and Use Committee of the University of Alberta approved the breeding and use of the various mouse lines.

2.2: Necropsy and organ collection

Adult animals were euthanized by CO₂ asphyxiation, while mice younger than 3 weeks were subjected to cervical dislocation according to the Canadian Council of Animal Care standard operating procedures. Organ weight datasets were collected from samples immediately following dissection without fixation. Tissues collected for other uses were washed in PBS followed by fixation. Adult samples used in histology or other procedures were fixed in 10% formalin overnight, or up to one week depending on sample size. Samples needing long-term storage were kept in ethanol or methanol at -20 degrees.

2.3: Micro-CT rendering

Whole mice were fixed in Bouin's fixative for up to one week and incrementally washed in a series until stored in 100% ethanol. The skeletal structures were serially X-rayed in a Skyscan 1076 at 35 μ m resolution. Computer tomography rendered the X-rays into a 3D skeletal model using programs CTAn, CTVol, CTVox, and DataViewer (Skyscan). The rendered models were visually inspected for craniofacial or skeletal defects.

2.4: Ovary cyst analysis

One of the samples was sent to Dr. Nation, University of Alberta veterinary pathologist, for the determination of pathology and detailed morphological analysis. Dr. Nation generated the hematoxylin and eosin stained sections. Samples were also sent to Dr. Russell, University of Alberta pathologist, for analysis of the potentially cancerous cells found during pathological analysis. Dr. Russell treated sections with anti-Cam5, Inhibin, and the Periodic acid-Schiff stain.

2.5: Urine and blood analysis

Urine from homozygous *Cecr2*^{tmem1.1Hemc} FVB/N and wildtype FVB/N animals was collected passively through restraint. Samples were collected daily for one week and tested within 20 minutes of collection on Chemstrip GP ten-patch dipsticks (Roche). Assessment followed manufacturers' protocols and provided colour standards.

Blood from homozygous *Cecr2*^{tmem1.1Hemc} FVB/N and wildtype FVB/N animals was obtained through cardiac puncture immediately following CO₂ euthanization. Coagulation was allowed to occur for 20 minutes at room temperature, followed by centrifugation at 6800 rcf (8000 rpm) for 10 minutes and the serum collected. Serum was then packaged on ice and shipped to Idexx Laboratories Edmonton for same-day processing on a VetTest chemical analyzer renal panel.

2.6: Embryo collection

All TS12-TS23 embryos were dissected in PBS (or DEPC-treated PBS) on ice. Embryos were further characterized under dissection microscopes to determine somite numbers and Theiler stage of the sample. Samples for use in histology or *in situ* hybridization were fixed in 4% paraformaldehyde for 3 hours. Samples for RNA collection were flash frozen immediately and stored at -80°C.

Embryos of TS24 and older for histology and morphological assessments were bisected and fixed in 10% neutral buffered formalin for one day, at which time kidneys were separated and re-fixed for a further 24 hours. TS24 kidneys used for *in situ* or qRT-PCR analysis were not fixed, and immediately flash frozen to -80 degrees. Adult tissue collection was followed by fixation in either Bouin's fixative or 10% neutral buffered formalin for over 24 hours.

Samples for *Cecr2*^{Gt45Bic} expression analyses were not fixed prior to staining. The *Cecr2*^{Gt45Bic} gene product was detected by X-gal staining of the

gene-trap as previously described (Banting et al., 2005). Expression samples to be sectioned were fixed and stored in methanol.

2.7: Embedding and histology

Samples were stored in ethanol or methanol at -20°C prior to vacuum processing into paraffin by the Advanced Microscopy Facility, University of Alberta. Blocks were cut to sections by microtome to between 5-8 µm. Sections were stained with hematoxylin, eosin, or methyl green for general histology.

2.8: Stereociliary analyses

Stereocilia assessment followed the procedures of Montcouquiol et al. (2003) with few deviations. Confocal microscopy was used to image the stereocilia at the basal (5%), middle (50%), and apical (75%) regions of the cochlea. A minimum of ten cells were assessed for each hair cell row. The orientation of stereocilia was determined against the plane parallel to basal membrane and cell rows. Cells rotated more than 30 degrees away from the mediolateral axis were considered misaligned. Chi-squared tests of independence were conducted, using a Bonferroni adjustment for multiple dataset analyses.

2.9: RNA extraction for quantification

The *Cecr2*^{Gt45Bic} microarray analyses were presented in Fairbridge et al. (2010). *Cecr2*^{Gt45Bic} embryos were collected whole and processed through the Lipid RNA Extraction Kit (Qiagen). RNA was extracted according to manufacturer's protocol and eluted into 30 µl of DEPC-treated water. RNA was tested on a Nanodrop Spectrophotometer and quality assessment on an Agilent 2100 Bioanalyzer RNA 6000 Nano and Pico chips (RIN over 8). Superscript III VILO cDNA synthesis kit (Invitrogen) was used to generate cDNA.

Cecr2^{Gt45Bic} embryos for microarray and qRT-PCR experiments were collected within a range of 11-14 somites just prior to wildtype cranial neural tube fusion (TS14). All embryos selected for microarrays were female. Genotyping of embryos was done on extraembryonic membranes separated at the time of collection.

Cecr2^{tm1.1Hemc} exon 1-deletion embryos and wildtype controls were bisected between the first and second branchial arch prior to RNA extraction. An older stage of 18-20 somites was collected in addition to the 10-14 somite ranges. Samples were processed through the Lipid RNA Extraction Kit (Qiagen). The Superscript III VILO cDNA synthesis kit (Invitrogen) used 275 ng of RNA to generate cDNA for qRT-PCR experiments using the *Cecr2*^{tm1.1Hemc} deletion line. For all experiments, RNA concentrations were obtained via Nanodrop Spectrophotometer prior to quality assessment on Agilent 2100 Bioanalyzer RNA 6000 Nano and Pico chips (RIN over 8).

2.10: Gene expression profiling: microarray

For cDNA synthesis, 1 µg of RNA was used per sample. The Center of Applied Genomics (Hospital for Sick Children, Toronto) performed the

chip hybridizations on Affymetrix Genechip Mouse Genome 430 2.0 Arrays according to the manufacturer's protocol. Datasets were normalized using R-statistical package R/gcRMA, dCHIP, and Arraystar 4.0 (King Jones, personal communications 2011). Having access to three means of assessing the data, each with differing methodology and assumptions, and each from two separate strain experiments, allowed for inter-comparison and generation of a highly stringent short-list of candidates. The Arraystar 4 program considers the relative intensity (amount) of the transcripts and may overlook low abundance transcripts. The gcRMA program overestimates low-abundant transcripts and generally overestimates fold-change values. The dCHIP program calculates probe intensity based on the 10 probe matches and is the only program to also consider the mismatch probe, which may better account for non-specific signal. To identify genes of interest, we filtered for significant changes ($p < 0.05$) under all analyses, and then ranked candidates by both fold-change and gene function.

Gene ontology analysis was conducted with the online GOEAST Affymetrix GeneChip® platform (Zheng and Wang, 2008). The analysis used hypergeometric sampling statistics and controlled false discovery through the use of the Yekutieli process for FDR under dependency. The resulting lists were formatted number of genes found with enriched GO terms, the total possible genes tagged with a given term within the array, the log odds-ratio, and the associated p-value. Gene ontology terms were ranked by odds-ratio and only those with $p < 0.05$ were considered. The shortlist candidate input data were separated into genes downregulated by the disruption of *Cecr2*, those upregulated, and those showing opposing strain/*Cecr2* effects.

2.11: Gene expression profiling: quantitative real-time PCR

Validation of microarray data was performed on cDNA samples from *Cecr2^{tm1.1Hemc}* heads. Amplicons were designed within, or just upstream of the Affymetrix Mouse MOE 430 2.0 target sequences for each gene of interest. Primers and universal probe hexamer were designed on the Roche ProbeFinder Version: 2.45. Probes were obtained from the Roche Universal Probe Library set. Reactions were performed on the Fluidigm Biomark 48.48 Access Array Integrated Fluidic Circuit, according to manufacturer's protocols. A pre-amplification step with all pooled primers was carried out with the TaqMan PreAmp Master Mix (Applied Biosystems). Quadruplicate technical replicates were run for each of the 4 biological replicates. An internal five-point standard dilution curve was run for each probeset. Fold change was calculated by the Pfaffle (2001) method taking PCR efficiency into consideration. PCR efficiency was derived from the five-point internal standard curve and used in the following equation:

$$Fc = (\text{TargetEfficiency}^{(wtCT - mutCT)}) / (\text{ReferenceEfficiency}^{(wtCT - mutCT)})$$

Target gene expression levels were normalized to reference genes *Tbp*, *Rps12*, *Ube3a*, *Gla*, *Elmo2* and the geometric averages of all fold change

equations were taken in accordance with Vandesompele et al. (2002). Reference genes were selected based upon previously reported use and having shown no change in any of the microarray analyses. TTESTs were performed on the delta-Ct datasets comparing the target gene delta-Ct values to reference genes. *Tbp*, *Rps12*, *Ube3a*, *Gla*, and *Elmo2* TTESTS did not significantly differ between any combination of reference genes, and so all were pooled into a single TTEST reference set to be tested against the candidate genes.

2.12: *In situ* hybridization

In situ hybridization procedures followed a modified protocol provided by Chang (personal communication 2009) using Blocking Reagent (Roche) during antibody steps to reduce background. Probes were generated through PCR amplification from embryonic TS13-14 or kidney TS23-24 cDNA. A 2-step PCR with a nested T7 initiation site primer preceded DIG labeled RNA synthesis using T7 RNA polymerase (Roche) and the DIG RNA labeling mix (Roche). Probe primer sequences are listed in Appendix 3. Alkaline phosphatase-linked anti-DIG FAB fragment (sheep, Roche) and NBT/BCIP stock solution (Roche) was used for staining.

2.13: Apoptosis TUNEL analysis

Apoptosis analyses were performed on tissue slides prepared using the *in situ* hybridization procedure and stained using the DeadEnd Colourimetric TUNEL System (Promega). The tests were performed on slides of tissue sections to 8-10 μ m. Positive controls were incubated with DNase 1 endonuclease to artificially create double-strand DNA breaks. The negative control samples underwent all procedure steps, without the critical end-labeling enzyme.

2.14 Statistical significance

There were a variety of statistical tests used throughout the presented work. Common tests included T-tests, U-tests, chi-squared analyses. The unique statistical methods of the microarray and qRT-PCR were presented in their own sections. Significance was set to $p < 0.05$ in nearly all cases. Where Bonferroni adjusted p-values applied, the significance cut-off began with $p < 0.05$ and was then adjusted depending on the number of tests within the same dataset.

3: Results

The presented work focuses on the developmental function of chromatin remodeling subunit CECR2 as interpreted by the mutation of *Cecr2* in mice and characterization of the associated abnormal phenotypes. I proposed that the original *Cecr2* gene-trap mutation affected the organogenesis of multiple systems beyond the reported neural tube defects (Banting et al., 2005). I further hypothesized that the gene-trap mutation was not a functional null, and that the generation of an independent exon 1 deletion mutation would provide a more thorough account of *Cecr2*-reliant phenotypes. The reasoning for such extensive characterization of the mouse mutants was the hypothesis that there may be shared traits affected in multiple *Cecr2*-associated phenotypes. If a common cell lineage or developmental process could be identified, directed studies would be followed to confirm whether CECR2 regulated or was necessary for that particular pathway.

A caveat of this approach was that the normal function of CECR2 at a molecular level remains largely unknown. CECR2 was identified as a chromatin remodeling protein (Banting et al., 2005), but our understanding of its role in development remained limited to the abnormal phenotypic effects of *Cecr2* mutations. Compensation by related remodeling processes could be masking some of its roles. Subtle or low penetrant defects may have been overlooked. I had further assumed that CECR2 acts, at least in part, to regulate gene transcription through its remodeling activity. The microarray and qRT-PCR studies presented herein tested the hypothesis that there would be misregulation of neurulation-related genes in *Cecr2* mutants during neural closure. Additional qRT-PCR and *in situ* hybridizations were conducted in developing renal tissue to confirm whether the same transcripts misregulated during neurulation were misregulated in other *Cecr2*-expressing tissues. The idea driving these experiments was that there may be a set of regions or specific gene targets for CECR2 remodeling consistent throughout development. Whether CECR2 directly acts as a regulator of transcription remained unresolved.

3.1: Generation of the *Cecr2^{tm1.1Hemc}* allele

Banting et al. (2005) first described the *Cecr2^{Gt45Bic}* mutant mouse line, produced by a B-geo gene-trap vector partially interrupting *Cecr2* splicing between exons 7 and 8. A congenic BALB/c line was established with over 10 backcrosses. The mutation remained useful for many of the studies presented throughout the following experiments, but I predicted that a deletion mutation would better serve to identify which developmental processes were disrupted by a full loss of CECR2 function.

The *Cecr2^{tm1.1Hemc}* allele presented here was generated through LoxP-Cre deletion of *Cecr2* exon 1. The selected genomic region contains exon 1 with the start codon, half of the DDT domain predicted to bind to SNF2L, and possible promoter elements (Figure 11). The initial LoxP non-deleted line was crossed onto the neural tube defect susceptible background BALB/c (Davidson et al., 2007). Early crosses onto the BALB/c backcross produced the expected

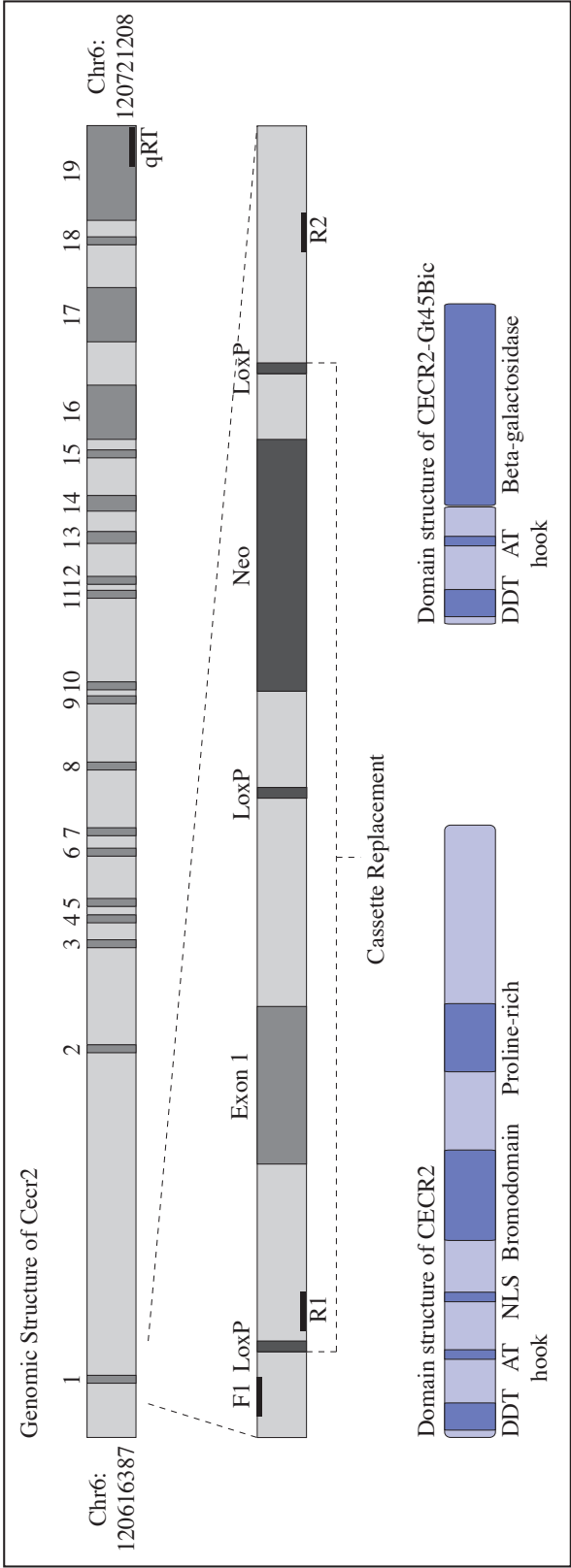


Figure 11:

Diagram of *Cecr2*^{tm1Hemc} conditional deletion gene structure and genotyping

Mouse *Cecr2* is comprised of 19 exons spanning roughly 100 kbp of chromosome 6F1. The *Cecr2*^{tm1Hemc} conditional deletion cassette was engineered by inGenious Targeting Laboratory through the replacement of *Cecr2* exon 1 with a LoxP flanked version of the exon as well as a *Neo* selectable marker. The genotyping primers indicated were used to distinguish the presence of the 5' Lox insertion from wildtype unmodified *Cecr2*, and a second reverse primer flanking the 3' Lox site detected the *Cecr2*^{tm1.1Hemc} deletion between the first and third Lox site following CRE-mediated deletion (primers F1= inGeniousLox1, R1= inGeniousSDL2, R2=CECR2_DEL3R, qRT=region identified by microarray and qRT-PCR studies, NLS=nuclear localization signal).

frequency of heterozygous *Cecr2^{tm1.Hemc}* pups and the adult heterozygous animals did not manifest abnormal phenotype or lethality. The *Cecr2^{tm1.Hemc}* LoxP cassette originated in four separate founding iTL BA1 embryonic stem cell lines. Each was bred to BALB/c-Tg(CMV-cre)1Cgn/J and four *Cecr2^{tm1.Hemc}* deletion lines were initially created. The mice of each line were designated DEL1 through DEL4 of *Cecr2^{tm1.Hemc}*.

Confirmation of the deletion involved a number of tests. Genomic PCR and sequencing confirmed the full deletion of the LoxP cassette and subsequent loss of exon 1. *Cecr2^{tm1.Hemc}* BALB/c cDNA was generated from embryonic RNA through random hexamer, polyT, and *Cecr2*-specific reverse transcription primers. RT-PCR failed to produce a band from exon 1 primers as expected of the deletion. However, RT-PCR bands specific to *Cecr2* could still be obtained from exon 2 through exon 18 (Niri, personal communication, 2011). This suggested an alternate start site for transcription must exist for *Cecr2*. Extensive database mining for ESTs failed to identify a potential secondary start site, as did a 5' RACE from exon 2 primers (Niri, personal communication, 2011). Other students have taken on the alternative RNA project, but no definitive conclusions have been reached. Without exon 1, or an identifiable alternate exon 1, the transcript lacks an the normal start site and the DDT domain. The next few available translational start sites are out of frame. The remaining sequence is not predicted to produce a functional protein. Preliminary evidence from a new CECR2 antibody undergoing characterization finds no CECR2 detectable by Western Blot in the *Cecr2^{tm1.Hemc}* homozygotes (Farshad Niri, personal communications, 2012), suggesting the alternative transcript is not translated.

To quantify the reduction in full-length *Cecr2* expression, qRT-PCR analysis of *Cecr2* indicated a 259±4-fold reduction ($p=7.38E-52$) in the *Cecr2^{tm1.Hemc}* BALB/c homozygotes. By comparison, the *Cecr2^{Gt45Bic}* BALB/c mutation full-length transcription was only reduced 6.4±0.2-fold ($p=2.1E-14$). These tests used the exon 19 primers and universal probe set for full length *Cecr2*. Thus, the exon 1 deletion greatly reduced the transcription of the full-length *Cecr2* transcript. The generation of the additional mutant allele allowed for further examination of *Cecr2*-related phenotypes with an additional genetic resource and the ability to confirm findings on two independent mutations.

3.2: Testing whether a disruption of *Cecr2* influences transcript expression during cranial neural closure

As a chromatin remodeler working with the ISWI family, CECR2 regulates chromatin state and may affect transcription in target regions. CECR2 was proposed to affect neural tube closure through the misregulation of target genes necessary for neural closure. Whether CECR2 is in fact a transcriptional regulator remains unresolved. However, there are a number of consistently misregulated genes associated with the *Cecr2* mutations during neurulation. Initially, the effected genes were predicted to include members of the planar cell polarity pathway and were tested by microarray and qRT-PCR analyses.

3.2.1: *Cecr2*^{Gt34Bic} BALB/c and *Cecr2*^{Gt34Bic} FVB/N microarray analyses found a set of generally low fold-change, but significant, candidate transcripts

Although *Cecr2*^{Gt45Bic} BALB/c homozygous pups show a high incidence of exencephaly while *Cecr2*^{Gt45Bic} FVB/N homozygotes do not, I hypothesized that the base molecular function of CECR2 would be conserved between strains. The function of CECR2 may be to act as a regulator of transcription. Although this assumption was consistent with the known roles of some ISWI proteins and complexes and the comparable BPTF protein (Landery et al., 2008), this roles had not been confirmed for CERF complexes. If correct, then gene expression changes should be detectable by microarray or qRT-PCR as relative changes in the expression levels of affected targets. Changes specific to the *Cecr2*^{Gt45Bic} BALB/c array may be expected to show larger fold-changes in NTD-associated genes, but these changes could be due to secondary effects resulting from the failure of the neural tube to close. The subsequent discoveries of *Cecr2*^{Gt45Bic} FVB/N homozygotes showing neural closure delay and that *Cecr2*^{tm1.1Hemc} FVB/N homozygotes develop exencephaly both support the assumption that the targeting and base function of CECR2 may be conserved between strains. Transcripts affected by *Cecr2* disruption in both strain arrays would represent the most significant target candidates under this assumption. Within the following analyses, the term upregulated refers to those transcripts whose relative expression increased when *Cecr2* was disrupted, while downregulated refers to transcripts whose relative expression was lower when *Cecr2* was disrupted.

Four biological replicates per homozygous genotype (FVB/N, BALB/c, *Cecr2*^{Gt45Bic} FVB/N, *Cecr2*^{Gt45Bic} BALB/c) were selected. Each sample represented an individual 11-14 somite female embryo whose development just preceded TS14 cranial closure. Analyses by gcRMA, dCHIP, and Arraystar 4.0 of Affymetrix mouse 420 2.0 *Cecr2*^{Gt45Bic} BALB/c homozygous versus BALB/c datasets found 418 downregulated and 109 upregulated transcripts (Appendix 2). Only 14 of the downregulated transcripts show over a 1.5-fold change under all analyses, and only 4 of those are over 2-fold. Within the 109 upregulated transcripts, 7 were over 1.5-fold and only 1 was over 2-fold. The microarray data indicated that the *Cecr2*^{Gt45Bic} BALB/c allele reduced the full length *Cecr2* transcript levels by only -8.1 to -8.5 times compared to wildtype levels. An -8.5-fold change indicates that up to ~12% of wildtype transcript remains in the *Cecr2*^{Gt45Bic} allele. Heterozygous animals show very low penetrance of defect or an intermediate phenotypic severity (Banting et al., 2005; Dawe et al., 2011). The heterozygous phenotypes suggest *Cecr2* is dosage sensitive. The analysis of Affymetrix 430 2.0 MOE microarray data of the *Cecr2*^{Gt45Bic} FVB/N homozygous mutation followed the same criteria presented above. The entire list of affected transcripts can be found in Appendix 3. The FVB/N array provided nearly double the number of affected transcripts with 730 showing a lower expression and 331 overexpressed in *Cecr2*^{Gt45Bic} FVB/N mutants compared to wildtype FVB/N animals ($p < 0.05$). In the downregulated group, 113 transcripts possessed over a 1.5-fold change, with 18 showing over a 2-fold effect. There were 83 overexpressed transcripts over the 1.5-fold mark and 6 over 2-fold.

The overall profile of transcriptional changes offered insight into how CECR2 remodeling complexes worked upon the chromatin in a very general sense. The vast majority of transcripts were downregulated during the disruption of *Cecr2*. Within the highest stringency lists, 76% of affected transcripts were lower in *Cecr2*^{Gt45Bic} embryos. Only 13% were upregulated in *Cecr2* mutants. There were 11% which showed opposing strain effects where the same mutation of different strains each caused significant expression changes in a transcript, but in one strain showed upregulation of the transcript while the other indicated a reduction. Similar ratios were reached when looking at *Cecr2*^{Gt45Bic} BALB/c to BALB/c or *Cecr2*^{Gt45Bic} FVB/N to FVB/N in isolation, where either shows ~75% of affected transcripts were downregulated. This trend suggested CECR2 activity was an activator, or that any indirect effects were predominantly through a loss of activation.

Although the *Cecr2*^{Gt45Bic} BALB/c embryos developed exencephaly while the *Cecr2*^{Gt45Bic} FVB/N did not, a specific model to explain the phenotypic difference was not available (Kooistra et al., 2011). Prior to the development of the *Cecr2*^{Gt45Bic} arrays, there was no evidence as to whether CECR2 targeted different genes depending in the background strain. Although *Epha7* was identified as a neural tube causing candidate specifically in the *Cecr2*^{Gt45Bic} BALB/c array (Appendix 2 and 3), many of the highest ranked candidates appeared affected on both strains.

Common to both *Cecr2*^{Gt45Bic} comparisons were 54 significantly changed transcripts (Table 1), representing 48 genes. Of these, 36 were downregulated on the mutant strains, 6 overexpressed on the mutant strains and 6 showed opposing effects on the datasets by strain. Those common to both arrays represented changes most likely to be direct functions of CECR2 activity, as the core function of CECR2 would very likely be conserved between strains. Dawe et al. (2010) confirmed a neural closure delay existed in *Cecr2*^{Gt45Bic} FVB/N mutants, which suggested the same initial neural closure defect was the same in both strains, but that FVB/N somehow overcame the wider distance between neural ridges.

Gene ontology analysis of the 48 unique genes to make the shortlist of candidates suggested a variety of processes are overrepresented within the dataset (Table 2). The GOEAST analysis was split into transcripts downregulated during the disruption of *Cecr2* (Table 2.A), those upregulated (Table 2.B), and those showing opposing strain effects (Table 2.C). Three quarters of all transcripts were downregulated in the *Cecr2*^{Gt45Bic} mutant microarrays. Half of the downregulated transcripts (n=19/36) were involved in developmental processes, with skeletal system development (n=3/36), ear morphogenesis (n=5/36), vascular development (n=5/36), gland development (n=5/36) and palate development (n=3/36) among the organ systems associated with downregulated gene candidates. Tissue development was associated with 16 of the 36 downregulated genes. Within this group, genes involved with epithelium development (n=13/36) and differentiation (n=7/36) were enriched, as was mesenchymal cell development (n=3/36) and tube morphogenesis (n=7/36). Neurogenesis (n=9/36) and axogenesis (n=5/36) associated genes were also enriched. Another common theme was the regulation

Table 1: Significant transcripts shared between strains as predicted by the microarrays														
PROBE ID		Gene	Cecr2 ^{G45Bic} FVB/N vs FVB/N						Cecr2 ^{G45Bic} BALB/c vs BALB/c					
			gcRMA		Arraystar 4		dCHIP		gcRMA		Arraystar 4		dCHIP BALB	
			Fold	p-value	Fold	p-value	Fold	p-value	Fold	p-value	Fold	p-value	Fold	p-value
1431014_at		Cecr2	-13.32	1.58E-05	-7.77	2.87E-05	-7.21	4.00E-06	-11.35	8.63E-09	-5.23	4.03E-04	-7.7	3.00E-06
1457039_at		Cecr2	-12.73	1.00E-08	-4.01	1.34E-06	-4.54	1.00E-06	-14.52	5.27E-08	-5.14	1.33E-06	-5.8	3.00E-06
1419735_at		Csn3	-3.31	4.04E-04	-1.76	2.45E-04	-1.64	7.74E-03	-3.01	1.43E-05	-2.14	3.44E-05	-1.8	7.21E-04
1445503_at		Gm715	-2.16	1.55E-02	-1.69	1.64E-02	-1.56	1.83E-02	-1.75	1.26E-03	-1.48	3.13E-03	-1.4	2.30E-02
1439972_at		Etnk1	-1.96	2.78E-02	-1.63	6.18E-03	-1.77	9.57E-03	1.63	1.60E-02	1.43	4.45E-02	1.58	4.93E-02
1437633_at		Ankrd11	-1.92	1.56E-02	-1.63	2.50E-02	-1.65	3.07E-02	1.47	1.58E-02	1.30	2.02E-02	1.33	2.82E-02
1435022_at		Alx1	-1.91	1.05E-03	-1.57	9.58E-04	-1.62	1.81E-03	-2.33	1.11E-05	-1.78	2.13E-04	-1.7	5.79E-03
1448213_at		Anxa1	-1.86	3.33E-04	-1.33	6.31E-04	-1.25	4.13E-02	-2.13	1.66E-02	-1.51	1.78E-02	-1.3	4.27E-02
1423422_at		Asb4	-1.62	1.39E-02	-1.53	1.19E-02	-1.59	8.16E-03	-1.54	4.33E-02	-1.43	3.55E-02	-1.5	2.93E-02
1427233_at		Tshz1	-1.59	4.51E-03	-1.51	4.90E-03	-1.48	9.98E-03	-1.29	6.34E-03	-1.29	1.79E-03	-1.2	2.93E-02
1418496_at		Foxa1	-1.58	1.94E-03	-1.48	3.75E-03	-1.49	2.06E-03	-1.34	1.30E-02	-1.27	1.14E-02	-1.2	4.40E-02
1434283_at		LOC100044968	-1.56	6.25E-04	-1.35	2.50E-03	-1.40	4.82E-03	-1.30	6.36E-03	-1.20	6.73E-03	-1.3	6.54E-03
1419583_at		Cbx4	-1.47	3.13E-04	-1.36	1.38E-03	-1.53	2.60E-03	-1.25	9.65E-03	-1.19	4.13E-03	-1.4	6.29E-03
1439774_at		Prrx1	-1.41	4.68E-03	-1.45	1.04E-02	-1.35	1.88E-02	-1.54	3.53E-02	-1.51	3.18E-02	-1.4	3.69E-02
1436985_at		Zfp644	-1.39	3.65E-02	-1.29	1.76E-02	-1.31	4.78E-02	1.36	2.05E-02	1.25	3.97E-02	1.26	3.82E-02
1434447_at		Met	-1.36	1.79E-02	-1.35	2.06E-02	-1.32	6.44E-03	-1.42	1.51E-03	-1.36	1.21E-03	-1.4	2.85E-03
1423537_at		Gap43	-1.36	1.51E-03	-1.27	4.00E-03	-1.32	1.01E-02	-1.34	5.72E-05	-1.27	5.73E-04	-1.3	3.33E-03
1436041_at		LOC100046086	-1.34	8.40E-03	-1.29	8.02E-03	-1.26	2.04E-02	-1.40	1.40E-03	-1.29	4.51E-03	-1.3	2.80E-03
1427277_at		Six1	-1.33	8.77E-03	-1.35	3.80E-03	-1.30	1.58E-02	-1.36	5.94E-03	-1.23	5.99E-03	-1.3	2.60E-02
1436472_at		Sifn9	-1.32	4.11E-03	-1.29	1.81E-03	-1.27	1.18E-02	-1.27	1.23E-02	-1.19	5.79E-04	-1.3	2.40E-02
1434848_at		---	-1.31	1.39E-02	-1.32	1.08E-02	-1.30	5.72E-03	-1.26	1.76E-02	-1.24	9.66E-03	-1.2	1.60E-02
1429177_x_at		Sox17	-1.31	4.65E-03	-1.27	7.67E-03	-1.26	1.11E-02	-1.42	1.82E-02	-1.29	2.69E-02	-1.3	7.56E-03
1427310_at		Bptf	-1.31	1.57E-02	-1.27	2.34E-02	-1.28	2.01E-02	1.28	1.10E-02	1.21	1.91E-02	1.27	1.46E-02
1451319_at		Senp1	-1.31	1.20E-02	-1.22	1.39E-02	-1.22	3.91E-02	1.28	2.45E-02	1.15	4.05E-02	1.2	4.93E-02
1450700_at		Cdc42ep3	-1.30	4.59E-03	-1.24	9.70E-03	-1.26	1.68E-02	-1.27	4.34E-03	-1.19	1.15E-03	-1.2	1.82E-02
1423635_at		Bmp2	-1.30	1.73E-02	-1.29	1.99E-02	-1.23	3.58E-02	-1.23	4.20E-02	-1.24	3.46E-02	-1.2	4.06E-02
1437556_at		Zfhx4	-1.29	9.52E-05	-1.28	1.77E-03	-1.24	3.32E-02	-1.38	2.76E-04	-1.33	7.23E-04	-1.3	4.91E-03
1449865_at		Sema3a	-1.28	2.05E-02	-1.29	1.57E-02	-1.21	4.32E-02	-1.34	5.11E-03	-1.25	8.73E-03	-1.3	1.43E-02

Table 1: Significant transcripts shared between strains as predicted by the microarrays													
PROBE ID	Gene	Cecr2 ^{6450c} FVB/N						Cecr2 ^{6450c} BALB/c					
		gcrma			dCHIP			gcrma			Arraystar 4		
		Fold	p-value	Fold	p-value	Fold	p-value	Fold	p-value	Fold	p-value	dCHIP BALB	p-value
1449863_a_at	Dlx5	-1.27	5.33E-03	-1.23	1.38E-02	-1.28	2.55E-02	-1.32	3.50E-03	-1.30	2.50E-05	-1.3	7.85E-03
1424659_at	Slit2	-1.27	9.95E-04	-1.27	8.11E-03	-1.30	1.39E-02	-1.22	8.29E-05	-1.17	9.87E-04	-1.2	1.82E-02
1416658_at	Frzb	-1.26	1.37E-03	-1.19	1.34E-02	-1.23	3.78E-02	-1.37	3.10E-02	-1.24	2.12E-02	-1.3	1.20E-02
1438971_x_at	Ube2h	-1.26	2.81E-02	-1.22	3.78E-02	-1.20	4.98E-02	-1.25	6.35E-03	-1.19	8.98E-03	-1.2	1.59E-02
1424842_a_at	Arhgap24	-1.23	1.71E-02	-1.20	4.26E-03	-1.23	4.45E-02	-1.29	2.69E-03	-1.23	9.15E-03	-1.2	2.73E-02
1435494_s_at	Dsp	-1.22	2.31E-02	-1.20	2.48E-02	-1.18	3.39E-02	-1.29	1.02E-02	-1.25	1.50E-02	-1.2	2.40E-02
1420603_s_at	Raet1	-1.21	2.98E-02	-1.21	3.75E-02	-1.32	1.06E-02	-1.18	7.38E-04	-1.19	5.66E-05	-1.2	3.81E-03
1429078_a_at	Cops7a	-1.21	9.83E-04	-1.17	5.47E-03	-1.21	9.11E-03	-1.24	5.29E-05	-1.21	1.05E-04	-1.3	7.63E-04
1431464_a_at	Pmm2	-1.21	1.28E-02	-1.21	3.15E-02	-1.27	7.86E-03	-1.23	9.96E-03	-1.22	2.06E-02	-1.2	3.20E-02
1451154_a_at	Cugbp2	-1.19	5.77E-03	-1.14	3.43E-02	-1.15	2.87E-02	-1.20	9.99E-03	-1.21	5.34E-03	-1.1	3.28E-02
1455792_x_at	Ndn	-1.16	5.08E-03	-1.15	4.39E-03	-1.16	1.68E-02	-1.24	2.06E-03	-1.18	2.68E-03	-1.2	1.11E-03
1435766_at	Pphln1	-1.16	2.94E-03	-1.15	8.17E-03	-1.17	6.97E-03	-1.15	4.19E-03	-1.11	2.78E-02	-1.1	4.91E-02
1434864_at	Nipa1	-1.16	2.57E-02	-1.16	4.36E-02	-1.17	4.46E-02	-1.18	1.24E-03	-1.15	1.01E-02	-1.1	4.19E-02
1423245_at	Cops7a	-1.14	1.92E-02	-1.16	4.49E-03	-1.14	2.31E-02	-1.27	4.52E-05	-1.19	5.62E-05	-1.1	3.67E-02
1435383_x_at	Ndn	-1.13	1.22E-02	-1.11	1.34E-02	-1.14	2.85E-02	-1.19	5.33E-03	-1.18	1.16E-03	-1.1	4.75E-02
1433478_at	Parl	-1.11	2.75E-02	-1.10	1.71E-02	-1.11	1.32E-02	-1.15	5.46E-03	-1.12	1.08E-02	-1.1	2.25E-02
1437853_x_at	Ndn	-1.09	3.03E-03	-1.09	4.41E-03	-1.14	4.51E-03	-1.17	2.93E-03	-1.14	6.46E-04	-1.1	2.69E-03
1435834_at	LOC100040608	-1.07	3.71E-02	-1.11	3.55E-04	-1.12	2.95E-02	-1.18	1.83E-02	-1.14	1.54E-02	-1.2	1.91E-02
1460542_s_at	Mdm4	1.22	1.99E-02	1.16	2.40E-02	1.15	1.67E-02	1.26	9.72E-03	1.23	1.16E-02	1.22	3.51E-02
1417493_at	Bmi1	1.24	9.96E-05	1.20	3.16E-04	1.17	2.08E-03	1.28	1.77E-02	1.23	1.76E-02	1.26	9.31E-03
1417356_at	Peg3	1.25	4.13E-03	1.21	5.68E-03	1.18	2.16E-02	1.17	3.24E-02	1.15	2.33E-02	1.18	4.60E-02
1448733_at	Bmi1	1.26	2.30E-04	1.20	1.18E-03	1.17	6.59E-03	1.18	1.73E-02	1.13	9.47E-03	1.14	3.35E-02
1436071_at	Ankrd26	1.36	1.03E-04	1.27	1.11E-03	1.27	5.16E-03	1.45	3.19E-03	1.29	3.53E-03	1.43	3.27E-03
1452040_a_at	Cdca3	1.62	1.68E-05	1.48	7.63E-05	1.37	6.50E-05	1.57	7.47E-06	1.45	1.11E-05	1.4	1.38E-03
1423847_at	Ncapd2	1.99	8.79E-05	1.80	1.58E-04	1.66	6.28E-03	2.32	4.84E-07	2.05	1.23E-06	1.87	5.00E-06
1439047_s_at	Recql	2.32	4.05E-05	1.71	9.43E-06	1.57	2.78E-04	-1.20	7.12E-03	-1.15	1.82E-02	-1.2	3.60E-02

Table 2.A: GOEAST of downregulated shortlist genes				
Gene Ontology Term	Genes Found	Array Total	Odds ratio	p-value
protein destabilization	2	14	7.48	6.42E-03
muscle cell migration	2	14	7.48	6.42E-03
chemorepellent activity	2	15	7.38	6.88E-03
glial cell migration	2	21	6.90	1.11E-02
neg. chemotaxis	2	27	6.54	1.52E-02
axonal fasciculation	2	29	6.43	1.72E-02
middle ear morph.	2	31	6.34	1.88E-02
cornified envelope	2	34	6.20	2.21E-02
neuron recognition	3	58	6.02	2.20E-03
peptide cross-linking	2	41	5.93	3.14E-02
ear morph.	5	140	5.48	3.72E-05
keratinocyte diff.	3	89	5.40	5.98E-03
inner ear morph.	4	123	5.35	7.07E-04
epidermal cell diff.	3	96	5.29	6.85E-03
palate development	3	102	5.20	7.76E-03
mesenchymal cell development	3	117	5.01	1.03E-02
neg. reg. to external stimulus	3	120	4.97	1.08E-02
mesenchymal cell diff.	3	124	4.92	1.14E-02
cell recognition	3	129	4.87	1.24E-02
epithelial cell diff.	7	307	4.84	2.59E-06
mesenchyme development	3	139	4.76	1.46E-02
ear development	5	234	4.74	3.22E-04
reg. of organ morph.	3	142	4.73	1.47E-02
reg. of Wnt receptor signaling	3	142	4.73	1.47E-02
ureteric bud development	3	143	4.72	1.47E-02
inner ear development	4	191	4.71	2.47E-03
embryonic skeletal morph.	3	156	4.59	1.79E-02
embryonic organ morph.	6	318	4.56	6.88E-05
epithelial tube morph.	6	355	4.40	1.23E-04
epithelium development	13	785	4.38	3.69E-11
morph. of an epithelium	9	572	4.30	6.60E-07
gliogenesis	3	197	4.25	3.24E-02
axon guidance	4	265	4.24	6.58E-03
tube morph.	7	465	4.24	3.21E-05
embryonic skeletal development	3	203	4.21	3.48E-02
heart morph.	3	211	4.16	3.77E-02
connective tissue development	3	216	4.12	4.00E-02
embryonic limb morph.	3	218	4.11	4.05E-02
appendage morph.	3	218	4.11	4.05E-02
gland morph.	3	232	4.02	4.67E-02
morph. of a branching	4	311	4.01	1.02E-02
cell fate commitment	4	312	4.01	1.02E-02
tissue morph.	9	714	3.98	2.41E-06
embryonic organ development	6	516	3.87	7.49E-04
angiogenesis	4	363	3.79	1.47E-02
embryonic morph.	9	833	3.76	7.28E-06

Table 2.A: GOEAST of downregulated shortlist genes				
Gene Ontology Term	Genes Found	Array Total	Odds ratio	p-value
blood vessel morph.	5	494	3.67	5.38E-03
axonogenesis	5	495	3.66	5.38E-03
gland development	5	496	3.66	5.38E-03
tissue development	16	1650	3.60	5.30E-11
pattern specification process	6	621	3.60	1.53E-03
tube development	7	727	3.59	3.98E-04
cell morph. involved in neuron diff.	5	548	3.52	7.44E-03
cell morph. involved in diff.	6	658	3.51	2.08E-03
sensory organ development	5	572	3.45	8.63E-03
neuron projection morph.	5	577	3.44	8.82E-03
chemotaxis	4	466	3.43	3.16E-02
taxis	4	466	3.43	3.16E-02
organ morph.	10	1193	3.39	9.77E-06
reg. of neuron diff.	4	489	3.36	3.64E-02
blood vessel development	5	615	3.35	1.08E-02
cell projection morph.	5	643	3.28	1.24E-02
vasculature development	5	644	3.28	1.24E-02
cell part morph.	5	655	3.26	1.32E-02
growth	4	525	3.26	4.44E-02
reg. of anatomical structure morph.	5	678	3.21	1.47E-02
reg. of cell development	5	680	3.20	1.47E-02
cell morph.	6	871	3.11	6.64E-03
neuron projection development	5	727	3.11	1.79E-02
locomotion	7	1058	3.05	2.52E-03
cell component morph.	6	940	3.00	8.82E-03
neg. reg. of response to stimulus	5	784	3.00	2.42E-02
embryo development	10	1619	2.95	1.23E-04
anatomical formation in morph.	6	977	2.94	1.03E-02
sequence-specific DNA binding	7	1159	2.92	4.19E-03
neg. reg. of gene expression	6	1002	2.91	1.11E-02
generation of neurons	9	1551	2.86	6.73E-04
nucleic acid binding TF activity	9	1605	2.81	7.63E-04
seq.-specific DNA binding TF activity	9	1605	2.81	7.63E-04
cardiovascular system development	6	1071	2.81	1.46E-02
circulatory system development	6	1071	2.81	1.46E-02
anatomical structure morph.	15	2730	2.78	8.06E-07
neuron development	5	917	2.77	4.37E-02
pos. reg. of cell biosynth.	8	1469	2.77	2.47E-03
neurogenesis	9	1666	2.76	9.03E-04
pos. reg. of biosynth.	8	1493	2.75	2.61E-03
pos. reg. of transcription	6	1122	2.74	1.68E-02
pos. reg. from RNAPII promoter	5	942	2.73	4.75E-02
neuron diff.	6	1134	2.73	1.75E-02
cell development	9	1706	2.72	9.96E-04
pos. reg. of RNA metabolic process	6	1139	2.72	1.78E-02

Table 2.A: GOEAST of downregulated shortlist genes				
Gene Ontology Term	Genes Found	Array Total	Odds ratio	p-value
pos. reg. of gene expression	6	1193	2.66	2.18E-02
pos. reg. of nitrogen compound	7	1405	2.64	1.00E-02
reg. of cell diff.	6	1310	2.52	3.34E-02
organ development	16	3525	2.51	2.07E-06
pos. reg. of macromolecule biosynth.	6	1330	2.50	3.56E-02
reg. from RNAPII promoter	7	1562	2.49	1.47E-02
pos. reg. of nucleobase compound	6	1348	2.48	3.76E-02
reg. of developmental process	8	1801	2.48	7.44E-03
cell diff.	17	3954	2.43	1.46E-06
reg. of multicell development	6	1402	2.42	4.41E-02
cell developmental process	17	4050	2.40	1.90E-06
pos. reg. of cell metabolic process	9	2181	2.37	5.23E-03
nervous system development	10	2514	2.32	2.61E-03
pos. reg. of metabolic process	9	2283	2.30	6.57E-03
system development	19	4887	2.28	6.60E-07
reg. of transcription, DNA-dependent	12	3188	2.24	7.94E-04
reg. of RNA biosynth.	12	3192	2.24	7.94E-04
reg. of RNA metabolic process	12	3264	2.20	9.03E-04
reg. of cell biosynth.	14	3870	2.18	2.15E-04
reg. of response to stimulus	10	2765	2.18	5.38E-03
reg. of biosynth.	14	3925	2.16	2.42E-04
reg. of multicell organismal process	8	2381	2.07	3.04E-02
anatomical structure development	19	5669	2.07	4.07E-06
reg. of nitrogen compound	13	3878	2.07	9.03E-04
reg. of cell macromolecule biosynth.	12	3610	2.06	2.20E-03
reg. of gene expression	13	3917	2.06	9.38E-04
reg. of macromolecule biosynth.	12	3696	2.02	2.52E-03
reg. of nucleobase compound	12	3807	1.98	3.16E-03
multicell organismal development	19	6043	1.98	9.77E-06
neg. reg. of cell process	11	3641	1.92	8.46E-03
reg. of macromolecule	15	5112	1.88	7.63E-04
DNA binding	11	3804	1.86	1.08E-02
reg. of metabolic process	17	5922	1.85	2.15E-04
reg. of cell metabolic process	15	5228	1.85	9.03E-04
developmental process	19	6631	1.84	3.79E-05
reg. of primary metabolic process	15	5268	1.84	9.04E-04
neg. reg. of biological process	11	4009	1.78	1.47E-02
pos. reg. of cell process	11	4188	1.72	1.92E-02
pos. reg. of biological process	12	4638	1.70	1.30E-02
multicell organismal process	19	7583	1.65	2.42E-04
reg. of biological process	22	12028	1.20	2.27E-03
reg. of cell process	20	11255	1.16	8.49E-03
biological reg.	22	12728	1.12	5.04E-03

Table 2.B: GOEAST of upregulated shortlist genes				
Gene Ontology Term	Genes Found	Array Total	Odds ratio	p-value
Cell division	3	739	4.93	3.60E-02

Table 2.C: GOEAST of strain-dependent shortlist genes				
Gene Ontology Term	Genes Found	Array Total	Odds ratio	p-value
DNA-dependent ATPase activity	2	115	7.03	2.82E-02

Table 2 Legend: biosynthesis (biosynth.), differentiation (diff.), morphology (morph.), negative (neg.), positive (pos.), regulation (reg.)

of gene expression (n=13/36), where many of the same genes found in the previous categories of tissue or organ development were also transcription factors. Among the upregulated gene candidates (Table 2.B), the only category to appear in common was cell division (n=3/6). The only category common to genes showing opposing strain misregulation was DNA-dependent ATPase activity (n=2/6) (Table 2.C). Not all of the genes were annotated, with 9 of the 48 total not registering within the analysis. Overall, it appeared that genes whose expression decreased with the loss of *CECR2* were often transcription factors involved in organogenesis, while candidates whose expression increased in the *Cecr2* mutants were involved in regulating cell division. An interesting, but perplexing, category was the candidates involved in DNA-dependent ATPase chromatin remodeling activities that showed different responses depending on the strain background. It may be that the FVB/N and BALB/c strains respond to chromosomal structural changes in different ways in terms of potential compensation or response of other ATP-dependent remodeling complexes.

The resulting lists offered a number of candidates, but the Affymetrix MOE 420 2.0 genechips did not contain a complete coverage of all mouse transcripts. Thus, important genes affected by the disruption of *Cecr2* may have been overlooked. Another important caveat is that these experiments have not confirmed that *CECR2* directly acts as a regulator of transcription. These candidates show misregulation, but may be indirectly affected through some yet unknown process. The probe regions of the arrays were confined to the 3' untranslated end of transcripts and so only changes in these regions would have registered. The use of whole embryos as an RNA source could have diluted regional specific changes, but this was favoured over the potential risk for tissue heterogeneity during micro-dissections. Although the focus of the arrays was neural closure, changes recorded from whole embryo samples may not represent neural-specific changes for a given candidate. Techniques such as flow cytometry and cell sorting may be capable of providing isolated cell populations, potentially increasing the relative fold-change of specific neural effects and ensuring any changes were relevant to the tissue of interest. Such specific isolations were not pursued, as at the time there was not a clear understanding of what cell markers, pathways, or candidates were of interest. Future studies should consider FACS for microarray or qRT-PCR applications if focusing on a particular candidate pathway or cell type. What these studies could provide was an extensive prediction of what pathways or genes were disrupted during development with a loss of *CECR2*.

3.2.2: Microarray and qRT-PCR analyses did not support a disruption in the relative expression of planar cell polarity transcripts during neural closure of *Cecr2*^{tm1.1Hemc} BALB/c homozygous embryos

If planar cell polarity signalling was effected in the *Cecr2* mutants, and if the assumption of *CECR2* acting as a transcriptional regulator was correct, then the misregulation of planar cell polarity-associated genes might be expected in *Cecr2* mutants during neurulation. However, no core PCP genes were found to be affected when comparing all three microarray analysis methods. A reduced

stringency was then considered by taking only the *Cecr2*^{GT45Bic} BALB/c gcRMA values into account, as gcRMA is thought to over-represent low abundance transcripts. Among the PCP receptors, a few showed low but significant changes in the gcRMA microarray of whole body embryos. The *Celsr2* receptor was suggestive with a low fold-change just over the significance cut-off (f.c.=1.26, p=0.06). *Wnt5b* (f.c.=1.59, p=4.16E-03) was the only secreted WNT to show a significant expression change. *Prickle1* (f.c.=1.21, p=0.07) and *Gsk3b* (f.c.=1.23, p=0.06) were other suggestive changes within the PCP signaling cascade. Finally, a member of the secondary PCP Fat/Dach/Fjx signaling networks *Lix1* (f.c.=1.55, p=3.33E-04) showed a significant fold-change.

The following qRT-PCR work was conducted alongside undergraduate Amanda Pisio to confirm whether changes in the expression of PCP genes were evident in the early *Cecr2*^{GT45Bic} and *Cecr2*^{tm1.1Hemc} homozygous embryos. A series of primers were designed for qRT-PCR confirmation. Included in this list were the core PCP genes absent from the microarray probesets, along with any PCP genes present on the microarrays that showed significant or suggestive expression changes in the *Cecr2*^{GT45Bic} samples. All of the microarray data were generated from mutants of the *Cecr2*^{GT45Bic} allele. For this reason, the follow-up confirmation of candidates was performed in new biological replicates from the *Cecr2*^{tm1.1Hemc} BALB/c mutation. Confirming the same effects were present using two mutant alleles would provide additional support that these changes were a real and repeatable consequence of *Cecr2* disruption. *Cecr2*^{tm1.1Hemc} and wildtype embryos were from two developmental stages: 10-14 somites (late TS13) and 18-20 somites (late TS14). These ages represented the stage immediately prior to when wildtype cranial neural folds come together, and shortly after cranial fusion would be complete. To focus on genes involved in cranial neurulation, only the head of the embryo was used for qRT-PCR.

The Fluidigm qRT-PCR results presented in Table 3 indicated *Cecr2* mutations do not disrupt the transcriptional regulation of the PCP genes tested during neural closure. The only primer set to indicate a significant change during closure was *Wnt5a* (f.c.=1.37, p=4.0E-03). However, upon further inspection this probe mapped to an intron of *Wnt5a* that was also an exon of a second unnamed gene transcript overlapping with the *Wnt5a* position. With the exclusion of the *Wnt5a/unknown* probe, no PCP transcripts were affected in the closing cranial neural tube.

The post-closure sample set of 18-20 somites (TS14) was tested using the same qRT-PCR primer sets. *Wnt7b* (f.c.=1.19, p=0.015), *Fzd7* (f.c.=1.17, p=0.043) and *Lix1* (f.c.=1.37, p=0.032) showed a significant expression change. By this stage, the results may represent secondary effects of CECR2 function following attempted neural tube closure or failure. Thus the transcriptional regulation of the PCP genes tested was not disrupted during neural closure of *Cecr2* mutants. This did not exclude the possibility that CECR2 may affect the PCP pathway in a non-transcriptional manner, during other stages of development, or in tissues outside of the embryonic head. The transcription of PCP genes was not affected by the disruption of *Cecr2* during cranial neurulation. This could

Table 3: PCP qRT-PCR of <i>Cecr2</i> ^{tm1.1Hemc} BALB/c cranial tissue versus wildtype BALB/c			
Genes	TS 13 (10-14 somites)		
	Fold	SE	p-value
<i>Celsr2</i>	1.02	0.08	8.72E-01
<i>Fat4</i>	1.15	0.05	2.85E-01
<i>Fgfr1</i>	1.10	0.03	3.10E-01
<i>Fjx1</i>	-1.02	0.02	9.14E-01
<i>Frzb</i>	1.10	0.06	5.50E-02
<i>Fzd1</i>	-1.00	0.03	9.17E-01
<i>Fzd10</i>	-1.21	0.06	1.95E-01
<i>Fzd2</i>	1.10	0.03	2.73E-01
<i>Fzd5</i>	-1.07	0.04	3.12E-01
<i>Fzd7</i>	1.21	0.04	1.02E-01
<i>Gsk3b</i>	1.08	0.02	3.24E-01
<i>Intu</i>	-1.03	0.03	9.06E-01
<i>Prickle</i>	1.02	0.03	8.69E-01
<i>Vangl1</i>	-1.07	0.05	4.92E-01
<i>Vangl2</i>	-1.18	0.06	2.47E-01
<i>Wnt5a</i>	-1.37	0.05	3.80E-03
<i>Wnt5b</i>	1.04	0.04	6.89E-01
<i>Wnt7b</i>	-1.06	0.07	5.68E-01

indicate that CECR2 was not a transcriptional regulator, or that PCP-associated genes were not downstream of its activity. The question became whether there were other genes misregulated in *Cecr2* mutants which could account for the neural tube defects.

3.2.3: Microarray analyses identified a number of candidate transcripts with roles in neural tube closure

The microarray datasets provided candidates that may indicate which, if any, genes or developmental pathways were disrupted in the *Cecr2* mutant embryos with neural tube defects. At least sixteen genes were identified on the *Cecr2*^{Gt45Bic} BALB/c microarray, by all three statistical methods, whose mutations develop some form of a neural tube defect. Of these, only *Alx1*, *Bmi1*, *Bmp2*, *Met*, *Dlx5*, *Mdm4*, and *Prrx1* also were affected in *Cecr2*^{Gt45Bic} FVB/N. These genes could be the targets of the proposed CECR2 transcriptional regulation, and due to their known roles in development may be the cause of the associated neural tube defects.

Transcript selection for further analysis at the time focused on those genes with expression differences on the *Cecr2*^{Gt45Bic} BALB/c array, predicted or confirmed function during neural tube closure, or early developmental expression similar to *Cecr2* (Table 4). Some candidates without known roles in neurulation were also tested if they met the other requirements. Five of fourteen transcripts tested were validated in the 10-14 somite (TS13) stage samples (*Alx1*, *Dlx5*, *Cecr2*, *Ncapd2*, and *Six1*; Table 4). In addition, at the 18-20 somite stage (TS14) a further three genes showed significant downregulation (*Epha7*, *Eya1* and *Lix1*). It is important to note that the microarray RNA was generated from whole bodies of homozygous *Cecr2*^{Gt45Bic} or wildtype embryos, while qRT-PCR analysis focused only on heads of stage-matched homozygous *Cecr2*^{tm1.1Hemc} or wildtype embryos. The possibility therefore remains that the unconfirmed transcripts are simply not expressed or altered in embryonic head, but may still show changes elsewhere in the body. Of the four candidate transcripts validated (*Alx1*, *Dlx5*, *Ncapd2*, and *Six1*; Table 4), all four were altered on both the *Cecr2*^{Gt45Bic} BALB/c and *Cecr2*^{Gt45Bic} FVB/N microarrays as predicted by all three statistical methods. Of the six probes not confirmed in the pre-neural closure embryos (*Elavl1*, *Epha7*, *Eya1*, *Lix1*, *Mdfr*, *Zfp9*; Table 4), none met the highest stringency selection of being affected on both strains by all statistical methods. These results strongly suggested that multiple microarray analytical methods should be consulted when generating predictive lists of transcriptional changes. They also indicated that the misregulation of *Alx1* and *Dlx5* was consistent in multiple *Cecr2* mutations. Changes in the expression of *Alx1* and *Dlx5* could be the cause of the neural defects in *Cecr2* mutations.

3.3: *Cecr2* microarray analyses revealed three regions showing chromosomal enrichment of transcripts that may identify direct target regions of CECR2 remodeling

The microarray dataset was analyzed further to identify potential regions

Table 4: QRT-PCR of <i>Cecr2</i> ^{mt1.Htmc} BALB/c homozygous cranial tissue versus wildtype BALB/c						
Genes	TS13 (10-14 somites)			TS14 (18-20 somites)		
	Fold	SE	p-value	Fold	SE	p-value
<i>Atx1</i>	-2.31	0.05	7.00E-05	-2.02	0.03	1.00E-06
<i>Cdk5rap1</i>	-1.2	0.2	7.00E-01	-1.4	0.2	2.00E-01
<i>Cecr2</i>	-258	4.00E-04	7.00E-52	-201	5.00E-04	3.00E-64
<i>Dlx5</i>	-1.42	0.03	2.00E-03	-1.41	0.03	5.00E-04
<i>Elavl1</i>	-1.09	0.03	2.20E-01	1.04	0.03	1.40E-01
<i>Epha7</i>	-1.41	0.3	7.00E-02	-2.3	0.3	1.00E-02
<i>Eya1</i>	-1.12	0.06	4.00E-01	-2.47	0.06	1.00E-05
<i>Ldhb</i>	1.14	0.03	7.00E-02	-1.06	0.05	8.40E-01
<i>Lix1</i>	-1.21	0.05	1.20E-01	-1.37	0.06	3.00E-02
<i>Mdfr</i>	-1.1	0.1	3.00E-01	-1.62	0.07	9.00E-06
<i>Ncapd2</i>	1.55	0.05	2.00E-05	1.53	0.05	4.00E-06
<i>Six1</i>	-1.20	0.04	2.30E-02	-1.49	0.04	6.00E-04
<i>Tfpi</i>	1.2	0.1	2.00E-01	-1.8	0.1	1.00E-03
<i>Zfp9</i>	-1.10	0.04	3.30E-01	-1.00	0.06	8.90E-01

Table 5: Chi-squared analyses for chromosomal regions enriched in significant transcripts										
Chromosome	Whole chromosome	Band A	Band B	Band C	Band D	Band E	Band F	Band G	Band H	
1	9.60E-02	2.45E-01	3.87E-02	6.66E-01	2.39E-01	7.88E-01	1.28E-02	8.49E-02	7.39E-01	
2	7.10E-01	1.33E-02	9.72E-01	9.20E-02	1.19E-01	6.75E-01	7.03E-01	5.04E-01	2.82E-01	
3	1.21E-01	6.01E-01	8.30E-01	1.81E-01	8.87E-01	2.66E-01	6.67E-01	9.39E-01	3.77E-02	
4	2.14E-01	2.21E-02	3.41E-02	4.21E-01	1.46E-01	1.95E-01				
5	4.12E-02	1.16E-02	9.47E-01	3.32E-01	2.67E-01	1.57E-01	3.98E-02	4.77E-01		
6	6.73E-13	2.94E-04	2.84E-01	5.06E-01	4.54E-01	6.35E-01	1.07E-10	1.28E-23		
7	4.34E-02	1.08E-02	1.54E-01	2.11E-05	6.84E-01	2.10E-01	1.67E-02			
8	1.06E-01	9.14E-01	1.92E-01	9.69E-01	7.57E-01	5.50E-02				
9	9.97E-01	3.96E-01	4.56E-01	3.71E-01	6.35E-01	6.79E-01	9.01E-01			
10	2.92E-03	1.12E-01	1.98E-01	2.36E-02	4.72E-01		7.03E-01			
11	9.12E-02	5.42E-01	8.61E-02	6.66E-01	3.62E-01	4.25E-01		8.49E-01		
12	1.25E-01	5.23E-01	2.26E-06	2.19E-01	6.66E-01	9.26E-01				
13	9.53E-01	1.91E-01	2.84E-01	6.03E-02	7.01E-01		6.15E-01			
14	7.96E-01	7.90E-01	9.47E-02	8.98E-01	8.81E-01	1.31E-01				
15	4.70E-01	1.61E-01	6.94E-01	7.13E-01	7.08E-01	8.27E-01	3.73E-02			
16	7.12E-03	4.03E-01	1.19E-01	2.92E-02						
17	7.45E-01	4.97E-01	3.10E-01	4.49E-01	1.70E-01	8.00E-01	6.70E-01			
18	4.37E-01	6.53E-02	1.68E-01	9.75E-01	5.62E-01	5.74E-01				
19	6.44E-01	5.11E-01	7.12E-01	4.61E-01	1.74E-02	6.96E-01		6.62E-01		
X	3.81E-03	2.84E-01	3.23E-01	5.90E-01	1.49E-01	6.99E-01	1.16E-02			
Y	8.91E-01	3.51E-01								
Unaffiliated	2.42E-25									
Bonferroni significant p<2.27E-03										
Bonferroni significance p<4.20E-04										

Table 6: Chromosome 6 qRT-PCR of <i>Cecr2</i> ^{Gt45Bic} homozygotes versus wildtype							
Gene	<i>Cecr2</i> ^{Gt45Bic} BALB/c			<i>Cecr2</i> ^{Gt45Bic} FVB/N			
	Fold	SE	p-value	Fold	SE	p-value	
<i>Clec1b</i>	-1.01	0.02	9.20E-01	3.6	0.1	9.00E-16	
<i>H2aff</i>	1.09	0.03	5.40E-01	-1.03	0.01	4.10E-01	
<i>Klhdc5</i>	1.07	0.03	1.60E-01	1.01	0.02	3.50E-01	
<i>Ldhb</i>	1.08	0.03	4.55E-02	-1.56	0.01	1.80E-09	
<i>Mbd4</i>	1.26	0.07	1.00E-01	-1.13	0.01	1.50E-02	
<i>Ncapd2</i>	1.63	0.02	5.00E-09	1.36	0.03	2.00E-07	
<i>Wnt5b</i>	-1.22	0.01	4.00E-02	1.20	0.04	4.00E-02	
<i>Zfp9</i>	-1.28	0.02	2.00E-02	-1.68	0.01	4.00E-07	

showing multiple affected transcripts or a scarcity of hits from a particular region. The basis for these analyses was the finding that the functionally-related ISWI *Bptf* mutations showed regional effects by microarray analyses. Thus ISWI complexes may work across specific, but broad, regions. This line of evidence would further suggest ISWI complexes can regulate, or at least affect, the transcription of genes within these regions. The hypothesis was that CECR2 would target different regions than BPTF, but that the general pattern of broad regions showing expression changes would be conserved.

All significantly changed transcripts from either strain dataset with annotated chromosomal positions were grouped by chromosome and subjected to Chi-squared analysis. Only chromosome 6 showed enrichment (found 125, expect 68, $p=6.73e-13$, Table 5) with nearly double the expected number of hits. The chromosomes were subdivided into chromosomal bands and reanalyzed. The refined chromosome 6 enrichment showed Chr6A enrichment (found 20, expect 9, $p=2.94e-04$, Table 5), and a span from Chr6F (found 34, expect 12, $p=1.07e-10$, Table 5) to Chr6G (found 37, expect 8, $p=1.28e-28$, Table 5). All other chromosomes were broken out into bands and two further enriched regions were Chr7C (found 11, expect 3, $p=2.11e-05$, Table 5) and Chr12B (found 9, expect 2, $p=2.26e-06$, Table 5).

Eight Chr6F-G transcripts were tested by qRT-PCR on the original whole embryo RNA used for the microarray analysis. *Clec1b*, *H2aff*, *Klhdc5*, *Ldhb*, *Mbd4*, *Ncapd2*, *Wnt5b* and *Zfp9* were predicted by the microarray to show expression changes in the FVB/N strain; while *Wnt5b*, *Ncapd2*, and *Zfp9* were identified on the BALB/c array. Table 6 lists the qRT-PCR fold-change results wherein *Clec1b*, *Ldhb*, *Mbd4*, *Ncapd2*, *Wnt5b*, and *Zfp9* were all confirmed (six of eight) as showing altered expression in *Cecr^{Gt45Bic}* FVB/N, and all three of the *Cecr^{Gt45Bic}* BALB/c predicted changes were confirmed.

As both the Chr7C and Chr12B regions were quite small, they were sensitive to affected genes with multiple transcripts/probes. All five of the significant regions were re-analyzed, sifting the enrichment data to include only a single-transcript per gene. Regions 6A ($p=6.33e-04$), 6F ($p=6.81e-05$), 6G ($p=1.95e-12$), and 12B ($p=4.92e-05$) still had significant enrichment based on single-transcript analysis; but region 7C did not (Bonferroni adjusted $p<0.01$). Thus Chr6A, 6F, 6G, and Chr12B may be the direct targets of CECR2 remodeling. Of an interesting and perhaps significant note, two of the genes from the neurulation candidate short-list *Dlx5* and *Met* map to the Chr6A enrichment and *Cecr2* maps to the Chr6F region. However, a major caveat of this study, and perhaps of Landry et al. (2008), is that the sensitivity of microarrays cannot distinguish expression changes due to the primary mutation from potential strain expression differences remaining from the initial generation of the mutation. The region surrounding the *Cecr2* mutation would be of the 129/Ola strain, and this could potentially account for the expression change enrichment of regions 6F-G.

3.4: Testing the hypothesis that the *Cecr2*^{Gt45Bic} mutants manifest multi-system congenital defects

A detailed report of the exencephaly present in the *Cecr2*^{Gt45Bic} mutant embryos (Banting et al., 2005) indicated the non-exencephalic *Cecr2*^{Gt45Bic} homozygotes of both the BALB/c and FVB/N strains were viable and fertile. Dawe et al. (2011) added stereocilia defects to the list of known *Cecr2* defects and further defined the nature of the neural closure defect. One of the initial goals of this project was to carefully document non-exencephalic animals for subtle abnormalities beyond the early neural tube defect and to begin a comprehensive study of the effect of the *Cecr2* mutation during embryogenesis. Wildtype BALB/c or FVB/N stage-matched animals, or wildtype littermates when possible, were used as controls in all phenotypic comparisons. A literature review and database search of the known phenotype and defects of the wildtype strains was also conducted. The expression of *Cecr2* throughout numerous organ systems strongly suggested a function not limited to neurulation (Banting et al., 2005). Many developmental processes such as convergent extension and PCP, gene network pathways, and even cell lineages are shared between diverse sites of organ development. If a number of *Cecr2*-disrupted affected organs could be identified, then one could speculate what developmental processes or pathways these traits have in common. Initially, traits were scanned for PCP-like defects.

3.4.1: *Cecr2*^{Gt45Bic} BALB/c non-exencephalic homozygous and heterozygous adult animals possessed caudal vertebrae defects

Many mutations in mice show some form of tail defect, a trait appearing quite often in association with other neural tube defects. Caudal vertebrae defects may indicate defects in the process of secondary neurulation. The MGI database contains some 845 genotypes associated with tail defects, 295 characterized with kinked tails and 133 with known caudal vertebrae deformities. Tail kinks often appear in conjunction with neural tube defects (Klootwijk et al., 2000; Matsuura et al., 1998; Robledo et al., 2002; Singh et al., 2008; Terzian et al., 2007; Ting et al., 2003) and also in association with cranial midline defects (Klootwijk et al., 2000; Naf et al., 2001; Petryk et al., 2004). Other than the phenotypic coexistence, few studies draw clear connections between the causes of the NTD and tail kinks. There is a difference in the developmental and cellular origins of the caudal neural tube compared to primary neurulation. The caudal neural tube is derived from mesenchymal cells undergoing mesenchymal-epithelial transition and cavitation through the process of secondary neurulation (Schoenwolf, 1983). Other mutant lines resembling *Cecr2* mutant tail defects include the *Knotty-tail* (Matsuura et al., 1998) and *Bent-tail* mutations (Klootwijk et al., 2000). These types of kinks arise from somitogenesis defects and abnormal mesenchymal apoptosis (Matsuura et al., 1998). Thus from phenotypic comparisons, the *Cecr2* mutant tail kinks are consistent with secondary neurulation defects and may support a general and consistent role for *Cecr2* in mesenchymal development, survival, and mesenchymal-epithelial transitions.

A set of non-exencephalic *Cecr2*^{Gt45Bic} BALB/c adult animals with visible

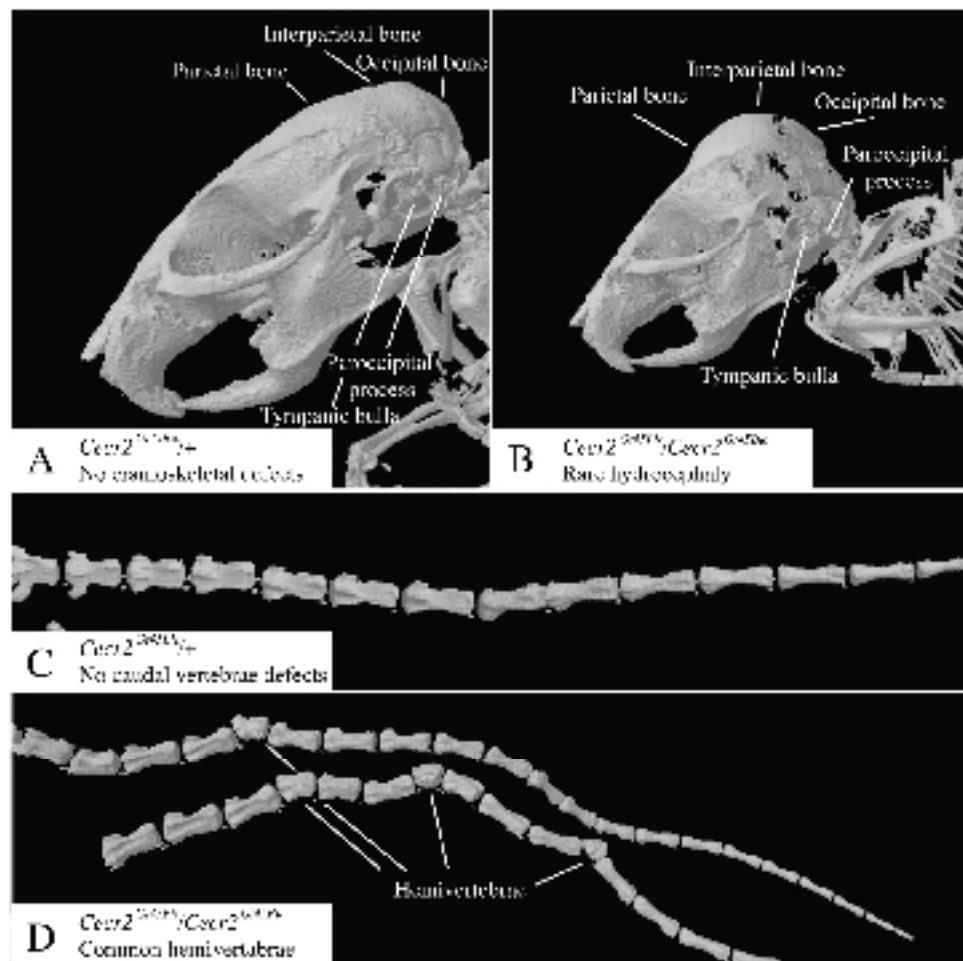


Figure 12:

Cranial and caudal-vertebrae skeletal defects developed in *Cecr2*^{Gt45Bic} BALB/c homozygotes

(A-B) Micro-CT imaging of *Cecr2*^{Gt45Bic} BALB/c heterozygous (A) and 3 of 4 homozygous animals did not exhibit skeletal defects under micro-CT. A single aberrant male *Cecr2*^{Gt45Bic} BALB/c homozygote presented with a bulbous skull and died 4 weeks after birth (B). Micro-CT scans revealed incomplete suture fusion likely due to the cranial distention of the tympanic bulla and paroccipital process displacement ventrally while the parietal, interparietal, and occipital bones were bulbous and forced outward (B). The morphology suggested hydrocephaly, but no other mutant animals were found to manifest this defect. (C-D) Caudal defects appeared as kinks along the tails of *Cecr2*^{Gt45Bic} BALB/c homozygous adults, and occasionally manifested within the *Cecr2*^{Gt45Bic} BALB/c heterozygotes. Heterozygous samples scanned by micro-CT showed typical vertebrae morphology (C). *Cecr2*^{Gt45Bic} BALB/c homozygous tails (D) indicated the kinked appearance originated from hemivertebrae spaced sporadically throughout the homozygous tails. Affected vertebrae were shortened, curved, and show unilateral malformations of the vertebral processes. The rendered images were not produced to the same magnification scale.

tail kinks was scanned for skeletal defects using computer tomography X-ray imaging. *Cecr2*^{Gt45Bic} FVB/N animals were not examined by micro-CT as they were not known to manifest the cranial defects associated with an open neural tube, nor did they show evidence of prominent tail kinks. Heterozygous animals examined (n=2 by CT) showed wildtype morphology (Figure 12.A). All but one non-exencephalic homozygous animal exhibited wildtype morphology of cranial sutures, snout morphology and craniofacial bone morphology (n=149 homozygous animals visually examined, 4 further scanned by micro-CT) (Figure 12.B). This unusual *Cecr2*^{Gt45Bic} homozygous animal developed a bulbous cranium suggesting hydrocephaly and was selected for micro-CT due to its obvious structural defect after being found dead soon after weaning. The rarity of this condition likely represents a random abnormality not associated with the *Cecr2*^{Gt45Bic} phenotype. However, given the range of phenotypes now associated with *Cecr2* mutation, it may be that hydrocephaly is a rare outcome. Putrification of the body prior to discovery, and the rarity of hydrocephaly, left me unable to confirm either possibility. All other homozygous animals imaged by micro-CT were selected from available mutant animals.

Given the strong *Cecr2* expression in the developing limbs, cartilage, and muscles throughout the embryo (Banting et al., 2005 and Man, personal communication, 2009), micro-CT-rendered models of *Cecr2*^{Gt45Bic} BALB/c homozygous adults were examined for peripheral skeletal defects. No abnormalities were noted among the limbs or digits studied (data not shown, n=4 examined by CT, n=1/149 of all homozygous animals visually examined), and to date no limb defects have been noted among *Cecr2* mutants during colony maintenance.

Cecr2^{Gt45Bic} BALB/c adult homozygous, and occasionally heterozygous, animals have been found to have tail kinks (McDermid, Dawe, Kooistra, Davidson, and Ames, personal communications, 2006-2012), although this thesis is the first to characterize the defect. The micro-CT revealed the kinks result from shortened and aberrant caudal vertebrae (Figure 12.C-D). Within a given tail most often only a single vertebra appeared affected, although instances of up to three kinks were noted by micro-CT. Affected vertebrae showed distortions of the vertebral body with abnormal transverse and spinal processes. The more severe aberrations would be classified as fully segmented dorsal or lateral hemivertebrae (Farley et al., 2001; Farley et al., 2006). The vertebral foramen remained unimpeded throughout the vertebra. No vertebrae fusions were noted, and the sacrum structures of *Cecr2*^{Gt45Bic} BALB/c mutants showed wildtype morphologies.

What may be more telling than the morphological assessments are the genes whose mutations are known to manifest tail kinks, that also appear on the *Cecr2*^{Gt45Bic} microarray highest stringency shortlist (Table 1). The age of the embryos used in the microarray does precede caudal vertebrae development and so any connections must assume the developmental genes disrupted during neural closure are consistent targets of CECR2 throughout development. Nonetheless, three candidates include *Mdm4* (Terzian et al., 2007), *Bmp2* (Bandyopadhyay et al., 2006; Singh et al., 2008), and *Dlx5* (Robledo et al., 2002). All three of these

TABLE 7 : Organ weight comparisons of <i>Cecr2</i> ^{G45Bc} mutants of both strains										
Strain	Sex	Age	N	Body Weight (g)	Brain Weight (g)	Brain/Body Ratio (%)	Kidney Weight* (g)	Kidney/Body Ratio* (%)	Testis Weight (g)	Testis/Body Ratio (%)
FVB/N										
Wildtype	M	6-8 weeks	12	24.0±0.5	0.436±0.005	1.82±0.04	0.203±0.007	0.85±0.01	76.59±0.15	0.320±0.007
<i>Cecr2</i> ^{G45Bc}	M	6-8 weeks	13	28.6±0.7	0.413±0.006	1.45±0.03	0.21±0.01	0.72±0.03	61.96±0.13	0.217±0.005
Wildtype	F	6-8 weeks	18	19.9±0.4	0.429±0.004	2.17±0.03	0.139±0.002	0.702±0.006	-	-
<i>Cecr2</i> ^{G45Bc}	F	6-8 weeks	11	23±1	0.404±.005	1.77±0.05	0.140±0.006	0.61±0.02	-	-
BALB/c										
Wildtype	M	6-8 weeks	6	24.2±0.7	0.44±0.01	1.83±0.04	0.253±0.004	1.05±0.02	78±1	0.327±0.005
<i>Cecr2</i> ^{G45Bc}	M	6-8 weeks	6	23±1	0.42±0.01	1.9±0.1	0.22±0.01	0.97±0.03	60±4	0.26±0.01
Wildtype	F	3 weeks	9	11.7±0.4	0.44±0.01	3.80±0.09	ND	ND	-	-
<i>Cecr2</i> ^{G45Bc}	F	3 weeks	5	11.7±0.8	0.410±0.007	3.6±0.3	ND	ND	-	-

genes show tail kinks when mutated, but are also necessary for neural closure and present with exencephaly as well as a range of midline or palate defects.

3.4.2: *Cecr2*^{Gt45Bic} non-exencephalic homozygous adult animals from both strains showed reduced brain weight compared to wildtype littermates

Non-exencephalic animals with the *Cecr2*^{Gt45Bic} mutation were initially characterized as phenotypically normal (Banting et al., 2005). However, given the range of *Cecr2* expression I hypothesized that the non-penetrant adult animals would develop additional subtle defects. *Cecr2*^{Gt45Bic} FVB/N homozygous embryos do not develop the exencephalic phenotype; yet, their neural folds show a delay in closure and appear farther apart than stage-matched wildtype FVB/N controls (Kooistra et al., 2011). From birth to adulthood, no overt behavioral defects have been noted during the care or handling of these animals. Additional subtle neural defects were the first category of defects to be examined in the *Cecr2* mutations.

Necropsy weight of whole brains from *Cecr2*^{Gt45Bic} FVB/N homozygous adults of both sexes indicated a reduction in brain mass compared to normal controls (Table 7). Within a 6 to 8-week-old cohort, the weight of *Cecr2*^{Gt45Bic} FVB/N homozygous brains averaged 0.413±0.006 g in males and 0.404±0.005 g among females. FVB/N age-matched brain weights were 0.436±0.005mg in males and 0.429±0.004 g in females. Mann-Whitney U-tests confirmed *Cecr2*^{Gt45Bic} FVB/N homozygous males (p=0.015) and females (p=4.3E-04) had a significant reduction in brain weight. Brain weights were further considered in terms of percent body mass where mutant male brains were 1.45±0.03% and the females 1.77±0.05% of body mass. FVB/N wildtype brains of males were 1.82±0.04% and in females 2.17±0.03% of their body masses. *Cecr2*^{Gt45Bic} FVB/N homozygote brain-to-body ratio was significantly reduced in both males (p= 3.85E-07), and females (2.02E-07).

A similar deficit was found in the *Cecr2*^{Gt45Bic} BALB/c non-exencephalic homozygous brain weight. A female dataset was collected at three weeks of age following weaning, where the *Cecr2*^{Gt45Bic} BALB/c homozygous brains averaged 0.410±0.007 g (n=5) and the wildtype littermates averaged 0.44±0.01 g (n=9). By body weight, the mutants averaged 3.6±0.3% and the wildtypes 3.80±0.09%. The *Cecr2*^{Gt45Bic} BALB/c homozygous female brains were significantly smaller by weight (p=0.030), but not by body ratio (p>0.05). Male *Cecr2*^{Gt45Bic} BALB/c homozygous 6 to 8-week brain weights were 0.421±0.008 g (n=6) and wildtype 0.458±0.009 g (n=11), which showed a significant reduction (p=0.024). The brain tissue represented 1.85±0.06% of mutant body mass and in wildtypes was 2.04±0.08%. The body ratio values were not significantly different in BALB/c samples (p>0.05).

The brain weight was reduced in both strains and sexes among *Cecr2*^{Gt45Bic} mutants. However, *Cecr2*^{Gt45Bic} FVB/N homozygous animals from the above dataset of both sexes showed a significant increase of 16-19% in body weight compared to normal controls (females p=9.90E-03, males p=1.49E-05 respectively). There may be changes in body weight from an increase in fat or muscle tone, but the cause of the variation has not been tested. The body weight

of *Cecr2*^{Gt45Bic} BALB/c mice did not differ from wildtype littermates. Even with the slight body-mass variation among FVB/N samples, the brain weight of *Cecr2*^{Gt45Bic} mutants of either strain showed a clear reduction in mass compared to wildtype littermates.

A histology project undertaken by Sara Afshar attempted to identify the regions of the *Cecr2*^{Gt45Bic} brain showing a size reduction. The preliminary examination did not identify a specific layer, substructure, or region showing a disproportional reduction. *Cecr2* expression in an adult brain is within the hippocampus and cerebellum (McDermid, personal communications, 2012), but these structures did not appear smaller (Afshar, personal communications, 2010). The reduced weight of mutants was thought to be diffuse and general across the entire brain; however, this was not confirmed. The general reduction in size, correlating with an early expression of *Cecr2*, may suggest a reduction in progenitor populations or reduced cellular proliferation of early progenitor cells of the neural tube. Gene ontology analysis of the microarray datasets during neural closure did show a small cluster of cell proliferation associated genes affected by the loss of *Cecr2*. Future work could consider PH3 cell proliferation assays of the early neural tube to characterize a potential delay in cell replication. Taken together, the data presented has established that neural tube closure is not the only role for *Cecr2* during neural development.

3.4.3: *Cecr2*^{Gt45Bic} adult males of both strains developed smaller testes with reduced weight compared to wildtype males

The same animals used to generate the brain weight data were used in analyzing the testis weight of *Cecr2*^{Gt45Bic} homozygotes. Thompson et al. (2012) found that male *Cecr2*^{Gt45Bic} BALB/c homozygotes showed significantly reduced litter sizes, although no structural defects of the testes or sperm were found during histology analysis. *Cecr2*^{Gt45Bic} FVB/N litter size did not differ from wildtype counterparts (Thompson et al., 2012). The adult testes were one of the few adult structures to show strong *Cecr2* expression (Thompson et al., 2012). As this expression began in early development, I hypothesized that the testes would show defect and that the defect may be a growth/weight issue similar to that of the adult *Cecr2*^{Gt45Bic} brain.

Dissection of the testes found a significant reduction in overall testes weight in both *Cecr2*^{Gt45Bic} BALB/c and *Cecr2*^{Gt45Bic} FVB/N homozygous animals. The *Cecr2*^{Gt45Bic} FVB/N homozygous males (Table 7) showed an average testis weight of 62.0±0.1 mg to the wildtype average of 76.6±0.2 mg. Accounting for body weight, the *Cecr2*^{Gt45Bic} FVB/N homozygous testis ratio was 0.217±0.005% and the FVB/N testis ratio was 0.320±0.007% of body weight. Despite showing no fecundity defect, the *Cecr2*^{Gt45Bic} FVB/N male testes were 81% (U-test p=1.4E-08) of wildtype mass and only 68% (U-test p=1.6E-09) of the expected wildtype testis-to-body ratio.

Cecr2^{Gt45Bic} BALB/c homozygous males possessed an average testis weight of 60±4 mg, or 0.26±0.01% of body weight. Age-matched BALB/c wildtypes showed an average testis weight of 79±1 mg, or 0.327±0.005% of body weight.

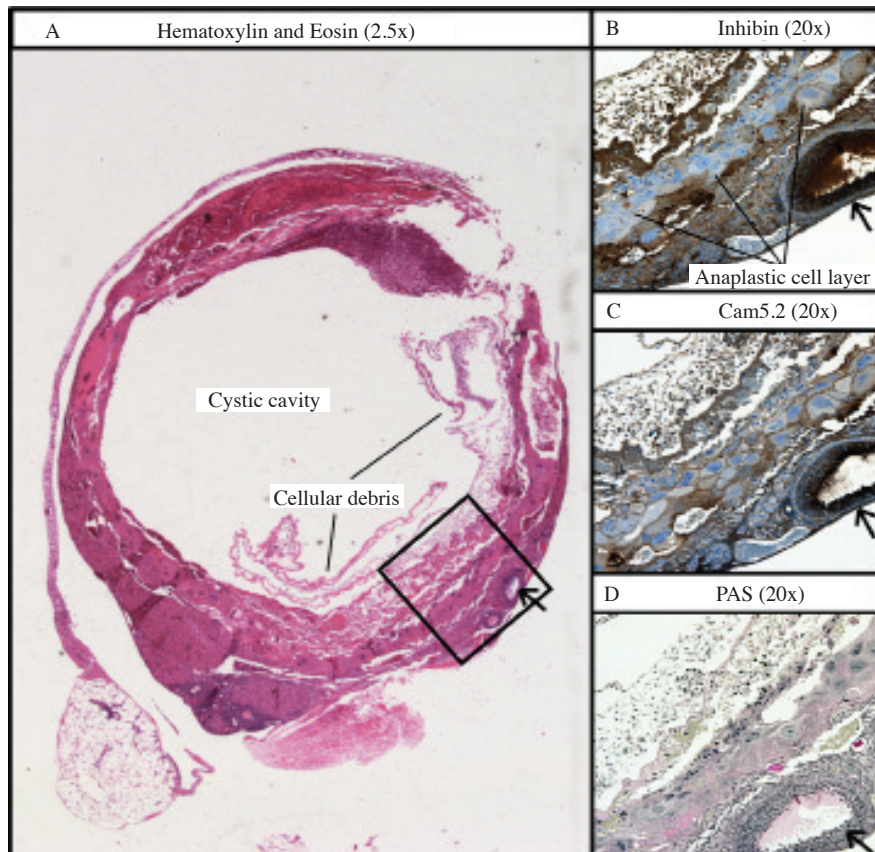


Figure 13:

Rare cancerous ovarian cysts were found in *Cecr2*^{Gt45Bic} FVB/N homozygous females

Abnormally large ovaries were found in *Cecr2*^{Gt45Bic} FVB/N homozygous with a dark red complexion from hemorrhaging vascular sinuses (arrows) (n=3). Cross-section of an affected ovary with hematoxylin and eosin staining had a large central cystic cavity with cellular debris and infiltrating neutrophils within the central surface (A, magnification 25x). Inhibin immunohistochemistry was used to differentiate ovarian sex cord-stromal tumours (B, magnification 200x), anti-Cam5.2 can was used to identify germ cell tumours (C, magnification 200x), and the Periodic acid-Schiff (PAS) stain (D, magnification 200x) demonstrated the presence of glycogen in various carcinomas. The assessment characterized the presumptive tumour as either an unusual dysgerminoma or atypical teratoma.

Cecr2^{Gt45Bic} BALB/c homozygous male testes were ~77% (U-test p=2.5E-05) of wildtype mass and ~80% (U-test p=1.4E-04) of the expected wildtype testis-to-body ratio. None of the males used in this study had breeding experience as all were housed with weaned brothers. Due to this restriction, the testis weight could not be directly compared to the partial-penetrance of males showing reduced litter size found in Thompson et al. (2012).

The testis is one of the only organs to show strong adult *Cecr2* expression (Thompson et al., 2011). Thompson et al. (2011) found no differences in testis histology or sperm count, motility, or morphology, despite a variable penetrance of reduced litter size among some animals. This could indicate a fertilization defect due to chromosomal or packaging defects. The reduction in testes mass does not appear to affect sperm output. Until the base cause of the fertilization defect and reduced testes mass is found, it is not yet possible to determine whether the reduced size causes or is related to the fertility issues.

3.4.4: Rare cases of hemorrhagic ovarian cysts developed in *Cecr2*^{Gt45Bic} FVB/N homozygous females

During the necropsy of *Cecr2*^{Gt45Bic} FVB/N homozygous females, three incidents (n=3/66) of hemorrhagic cystic ovaries were found. In each case, the abnormality presented as a unilateral hemorrhagic ovary approximately three times normal size and with a chocolate-brown colouration. Histopathology performed by pathologist Dr. Nation assigned tentative identification as an atypical dysgerminoma, a type of germ cell tumour. The structure of the affected ovary showed a single large cyst with limited ovarian tissue compressed to the edges (Figure 13.A). Abnormal cells within the cyst wall were anaplastic with huge nuclei and nucleoli with a large cytoplasmic volume that was stippled or finely vacuolated (Figure 13.B-D). Degenerated cellular debris and the occasional infiltrating neutrophil made up the inner surface of the cyst. The hemorrhaging occurred from irregular vascular sinuses around the cyst (Figure 13, arrows). The size of the cysts accompanied by their dark, contrasting colour would not be easily overlooked during routine embryo collections. No cases of these cysts were noted during the dissection of wildtype FVB/N females among members of the McDermid laboratory, nor does such a phenotype appear on the Jackson Laboratory strain descriptions of the FVB/N line. At a frequency of ~3/66 individuals, the defect may represent an independent aberration or cancer. However, with three similar cases in mutants and none found in wildtype mice, the cystic ovaries should not be discounted as a potential *Cecr2* mutant phenotype.

The samples were sent on to Dr. Russell for further analysis of the presumptive tumour. Dr. Russell performed the Inhibin (Figure 13.B), Cam5.2 (Figure 13.C), and Periodic acid-Schiff (PAS) (Figure 13.D) staining. Dr. Russell's initial diagnosis was ectopic pregnancy of the ovary; however, the female examined had never been bred or housed with males following weaning. The sample originates from a female housed with sister littermates, all of which were confirmed female during culling and dissection. Dr. Russell was unable

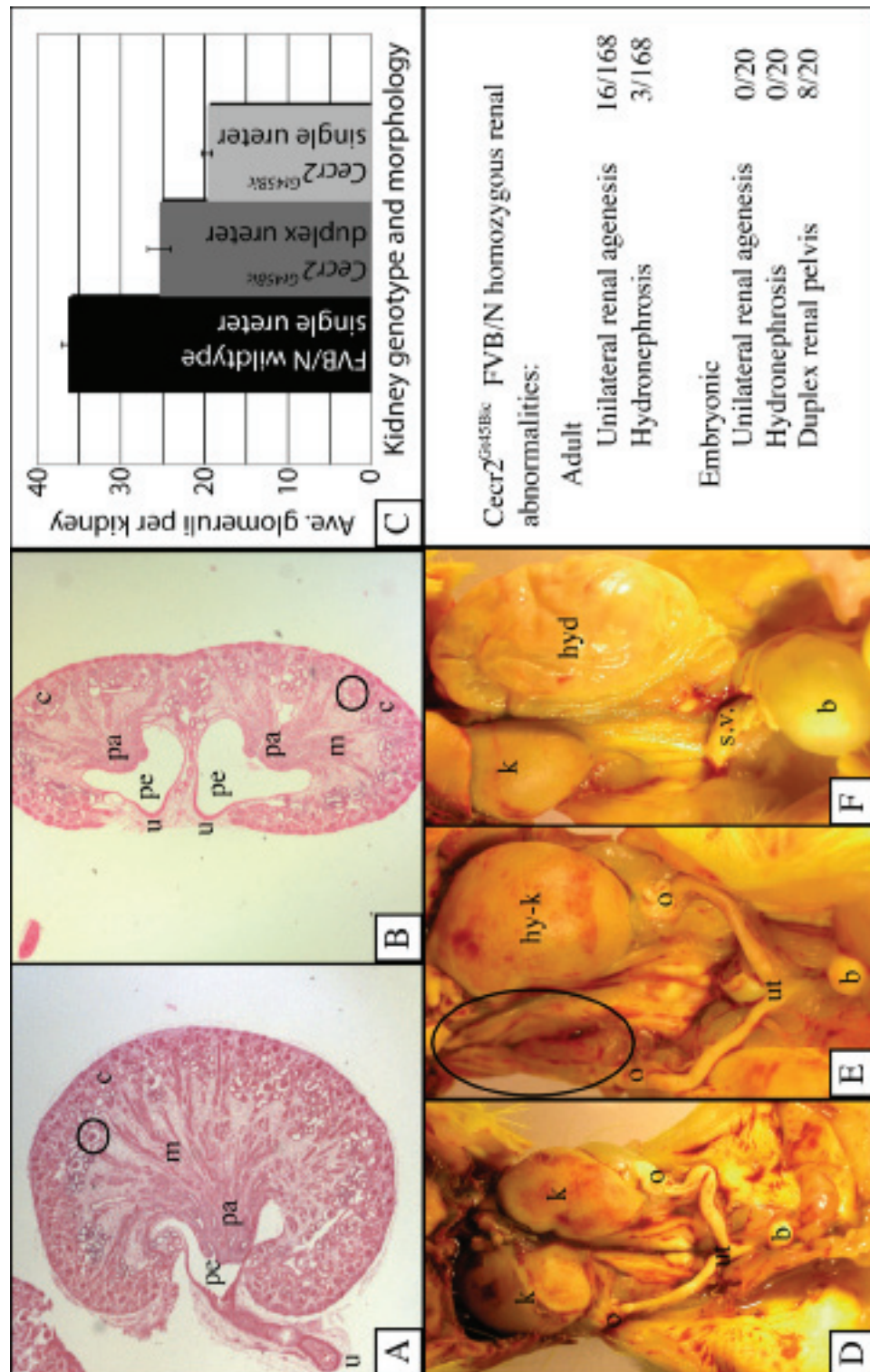


Figure 14:
Congenital abnormalitie of the kidney and urinary tract manifested in
***Cecr2^{Gt45Bic}* FVB/N homozygotes.**

(A-B, magnification 25x) Embryonic Theiler stage 24 (16.5dpc) wildtype (A) and *Cecr2^{Gt45Bic}* FVB/N homozygous (B) kidney histology with eosin staining. Wildtype FVB/N kidneys had normal renal cortex, medulla, renal pelvis, and ureter morphology as expected (A). *Cecr2^{Gt45Bic}* FVB/N homozygotes showed 40% penetrance of duplex kidneys with separate renal pelvis structures and fused cortex (duplex kidney, B) (c=cortex, m=medulla, pa=papilla, pe=pelvis, u=ureter). Both duplex and single-ureter *Cecr2^{Gt45Bic}* FVB/N homozygous kidneys were generally smaller than wildtype kidneys. The reduction in size at TS24 was quantified through the assessment of glomeruli number as these represent the functional units of kidney filtration (C) (circles highlight example glomeruli). *Cecr2^{Gt45Bic}* FVB/N homozygous duplex kidneys possessed 70% of the wildtype number of forming glomeruli (n=4, p=2.5e-06), while single-ureter *Cecr2^{Gt45Bic}* FVB/N homozygous kidneys had ~50% of wildtype levels (n=24, p=2.4e-33). (D-F, magnification variable) Necropsy of adult abdomens showed a range of *Cecr2^{Gt45Bic}* FVB/N homozygotes adult defects. Wildtype FVB/N abdomens from diaphragm to bladder had no abnormal phenotypes (D). Adult *Cecr2^{Gt45Bic}* FVB/N homozygous mice demonstrated unilateral agenesis of a kidney (n=16/168, circled region in E). The remaining kidney in these samples was hypertrophic (E). *Cecr2^{Gt45Bic}* FVB/N homozygous animals occasionally showed extreme unilateral hydronephrosis and possible distention of the bladder (F). The fluid-filled kidney remnant ruptured during dissection and appears here deflated (b=bladder, hyd=hydronephrosis, hy-k=hypertrophc kidney, k=kidney, o=ovary, s.v.=seminal vesicle, ut=uterus).

to classify the cause of the ovary cyst, and characterized the abnormal cells as perhaps an unusual teratoma. The cellular and cystic ovary phenotypes presented by *Cecr2*^{Gt45Bic} FVB/N homozygous could not be classified and may represent a novel germline cancer.

These cases were the first to associate *Cecr2* with ovary development and the first to link CECR2 function with cancerous cells. As the phenotype remains pathologically unclassified, we do not know whether the abnormal germline cells brought about the eventual cyst, or whether a structural cystic defect stressed surrounding cells causing the abnormal cellular morphologies. The cysts themselves were large with a deeply contrasting colour to normal ovaries and so are not likely to be under-reported in our mice. Abnormal ovarian cells, without the cyst manifestation, within the *Cecr2* mutant population could have been overlooked. Detailed histological examinations of non-cystic ovaries were not performed routinely. The dataset may be biased toward *Cecr2*^{Gt45Bic} FVB/N females by the embryonic lethality of exencephaly and midline clefts, but if females of *Cecr2*^{Gt45Bic} BALB/c or the *Cecr2*^{tm1.1Hemc} mutation are available, they could be screened.

3.4.5: Congenital abnormalities of the kidney and urinary tract were found in *Cecr2*^{Gt45Bic} FVB/N homozygous animals

Further phenotypic analysis of *Cecr2*^{Gt45Bic} homozygotes in the FVB/N background revealed congenital renal defects. Whereas FVB/N kidneys examined at TS24 appear morphologically normal (Figure 14.A), TS24 fetal kidneys of *Cecr2*^{Gt45Bic} FVB/N homozygous embryos showed 40% (8/20) possessed duplex kidneys (Figure 14.B) with two distinct renal pelvi leading to separate ureters. Despite the duplication of structure, the duplex kidney sections appeared visually smaller in area on histological cross-section than kidneys of wildtype FVB/N age-matched animals. Single-ureter *Cecr2*^{Gt45Bic} FVB/N homozygous kidneys appeared smaller than their duplex counterparts.

The reduced size of the TS24 *Cecr2*^{Gt45Bic} FVB/N homozygous kidneys correlated with a reduction in glomeruli numbers identified during histology. Glomeruli numbers were assessed on histological slides by taking the average number of glomeruli found per section across three different sections per kidney, each showing a central cross-section that included ureter, pelvis, medulla, and cortex tissues. Wildtype kidneys (n=25) averaged 36.3±0.8 glomeruli per kidney cross-section. Single-ureter *Cecr2*^{Gt45Bic} FVB/N homozygous kidneys (n=24) averaged 19.7±0.6 glomeruli while the duplex *Cecr2*^{Gt45Bic} kidneys (n=4) averaged 25±1 across comparable cross-sections. The *Cecr2*^{Gt45Bic} FVB/N homozygous kidneys possessed only 54% wildtype glomeruli normally present (TTEST p= 2.4e-33) and even in a duplex kidney the glomeruli numbers found were at 70% of wildtype levels (TTEST p= 2.5e-06). Therefore, both duplex and single-ureter *Cecr2*^{Gt45Bic} FVB/N homozygous kidneys showed a significant reduction in the number of forming glomeruli in the TS24 kidney (Figure 14.C). Examinations of hematoxylin and eosin stained sections has not identified a specific embryonic tissue loss or abnormal tubule structures beyond the duplex state. The renal pelvis

volume of TS24 *Cecr2*^{Gt45Bic} FVB/N homozygous samples appeared distended, but volumetric comparisons were not done.

Adult *Cecr2*^{Gt45Bic} FVB/N homozygotes were viable and fertile; however, kidneys from adult *Cecr2*^{Gt45Bic} FVB/N homozygotes occasionally were found with unilateral agenesis (loss of one kidney) with compensatory hypertrophy in the other kidney (Figure 14.E). The occurrence of compensatory hypertrophic growth suggests that CECR2 is not necessary for the signaling or response of the repair pathway (Nagasu et al., 2012), and may only be active during initial organogenesis. Surgical unilateral nephrectomy of *Cecr2*^{Gt45Bic} heterozygous mice could confirm whether CECR2 is re-activated and expressed during the compensatory process. Among adults, 9.5% (n=16/168) of *Cecr2*^{Gt45Bic} FVB/N homozygous animals possessed only a single kidney. No remnant kidney structures or ureteric tissue could be located in these cases during dissection or histology of the excised region. Unilateral agenesis was not seen in the embryos surveyed; however, with low penetrance of the condition, the defect may not have presented in the smaller sample set. Wildtype FVB/N animals do not show unilateral renal agenesis (Jackson Laboratories, <http://jaxmice.jax.org/strain/001800.html>, 2012)

Severe hydronephrosis presented in 3 of 168 *Cecr2*^{Gt45Bic} FVB/N homozygous adult animals (Figure 14.F). Wildtype FVB/N examined during this trial (n=54) as well as all other FVB/N adult animals examined in the McDermid laboratory during routine dissections have not been found to spontaneously present with advanced hydronephrosis, which would be obvious during any dissection in its later stages. All cases were unilateral and affected animals did not show outward signs of distress. Distortions caused by the affected kidneys were palpable and visible along the flank and abdomen. Histological examination of a breeding aged female's hydronephrotic kidney by pathologist Dr. Nation found a loss of all medullar and internal structures with a thin and stretched cortex containing crushed glomeruli encasing the single large cyst (personal communications 2010). An incident of full hydronephrosis with distention and structural loss was found in a three-week-old pup. Hydronephrosis is associated with duplex kidneys and multiple ureters (Kume et al., 2000; Mackie and Stephens, 1975; Miyazaki et al., 2000). Mouse models with the additional and ectopic ureter branches near or within the bladder are prone to bladder backpressure (Kume et al., 2000; Miyazaki et al., 2000). The duplicated ureters also have smaller lumens than single-ureters, which along with bladder pressure from ectopic sites both increase the risk of hydroureter or hydronephrosis. The rarity of hydronephrotic kidneys among *Cecr2* homozygous mutants hampers efforts to confirm whether blockages or ectopic positioning is the cause. The hydronephrosis may be an indirect consequence of backpressure or blockage predisposed by the presence of duplex kidneys and double ureters among the *Cecr2* mutations.

Although the *Cecr2*^{Gt45Bic} FVB/N homozygous embryonic kidney samples indicated a reduction in the size and glomeruli number of the developing metanephric kidney, the *Cecr2*^{Gt45Bic} FVB/N homozygous adult kidney samples

showed no difference in weight averages compared to FVB/N (Table 7). Hypertrophy of the remaining *Cecr2*^{Gt45Bic} FVB/N homozygous adult kidney in cases of unilateral agenesis accounted for the largest of the samples. Mann-Whitney U-tests did not show a significant change in kidney weight between *Cecr2*^{Gt45Bic} FVB/N homozygous and wildtype kidneys. Wildtype 6 to 8-week male kidneys (n=24) weighed 203±7 mg while the 8-week *Cecr2*^{Gt45Bic} FVB/N homozygous kidneys (n=26) weighed 210±10 mg. Female kidneys weights were 139±2 mg for wildtype and 140±6 mg for *Cecr2*^{Gt45Bic} FVB/N. This suggested the adult *Cecr2*^{Gt45Bic} FVB/N homozygous kidneys were able to continue growth and match wildtype kidneys in terms of overall kidney mass. It must be noted that this data was collected prior to the discovery of the duplex kidney state, and thus the average weight does not distinguish between single-ureter and duplex kidneys in *Cecr2*^{Gt45Bic} FVB/N homozygotes. *Cecr2* homozygous mutant duplex kidneys were larger than *Cecr2* homozygous mutant single-ureter kidneys and could be masking a single-ureter size reduction when all samples are averaged.

The sum of the renal defects indicated that *Cecr2*^{Gt45Bic} FVB/N homozygous animals develop smaller metanephric kidneys embryonically, with significantly fewer glomeruli. Whether through compensatory hypertrophy or a masking effect of increased duplex kidney size, the mutants had comparable wildtype kidney mass by 6 to 8 weeks after birth - excluding cases of agenesis or hydronephrosis. The *Cecr2*^{Gt45Bic} FVB/N homozygous kidneys showed structural congenital defects of complete agenesis or duplex kidneys, with hydronephrosis occasionally manifesting. However, they do not manifest polycystic kidney disease. This classified *Cecr2* mutations within the category of Congenital Abnormalities of the Kidney and Urinary Tract (CAKUT) (Miyazaki and Ichikawa, 2003; Nakanishi and Yoshikawa, 2003; Song and Yosypiv, 2011) with a unique set of characteristics not consistent with CE or PCP-like defects.

3.5: Testing the hypothesis that a novel *Cecr2*^{tm1.1Hemc} deletion allele would show increased severity and range of *Cecr2*-mutant aberrant phenotypes

Splicing around the gene-trap in *Cecr2*^{Gt45Bic} mutant tissue was discovered during qRT-PCR testing where ~10-20% of wildtype *Cecr2* transcript levels were expressed of the region beyond the genetrapp (Tassone, personal communications 2008). Steps were then taken to produce a new mutant allele for *Cecr2*. I hypothesized a homozygous null mutation of *Cecr2* would show increased penetrance, severity, and range of aberrant phenotypes compared to the *Cecr2*^{Gt45Bic} mutation. The novel mutation confirmed all of these predictions.

3.5.1: *Cecr2*^{tm1.1Hemc} BALB/c embryos showed an increased penetrance of exencephaly compared to the *Cecr2*^{Gt45Bic} BALB/c line

Each of the DEL1-DEL4 *Cecr2*^{tm1.1Hemc} lines was analyzed for embryonic defects early in their lineages (N3-4 BALB/c) through heterozygous crosses. The prominent anomaly present was exencephaly with an absent cranium dome, exposed brain tissue, and an aberrant morphology consistent with a failure to close the cranial neural tube. Open eyelids were present in exencephalic animals

but did not manifest independently. The *Cecr2^{tm1.1Hemc}* BALB/c homozygous exencephalic and open eyelid morphologies were the equivalent of the *Cecr2^{Gt45Bic}* BALB/c homozygous abnormalities.

Exencephaly was confirmed in the homozygotes of DEL1 (n=2/2), DEL2 (n=15/15), and DEL4 (n=3/4). One of the DEL4 exencephalic mutants displayed midline facial clefts, a phenotype more commonly found in the *Cecr2^{tm1.1Hemc}* FVB/N homozygotes (see Section 3.5.2). This was the only midline cleft found in the *Cecr2^{tm1.1Hemc}* BALB/c background (n=1/66, combining all lines). The DEL3 homozygous embryos were not characterized as the line failed to generate enough heterozygotes.

The DEL2 lineage contained a larger embryonic sample set due to a larger availability of heterozygous females. Following the initial confirmation that all four germ-line transmissions of *Cecr2^{tm1.1Hemc}* showed identical deletions as scored by PCR genotyping, the DEL2 line was selected as the representative *Cecr2^{tm1.1Hemc}* mutation and the other three lines were culled. All future data and references to the *Cecr2^{tm1.1Hemc}* mutation refer to the DEL2 lineage.

The penetrance of exencephaly in the *Cecr2^{tm1.1Hemc}* BALB/c background (generation N3-4) was higher than the penetrance published for *Cecr2^{Gt45Bic}* by Banting et al. (2005) and later confirmed by Kooistra et al. (2011). *Cecr2^{tm1.1Hemc}* BALB/c embryos presented with an open cranial neural tube in 97% of embryos (n=58/60). Among litters where all embryos were genotyped, the number of wildtype (n=62), heterozygous (n=101), and homozygous embryos (n=51) *Cecr2^{tm1.1Hemc}* BALB/c embryos did not show deviation from the expected Mendelian ratios (Chi Squared p>0.05). The new *Cecr2^{tm1.1Hemc}* BALB/c allele did not show a significant reduction in recovered homozygous embryos (TS13-26). The *Cecr2^{tm1.1Hemc}* BALB/c penetrance of exencephaly was significantly higher than *Cecr2^{Gt45Bic}* BALB/c allele (Chi Squared p=0.001). The overall type of neural tube defects in *Cecr2^{tm1.1Hemc}* BALB/c and the morphology of the defects were similar to *Cecr2^{Gt45Bic}* BALB/c neural tube defects (Banting et al., 2005). The only exception to this was a single (n=1/66) case of midline facial cleft found in the DEL4 line. As the *Cecr2^{tm1.1Hemc}* BALB/c line approaches congenic BALB/c, I predict the penetrance of exencephaly will effectively reach 100% and the midline clefts will no longer manifest.

3.5.2: The *Cecr2^{tm1.1Hemc}* FVB/N homozygous embryos partially overcame FVB/N strain resistance modifiers and manifested both the neural tube defects exencephaly and midline facial clefts

The neural tube defect penetrance of the *Cecr2^{Gt45Bic}* gene-trap mutation was highly dependent on the background genetic strain (Banting et al., 2005; Davidson et al., 2007; Kooistra et al., 2011). I crossed the *Cecr2^{tm1.1Hemc}* deletion mutation onto the NTD-resistant FVB/N strain to assess whether the more severe deletion would still show strain specificity. *Cecr2^{tm1.1Hemc}* FVB/N homozygotes were assessed following 3-4 backcrosses onto the FVB/N strain. The penetrance of exencephaly in the homozygous *Cecr2^{tm1.1Hemc}* FVB/N embryos was 31% (n=11/35), compared to <1% with the *Cecr2^{Gt45Bic}* mutation on that background

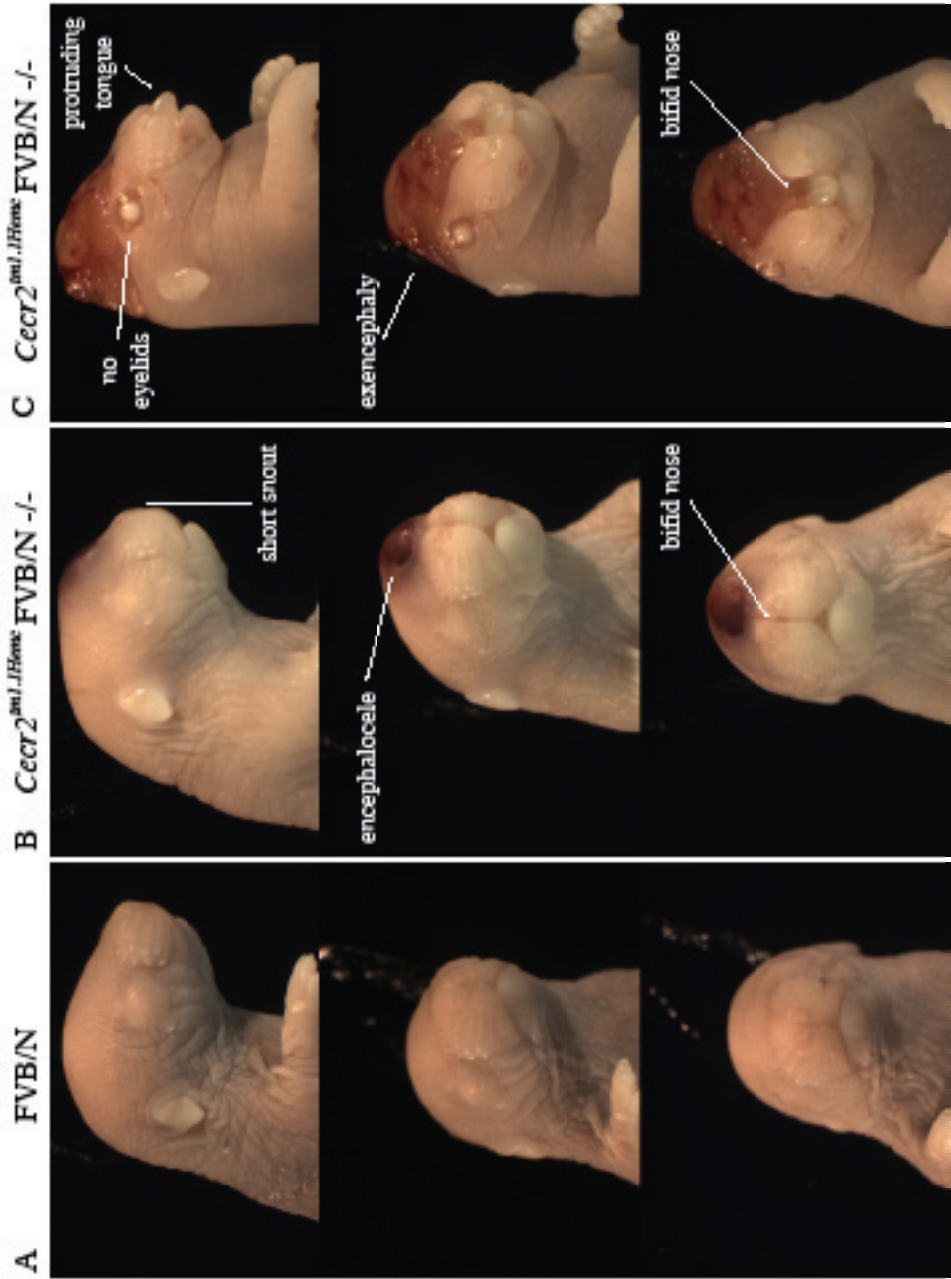


Figure 15:

***Cecr2*^{tm1.1Hemc} FVB/N homozygous pups developed exencephaly and midline facial clefts**

(A-C) Cranial morphology of FVB/N and *Cecr2*^{tm1.1Hemc} FVB/N TS 26 (18.5dpc) embryos displayed aberrant phenotype among homozygous mutants. Wildtype FVB/N samples showed the expected craniofacial morphology (A). At 3-4 FVB/N backcross generations, 11% (n=4/35) of *Cecr2*^{tm1.1Hemc} FVB/N homozygous embryos developed midline facial clefts. Some clefts appeared independently of exencephaly (B) with bifid noses and maxilla, and with encephaloceles as shown in the figure. A partially overlapping group of 31% (n=11/35) of *Cecr2*^{tm1.1Hemc} FVB/N homozygotes also manifested exencephaly (C), showing the largest midline displacement (n=7/35 show exencephaly alone, data not shown). Exencephalic embryos lacked eyelids, an association common to *Cecr2*^{Gt45Bic} and *Cecr2*^{tm1.1Hemc} BALB/c homozygous exencephalic cases. The snouts of *Cecr2*^{tm1.1Hemc} FVB/N pups with midline defects appeared shorter than wildtype littermates and in severe cases the tongue protruded past the jaw. The mandibles and tongues did not show evidence of bifid clefts.

(generation N5-6, 0/45, Banting et al., 2005).

As the new line was also predicted to show an increased range of phenotypes, the embryos were examined for additional defects. Midline facial clefts appeared in the *Cecr2^{tm1.1Hemc}* FVB/N embryos (11%, n=4/35), as well as in conjunction with exencephaly or with forebrain encephaloceles (Figure 15.B-G). The clefts were classified as an extreme Tessier 0 or 14 midline cleft showing hypertelorism with bifid nose and associated meningocele/encephaloceles (Tessier, 1976). As with exencephaly, no pups with midline clefts survived birth and remains were likely cannibalized. The single midline cleft (see Section 3.5.1) in the *Cecr2^{tm1.1Hemc}* BALB/c appeared very early in the BALB/c backcrosses (after 3 BALB/c backcrosses) and no further midline clefts were found among *Cecr2^{tm1.1Hemc}* BALB/c mutants in later crosses (after 4-6 BALB/c backcrosses). Therefore, the penetrance of midline facial clefts appeared strain dependent. The inverse relationship found between exencephaly and midline clefts is similar to the strain penetrance of the *Ski* mouse mutation (Colmenares et al., 2002). Disruption of *Ski* results in 83% exencephaly and 0% facial clefting on a 129P2 strain background, and 5–6% exencephaly and 87–93% facial clefting on a C57BL/6J strain background (Colmenares et al., 2002). The *Ski* mutation, and now the *Cecr2* data, show strain modifiers influence midline cleft development with an inverse relationship with exencephaly.

In addition, the *Cecr2^{tm1.1Hemc}* FVB/N homozygous state was often lethal even in the absence of clefts or neural tube defects. There were 20 wildtype, 39 heterozygous, and 5 homozygous mutant pups weaned from heterozygous *Cecr2^{tm1.1Hemc}* FVB/N crosses. This significantly deviated from the expected Mendelian ratio (Chi-squared p=0.0064). If we take into account the ~20% of pups lost at birth to exencephaly or midline facial clefts at this backcross, the ratios of surviving pups suggested over half of all non-exencephalic/non-midline cleft pups die between birth and weaning. This is supported by the abundance of homozygous pups found dead within the first two days after birth (Rasmussen, personal communication, 2010). A necropsy performed by pathologist Dr. Nation noted a failure to fully inflate lungs in one *Cecr2^{tm1.1Hemc}* FVB/N homozygous pup found dead. However, no other morphological defects were noted during necropsy and respiratory failure was not thought to account for the pups surviving 36 hours before death.

3.5.3: Inner ear analyses confirmed the stereocilia alignment defects were present in a *Cecr2^{tm1.1Hemc}* BALB/c mutant background

Dawe et al. (2011) found cochlear defects among *Cecr2^{Gt45Bic}* BALB/c TS26 pups; which included smaller inner ears, shorter and wider cochlear ducts, extranumerary stereocilia hair cells, and increased misalignment of the stereocilia cells. These studies added to the growing body of evidence that planar cell polarity developmental pathways may be disrupted in the *Cecr2* mutants. Concurrent with the *Cecr2^{Gt45Bic}* study, my analysis of the *Cecr2^{tm1.1Hemc}* BALB/c mutation tested whether a similar range of inner ear defects were present in the new line at a greater penetrance or severity as predicted. The *Cecr2^{tm1.1Hemc}*

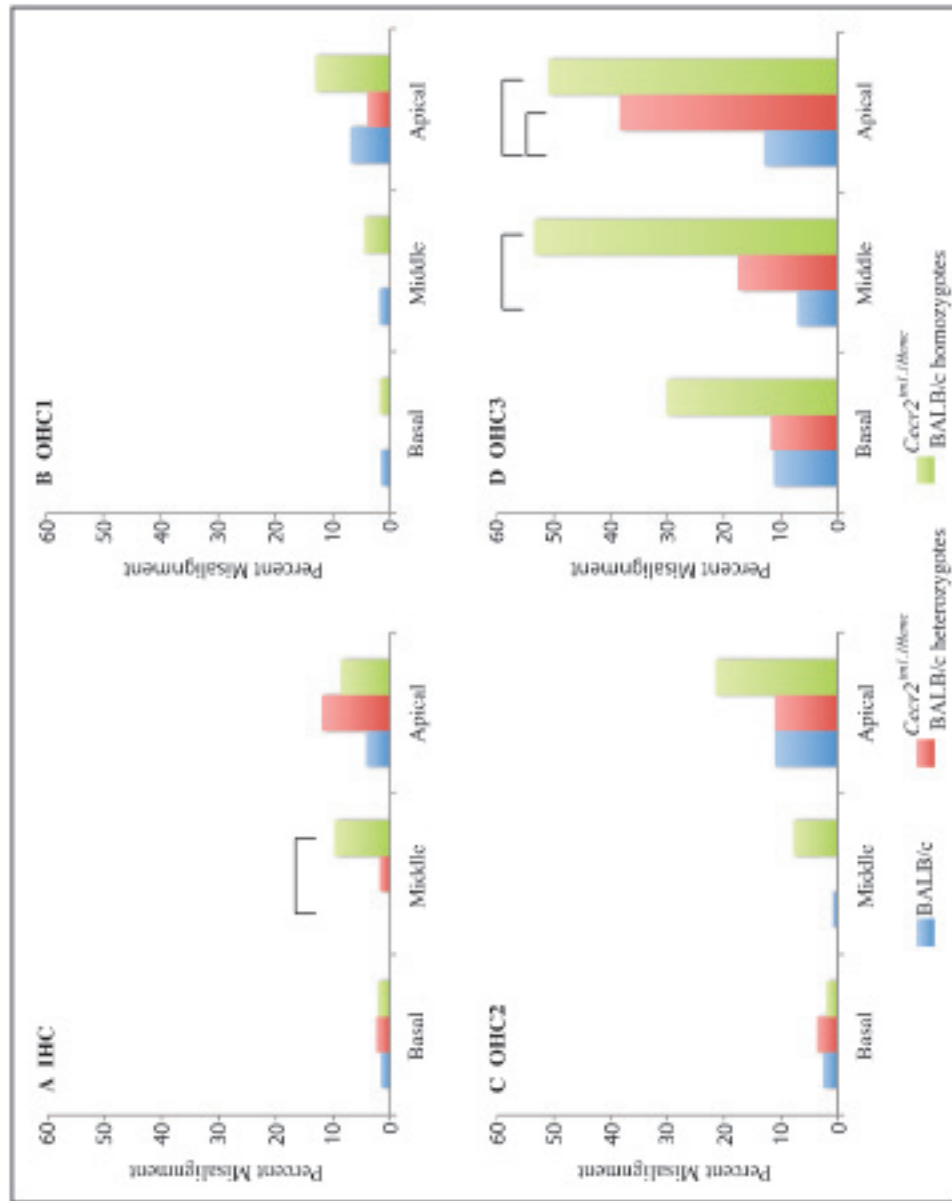


Figure 16:

***Cecr2*^{tm1.1Hemc} BALB/c homozygous and heterozygous embryos developed stereocilia polarity defects**

The mispolarization of stereocilia was determined based on a 30-degree threshold set by Montcouquiol et al. (2003). Wildtype percent mispolarization is represented by blue, heterozygous *Cecr2*^{tm1.1Hemc} BALB/c mispolarization is red, and the homozygous *Cecr2*^{tm1.1Hemc} BALB/c samples are shown as green bars. The data are presented according to each stereocilia cell layer. The overall data trend showed homozygous stereocilia were highly disorganized in the outer hair layers (OHC), an effect that was less pronounced within the inner cell layers (IHC). Heterozygous trends appeared partially affected, falling between the wildtype and mutant samples. However, only the most extreme changes appeared significant within the dataset. Significantly different levels are represented by encompassing brackets ($p < 0.05$).

BALB/c phenotype confirmed the stereocilia defects were not due to a gain of function mutation due to the fusion protein, and that the mispolarization of the stereocilia were due to the loss of CECR2 activity.

Inner ears were dissected from exencephalic *Cecr2^{tm1.1Hemc}* BALB/c homozygotes (n=6), heterozygotes (n=5), and wildtype littermates (n=2). The wildtype values were added to the BALB/c wildtype collection available from the Dawe et al. (2011) *Cecr2^{Gt45Bic}* study. The cochlear ducts were recovered and incubated with Phalloidin and anti-acetylated tubulin to label the stereocilia. Confocal microscopy was used to image the stereocilia of the inner (IHC) and three outer hair cell (OHC) rows. Analyses were completed at the basal (5%), midway (50%) and apical (75%) points along the cochlear duct.

The stereocilia of *Cecr2^{tm1.1Hemc}* BALB/c homozygotes presented with misalignment defects. The percent of misalignment was consistent, but slightly lower, than the levels reported by Dawe et al. (2011) for *Cecr2^{Gt45Bic}* BALB/c. The angle of cell orientation was measured perpendicular to the row of basal pillar cells. The analysis was based upon the criteria established by Montcouquiol et al. (2003), where an orientation over 30 degrees variant from perpendicular was considered aberrant. The basal IHCs are the most structured and the closest to perpendicular alignment. The overall organization decreased towards the apical cochlea. Decreasing organization was present as well when progressing dorsally, with the OHC3 layer showing the greatest misalignment at all cochlear positions. The *Cecr2^{tm1.1Hemc}* BALB/c homozygous IHCs were misaligned in 2.3% (n=1/44) of cells at the basal cochlea, 9.9% (n=9/91) medially, and 8.7% (n=4/46) at the apical cochlea (Figure 16.A). Homozygous OHC1 showed 1.9% (n=1/52) misalignment basally, 4.7% (n=5/107) medially, and 13.1% (n=8/61) apically (Figure 16.B). OHC2 showed 2.0% (n=1/50) misalignment basally, 7.9% (n=9/114) medially, and 21.6% (n=11/51) apically (Figure 16.C). The outermost OHC3 later was misaligned in 30.2% (n=16/53) of basal cells, 53.5% (n=61/114) medially, and 51.0% (n=25/49) at the apical cochlea (Figure 16.D). The mutant stereocilia showed misalignment consistent with a defect in planar cell polarity, but they were not more severe than the *Cecr2^{Gt45Bic}* BALB/c as originally expected (Dawe et al., 2011).

Cecr2^{tm1.1Hemc} BALB/c homozygotes possessed an increased number of extranumerary hair cells. The IHC layer showed 0% (n=0/43) extra cells appearing beneath or outside of the structured line of cells at the basal cochlea, 4.3% (n=4/93) midway, and 9.3% (n=4/43) at the apical cochlea. Extranumerary outer hair cells appeared as duplicated cell rows inserted between the expected three structured rows of OHC layers and the surrounding supportive pillar cells. As both the stereocilia and pillar cells were duplicated in the partial rows, it was not possible to directly assign them to a given OHC row. Overall, there was an average of 1.3% (n=2/155) extra cells appearing beneath or outside of the structured rows of cells at the basal cochlea, 3.5% (n=11/318) midway, and 9.8% (n=15/153) at the apical tip. Thus, the misalignment data presented above under-reports the full nature of the misorganization as many of the extranumerary cells could not be assigned to a particular layer, and were also misaligned.

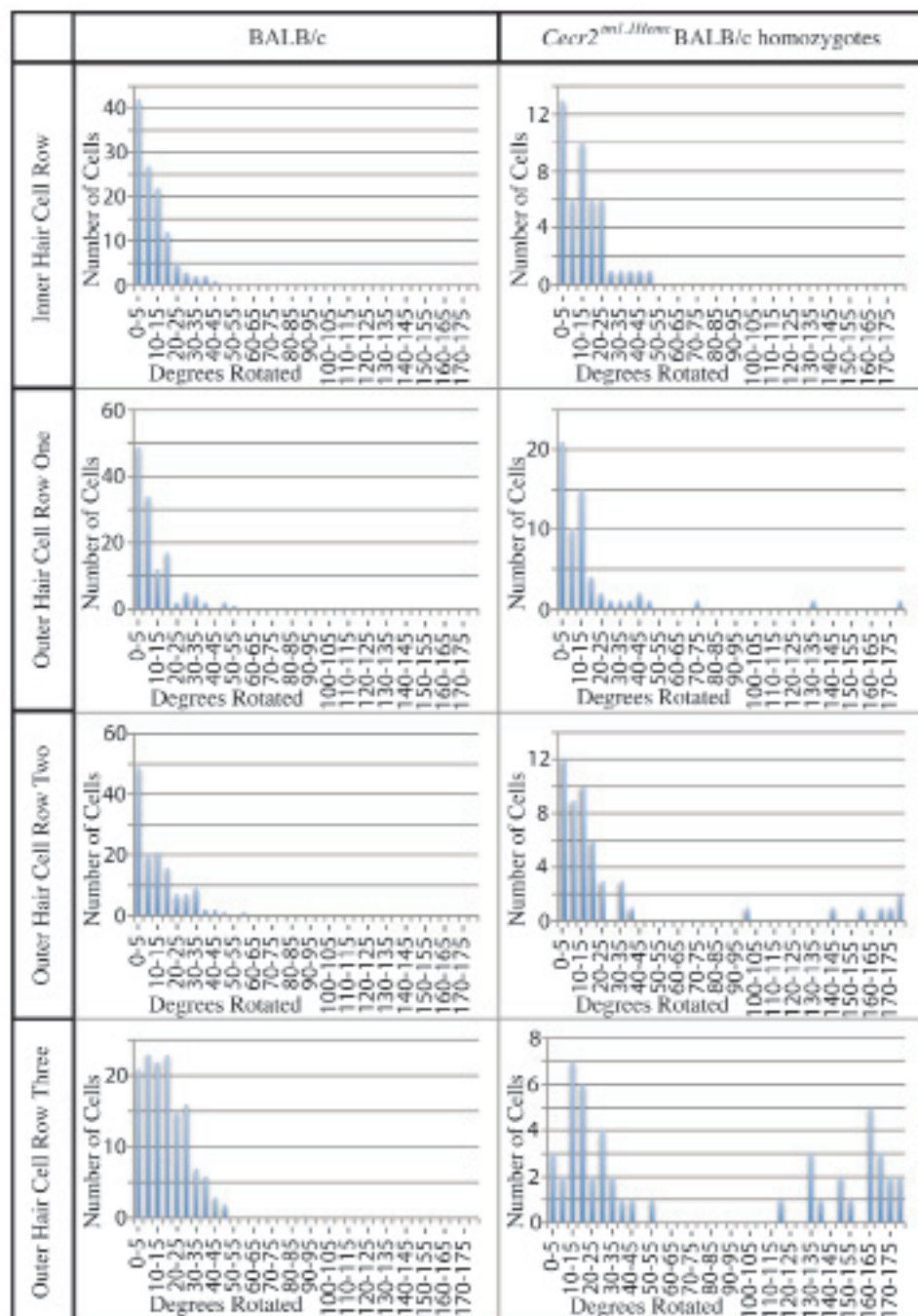


Figure 17:
***Cecr2*^{tm1.1Hemc} BALB/c homozygous and heterozygous stereocilia displayed an increase in angle variation**

Histograms of variance were plotted according to the degree a stereocilia cell had rotated away from perpendicular to the cell row. Wildtype samples had tight adherence to the midline with minimal variance and no angle exceeded 50-degrees. The outer hair cells showed an increased spread away from perpendicular but still did not exceed 50-degrees. The *Cecr2*^{tm1.1Hemc} homozygous inner hairs cells resembled a wildtype spread. The outer hair cells of mutants had increased variance, with multiple cells beyond the 50-degree wildtype extremes.

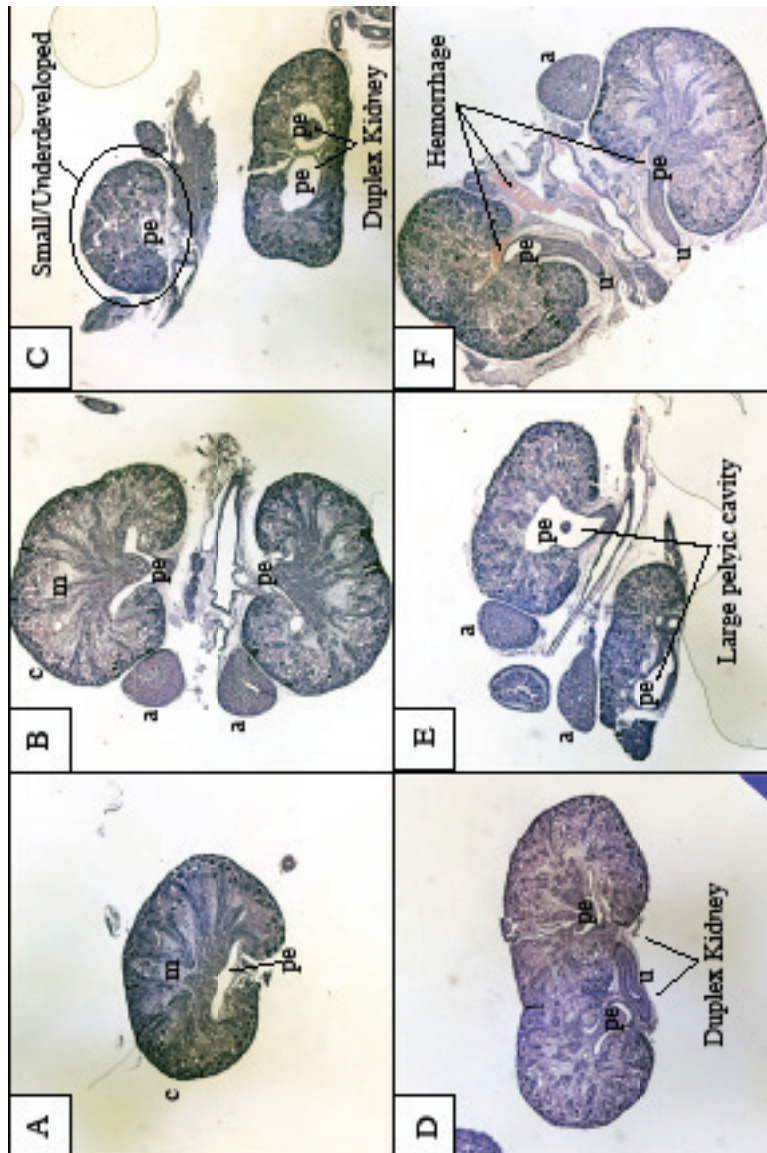


Figure 18:

***Cecr2*^{tm1.1Hemc} FVB/N homozygous embryos recapitulated the CAKUT phenotypes**

(A-F, magnification 25x) Theiler stage 24 *Cecr2*^{tm1.1Hemc} FVB/N homozygous metanephric kidneys indicate a range of defects. Kidneys were fixed in 10% formalin, sectioned to 8 μ m, and stained with hematoxylin and eosin. FVB/N littermates had the expected wildtype morphology (A) (a=adrenal gland, c=cortex, m=medulla, pe=pelvis, u=ureter). Among *Cecr2*^{tm1.1Hemc} FVB/N homozygotes, the mildest cases appeared unaffected, with wildtype size and morphology (B). Markedly smaller kidneys existed within the mutant samples although the size was variable (C). Duplex kidneys manifested at a similar penetrance to the *Cecr2*^{Gt45Bic} FVB/N samples (n=5/12) (C-D). A subset of mutant samples appeared to show enlarged or inflated pelvis lumens (E), although this remains subjective as it was not quantified. Extensive hemorrhaging of the renal region manifested in a quarter of mutant animals (n=3/12), both surrounding and within metanephric tissues (F). Wildtype FVB/N controls showed negligible size variance and have not been found with the aberrant phenotypes of *Cecr2*^{tm1.1Hemc} FVB/N kidneys.

The inner ears of heterozygous *Cecr2^{tm1.1Hemc}* BALB/c pups displayed the aberrant phenotypes associated with their homozygous littermates, but were less severity. The heterozygous IHCs showed 2.4% (n=1/41) misalignment basally, 1.9% (n=1/52) medially, and 12% (n=3/25) at the apical cochlea length (Figure 16.A). The OHC1 rows showed 0% (n=0/51) misalignment basally, 0% (n=0/56) medially, and 4% (n=1/25) apically (Figure 16.B). OHC2 showed 3.6% (n=2/55) misalignment basally, 0% (n=0/59) at 50%, and 11.1% (n=2/27) apically (Figure 16.C). The OHC3 cells were misaligned in 11.8% (n=6/51) basally, 17.5% (n=10/57) medially, and 38.5% (n=10/26) apically (Figure 16.D). The *Cecr2^{tm1.1Hemc}* BALB/c heterozygous stereocilia were rarely extranumerary. No extra OHC layers were located in the sample and a single extranumerary IHC (n=1/24) appeared in the apical cochlea.

Misalignment in wildtype BALB/c samples in the inner hair cells showed 1.7% (n=1/60) misalignment basally, 0% (n=0/95) medially, and 4.3% (n=5/116) at the apical cochlea length (Figure 16.A). OHC1 showed 0% (n=0/72) misalignment basally, 2.0% (n=2/102) medially, and 7.0% (n=9/128) apically (Figure 16.B). OHC2 showed 2.6% (n=2/76) misalignment basally, 0.9% (n=1/107) medially, and 11.1% (n=15/135) apically (Figure 16.C). The outermost OHC3 rows were misaligned in 11.3% (n=8/71) of cells basally, 7.1% (n=8/112) medially, and 13.0% (n=18/138) at apically (Figure 16.D). Wildtype samples had no indications of extranumerary cells or layers.

Overall, the homozygous stereocilia were significantly mispolarized compared to wildtype within IHC and OHC3 of the medial cochlea, and within OHC3 at the apical tip. Heterozygous animals were significantly different from wildtype only at the OHC3 layer of the apical cochlea. The data suggested a trend increasing toward the apical tip even when not statistically significant. When compared to the *Cecr2^{Gt45Bic}* BALB/c data presented by Dawe et al. (2011), the *Cecr2^{tm1.1Hemc}* BALB/c misalignment values were nearly half that expected. Although the OHC3 layers nearly matched at the midway and apical cochlea, *Cecr2^{tm1.1Hemc}* BALB/c stereocilia of the other layers and locations showed between 1/3 and 1/2 the *Cecr2^{Gt45Bic}* BALB/c percentage of misalignment. Thus the stereocilia were significantly disorganized among *Cecr2^{tm1.1Hemc}* BALB/c mutants, but not to the full degree expected compared to *Cecr2^{Gt45Bic}* homozygotes. At the time of the study, *Cecr2^{tm1.1Hemc}* had fewer BALB/c backcross generation compared to the gene-trap allele (N3-4 vs. congenic) and residual strain effects may account for the inner ear differences.

Although the 30-degree limit is a standard measure of stereocilia variance (Montcouquiol et al., 2003), it reduces the data to a binomial call of either aligned or misaligned. The data also can be presented as histograms (Figure 17) to visualize the full spread of variance. This mode was less amenable to statistical examination but better highlighted subtle shifts in the dataset. Wildtype samples showed a tight adherence to centered (0-degree) alignment with steep drops away from parallel. Heterozygous and homozygous samples at all stages showed a spread away from parallel (Figure 17). Whereas the maximum wildtype BALB/c misalignment was within 50 degrees of parallel, *Cecr2^{tm1.1Hemc}*

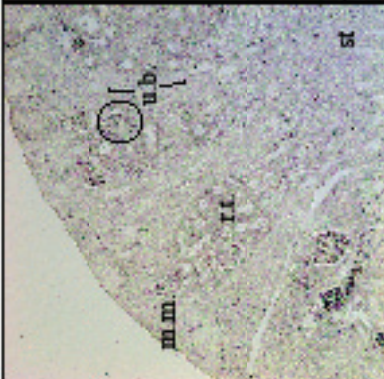
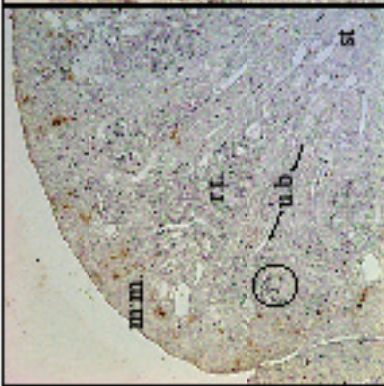
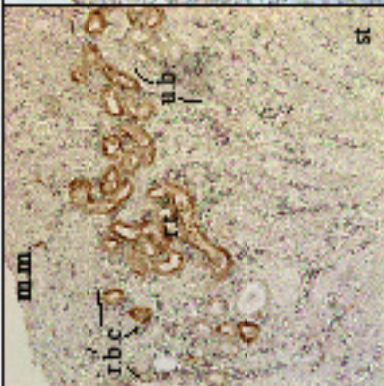
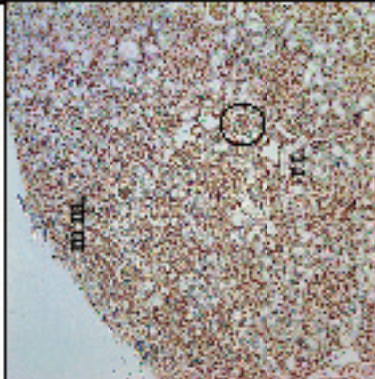
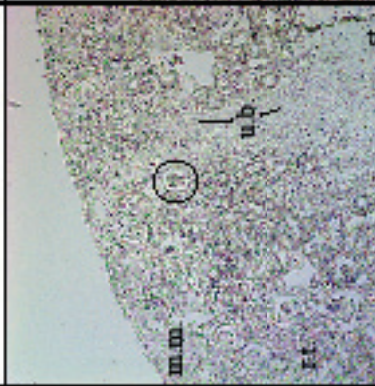
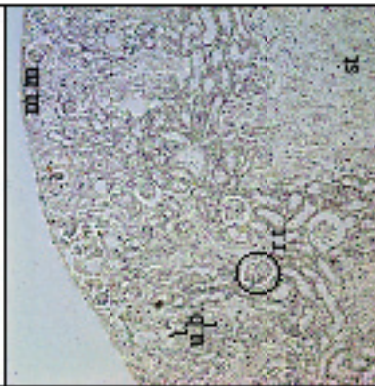
Minimum Apoptosis	<i>Cecr2</i> ^{tm1.1Hmc} homozygotes	Extensive Apoptosis
		
Positive Control	Negative Control	Wildtype FVB/N
		

Figure 19:

The neonatal renal cortex displayed abnormal apoptosis in *Cecr2^{tm1.1Hemc}* FVB/N homozygotes

Newborn (P0-2) kidneys from pups found dead are shown as sagittal sections stained with the DeadEnd colorimetric TUNEL system to detect apoptosis. Control samples were taken from wildtype FVB/N pups also found dead in order to better account for post-death effects on the renal tissues or apoptosis rates. Homozygous *Cecr2^{tm1.1Hemc}* FVB/N neonatal kidneys showed a range of apoptotic abnormalities. The least affected mutant samples (n=2/12) resembled wildtype FVB/N. Other samples (n=2/12) of *Cecr2^{tm1.1Hemc}* FVB/N homozygotes had sporadic apoptosis within the outer cortex metanephric mesenchymal (m.m.) cells clustered around cap mesenchyme, as well as occasional epithelial cells of the renal tubules (r.t.). Samples with hemorrhaging (n=4/12) in renal tissues showed extensive apoptosis of renal tubules in addition to the sporadic cortex apoptosis in mesenchymal cells. The excessive red blood cells (r.b.c.) were distinguishable in hemorrhaging samples. The most severe cases (n=4/12) indicated nearly all renal cells had undergone apoptosis. The severe mutant cases appeared only slightly less-affected than the positive control samples treated with blunt-end restriction enzyme to simulate apoptosis. The cause of death remains unknown in all cases. Wildtype FVB/N samples showed no signal from the negative control lacking the TUNEL enzymes, and fully treated wildtype FVB/N kidneys had minimal levels of cellular apoptosis within the outer cortex mesenchyme. In all cases, apoptotic staining appeared as brown colouration against the unstained tissue. Other structures indicated include mature glomeruli (example circled), stromal cells (st), and ureteric branches (u.b.). All images were magnified 200x.

BALB/c cells showed up to 180-degree rotations. The histograms and 30-degree calls consistently showed that the *Cecr2* mutants show mispolarization and disorganization of the inner ear stereocilia. These data support the hypothesis that CECR2 may regulate or effect the establishment of planar cell polarity.

3.5.4: Congenital abnormalities of the kidney and urinary tract were seen in *Cecr2*^{tm1.1Hemc} FVB/N homozygotes and recapitulated *Cecr2*^{Gt45Bic} FVB/N defects

The abnormal phenotypes associated with the *Cecr2*^{Gt45Bic} gene-trap allele were expected to also manifest in the *Cecr2*^{tm1.1Hemc} deletion mutation, but that the deletion allele may show increased penetrance and severity of defects. The *Cecr2*^{tm1.1Hemc} deletion mutation crossed onto the FVB/N strain recapitulated the duplex kidney and other renal phenotypes found in the *Cecr2*^{Gt45Bic} FVB/N line (generation N2-3, Figure 18). The general morphology of the duplex state (n=5/12) matched that first described in the *Cecr2*^{Gt45Bic} FVB/N mutation (Figure 18.C-D). Apparent among the embryonic kidney cross-sections was a variable reduction in TS24 *Cecr2*^{Gt45Bic} FVB/N homozygous kidney size (Figure 18.C), and an increase in renal pelvis distention (Figure 18.E). One quarter of samples showed signs of a renal aneurysm, with hemorrhaging blood surrounding and within the kidney (n=3/12) (Figure 18.F).

Hematoxylin and eosin staining of the P0-P2 homozygous kidneys of pups found dead (n=4) generally followed the description of that already stated for embryonic TS24 kidneys, which included duplex structures with two ureters (n=1/4) and an overall smaller size in cross-section. The small sample size of pups found dead prevented informative penetrance comparisons to embryonic samples. One of the neonatal samples found dead showed extensive hemorrhage and hyperemia, with red blood cells evident within nearly all the interstitial space of the kidney similar to the cases of TS24 renal hemorrhage. Before the discovery of renal hemorrhage, this phenotype was not actively searched for during other renal examinations. Although the hemorrhaging may be related or be the ultimate cause of death, a causative relationship was not established.

Hemorrhages were also associated with *Cecr2* homozygous mutant cases of exencephaly. Exencephalic pups dissected after TS22 were often pale compared to normal littermates, and the amniotic fluid contained blood. Hemorrhaging is generally associated with exencephaly (Matsumoto et al., 2002), and it is not established whether the two conditions are causally related in *Cecr2* mutant embryos. Gene ontology analysis (Table 2) of *Cecr2*-affected microarray shortlist candidates indicates that blood vessel development genes are overrepresented in the dataset (*Hand2*, *Sox17*, *Prrx1*, *Slit2*, and *Arhgap24*). Future work may find *Cecr2* mutant defects in vessel development, but vascular defects are unlikely to cause either the duplex kidney or open neural tube defects.

Table 8 : Urine analysis of <i>Cecr2^{tm1.1Hemc}</i> FVB/N homozygotes surviving to adulthood											
Mouse ID	Genotype	Sex	SG	pH	Nitrile	Protein	Glucose	Ketones	Urobilirubin	Bilirubin	Blood
45	-/-	Female	1.024	5.688	neg	neg	neg	neg	neg	neg	neg
55	-/-	Female	1.021	6.125	neg	neg	neg	neg	neg	neg	neg
58	-/-	Female	1.010	7.500	neg	neg	neg	neg	neg	neg	neg
377	+/+	Female	1.025	5.500	neg	neg	neg	neg	neg	neg/1	neg
378	+/+	Female	1.020	6.875	neg	neg	neg	neg	neg	neg	neg
379	+/+	Female	1.015	6.000	neg	neg	neg	neg	neg	neg	neg
51	-/-	Male	1.022	6.217	neg	1	neg	neg	neg	neg	neg/3
70	-/-	Male	1.021	6.220	neg	1	neg	neg	neg	neg	neg
71	+/+	Male	1.023	6.433	neg	1	neg	neg	neg	neg	neg
72	+/+	Male	1.025	6.410	neg	1	neg	neg	neg	neg	neg

Table 9 : Blood chemistry of <i>Cecr2^{tm1.1Hemc}</i> FVB/N homozygotes surviving to adulthood											
Mouse	Genotype	Sex	Urea	Creatine	Sodium	Potassium	Chloride	Bicarbonate	Anion Gap	Calcium	Phosphorus
ID			mmol/L	umol/L	mmol/L	mmol/L	mmol/L	mmol/L	mmol/L	mmol/L	mmol/L
55	-/-	Female	8.7	20	146	9.3	105	27	23.3	2.45	2.89
58	-/-	Female	6	13	146	10.3	108	26	22.3	2.47	2.52
377	+/+	Female	7	15	147	7.6	106	26	22.6	2.43	2.62
378	+/+	Female	7.6	15	148	7.4	107	25	23.4	2.45	2.8
379	+/+	Female	6.6	10	146	8.5	103	25	26.5	2.42	3.07
70	-/-	Male	10.4	18	149	8.8	106	28	23.8	2.48	2.62
71	+/+	Male	8.7	15	148	8.7	107	27	22.7	2.46	2.61
72	+/+	Male	10.7	12	148	8.1	106	27	23.1	2.45	2.85

3.5.5: *Cecr2*^{tm1.1Hemc} FVB/N homozygous neonates possessed extensive renal apoptosis

The discovery of neonatal death within 36 hours of birth among non-exencephalic *Cecr2*^{tm1.1Hemc} FVB/N homozygotes prompted an examination of the pups in order to uncover the cause of lethality. General necropsy could not identify a clear cause (Nation, personal communications 2009). As this strain was shown to develop a series of renal defects, I hypothesized that the renal defects may occasionally result in renal failure. I was unable to assess renal function by urine or blood markers from neonates and so turned to histological examination of kidneys from the mice found dead.

The apoptosis experiments were split initially between this researcher and a series of undergraduate projects that intended to expand the dataset and including TS24 embryonic renal samples. Unfortunately, not all aspects of the undergraduate projects were completed within the given timeframe. The following analysis was based upon a limited dataset and should be considered preliminary evidence.

Using TUNEL staining, a range of abnormal apoptotic patterns were detected in the *Cecr2*^{tm1.1Hemc} FVB/N neonatal kidney of pups found dead (n=6 animals, 12 kidneys) (Figure 19). One wildtype pup found dead indicated rare apoptotic cells occasionally found within scattered cells of the kidney cortex. Wildtype epithelial cells of the collecting ducts within the renal pelvis papilla contained many apoptotic cells (data not shown), a pattern shared in *Cecr2*^{tm1.1Hemc} FVB/N kidneys tested and a normal aspect of papilla remodeling (Kim et al., 1996). As the wildtype sample was found dead, it likely had undergone similar desiccation and time-dependent necrotic events. The mesenchymal apoptosis detected appeared specific to the *Cecr2*^{tm1.1Hemc} FVB/N homozygous pups and not a secondary factor of death. A range of apoptotic states was found in *Cecr2*^{tm1.1Hemc} FVB/N homozygous kidneys varying from complete apoptosis of all renal cells to sporadic apoptotic cells in the condensing mesenchyme surrounding what would be *Ret*-expressing leading branch epithelium (Figure 19). Two cases of extensive apoptosis within the forming convoluted tubules were found in addition to the sporadic mesenchyme apoptosis (Figure 19). The sample with the strongest tubule apoptosis was the same one that possessed extensive hemorrhage and hyperemia. The cause of such variation remains unknown, but overall demonstrated an apoptotic defect in *Cecr2*^{tm1.1Hemc} FVB/N homozygous neonatal kidneys.

3.5.6: *Cecr2*^{tm1.1Hemc} FVB/N homozygous adults had hyperkalemia, but all other renal markers are within normal ranges

Given the variety of renal defects discovered in *Cecr2*^{tm1.1Hemc} FVB/N animals, I hypothesized that the adult animals may show indications of renal disfunction. *Cecr2* was expressed throughout early nephron development, the key morphological structure necessary for filtration. I could not detect morphological abnormalities in the nephron structure, but standardized blood and urine veterinary tests could determine whether the nephrons were physiologically defective. These tests were tempered by two caveats. The first was that the rare

Table 10: Candidate transcripts with gene mutations showing phenotypes similar to <i>Cecr2</i> mutations						
Gene	Facial	NTDs	Otic	Renal	Gonadal	Phenotypic Score
<i>Cecr2</i>	1	1	1	1	1	5
<i>Eya1</i>	1	0	1	0.75	0.5	3.25
<i>Fgfr1</i>	1	0.5	0.75	1	0	3.25
<i>Foxc1</i>	0.5	0.5	0	1	1	3
<i>Mdm4</i>	0.75	1	0	1	0	2.75
<i>Fzd2</i>	0.75	1	1	0	0	2.75
<i>Tgfb2</i>	0.75	0.75	0	0.5	0.5	2.5
<i>Zeb2</i>	1	1	0	0	0.5	2.5
<i>Gata3</i>	0.5	0.5	0.5	0.5	0.25	2.25
<i>Dlx5</i>	0.75	1	0.5	0	0	2.25
<i>Pdgfc</i>	1	0.75	0	0.5	0	2.25
<i>Bmp2</i>	0.25	1	0.25	0	0.5	2
<i>Six1</i>	0.25	0.25	0.75	0.75	0	2
<i>Foxg1</i>	0.75	0.25	1	0	0	2
<i>Prrx1</i>	0.75	0.75	0.5	0	0	2
<i>Alx1</i>	1	1	0	0	0	2
<i>Pds5a</i>	1	0	0	1	0	2
<i>Luzp1</i>	1	0.75	0	0	0	1.75
<i>Ripk4</i>	0.25	0	0	0.75	0.75	1.75
<i>Abl2</i>	0	0.5	0.5	0	0.75	1.75
<i>Zfp148</i>	0	1	0	0	0.75	1.75
<i>Prkaca</i>	0	1	0	0.25	0.5	1.75
<i>Mecp2</i>	0.25	0.75	0.5	0	0.25	1.75
<i>Laspl</i>	0.75	0.75	0	0	0.25	1.75
<i>Col2a1</i>	0.5	0.5	0.5	0.25	0	1.75
<i>Tenc1</i>	0	0	0	0.75	0.75	1.5
<i>Rad23b</i>	0.75	0	0	0	0.75	1.5
<i>Smad1</i>	0.25	1	0	0	0.25	1.5
<i>Hectd1</i>	0.5	1	0	0	0	1.5
<i>Csnk2a1</i>	0.25	0.5	0.5	0	0	1.25
<i>Col4a1</i>	0	0	0	0.5	0.75	1.25
<i>Cdc73</i>	0	0	0	0.5	0.75	1.25
<i>Thbs1</i>	0	0	0	0.5	0.75	1.25
<i>Vps54</i>	0.25	0.25	0	0	0.75	1.25
<i>Mill</i>	0.25	0	0.25	0.25	0.5	1.25
<i>Eya4</i>	0.5	0	0.25	0	0.5	1.25
<i>Spnb2</i>	0.25	0.25	0.25	0.25	0.25	1.25
<i>Met</i>	0.5	0	0	0.75	0	1.25
<i>Akap13</i>	0.5	0	0	0.75	0	1.25
<i>Pcsk5</i>	0.5	0.25	0	0.5	0	1.25
<i>Jag1</i>	0	0.5	0.75	0	0	1.25
<i>Efnb1</i>	0.75	0.25	0.25	0	0	1.25
<i>Rere</i>	0.25	1	0	0	0	1.25
<i>Ikbkap</i>	0.25	1	0	0	0	1.25
<i>Pax3</i>	0.25	1	0	0	0	1.25

Table 10: Candidate transcripts with gene mutations showing phenotypes similar to <i>Cecr2</i> mutations						
Gene	Facial	NTDs	Otic	Renal	Gonadal	Phenotypic Score
<i>Cecr2</i>	1	1	1	1	1	5
<i>Disp1</i>	0.5	0.75	0	0	0	1.25
<i>Kitl</i>	0	0	0	0	1	1
<i>Bcl2l1l</i>	0	0	0	0.25	0.75	1
<i>Aspm</i>	0.25	0	0	0	0.75	1
<i>Prdm1</i>	0.25	0	0	0	0.75	1
<i>Fzd4</i>	0	0	0.5	0	0.5	1
<i>L1cam</i>	0.25	0.25	0	0	0.5	1
<i>Brd4</i>	0.5	0	0	0	0.5	1
<i>Tshz3</i>	0	0	0	1	0	1
<i>Dlx2</i>	0.75	0	0.25	0	0	1
<i>Unc5b</i>	0	1	0	0	0	1
<i>Epha7</i>	0	1	0	0	0	1
<i>C2cd3</i>	0	1	0	0	0	1
<i>Nipbl</i>	0.25	0.75	0	0	0	1
<i>Bmi1</i>	0.5	0.5	0	0	0	1
<i>Ndst1</i>	1	0	0	0	0	1
<i>Elavl1</i>	1	0	0	0	0	1
<i>Foxa2</i>	0.25	0.5	0	0	0.25	1
<i>Dlx1</i>	0.75	0	0.25	0	0	1
<i>Tcf12</i>	0	1	0	0	0	1
<i>Pfn1</i>	0	1	0	0	0	1
<i>Mbd4</i>	0.25	0.75	0	0	0	1
<i>Gsk3b</i>	1	0	0	0	0	1
<i>Gsk3b</i>	1	0	0	0	0	1
<i>Slit2</i>	0	0	0	1	0	1
<i>Tshz1</i>	0.5	0	0.25	0	0	0.75
<i>Fdft1</i>	0	0	0	0	0.75	0.75
<i>Zbtb16</i>	0	0	0	0	0.75	0.75
<i>Dlk1</i>	0	0	0	0	0.75	0.75
<i>Gmcl1</i>	0	0	0	0	0.75	0.75
<i>Nr2c2</i>	0	0	0	0	0.75	0.75
<i>Pa2g4</i>	0	0	0	0	0.75	0.75
<i>Rif1</i>	0	0	0	0	0.75	0.75
<i>Gpd2</i>	0	0	0	0	0.75	0.75
<i>Upp1</i>	0	0	0	0	0.75	0.75
<i>Abcd1</i>	0	0	0	0	0.75	0.75
<i>Hip1</i>	0	0	0	0	0.75	0.75
<i>Atp2a2</i>	0	0	0	0	0.75	0.75
<i>Rad18</i>	0	0	0	0	0.75	0.75
<i>Tns1</i>	0	0	0	0.25	0.5	0.75
<i>Stat3</i>	0	0	0	0.25	0.5	0.75
<i>Cutl1</i>	0	0	0	0.25	0.5	0.75
<i>Igf1r</i>	0.25	0	0	0	0.5	0.75
<i>Antxr1</i>	0.25	0	0	0	0.5	0.75
<i>Ddr2</i>	0.25	0	0	0	0.5	0.75
<i>Wwtr1</i>	0	0	0	0.5	0.25	0.75
<i>Pbx1</i>	0	0	0.25	0.25	0.25	0.75
<i>Dnajc5</i>	0	0	0.5	0	0.25	0.75

Table 10: Candidate transcripts with gene mutations showing phenotypes similar to <i>Cecr2</i> mutations						
Gene	Facial	NTDs	Otic	Renal	Gonadal	Phenotypic Score
<i>Cecr2</i>	1	1	1	1	1	5
<i>Actb</i>	0	0	0.5	0	0.25	0.75
<i>Six2</i>	0	0	0	0.75	0	0.75
<i>Ngfr</i>	0.25	0	0.5	0	0	0.75
<i>Pitx1</i>	0.5	0	0.25	0	0	0.75
<i>Sox10</i>	0	0.75	0	0	0	0.75
<i>Intu</i>	0	0.75	0	0	0	0.75
<i>Mdfr</i>	0	0.75	0	0	0	0.75
<i>Kif1b</i>	0	0.75	0	0	0	0.75
<i>Mib1</i>	0.25	0.5	0	0	0	0.75
<i>Hsd17b7</i>	0.25	0.5	0	0	0	0.75
<i>Hey2</i>	0.25	0.5	0	0	0	0.75
<i>Crim1</i>	0	0	0	0.75	0	0.75
<i>Fjx1</i>	0	0	0	0.75	0	0.75
<i>Bcr</i>	0	0	0.25	0.5	0	0.75
<i>Gpc3</i>	0.25	0	0	0.5	0	0.75
<i>Pou3f3</i>	0.25	0	0.25	0.25	0	0.75
<i>Sostdc1</i>	0.5	0	0	0.25	0	0.75
<i>Pax9</i>	0.5	0	0.25	0	0	0.75
<i>Cfl1</i>	0	0.75	0	0	0	0.75
<i>Stk4</i>	0	0.75	0	0	0	0.75
<i>Enah</i>	0	0.75	0	0	0	0.75
<i>Smarcc1</i>	0	0.75	0	0	0	0.75
<i>Fgf18</i>	0.75	0	0	0	0	0.75
<i>Id2</i>	0	0	0	0.75	0	0.75
<i>Igfbp2</i>	0	0	0	0.5	0	0.5
<i>Ankrd26</i>	0	0	0	0.5	0	0.5
<i>Serpinh1</i>	0	0.5	0	0	0	0.5
<i>Prkg1</i>	0	0	0	0	0.5	0.5
<i>Elavl4</i>	0	0	0	0	0.5	0.5
<i>Unc5c</i>	0	0	0	0	0.5	0.5
<i>Gja4</i>	0	0	0	0	0.5	0.5
<i>Amph</i>	0	0	0	0	0.5	0.5
<i>Reln</i>	0	0	0	0	0.5	0.5
<i>Acsl4</i>	0	0	0	0	0.5	0.5
<i>Crtc1</i>	0	0	0	0	0.5	0.5
<i>Mtap1b</i>	0	0	0	0	0.5	0.5
<i>Galnt3</i>	0	0	0	0	0.5	0.5
<i>Dhcr24</i>	0	0	0	0	0.5	0.5
<i>Qk</i>	0	0	0	0	0.5	0.5
<i>Cadm1</i>	0	0	0	0	0.5	0.5
<i>Ccnd2</i>	0	0	0	0	0.5	0.5
<i>Mll5</i>	0	0	0	0	0.5	0.5
<i>Smad4</i>	0	0	0	0	0.5	0.5
<i>Kit</i>	0	0	0	0	0.5	0.5

Table 10: Candidate transcripts with gene mutations showing phenotypes similar to *Cecr2* mutations

Gene	Facial	NTDs	Otic	Renal	Gonadal	Phenotypic Score
<i>Cecr2</i>	1	1	1	1	1	5
<i>Runx1t1</i>	0	0	0	0	0.5	0.5
<i>Lrp1</i>	0	0	0	0	0.5	0.5
<i>Wt1</i>	0	0	0	0.25	0.25	0.5
<i>Ada</i>	0	0	0	0.25	0.25	0.5
<i>Arid4b</i>	0	0	0	0.25	0.25	0.5
<i>Ephb2</i>	0	0	0.25	0	0.25	0.5
<i>Bmpr1b</i>	0.25	0	0	0	0.25	0.5
<i>Mbtps1</i>	0.25	0	0	0	0.25	0.5
<i>Cbx2</i>	0.25	0	0	0	0.25	0.5
<i>Clcn5</i>	0.25	0	0	0.25	0	0.5
<i>Ece1</i>	0.25	0	0.25	0	0	0.5
<i>Ep400</i>	0	0.5	0	0	0	0.5
<i>Itga5</i>	0	0.5	0	0	0	0.5
<i>Strap</i>	0	0.5	0	0	0	0.5
<i>Tfpi</i>	0.25	0.25	0	0	0	0.5
<i>Ptk2</i>	0.25	0.25	0	0	0	0.5
<i>Huwe1</i>	0.25	0.25	0	0	0	0.5
<i>Schip1</i>	0.5	0	0	0	0	0.5
<i>Cdh4</i>	0	0	0	0.5	0	0.5
<i>Lypla3</i>	0	0	0	0.5	0	0.5
<i>Hs2st1</i>	0	0	0	0.5	0	0.5
<i>Trio</i>	0	0.5	0	0	0	0.5
<i>Sall3</i>	0.5	0	0	0	0	0.5
<i>Sod1</i>	0	0	0.25	0	0	0.25
<i>Nrip1</i>	0	0	0	0	0.25	0.25
<i>Clip1</i>	0	0	0	0	0.25	0.25
<i>Ocln</i>	0	0	0	0	0.25	0.25
<i>Epha4</i>	0	0	0	0	0.25	0.25
<i>Zfx</i>	0	0	0	0	0.25	0.25
<i>Il6st</i>	0	0	0	0	0.25	0.25
<i>Lin9</i>	0	0	0	0	0.25	0.25
<i>Lpp</i>	0	0	0	0	0.25	0.25
<i>Cxcl12</i>	0	0	0	0	0.25	0.25
<i>Vav3</i>	0	0	0	0.25	0	0.25
<i>Ift20</i>	0	0	0	0.25	0	0.25
<i>E2f2</i>	0	0	0	0.25	0	0.25
<i>St8sia4</i>	0	0.25	0	0	0	0.25
<i>Med1</i>	0.25	0	0	0	0	0.25
<i>Ankrd11</i>	0.25	0	0	0	0	0.25
<i>Dag1</i>	0.25	0	0	0	0	0.25
<i>E2f5</i>	0.25	0	0	0	0	0.25
<i>Foxo1</i>	0.25	0	0	0	0	0.25
<i>Nfatc4</i>	0.25	0	0	0	0	0.25
<i>Wnk1</i>	0	0	0	0.25	0	0.25

Table 10: Candidate transcripts with gene mutations showing phenotypes similar to <i>Cecr2</i> mutations						
Gene	Facial	NTDs	Otic	Renal	Gonadal	Phenotypic Score
<i>Cecr2</i>	1	1	1	1	1	5
<i>Fah</i>	0	0	0	0.25	0	0.25
<i>Tcfap2b</i>	0	0	0	0.25	0	0.25
<i>Sim1</i>	0	0	0	0.25	0	0.25
<i>Bicc1</i>	0	0	0	0.25	0	0.25
<i>Chd2</i>	0	0	0	0.25	0	0.25
<i>Ifngr1</i>	0	0	0	0.25	0	0.25
<i>Mtss1</i>	0	0	0	0.25	0	0.25
<i>Foxp2</i>	0	0	0.25	0	0	0.25
<i>Pdpr1</i>	0.25	0	0	0	0	0.25
<i>Mef2c</i>	0.25	0	0	0	0	0.25
<i>Baz1b</i>	0.25	0	0	0	0	0.25
<i>Cdx1</i>	0.25	0	0	0	0	0.25
<i>Maf</i>	0.25	0	0	0	0	0.25
<i>Sumf1</i>	0.25	0	0	0	0	0.25
<i>Map3k3</i>	0.25	0	0	0	0	0.25
<i>Flnb</i>	0.25	0	0	0	0	0.25
<i>Cttna1</i>	0.25	0	0	0	0	0.25

survivors already represent the least-affected individuals developmentally and the sample size was small. Also, renal function must be severely compromised before the animals would show physiological effects and the urine markers used were insensitive and nonspecific (Star, 1998). Nonetheless, these tests were the established and available means to assess renal function.

Three homozygous *Cecr2^{tm1.1Hemc}* FVB/N females and two males surviving to adulthood underwent a series of biochemical analyses on blood and urine to detect markers of kidney dysfunction. The *Cecr2^{tm1.1Hemc}* FVB/N homozygous females showed a significant reduction in body weight compared to age-matched FVB/N animals housed and fed under the same conditions. *Cecr2^{tm1.1Hemc}* FVB/N homozygous females (n=3) body weight averaged 20.41 g, while FVB/N wildtype females (n=3) weighed an average 25.78 g at 6 to 8-weeks old. Although the sample size was small, it showed an opposing effect from that of the *Cecr2^{Gt45Bic}* FVB/N homozygotes where FVB/N body mass was less than *Cecr2^{Gt45Bic}* FVB/N homozygotes.

Urinalysis showed no abnormal urine nitriles, protein levels, glucose, ketones, urobilirubin, bilirubin or blood in the urine (Table 8). Specific gravity averaged 1.021 (n=5 animals, daily values averaged over 1 week) among the mutants and 1.022 (n=5 animals, daily values averaged over 1 week) for wildtypes, which was not significantly different. The pH did not differ significantly amongst genotypes, which averaged 6.16 (n=5 animals, daily values averaged over 1 week) in mutant and 6.39 (n=5 animals, daily values averaged over 1 week) in wildtype. Male urine samples contained a slightly higher protein level than female, although no other sex-related differences were found.

Animals were culled by cardiac puncture following CO₂ asphyxiation. The serum was collected for analysis of renal blood markers as summarized in Table 9. Mann-Whitney U tests indicated statistically significant increases in potassium levels of homozygous *Cecr2^{tm1.1Hemc}* FVB/N blood serum. Wildtype FVB/N potassium levels averaged 8.06 mmol/L (n=5) while *Cecr2^{tm1.1Hemc}* FVB samples averaged 9.47 mmol/L (n=3). Both wildtype and mutant potassium readings were above the expected physiological baseline, which was consistent with euthanasia via CO₂ as reported by Traslavina et al. (2010). The wildtype serum potassium levels were within the expected range for CO₂ euthanasia, but *Cecr2^{tm1.1Hemc}* FVB/N homozygous concentration was estimated to be in the moderate to severe hyperkalemia range. Blood serum urea, creatine, sodium, chloride, bicarbonate, anion gap, calcium and phosphorous levels were unaffected by genotype.

Renal dysfunction can cause hyperkalemia, but the other renal markers did not indicate disease. If *Cecr2^{tm1.1Hemc}* FVB/N homozygous kidney defects lead to hyperkalemia, then it was a specific effect and not due to general renal failure. Acidosis was an unlikely cause of the increased potassium as pH levels were unaffected. Likewise, trauma could be ruled out as a cause of the hyperkalemia. Nearly a month after the urine analysis, one of the *Cecr2^{tm1.1Hemc}* FVB/N homozygous males was found dead (<3 months old). Due to timing of discovery and the condition of the body no necropsy was performed. Severe hyperkalemia could cause abnormal heart rhythms and cardiac arrest (Janse and Wit, 1989),

although I was unable to determine a cause for this particular death. Future studies could consider testing *Cecr2*^{tm1.1Henc} FVB/N homozygous adults with electrocardiography to determine whether the hyperkalemia is sufficiently high to affect the heart.

The animals capable of surviving to adulthood do not show evidence of renal disease at the time of sampling as the blood and urine markers do not indicate renal failure. Neonatal serum could be tested in future studies; however, the serum volume of neonates was too small for this author to analyze by the available methods.

3.6: Testing whether CECR2 targets a core set of conserved transcripts during its roles in multiple developmental systems

The expanded phenotypic characterization of *Cecr2* mutations from this work as well as those of Dawe et al. (2010), Kooistra et al. (2011), and Thompson et al. (2012), suggested multiple roles for CECR2 throughout development. The most straightforward hypothesis predicted CECR2 to have a single molecular function affecting a consistent set of molecular targets in various tissues. The microarray and qRT-PCR comparisons of *Cecr2* homozygotes to wildtype littermates during neurulation provided gene candidates effected during neurulation which could be tested in other sites of CECR2-associated organogenesis. A subset of these genes were expected to be misregulated in *Cecr2* mutant kidneys if CECR2 targets a conserved set of genes throughout development.

3.6.1: Candidate gene mouse mutations allowed for the review and comparison of candidates based on associated developmental defects

Overall, the *Cecr2*-associated phenotypes can be grouped into five broad categories of craniofacial, neural tube closure, inner ear, renal, and gonad/fertility. If CECR2 alters a consistent set of developmental processes throughout development, then the gene candidates and their mutations should share multiple phenotypic similarities to the *Cecr2* mutations. These classifications were derived from MGI database entries, as MGI is the primary source of phenotypic data used in the following analysis. This database offered a consistent and catagorized means of characterizing mutant phenotypes as well as a comprehensive set of gene mutations. Genes that appeared affected in the microarray datasets and have gene-mutation phenotypes within the five broad phenotypic categories were compiled into Table 10. These datasets were restricted to genes with mouse mutants available and only those whose publications had been compiled by the MGI database (2011).

The resulting list of 209 genes showed significant expression changes on either the FVB/N to *Cecr2*^{Gt45Bic} FVB/N, BALB/c to *Cecr2*^{Gt45Bic} BALB/c, or both microarray analyses, and had relevant mutant phenotypes. With such an extensive list, it warrented a means to further rank how similar these mutations may have been to *Cecr2* mutants across the various catagories. A subjective phenotypic score was assigned to each gene depending on how closely its mutant

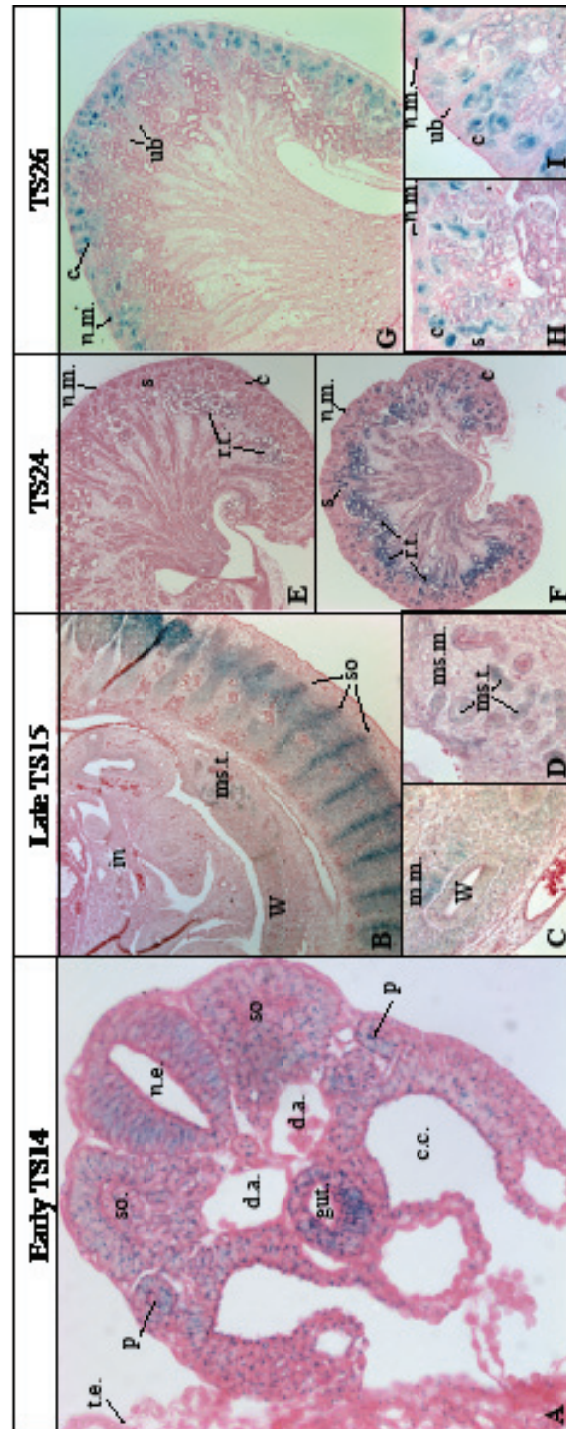


Figure 20:

***Cecr2* expression persisted throughout pro-, meso- and metanephric development**

(A-I) X-gal staining of the *Cecr2*^{Gt45Bic} B-gal fusion protein, counterstained with eosin demonstrated *Cecr2* expression during renal development. Expression of *Cecr2* was detected in the pronephros (p) of the early TS14 (16-17 somites) *Cecr2*^{Gt45Bic} FVB/N embryo (A, provided by Christine Dawe, magnification 630x), but appeared in all embryonic tissues except the trophectoderm (t.e.). Labels indicate the neuroepithelium (n.e.), outer somites (so), and gut epithelium (gut). *Cecr2*^{Gt45Bic} FVB/N TS15 embryos (27 somite) sagittally sectioned had staining within the renal regions within the mesonephric tubules (ms.t.) and lightly around the Wolffian (W) duct (B, magnification 100x). The somites (so) had consistent *Cecr2* expression dorsal to the renal expression, while the intestine (in) and other internal organs ventral to the renal regions had no expression (B). Increased magnification of the TS15 embryo identified the presumptive metanephric mesenchyme (m.m.) with *Cecr2* expression in the caudal Wolffian duct (C, magnification 400x). The mesonephric tubule epithelial cells had strong staining, but there was little staining in the surrounding mesonephric mesenchyme (ms.m.) (D, magnification 400x). The TS24 (16.5dpc) metanephric staining interpretation remained ambiguous in the proximal and distal renal tubules (r.e.) due to weak endogenous X-gal staining in wildtype samples (E, magnification 100x). *Cecr2*^{Gt45Bic} FVB/N TS24 kidneys did have specific staining within condensing cortex nephrogenic mesenchyme (n.m.), Comma-shaped bodies (c), and S-shaped bodies (s) (F, magnification 100x). TS26 Neonatal *Cecr2*^{Gt45Bic} FVB/N kidneys retained the cortex staining and no longer showed endogenous tubule staining (G, magnification 100x). (H-I, magnification 400x) The strongest staining exists within the Comma-shaped bodies (c), the elongated S-shaped bodies (s) and regions of condensing nephrogenic mesenchyme. The leading ureteric bud branches (ub) did not show expression.

phenotype was thought to matched *Cecr2*-associated defects across all five phenotypic categories. The *Cecr2* mutants were associated with midline facial clefts, encephalocele, and open eyelids for craniofacial defects (score 1 of 1); the NTD exencephaly, and tail kinks (score 1 of 1); inner hair cell disorganization with extranumerary stereocilia, and small inner ear (score 1 of 1); small or absent kidneys, hydronephrosis, fewer glomeruli, and duplex kidneys (score 1 of 1); and reduced male fertility showing reduced litter size, small testes, ovarian cysts, and ovarian hemorrhaging (score 1 of 1). A score of 0 in a given category could represent either a studied system with no abnormal phenotypes or a system that has not yet been studied. A score of 0.25 was assigned if the gene of interest had phenotypes in a given category, but with no specific similarities to *Cecr2* mutants. A 0.5 represented a partial match. Entries sharing multiple traits with *Cecr2* mutants were assigned 0.75, or up to 1.0 for a near-perfect match. This ranking may represent arbitrary distinctions, but offers one means to screen through candidates for genes which may be affected by CECR2 regulation in multiple organ systems.

When ranked by this relative phenotypic score, *Eya1* and *Fgfr1* phenotypes were tied in showing the closest overall phenotypic similarity to *Cecr2* abnormalities (Table 10). The fold-change of these transcripts was relatively low on both arrays. The *Eya1* mouse mutants have been associated with cleft palates, abnormal cranial morphology, open eyelids, stereocilia hair cell disorganization, absent or hypoplastic kidneys with impaired uterine bud branching and metanephric mesenchyme abnormalities, and infertility. A lack of neural tube defects reported in *Eya1* mice was the only category not showing a marked similarity to the *Cecr2* phenotype. *Fgfr1* mice present with full midline facial clefts, kinked neural tubes, abnormal stereocilia hair cell development, impaired uterine branching, hydronephrosis, and small kidneys with reduced glomeruli numbers. The mouse models of *Fgfr1* are not known to possess fertility defects, although human mutations have been associated with hypogonadism (Kim et al., 2005). The *Cecr2* homozygous fertility defects are subtle and similar abnormalities could be overlooked in other lines.

Other candidate genes included *Foxc1*, *Gli3*, *Mdm4*, *Fzd2*, *Zeb2*, *Tgfb2*, *Dlx5*, *Pdgdc*, *Gata3*, *Alx1*, *Prrx1*, *Six1*, *Gtf2ird1*, *Luzp1*, *Foxg1*, and *Pds5a*. From those genes only *Mdm4*, *Dlx5*, *Alx1*, *Prrx1*, and *Six1* showed a significant fold-change on all microarray datasets.

The phenotypic score analysis offered suggestive evidence that a core set of affected transcripts were common in all mutant arrays from both strains. A total of 26 transcripts with relevant phenotypes show consistent fold-changes on both arrays. The subjective phenotypic scores of these 26 transcripts averaged 1.27 on the relative 5 point scale across craniofacial, neural tube, inner ear, renal and fertility defects. The remaining strain-dependant transcripts showing changes on only one of the two strains averaged only 0.83 on the same scale. Candidates significantly changed on both arrays show a significantly closer phenotypic match to *Cecr2* mutants (two-tailed TTEST $p=0.01$) than the strain-dependant candidates.

Table 11: TS24 renal <i>Cecr2</i> ^{tml;Hhmc} FVB/N qRT-PCR versus wildtype FVB/N							
Genes	<i>Cecr2</i> ^{tml;Hhmc} FVB/N kidneys			Homozygous P3 versus wildtype			
	Fold	SE	p-value	Fold	SE	p-value	
<i>Alx1</i>	1.10	0.05	2.1E-01	-1.02	0.05	7.9E-01	
<i>Cecr2</i>	-28	3.E-03	3.0E-21	-37	2.E-03	4.0E-06	
<i>Dach1</i>	1.05	0.07	4.0E-01	1.33	0.06	5.0E-03	
<i>Dlx5</i>	1.10	0.09	2.7E-01	-1.30	0.04	7.0E-02	
<i>Foxl</i>	1.15	0.08	2.1E-01	1.44	0.08	6.0E-05	
<i>HoxD1</i>	1.2	0.1	4.3E-02	1.37	0.09	6.0E-04	
<i>Lix1</i>	-1.05	0.07	6.0E-01	1.13	0.07	5.4E-01	
<i>Nudt21</i>	2.0	0.4	4.5E-03	3.3	0.3	1.0E-02	
<i>Pax2</i>	1.4	0.2	1.0E-01	2.5	0.1	3.0E-10	
<i>Pax6</i>	1.09	0.07	3.4E-02	-1.12	0.04	3.9E-01	
<i>Prrxl</i>	1.09	0.07	9.2E-02	1.03	0.05	1.6E-01	
<i>Six1</i>	1.2	0.2	2.0E-01	-1.0	0.1	9.0E-01	
<i>Tshz1</i>	1.15	0.08	1.7E-01	1.52	0.06	2.0E-07	
<i>Tshz3</i>	1.08	0.06	2.3E-01	1.18	0.06	1.2E-01	
<i>Wnt5a</i>	1.2	0.1	2.0E-01	1.7	0.1	6.0E-02	
<i>Wnt5b</i>	-1.02	0.05	7.5E-01	1.26	0.05	9.0E-02	
<i>Zfp9</i>	1.16	0.04	1.7E-01	1.22	0.05	1.7E-01	

Thus by cross-referencing the phenotypic data with significant hits from all arrays we arrive at a shortlist of candidate genes most likely to represent a core functionality of *Cecr2*. This list is *Alx1*, *Ankrd11*, *Ankrd26*, *Bmi1*, *Bmp2*, *Dlx5*, *Mdm4*, *Met*, *Prrx1*, *Six1*, *Slit2*, and *Tshz1*. These candidates show multiple roles in not only neural closure, but also a variety of other developmental processes. As many of the candidates had known expression and roles in renal development, mesonephric and metanephric development was selected for further testing.

3.6.2: *Cecr2* expression was limited to the mesonephric tubules, metanephric mesenchyme and newly formed epithelium of comma-shaped and S-shaped bodies during renal development

I have established a variety of congenital abnormalities of the kidney and urinary tract within the *Cecr2* mutants lines. The characterization of the defects suggested an early role for CECR2 during metanephric induction, as well as a continued role during nephrogenesis. I hypothesized that the expression of *Cecr2* should present throughout renal development. If my general hypothesis that *Cecr2* is associated with mesenchymal-epithelial transitions is correct, then I expect renal *Cecr2* expression within the condensing metanephric mesenchyme and early tubules.

The *Cecr2^{Gt45Bic}* fusion protein allowed for X-gal staining for the fusion protein expression as outlined by Banting et al. (2005). *Cecr2* reporter within a TS14 embryo showed strong expression throughout the embryo proper, including the pronephros (Figure 20.A). By TS15 (Figure 20.B), *Cecr2* staining persisted in the mesenchyme surrounding the Wolffian duct (Figure 20.C) as well as the mesonephric tubules (Figure 20.D). The TS24 metanephric kidney had developed the distinctive structures and shape of the mature kidney. Wildtype kidneys presented a variable amount of endogenous staining within the renal ducts of the TS24 kidney (Figure 20.E). At this stage, *Cecr2* staining no longer appeared within the epithelium of the collecting ducts or leading ureteric branches (Figure 20.F). *Cecr2* expression was limited to the cortex (Figure 20.F), specifically within the areas of condensing mesenchyme, the comma-shaped bodies, and S-shaped bodies. Immature glomeruli retained light *Cecr2* staining, which appeared to fade as the nephron matures (Figure 20.F). This staining persisted into the neonatal kidney (Figure 20.G) in the condensing nephrogenic mesenchyme, the resulting comma-shaped and S-shaped bodies (Figure 20.H-I) where new nephrons were continuously developing, but remained absent from the ureteric branches (Figure 20.I).

3.6.3: *Cecr2^{Gt45Bic}* FVB/N microarray analysis revealed a number of candidate transcripts showing changes during neurulation, which also were known to be involved in renal development

The *Cecr2^{Gt45Bic}* FVB/N microarray analyses revealed 51 transcripts with known roles in kidney development, a number of which had mutations that manifested similar phenotypes to *Cecr2* mutants (Table 10). This observation was consistent with my hypothesis that CECR2 may regulate similar developmental

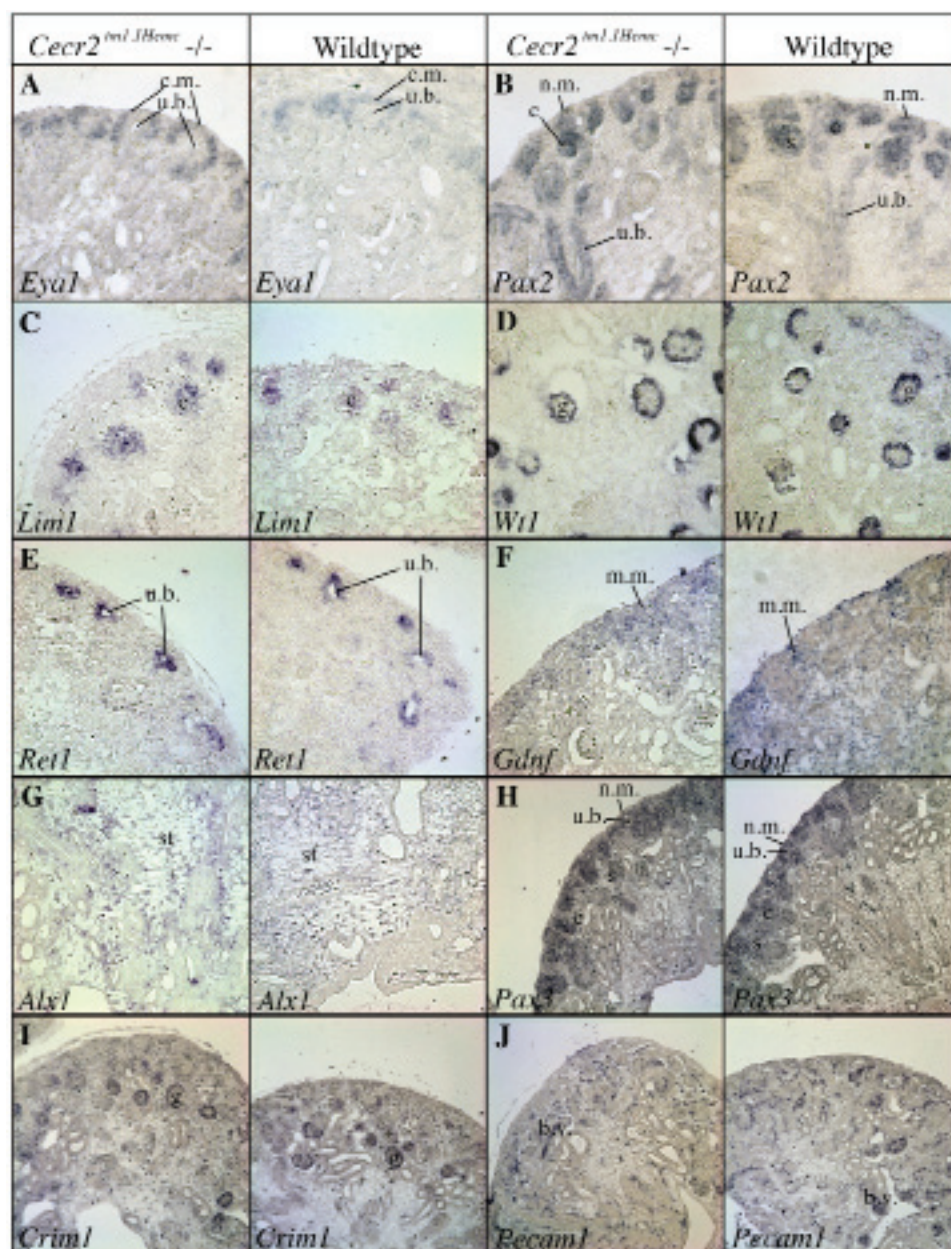


Figure 21:

***In situ* hybridizations of *Cecr2*^{tm1.1Hemc} FVB/N homozygous metanephric renal markers do not indicate a change in tissue morphology**

Cecr2^{tm1.1Hemc} FVB/N homozygous samples are shown to the left of FVB/N controls. Most images represent the renal cortex edge, with the exception of *Wt1* at the cortex/medulla boundary and *Cart1* within the renal medulla. In all cases, no probe showed significant differences between the FVB/N and *Cecr2*^{tm1.1Hemc} FVB/N homozygous kidneys. *Eya1* was limited to the cap mesenchyme (c.m.) of the cortex surrounding the leading ureteric branch (u.b.) (A). *Pax2* was found throughout the condensing nephrogenic mesenchyme (n.m.) epithelial tissue of the ureteric branches, and the comma-shaped (c) and S-shaped (s) bodies (B). *Lim1* was expressed in the comma-shaped bodies (C). *Wt1* probe strongly stained the podocytes of the glomeruli (g) (D). *Ret1* stained the leading tip of ureteric branches surrounded by the *Eya1* cap mesenchyme (E). *Gdnf* overlapped with *Eya1* in the outer cortex mesonephric mesenchyme (m.m.), but with broader expression throughout all cortex mesenchyme (F). *Alx1* probe highlighted the medulla mesenchymal stromal cells (st) (G). *Pax3* expression began in the cap mesenchyme and persisted through the Comma- and S-shaped bodies (H). *Crim1* started in the comma- and S-shaped bodies, and continued into the podocytes of maturing glomeruli (I). *Pecam1* was limited to the endothelial blood vessels (b.v.) and lymphocytes (J). Images taken at 400x magnification.

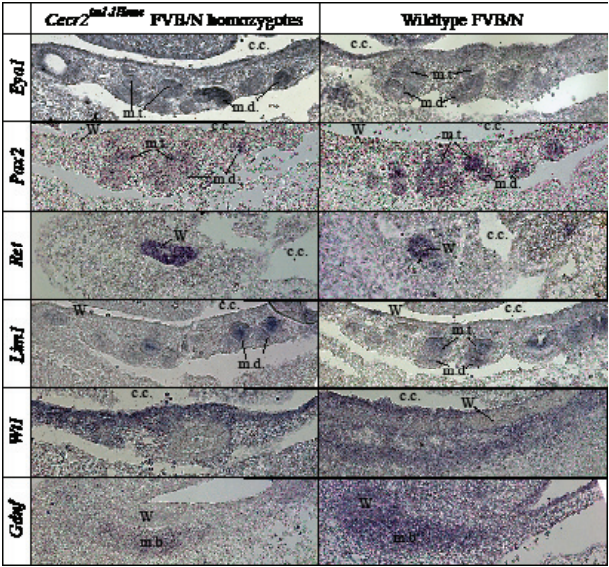


Figure 22:

***In situ* hybridizations of *Cecr2*^{tm1.1Hemc} FVB/N homozygous mesonephric renal markers indicated minimal change in tissue morphology**

In situ hybridization of sagittal sections from TS17 (10.5dpc) *Cecr2*^{tm1.1Hemc} FVB/N homozygous mesonephric regions showed minimal tissue changes. *Cecr2*^{tm1.1Hemc} FVB/N homozygous samples are shown above the FVB/N control. *Eya1* expression was weak (the sample imaged was allowed to overdevelop) at this stage surrounding the mesonephric tubules (m.t.) and mesonephric ducts (m.d.). *Pax2* was expressed within the mesonephric tubule and duct epithelium. *Lim1* was within the mesonephric tubules and to a lesser extent within mesonephric ducts. *Ret* expression was limited to the Wolffian duct. *Wt1* expression was throughout the mesonephric mesenchyme, showing greater intensity toward the ventral edge facing the coelomic cavity (c.c.). The *Cecr2*^{tm1.1Hemc} FVB/N samples showed a distinguishable dorsal-ventral boundary, which appears more diffuse and ubiquitous through the FVB/N mesonephric mesenchyme. A region of *Gdnf* expression resided dorsal to the Wolffian duct and caudal to the mesonephric tubules. The region marked the forming metanephric blastema (m.b.). The wildtype sample was over-stained, but the region showing strong *Gdnf* expression appeared similar to the pattern found in the *Cecr2*^{tm1.1Hemc} FVB/N homozygote. Images taken at 200x magnification.

pathways shared between neural and renal development. If correct, then key candidates should themselves show important role in both structures and show misregulation in the kidney.

Duplex kidneys, although a common idiopathic disorder among humans, has been associated with relatively few mouse gene mutants. *Fat4/Fjx1* double mutants possess duplex kidney structure (Saburi et al., 2008), however; they were further associated with polycystic phenotypes not noted among *Cecr2* mutants. The *Cecr2^{Gt45Bic}* FVB/N microarray results indicated *Fat4* transcriptional expression levels were unaffected by the *Cecr2* mutations while *Fjx1* levels were reduced (f.c.= -1.38, p=2.26E-02). FJX1 acts as a secreted peptide thought to interact with the FAT/DCHS1 signal pathway. It is currently unknown how FJX1 may influence ureteric bud induction.

Transcription factor FOXC1 and signaling molecule SLIT2 work in concert in the metanephric mesenchyme to restrict *Gdnf* expression, and in turn restrict ureteric budding to a single site (Grieshammer et al., 2004). Disruption of either gene is associated with multiple ureters from an expansion of the *Gdnf*+ region (Kume et al., 2000; Grieshammer et al., 2004). FOXC1 is not thought to act directly on *Gdnf*, but rather through restricting the expression of *Eya1* (Kume et al., 2000). The EYA transcription factors work within a complex including Sin oculis (SIX) transcription factors and DACHSHUND homologues to regulate *Gdnf* expression and metanephric mesenchyme differentiation (Xu et al., 1999 and 2003; Ikeda et al., 2002). Loss of *Eya1* or *Six1* gene products results in loss of metanephric induction, where a lack of ureteric bud outgrowth leads to renal agenesis. The levels of a variety of *Eya/Six/Dach* or renal induction-related genes were reduced in the *Cecr2^{Gt45Bic}* FVB/N mutants compared to wildtype mice based on the array (Table 10, Appendix 3). Genes of this pathway have shown dosage sensitivity and interaction. *Eya1/Six1* double heterozygotes are sufficient to cause a loss of kidney induction or hypoplasia (Zou et al., 2006).

3.6.4: QRT-PCR of *Cecr2^{tm1.1Hemc}* FVB/N homozygous metanephric kidneys did not confirm the same transcript disruptions as found during neurulation

The preceding section established that a number of candidates identified by the neural microarray may also be relevant to renal development. However, they must also be misexpressed during renal development. The stage tested by the microarray studies preceded ureteric bud formation. The embryos used in the arrays would have had intermediate mesenchyme present, along with the nephrogenic cord and forming mesonephric tubules. However, multiple candidate genes with altered expression such as *Eya/Six/Dach* or *FoxC1/Slit2* are known to regulate later metanephric induction (Xu et al., 1999 and 2003; Kume et al., 2000; Grieshammer et al., 2004; Zou et al., 2006). Candidate genes from the microarrays also predicted to be active during nephrogenesis were tested by qRT-PCR. Theiler stage 24 kidneys were selected to compare *Cecr2^{tm1.1Hemc}* FVB/N to FVB/N candidate expression (Table 11), as this stage shows the relevant nephrogenic stages, *Cecr2* expression, and the reduced number of glomeruli. By TS24 the metanephric kidney is morphologically distinct and nephrogenesis is

producing the first proximal and distal tubules. *Cecr2* expression was decreased in *Cecr2^{tm1.1Hemc}* renal samples (-27.7 fold, $p=3.4e-21$). The overall kidney size reduction at this stage was reflected in a significantly lower RNA yield from *Cecr2^{tm1.1Hemc}* kidneys that averaged 44.5 ng/ μ l compared to the wildtype yield average of 73 ng/ μ l (U-Test $p=0.03$). The relative expression of internal reference controls did not show a deviation between mutant and wildtype samples (data not shown).

During collection, non-duplex *Cecr2^{tm1.1Hemc}* kidneys were selected by gross morphology for this analysis in order to avoid secondary changes due to structural alterations of a second ureter. Duplex kidneys might be expected to show increases in ureteric-related, pelvis-related or other genes whose relative expression would increase if the unique structure expressing them were to be doubled. It was noted that one of the four *Cecr2^{tm1.1Hemc}* FVB/N biological replicates (denoted P3) was far outside the expected CT variation for certain primer sets. Treating this sample individually and analyzing against all four FVB/N samples it significantly differed at a number of genes (Table 11), but was consistent with other *Cecr2^{tm1.1Hemc}* FVB/N samples for most other genes tested. Importantly, all reference genes and the majority of target genes did not differ. The technical replicates were also consistent. This all suggested that the changes in the one unusual sample were biological. Potentially, this could have been due to partial penetrance of a renal defect. *Dach1*, *Fjx1*, *Pax2* and *Tshz1* all showed an upregulation in this single sample (Table 11) and *Dlx5* was suggestive. The increased expression of these genes in one sample may represent a duplex kidney, or perhaps a sample showing early hydronephrosis, or other defect. What was found was that three of the four biological replicates did not support consistent fold-changes of the candidate transcripts tested in the metanephros at an advanced developmental stage.

3.6.5: Metanephric tissue assessment by *in situ* hybridization supported the qRT-PCR results

The stages tested by qRT-PCR may have been too late in development, or may not have been able to detect subtle shifts in the expression pattern of key renal regulators. I therefore turned to *in situ* hybridization of a similar, and earlier, developmental stage in order to establish whether there were changes in the expression pattern of important renal genes. *In situ* hybridization indicated a wildtype pattern of expression for *Eya1*, *Six1*, *Alx1*, *Pax2*, *Pax3*, *Crim1*, *Gdnf*, *Pecam1*, *Ret*, and *Wt1* in *Cecr2^{tm1.1Hemc}* FVB/N homozygous TS24 kidneys. This set of probes was selected as markers for morphological structures throughout nephron and metanephric development. The expected wildtype expression of some candidates was previously published (Narlis et al., 2007; Willecke et al., 2011). *Eya1* stained the outer cortex in arches of mesenchymal cells (Figure 21.A) capping the ureteric branch of the *Ret*-expressing epithelium (Figure 21.E). *Pax2* overlapped strongly with the *Eya1*-staining caps of mesenchyme as well as possessing weaker expression continuing through the early comma-shaped bodies and collecting ducts (Figure 21.B). *Lim1* specifically stained the comma-shaped

bodies (Figure 21.C). The podocytes of the glomeruli intensely and specifically expressed *Wtl* (Figure 21.D). *Gdnf* overlapped with *Eya1*+ outer cortex mesenchyme, although more dispersed throughout the outer mesenchyme (Figure 21.F). *Alx1* marked stromal cells of the medulla (Figure 21.G). Also within the condensing mesenchyme and comma-shaped bodies, *Pax3* appeared strongest in the early condensing bodies, lightly in the area of *Eya1*+ caps, and throughout the collecting ducts/leading branches (Figure 21.H). *Crim1* began in the comma- and S-shaped bodies and intensified in the podocytes of the forming glomeruli (Figure 21.I). Throughout the kidney, *Pecam1* marked endothelial cells of blood vessels as well white blood cells within (Figure 21.J).

Cecr2 expression (Figure 20) staining intensified within the epithelial cells of the condensing comma- and S-shaped bodies and this intense staining partially overlapped with probes *Lim1*, *Crim1*, *Pax2* and *Pax3*. No changes were noted in the intensity, structure, or regional expression of any of the markers tested in the *Cecr2^{tml.1Hemc}* FVB/N kidney compared to wildtype FVB/N controls. Duplex kidneys and exceptionally small kidneys of *Cecr2^{tml.1Hemc}* FVB/N homozygotes retained the expression of all markers at equivalent levels. The analyses of markers suggested that the overall developmental structures were preserved.

3.6.6: Mesonephric tissue assessments by *in situ* hybridization did not reveal a loss of tissue identity

A series of *in situ* hybridization gene probes were selected as markers of mesonephric structures. The identification of key tissue and cellular markers during organogenesis was used in conjunction with structural morphology to assess for disrupted developmental processes. *In situ* hybridization was performed on TS17 embryonic sections to assess the Wolffian duct, mesonephric tubules and early metanephric blastema (Figure 22). The *Eya1* probe stained lightly and ubiquitously throughout the mesonephric region (Figure 22). The *Eya1* samples were overstained in an attempt to detect any *Eya1* signal present at this stage. No clear intensity or regional changes were noted in the *Cecr2^{tml.1Hemc}* FVB/N slides compared to wildtype samples. *Pax2* specifically marked mesonephric tubules and Wolffian duct epithelium equally in samples and controls (Figure 22). *Lim1* stained the mesonephric tubules, where the ventral tubules appeared darker in both genotypes with little staining in the Wolffian ducts (Figure 22). *Wtl* stained throughout the mesonephric mesenchyme and remained absent from duct epithelium (Figure 22). *Ret* staining was intense in the Wolffian duct epithelium while the *Gdnf* staining was weak throughout the region with an amalgamation in the forming metanephric blastema (Figure 22).

No mesonephric duct abnormalities were noted in the *Cecr2^{tml.1Hemc}* FVB/N mutant samples. Representative pictures in Figure 22 illustrate the common pattern found among replicates (n=2-3). The Wolffian duct retained strong *Ret* (Figure 22) and *Pax2* expression. Similarly, no changes in tubule markers *Lim1*, *Pax2* were noted among the replicates. The *Wtl*, *Eya1*, and *Gdnf* mesenchyme markers did not show a clear change among mutant samples. Thus, the tissue morphology and cellular markers of the earlier mesonephric structures were not

affected by the disruption of *Cecr2* as measured by RNA *in situ* hybridization.

4: Discussion

The presented work offers a substantial expansion of the known developmental and transcriptional consequences of CECR2 loss in the developing mouse. Prior research had established CECR2 as an ISWI chromatin remodelling subunit which was necessary for neural closure (Banting et al., 2005). I can now attribute the loss of *Cecr2* to the manifestation of exencephaly, midline facial clefts, smaller brains, smaller testes, fewer glomeruli, smaller embryonic kidneys, duplex kidneys, absent kidneys, renal hemorrhage, ovarian cysts, disorganized stereocilia, and hemivertebrae malformations. My work then focused on which pathway or process of neurulation may be disrupted by the mutation of *Cecr2*. The data both argued against an effect on the regulation of planar cell polarity while simultaneously supporting a misregulation of key mesenchymal/epithelial transcription factors involved in early organogenesis.

Although the microarray and qRT-PCR data supports the hypothesis that CECR2 regulates or can affect transcriptional regulation, the precise roles of CECR2 at a molecular level remain unknown. The enrichment of transcripts showing misregulation in *Cecr2* mutants suggests that ISWI remodelling may affect broad, but specific, regions of the genome consistent with the data presented by Landry et al. (2008). CECR2 acting in part to regulate transcription remains the primary hypothesis for what CECR2 may be doing during development. However, as little has been confirmed, the role of CECR2 should be reassessed.

4.1: Re-evaluating the molecular function of CECR2

The *Cecr2*^{Gt45Bic} microarray enrichment data suggest that there may be chromosomal regions targeted directly by CECR2 remodeling and influencing the transcription from these regions. The CECR2 data are consistent with a BPTF-like role in the regulation of broad regions (Landry et al., 2008) and ISWI transcriptional regulation of developmental genes (Deuring et al., 2000; Badenhorst et al., 2002; Barak et al., 2003). However, CECR2 was recently found to be necessary for double strand break repair and γ -H2AX alternate nucleosome formation (Lee et al., 2012). This suggests a role for CECR2 that is separate from transcriptional regulation. Lee et al. (2012) did not confirm whether the role of CECR2 in double strand break repair was a direct role, and proposed there could be a secondary effect on repair pathways indirectly from a CECR2-regulated target gene. Conversely, I do not believe that a single role for CECR2, limited to repair, would influence the regional expression of early embryonic genes in multiple biological replicates at consistent chromosomal sites with consistent transcriptional effects, as was found in the *Cecr2* microarray and qRT-PCR datasets. Gene ontology analysis of the *Cecr2*^{Gt45Bic} microarray did not suggest a role in transcriptionally regulating DNA repair pathways, but certainly could not rule out a transcription-independent function during repair. Thus, there may be multiple functional roles for the CECR2 protein.

The original characterization of the CERF complex did not identify cofactors involved in DSB repair (Banting et al., 2005), and so there may be additional CECR2 containing complexes specific for DSB repair. Thompson et al.

(2011) reported a second CECR2-containing complex associated with SNF2H and other, unidentified, components. Is the version of CECR2 that mitigates neural closure the same CECR2 protein necessary for proper renal development or other affected systems? Is the adult testis CECR2 protein identified in the CECR2-SNF2H complex (Thompson et al., 2011) spliced or modified differently from embryonic forms? Is there a CECR2-containing complex interacting with DSB repair, and is this the same or a different complex as that found during normal embryonic development? He et al. (2008) presented a model in which the non-catalytic, bromodomain-containing members of ISWI complexes would determine the biological *in vivo* function of the ISWI complexes. CECR2 structure and potential splicing may change the ISWI targeting, activity, or even alter which ISWI complex CECR2 forms. A future test should be a thorough RT-PCR and Western blot assessment of what splice variants and isoforms of *Cecr2*/CECR2 exists throughout mouse development at various stages and organs.

Histological examination of *Cecr2*^{Gt45Bic} X-gal staining in numerous stages and tissues reveals what may be at least two distinct subcellular locations of the CECR2-fusion protein in embryonic cells. The cellular expression most often associated with *Cecr2* (Banting et al., 2005; Dawe et al., 2011), is in epithelial tissue showing strong X-gal staining of the fusion protein throughout the cellular body and predominantly nuclear. However, in the surrounding mesenchymal non-epithelial tissue the X-gal staining exists as a defined rod or doublet within each cell (partially visible in Figure 20.A/C/D/H/I; data not shown) that appears to be within the nucleus. This is not an artifact of the tissue type, as wildtype samples underwent the same procedure and did not show these patterns. The fusion protein could have altered the localization of CECR2, and so immunohistochemistry should be employed to confirm these finding once an antibody to the native CECR2 becomes available. Tate et al. (1998) showed CECR2-fusion protein localized along the euchromatin and excluded from heterochromatin of embryonic stem cells. This appears consistent with the staining within the neuroepithelium, but quite dissimilar from the mesenchymal pattern. The CECR2 subcellular localization reported by Liu et al. (2002) shows both a doublet of strong nuclear staining or a border/line on one side of the nucleus that appears quite similar to the pattern noted in the *Cecr2*^{Gt45Bic} mesenchyme. High-resolution imaging of the X-gal staining may confirm whether the *Cecr2*^{Gt45Bic} subnuclear position and variation matches that reported by Liu et al. (2002). Thompson et al. (2011) confirmed at least two distinct CECR2 complexes, and there may be two or more distinct subcellular locations of the CECR2 protein. Before future projects delve into complicated gene interaction studies or pull-down experiments, confirmation first must be made as to which variants or complexes of CECR2 are biologically significant for the questions at hand. Not knowing these answers may not directly limit the ability to pursue other *Cecr2*-related studies, but I believe it will ultimately impede our ability to properly interpret and apply the data.

4.2: Planar cell polarity gene transcription is not affected by CECR2 remodeling during neurulation

Misregulation of planar cell polarity (PCP) pathways was a strong hypothesis to explain some of the *Cecr2* mutant phenotypes. Neural tube closure defects, open eyelids, aberrant inner ear morphology with stereocilia disorganization, and kidney defects can be hallmarks of planar cell polarity defects. However, within each of the organ systems the *Cecr2* phenotypes do not directly conform to classic PCP morphology. The facial clefts and exencephaly of *Cecr2* mutants are specific to the cranial regions and distinct from the systemic craniorachischisis found in the many PCP defects (reviewed by Coskun et al., 2009), although some PCP-associated gene mutations do manifest exencephaly (Hamblet et al., 2002; Wang et al., 2002; Qian et al., 2007). The renal defects most often associated with PCP include polycystic kidney and tubule morphology defects (reviewed by McNeil, 2010), which have not been found with either *Cecr2* mutation. *Cecr2* mutations and PCP defects both affect renal development, but in markedly different ways. Finally, Dawe et al. (2011) considered the stereocilia misalignment and extra outer cell layers in the *Cecr2* mutant inner ears to be the strongest indication of a PCP effect, but these conditions also resemble the *Eya1* mutant mouse phenotypes not associated with PCP (Zou et al., 2008).

The microarray and qRT-PCR used in this study detected no transcriptional differences in the core PCP genes by the CECR2 protein during neurulation. The microarray and qRT-PCR data collected from either *Cecr2* mutant allele on either strain all support this statement. In place of PCP, the array data suggest a number of known NTD-causing transcripts (*Alx1*, *Bmi1*, *Bmp2*, *Met*, *Dlx5*, *Mdm4*, and *Prrx1*) are affected by the mutation of *Cecr2*. This runs counter to the hypothesis that CECR2 regulates the transcription of PCP pathways during neurulation.

Dawe et al. (2011) first noted inner ear disorganization of *Cecr2*^{Gt45Bic} animals including smaller inner ears, and a disorganization of the stereocilia. This work confirmed the same defects are present in the *Cecr2*^{tm1.1Hemc} BALB/c line. This evidence is considered the strongest support for an involvement for PCP, and the stereocilia of both *Cecr2* alleles do show polarity defects. However, similar defects can be found among other mouse mutants not directly connected to PCP defects or regulation. *Eya1* mutant animals show that normal inner ear development is highly dosage sensitive (Zou et al., 2008). When *Eya1* expression is between 40% (*Eya1*^{bor/bor}) to 49% (*Eya1*^{+/-}) of wildtype levels, inner ear morphology has a severe disorganization and mispolarization of the stereocilia (Zou et al., 2008). Within the *Cecr2*^{tm1.1Hemc} BALB/c TS15 embryos (18-20 somites), *Eya1* expression is 40% (fold change of -2.47) of wildtype levels and within the range shown by Zou et al. (2008) to cause mispolarization. This suggests a model in which CECR2 regulates the early *Eya1* specification of the inner ear, resulting in *Eya1*-induced defects in the *Cecr2* mutant. The stereocilia arise from a mesenchymal-epithelial transition (Hu and Corwin, 2007) and *Eya1* is thought to facilitate the condensation and differentiation of the early ear mesenchymal cell populations (Kalatzis et al., 1998). A *Cecr2*->*Eya1* effect could be impacting the condensing mesenchyme undergoing mesenchymal-epithelial

transitions of both inner ear and renal development. The cause of the *Cecr2* ear defects may rely on changes to multiple candidates in addition to *Eya1*. Gene ontology analysis (Table 2) found a collection of genes affected by the loss of *Cecr2* during neurulation, that also have known roles in ear development. The candidates include *Frzb*, *Tshz1*, *Six1* and *Prrx1* that are expressed in the otic placode or have known roles in ear development, and *Dlx5* should be included in that list (Sajan et al., 2011).

4.2.1: Proposed future directions of PCP-related CECR2 research

Three lines of inquiry remain unanswered by the presented data, which could potentially still connect *Cecr2* and a PCP association. Are there PCP-associated transcripts not tested within the microarray datasets, or have candidates showing marginal effects on the arrays been overlooked? How does a disruption of *Cecr2* lead to the misalignment of stereocilia if not through the PCP pathway? Why do *Cecr2* mutants show genetic interaction when crossed with *Vangl2* (Dawe et al., 2011; Dawe, personal communications, 2011)?

Two genes represented on the microarray showed small expression changes in the mutant samples. *FRZB* is a secreted frizzled receptor and presumptive antagonist to WNT signaling. The *Frzb* transcript on the whole embryo microarray shows an average reduction of 1.27-fold. This was not confirmed in the cranial region of *Cecr2^{tm1.1Hmec}* BALB/c embryos where it showed no effect. *Frzb* reduction was subsequently confirmed in the embryonic trunk (Pisio, personal communications, 2010). Thus *Frzb* is not a candidate for neural closure, but perhaps has a role in renal or other systems. The second candidate is *Lix1*. The microarray data from the *Cecr2^{Gt45Bic}* FVB/N arrays show no significant difference, but a -1.4-fold change is observed on the *Cecr2^{Gt45Bic}* BALB/c arrays. The LIX1 protein is thought to be part of the mammalian FAT/HIPPO/WARTS alternate PCP pathway (Mao et al., 2009). Mutations in this alternate signaling pathway can resemble core PCP defects. Mouse *Fat4/Fjx* double-mutants are one of the few mouse models found to develop duplex kidneys (Saburi et al., 2008). Thus a tentative link could exist between *Cecr2* loss and the FAT/HIPPO/WARTS alternative PCP pathway. The qRT-PCR confirmation of *Lix1* in the cranial tissue of the *Cecr2^{tm1.1Hmec}* BALB/c homozygotes shows no significant reduction at the time of neural closure ($p > 0.05$), but does change in the post neural closure embryos (f.c.=-1.37, $p=0.032$) in the BALB/c background. *Lix1* is not affected by *Cecr2* mutation in the FVB/N strain and thus may not be a direct target.

I do not believe *Lix1* to be a leading candidate compared to the chromosomal regions and other candidate genes to be discussed in Sections 4.4.2. However, future inquiries looking to investigate *Lix1* and the FAT/HIPPO/WARTS PCP pathway as a potential cause of the *Cecr2* defects must first find an association between LIX1 and CE or PCP in the mouse. A direct link has not been found, and the field is unclear regarding what *Lix1* does and how or if it is associated with polarity. *Lix1*-tagged and mutant cell lines are available, but a mouse mutant has not been characterized. Chromatin immunoprecipitation (ChIP) or other studies implicating *Lix1* either as a direct target of CECR2, or to have

CE/PCP-like roles during development, need to be performed prior to devoting resources to explore this candidate during neurulation; primarily, the creation and characterization of a *Lix1* mouse mutant.

The majority of microarray and qRT-PCR data presented within this text have been limited to the early embryo and the cranial neural tube. It does not eliminate the possibility that *Cecr2* mutants show core PCP transcript disruption in other tissues or stages. If CECR2 has any connections to the disruption of the classic PCP or FAT/HIPPO/WARTS pathways, they should be manifesting in the developing cochlea where the stereocilia are mispolarized (Dawe et al., 2011). A similar qRT-PCR experimental setup could be used to test for transcriptional changes specifically during cochlear development. The mispolarization defects are found in *Cecr2* mutant TS26 embryos (Dawe et al., 2011), and a qRT-PCR approach should examine the earliest cochlear samples in which the stereocilia are first aligning (TS23-26). As part of the qRT-PCR analysis, the neural candidates such as *Alx1*, *Dlx5*, *Met* and the others found should be included to test whether CECR2 targets are conserved between tissues. As well, the *Eya/Six/Dach* gene network should be thoroughly screened as *Eya1* mutants show similar ear defects (Zou et al., 2008).

Subcellular localization of the PCP proteins plays a critical role in the establishment of polarity, and so a lack of transcriptional changes at the RNA level does not eliminate the possibility that any number of PCP proteins could have activation-state or subcellular location changes. PCP-like defects have been found in *Sec24b* mutants due to a packaging and transport defect of the ER/Golgi machinery, which in turn interrupts VANGL2 processing (Merte et al., 2010). *Sec24b* is not affected on the *Cecr2* arrays, but a similar and indirect candidate could remain undiscovered in the datasets. Immunohistochemistry could be applied to determine the subcellular localization of the various PCP components within the stereocilia bundles of *Cecr2* mutants. If PCP protein localization is not affected in the mispolarized stereocilia cells, then there is little argument left to support PCP as a target of CECR2 remodeling activities.

Work by Dawe et al. (2011) established a genetic interaction between *Cecr2* and *Vangl2* mutations. The interaction manifests as spina bifida in *Cecr2* homozygous and *Vangl2* heterozygous pups, and vaginal atresia in adult double heterozygous females (Dawe, personal communication 2011). Although *Vangl2* heterozygotes can develop both of these defects in isolation (Wilson and Center, 1977), the manifestation of vaginal atresia in the double heterozygote shows twice the penetrance of *Vangl2* heterozygotes. The cross indicates a complex and selective interaction, but does indicate is that CECR2 may play a larger role during caudal spinal closure than previously thought and that there is a role during vaginal development.

The *Cecr2*^{tm1.1Hmc} homozygous mutant pups may show a delay or aberration in the closure of the caudal neural tube. This could be scored during embryo collection of TS14-16 staged embryos by photographing the wholemount progression of tube closure and comparing to stage-matched wildtypes. A delay, widening, or other anomaly would warrant more thorough examinations through

serial sectioning of the closing caudal neural tube. Likewise, the role of CECR2 during vaginal development could be further explored. Christine Dawe (personal communications, 2011) began a preliminary study of *Cecr2* expression during vaginal development, but this should be further characterized and compared to *Vangl2* expression. Finally, as misalignment of stereocilia is the archetypical example of PCP, the stereocilia of the various *Cecr2/Vangl2* crosses need to be assessed.

4.3: CECR2-affected transcripts cluster to broad localized chromosomal regions during neurulation

Although a number of strong candidates are revealed by the microarray analysis, most are dispersed throughout the genome. In stark contrast is the extensive number of clustered changes within the chromosome bands 6A, 6F-G, and 12B. Transcripts showing expression changes within these regions are often flanked by unaltered genes, and do not appear as adjacent runs. The proximity of multiple genes indicates the loss of *Cecr2* disrupts these regions through a targeted, but broadly spread mechanism. This suggests that although CECR2 may be necessary for the proper regulation of these chromosomal segments, it is not sufficient to control the regulation of all genes within the region. Individual genes likely still require additional and specific transcription factors, or other secondary signals, many of which may not have been active at the stage of development tested. The overall profile of the region shows the majority (~60%) of transcripts are downregulated by the mutation of *Cecr2*, but with ~40% showing upregulation, the role of CECR2 cannot clearly be defined as an activator of this region. The overall microarray skew with ~75% of transcripts downregulated by *Cecr2* disruption suggests CECR2 may primarily be opening/activating. However, if secondary factors are still necessary to affect transcription, then repressors may also be gaining increased access to target regions ‘opened’ by CECR2 if that is its activity. The arrays suggest CECR2 may be increasing access of a region, but the response of any given gene may be dependent on the presence of specific activators/repressors specific to that gene.

The clustering of data suggests these regions are direct targets of CECR2 functional complexes in Theiler stage 13-14 embryos during neural closure. Five of seven genes showing a change in the 6F-G region of *Cecr2*^{Gt45Bic} FVB/N homozygotes were confirmed by qRT-PCR, and three of three genes tested and showing a change in the 6F-G region of *Cecr2*^{Gt45Bic} BALB/c homozygotes were also confirmed. Although not extensive, this sampling indicates the overall enrichment in the dataset is unlikely to be an array artifact.

The chromosome 6F-G enrichment contains many of the largest fold-changes present throughout the microarray and clusters within a roughly 30 Mbp span that includes *Cecr2*. There is a conceptual gap when attempting to link transcripts found affected in this region with the developmental mechanisms thought to embody the *Cecr2* mutant phenotypes. The majority of transcripts affected by the disruption of *Cecr2* from Chr6F-G are not currently known to control neurulation or renal development. The one potential candidate to fulfill the

above criteria is *Ankrd26* from Chr6F1. *Ankrd26* mouse mutants possess increased kidney weight, but also a severe obesity from insulin resistance and gigantism (Bera et al., 2008). The *Cecr2* microarray data show *Ankrd26* is upregulated, whereas the Bera et al (2008) mutation is a proposed hypomorph. Mouse lines overexpressing *Ankrd26* are not available, but may show opposing phenotypes to the hypomorph such as smaller kidneys. This lead is speculative at best, but is the only current candidate in the Chr6F-G region with a known association to *Cecr2*-affected organ systems.

The gene *Ret* is present in the chromosome 6F-G region its expression is not affected based on the microarrays. RET and GDNF regulation of the ureteric bud and branching could be a candidate for *Cecr2* defects based on the types of phenotypes manifested; however, *in situ* hybridization analysis of *Ret* in the *Cecr2^{tm1.1Hemc}* FVB/N kidney did not show a visible expression change. Quantification of *Ret* by qRT-PCR was not attempted on metanephric kidney samples and the *in situ* hybridizations may lack the precision to detect the subtle changes characteristic of the *Cecr2* mutant transcription effects. The microarray dataset was collected at a stage preceding normal *Ret* expression. If CECR2 does regulate the chromosome 6F-G region and this is a consistent target throughout development, then an effect on *Ret* may be expected in the forming kidney when secondary factors would be present for its activation. Further qRT-PCR of *Ret* could test this hypothesis in metanephric kidneys during ureteric budding and branching (TS17-20). A number of uncharacterized zinc finger transcription factors also appear within Chr6F-G. Future work may eventually link one or more of these factors to neural closure. Thus at present, no candidate from the Chr6F-G region currently links this enriched region to the *Cecr2* mutant developmental abnormalities.

The chromosome 6A enriched band offers more promise. *Dlx5* and *Met* both reside within this region that show marked *Cecr2*-induced misregulation across all strains, mutations, and statistical methods tested. *Dlx5* and *Met* also show a developmental function consistent with the *Cecr2* phenotypes (Acampora et al., 1999; Depew et al., 1999; Graveel et al., 2004; Relaix et al., 2003). *Dlx5* and *Met*, or their coordinated disruption, may represent the initial dysfunction leading to the subsequent developmental and transcriptional changes.

The Chr12B region is the smallest region identified to show clustered transcripts. The few changes found are strain dependent and no one candidate stands out under all conditions. *Foxg1* shows a significant change in *Cecr2^{Gt45Bic}* BALB/c embryos, but not *Cecr2^{Gt45Bic}* FVB/N. *Foxg1* mutant mice (Hebert and McConnell, 2000) also manifest a number of similarities to *Cecr2* mutations. This particular genomic region and gene stand out as SNF2L binds and specifically regulates *Foxg1* (Yip et al., 2012). Given that SNF2L relies on BAZ-like partners BPTF or CECR2 to actually bind nucleosome/DNA, this finding suggests that CERF may be the complex involved in the neural development pathway reported by Yip et al., 2012. However, Yip et al. (2012) found SNF2L regulation represses *Foxg1*, whereas the disruption of *Cecr2* appears to reduce *Foxg1*, suggesting positive regulation. This region shows all seven transcripts to be downregulated

by the loss of CECR2. This could suggest an activator function for CECR2, but the sample set is quite small in this region. Again, many genes of the region are not affected according to the array data and this may be an indication of a requirement for secondary gene-specific factors.

In all cases, the use of chromosomal band boundaries were selected based on the pre-existing designations within the reference data archives. The actual borders and span of the affected regions may not be in any way related to the band boundaries. This appears to be the case in Chr6F-G, where both appear to blend together into one region of effect. Bands do represent regional changes in AT/GC enrichment and bands can show specific signatures in the overall histone modifications (Florian et al., 2009). So, they could serendipitously represent real CECR2 boundary effects, but multiple microarray runs or direct binding analysis such as ChIP-seq would be required to further define the boundaries. The bands themselves are reliant on mapping data and so even the boundaries and placement of genes near the borders may be inaccurate.

4.3.1: Comparing CECR2 to BPTF chromosomal targets

Landry et al. (2008) presented microarray analyses of *Bptf* mutants from cell culture. ES lines were cultured in the presence of retinoic acid and in the absence of leukemia inhibitory factor. The RA- LIF+ culture media maintained the pluripotency of the ES state. Differentiated and undifferentiated lines were compared. Landry et al. (2008) did not specify a differentiation cell type studies and Lioudmila et al. (2007) found these conditions did not compete differentiation into a particular cell line within the 3 day period used by Landry et al. (2008). Thus, Landry et al. (2008) tested for the general loss of pluripotency and not the differentiation into a particular cell type. Although their conditions and methods were quite dissimilar to those used during the *Cecr2* arrays, both represent the transcriptional changes brought about by the disruption of BAZ-like targeting components from the two mammalian ISWI chromatin remodeling complexes. Comparing the two sets of affected transcripts reveals a potential common mechanism of BAZ-like targeting and transcriptional regulation of localized but broad chromosomal regions.

Bptf mutations are reported to have altered the regulation of 25 small clusters of transcripts (Landry et al., 2008). One of the reported regions overlaps with the Chr6G enriched region found within the *Cecr2* microarray. However, the *Bptf* enrichment is much smaller, and only a single transcript of *Emp1* appears common to both lists. *Emp1* is upregulated in the loss of *Bptf* while it is reduced in *Cecr2* mutants. The genes and regions affected by *Bptf* in the ES cell cultures are generally not consistent with those found in the *Cecr2* embryo datasets. This is consistent with the hypothesis by He et al. (2008) that the BAZ-like proteins distinguish the targeting of ISWI complexes. The two mouse lines also displayed diverse phenotypes, which suggest different affected genes and pathways (Banting et al., 2005; Landry et al., 2008). The two datasets appear to generally have different target regions as predicted, but both demonstrate broad regionalized transcriptional changes.

The 25 regions identified by Landry et al. (2008) were separated into upregulated and downregulated enriched regions. The data were provided in a supplementary figure with little further explanation or analysis. I further analyzed the data presented and found the *Bptf* regions spanned ~0.3 to ~2 Mbp in size. Although they stratified their data as up vs downregulated, in two regions (Chr10 and Chr16) the span of enrichment overlapped with both upregulated and downregulated enrichments contained in the same area. The BPTF data showed only ~10% (n=8/81) to ~55% (n=5/9) of the genes in a region had transcriptional changes. By having interspersed genes unaffected, along with the co-localization of both upregulated and downregulated transcripts, this suggests that BPTF remodeling is not sufficient to alter the expression of genes within affected regions. This is consistent with the CECR2 data and implies both are reliant upon secondary factors that drive gene-specific regulation.

What such factors might be, and whether CECR2 is specifically working in conjunction with another transcriptional complex is currently unknown. Landry et al. (2008) demonstrated that many relevant *Bptf*-affected genes were also SMAD regulated transcripts, suggesting SMAD likely functions as one such secondary factor during BPTF remodeling. Future studies might consider promoter analysis of the transcripts showing changes in the *Cecr2* arrays to determine whether there are common promoter-binding sites among affected transcripts that may indicate secondary factors working within the CECR2 remodeled regions.

The size of the BPTF identified regions is not restricted to band designations. Future studies may wish to apply local cluster analysis of the *Cecr2* microarray datasets using algorithms independent of the band-mapping and based upon physical clustering of targets by spatial relation. Presumably, such an algorithm was how Landry et al. (2008) generated their enrichment database for BPTF; however, they did not publish the methods used in their analysis. The same algorithm should be applied to the CECR2 database in order to directly compare the regional effects of these two related BAZ-like proteins.

Absent from the *Bptf* dependent clusters is a Chr12B-containing region, or a specific misregulation of *Foxg1*. This may further indicate that CECR2, and not BPTF, is responsible for the SNF2L regulation of *Foxg1* (Yip et al., 2012). Also absent from the Landry et al. (2008) data is an effect or targeting of the *Engrailed* genes. Barak et al. (2003) demonstrated by chromatin immunoprecipitation that BPTF and SNF2L specifically bound to the *Engrailed* promoters. The lack of association with the *Engrailed* gene was not addressed by Landry et al. (2008). *En1* and *En2* are not located within the 25 *Bptf* enriched regions. A caveat of these comparisons is that the datasets are generated from different tissue types. Histone modifications can be transient and so the targets of ISWI remodeling may also be transient.

The underlying mechanisms forming broad regional effects are not yet known; however, such effects are at least consistent with the regionalized patterns of some histone modifications (Pauler et al., 2009). This suggests that mammalian ISWI remodeling may either be responding to, or establishing, regionalized

histone modifications in a manner not restricted to single-gene regulation. Both the *Bptf* and the *Cecr2* mutant microarrays contained many transcripts showing altered expression not within localized enriched clusters. Many of these altered transcripts may be indirect effects, but may also indicate either gene-specific targeting or that small regions are underrepresented and remain unidentified.

Finally, the *Bptf* transcript itself is downregulated in the *Cecr2*^{Gt45Bic} FVB/N arrays and upregulated in the *Cecr2*^{Gt45Bic} BALB/c arrays. These changes are significant across all statistical tests used, but the opposing strain effect is not easily explained. A direct regulation of *Bptf* by CECR2 would normally be expected to show a similar regulatory effect independent of strain. Given the functional similarities of these proteins there is the possibility of compensation, but if BPTF/NURF were to be compensating for the loss of CECR2/CERF, it would again be expected to increase its expression in both strains. This indicates that the relationship between BPTF and CECR2, or NURF and CERF, may be quite complex. The *Bptf* microarray dataset (Landry et al., 2008) did not report a change in *Cecr2*; however, the complete list of significant changes was not published or registered with the Gene Expression Omnibus repository. The Landry et al. (2008) array may show a change in *Cecr2* if there is compensatory regulation between *Cecr2* and *Bptf*. Methods for quantitative Western blotting of the NURF components have been established (Landry et al., 2011), and these means could be applied to *Cecr2* homozygous mutant protein isolates from the closing neural tube in the FVB/N and BALB/c backgrounds in order to confirm how these changes are reflected in the functional complexes. A change in the function of NURF in addition to the disruption of CERF, or the possibility for regulatory feedback or compensation between the ISWI complexes, would offer intriguing new avenues of research to the increasingly complex field of ISWI chromatin remodeling.

4.3.2: Proposed future directions of CECR2 chromosomal targeting research

The microarray datasets suggests a number of genes are misregulated during neural closure in *Cecr2* mutant embryos. However, the microarray cannot distinguish which, if any, changes are a direct regulatory target of CECR2 from those arising from downstream cascades. Once CECR2 antibodies become available, chromatin immunoprecipitation (ChIP) studies should be considered. Candidates for direct CECR2 binding may be tested initially through ChIP-PCR using the methods of Barak et al (2003). This approach suffers from the limitation of having to predict and design the proper probe regions without knowing where the regulatory site might be located. Whereas successful ChIP-PCR would be informative, negative results could simply have overlooked key regions or improper probe placement. There are also a multitude of candidates requiring testing.

An alternative and preferred technique would be ChIP-seq, which would generate a broad report of all regions bound by CECR2-ISWIs and the resulting database could be cross-referenced to the microarray candidate lists. This author predicts at least a portion of the chromosome 6A and 6F-G and 12B regions

would be direct targets that would appear within a CECR2 ChIP-seq dataset. ChIP-Seq analysis could also identify whether there is sequence specificity to regions of CECR2 binding. However, CECR2 is predicted to bind modified histone as a BAZ-like protein of ISWI complexes. The acetylated modification must themselves be targeted in some fashion to target regions prior to CECR2 recruitment. SWI/SNF remodeler ACF utilizes a 40 bp sequence to direct nucleosome positioning (Rippe et al., 2007), and if similar underlying elements exist for CECR2 targeting they should appear as common sequence elements in CECR2 ChIP-seq. Precise sample collection should be considered the most limiting factor, as the targeted histone modifications could change over time or by tissue. This could be tested through ChIP-seq testing of divergent cell types or time-points involving CECR2. Although the initial ChIP-seq should be conducted on whole embryo (or cranial dissection) of TS13-14 embryos to allow comparison to the microarray, other ChIP-seq experiments from the forming kidney, testes, or other regions of interest should be considered to test whether genes targeted by CECR2 are conserved throughout development.

Also of interest would be to identify what specific histone modifications recruit CECR2. Co-immunoprecipitation of histones by anti-CECR2 pulldowns could be tested by Western blotting with antibodies to the various acetylation, methylation, or variant peptide alterations to the histone core (Egelhofer et al., 2011). BPTF was found to specifically bind H3(1–15)K4me3 modified histones, and the same methods could identify the CECR2-specific target (Li et al., 2006). Alternatively, the advent of publically available histone modification databases may allow predictions to be made as to which modifications are relevant through the cross-referencing of these databases with the *Cecr2*^{Gt45Bic} microarray and ChIP datasets. This approach would still require confirmation via co-immunoprecipitation or binding assays as presented by Li et al. (2006).

It is this author's opinion that the mechanisms of chromatin remodeling—in how CECR2 regulates target regions, the potential for inheritance or change of this regulation through developmental cell lineages, and the integration of CECR2 data into a better understanding of CERF and ISWI function—represent the greatest potential impact of this and future work on CECR2.

4.4: CECR2 affects the transcription of genes during neurulation with known roles in open neural tube defects

The initial assumption that the *Cecr2*^{Gt45Bic} BALB/c dataset would show both a greater frequency and intensity of fold-change has been overturned. Examination of the data reveals multiple candidates with suggested roles in neurulation that were equivocally affected in both the *Cecr2*^{Gt45Bic} BALB/c and *Cecr2*^{Gt45Bic} FVB/N datasets. Thus whatever the CECR2 modifier effects may be (Davidson et al., 2007; Kooistra et al., 2011), it is concluded that the modifiers either do not alter CECR2/CERF chromatin remodeling transcriptional regulation, or are not active until after Theiler stage 14. This conclusion initiated the examination of *Cecr2*^{Gt45Bic} FVB/N neural closure and the discovery of neural closure delay even in the *Cecr2*^{Gt45Bic} FVB/N mutant embryo (Kooistra et al.,

2011). It was further noted that the dominant strain modifiers of the FVB/N background were not able to suppress the *Cecr2*^{tm1.1Hemc} FVB/N neural tube phenotype to the same degree as in *Cecr2*^{Gt45Bic} FVB/N (Davidson et al., 2007). Mutant NTD penetrance in the resistant FVB/N background remained much lower than the susceptible BALB/c strain. The initial penetrance assessment was performed early in the FVB/N backcrossing and found a ~30% (11/35) penetrance. Later work by Rasmussen (personal communication 2010) found a reduction after a further three FVB/N backcrosses to ~20% NTD penetrance. Either rate is substantially higher than the 2.9% initially reported for *Cecr2*^{Gt45Bic} BALB/FVB F1 hybrids and the 0% exencephaly penetrance after five FVB/N backcrosses (Davidson et al., 2007).

The presence of encephaloceles indicates the *Cecr2*^{tm1.1Hemc} clefts likely originate from a failure to close the anterior neuropore (Hedlund, 2006). Strain dependant location or timing of the anterior closure site may be of greater importance than the midbrain/hindbrain location. Although positional variation of the anterior closure site is not found within the literature, Juriloff et al. (1991) surveyed mouse closure sites from various strain backgrounds and found a strain-dependant timing variation when the anterior site initiates. The BALB/c and FVB/N strains were not compared. The BALB/c anterior closure site may be more rostral and the FVB/N counterpart more caudal relative to each other. Davidson et al. (2007) tested whether closure site 2 varied between the strains, and found no difference. Anterior differences may have been overlooked, as they were not the focus of the study. A more posterior position of the FVB/N forebrain closure site 3 could reinforce the weakened *Cecr2*^{tm1.1Hemc} cranial site 2 closure process, countering the development of exencephaly, but in turn leave the anterior-most region of site 3 susceptible to midline defects. A more anterior position of the BALB/c forebrain site could elicit the opposite effects. Future projects could consider high-resolution SEM imaging to view the anterior closure site locations in *Cecr2*^{tm1.1Hemc} FVB/N and *Cecr2*^{tm1.1Hemc} BALB/c embryos to determine this theory's validity.

From the short-list of genes considered as candidates, *Alx1*, *Bmi1*, *Met*, *Dlx5*, *Mdm4*, and *Prrx1* mutations also manifest facial cleft defects (Martin et al., 1995; Depew et al., 1999; Qu et al., 1999; Akasaka et al., 2001; Schaeper et al., 2007; Terzian et al., 2007), and may represent a common mechanism disrupted in both *Cecr2*-related exencephaly and midline clefts. However, no candidate gene mutation develops all aberrant defects of the *Cecr2* mutants, many of the candidates manifest other defects not found in *Cecr2* mutants, and the expression change of most candidates is below a 2-fold change. This suggests the combined disruption of multiple small changes acting together in the *Cecr2* mutation might result in the *Cecr2* mutant defects.

4.4.1: A proposed role for *Cecr2* in neural closure

A role associated with the planar cell polarity pathway showing defects in convergent extension, ciliogenesis, or WNT-signaling, was the preferred model for CECR2 activity presented by Dawe et al., (2011). In favour of a PCP

mechanism were general similarities between the *Cecr2* and core PCP aberrant phenotypes, supported by the discovery of disorganized stereocilia in *Cecr2^{Gt45Bic}* inner ears (Dawe et al., 2011). The data presented here argues against a PCP association during neurulation. Other potential explanations for the NTDs, such as neural tube hinge point, or fusion defects, were discarded after detailed morphological examination of the *Cecr2^{Gt45Bic}* neural epithelium (Dawe, 2011).

The microarray analyses of *Cecr2^{Gt45Bic}* mutants compared to wildtype indicate a number of misregulated candidate genes with known roles in neural tube closure. The primary candidates now include *Dlx5*, *Met*, *Alx1*, and *Epha7*. The individual disruption of these candidate genes resembled *Cecr2* defects, and I suggest that the combined disruption of multiple candidate genes is what alters mesenchymal regulation and ultimately leads to exencephaly.

The generation of the *Cecr2^{tm1.1Hemc}* allele further supported the idea that the the cranial mesenchyme is disrupted. As a more severe mutation, it was expected to demonstrate more pronounced phenotypic defects. Rather than displaying defects such as craniorachischisis, which was expected if aggravating a PCP defect, the new mutants showed anterior midline facial clefts, which is more characteristic of *Dlx5* (Acampora et al., 1999) and *Alx1* mutations (Uz et al., 2010).

A speculative network can be drawn when considering the chromosome 6A enrichment that would suggest *Dlx5* and *Met* are among the more direct CECR2 targets. A network of *Cecr2*->*Dlx5*->*Alx1* during the formation of the neural and midline defects could explain how a disruption of *Cecr2* leads to *Alx*/*Dlx*-like defects. However, the relationship must be more complicated than a linear model as neither *Dlx5* nor *Alx1* heterozygous mutations present neural tube defects. The combined disruption of *Met* or other genes may also be required for the manifestation of neural defects (Relaix et al., 2003). Likewise, *Epha7* misregulation found only in the *Cecr2* BALB/c mutations may be necessary in combination with *Dlx5/Alx1/Met* disruption to bring about the strain specific neural defects. There may also be other candidate transcripts absent from the Affymetrix MOE 420 2.0 microarray chips that have not yet been identified. Moreover, the *in vivo* molecular function of the CECR2 remodeling complexes has not been confirmed, and so how *Cecr2* mutation results in the misregulation of these genes during development is not understood.

4.4.2: Proposed future directions of CECR2 neurulation research

The transcriptional changes brought about by *Cecr2* mutation are proposed to cause the NTDs. Although the changes are individually subtle, is the combined effect upon the series that is proposed to bring about the defects. *Cecr2* mutant embryos should then show rescue of neural closure if the expression of key candidate genes are returned to wildtype levels. Gray and Ross (2011) recently published methods allowing cranial neural tube closure to progress under *in vitro* whole embryo culture conditions. Applying such techniques to *Cecr2^{Gt45Bic}* or *Cecr2^{tm1.1Hemc}* homozygous embryos could be used to test rescue of neural closure through reintroduction of the target candidates. Recombinant retroviruses have

been successful for neural tube expression (Nakagawa and Takeichi, 1998) and embryonic culture expression rescue experiments (Shi et al., 2004), and so should be amenable for experiments designed to restore transcripts downregulated by *Cecr2* mutation. Upregulated transcripts could in turn be reduced by siRNA. Embryonic culture and rescue experiments could also establish secondary regulatory cascades such as the proposed *Alx1* regulation by DLX5. The return of DLX5 to normal levels should see a corresponding rescue of *Alx1* expression by qRT-PCR. Throughout this thesis, certain candidates such as the *Eya/Six/Dach* gene network have been proposed to be secondary effects. To validate these conclusions one would expect them not to be associated with regions identified by ChIP-Seq and they should show rescue if tested by qRT-PCR when intermediate factors are returned.

Overall, the potential combination of targets may be quite complex and thus difficult to demonstrate. A second approach could address how mesenchymal or MET processes, rather than individual genes, are mechanistically affected in *Cecr2* mutants. Based on the discovery of renal apoptosis, an apoptotic loss of mesenchymal tissue is hypothesized to result in reduced neural fold support in a manner matching that reported in *Alx1* mutations (Zhao et al., 1996). Serial sections followed by TUNEL or activated caspase immunohistochemistry should identify any apoptotic aberrations if present in the forebrain mesenchyme.

Alternatively, as the general *Cecr2* expression and a number of candidates appear linked to processes of mesenchymal development (*Alx1*, *Bmp2*, *Hand2*), or epithelial morphogenesis and transitions (*Alx1*, *Bmp2*, *Met*, *Foxa1*, *Frzb*, *Hand2*, *Sema3a*, *Six1*, *Slit2*, *Sox17*), future work could attempt to establish whether cells of the closing neural tube are undergoing such CECR2-regulated mesenchymal-epithelial or epithelial-mesenchymal transitions. Neural mesenchymal-epithelial defects are most often associated with secondary neurulation of the tail, while epithelial-mesenchymal transitions are the primary focus of the cranial neural tube generating neural crest mesenchyme (reviewed by Hay, 2005). However, known mesenchymal-epithelial regulators such as PAX3 (Wiggin et al., 2002) and MET (Relaix et al., 2003) can disrupt cranial neural closure. Vital dye analysis (Serbedzija et al., 1992; Kawakami et al., 2011) of cultured whole embryos during neural closure (Gray and Ross, 2011) could assay whether *Cecr2*-expressing cells are showing defects in MET/EMT transition and migrations by following cell migration through MET/EMT and comparing transition rates in mutant versus wildtype samples. Although the x-gal staining of *Cecr2*^{Gt45Bic} embryos is in both mesenchymal and epithelial tissues of the early embryo, it may be that one of the two represents the initial source of *Cecr2* activation, while the other site contains cells with the CECR2-fusion protein after a cellular MET/EMT. The predominantly epithelial expression of *Cecr2* is at odds with the mesenchymal genes found affected, and having CECR2 involved in a transition could explain the discrepancy.

The microarray analysis offered many candidates, but the following discussed genes are considered the leading candidates whose disruption likely plays a part in the presentation of exencephaly:

Epha7

The expression of *Epha7* is regionally restricted throughout the future prosencephalon and pro-rhombomere as well as the paraxial mesenchyme of the head and somites and dorsal limb mesenchyme (Araujo et al., 1998; Taneja et al., 1996). The expression of *Epha7* shows only a limited spatial and temporal overlap with the broader regions of *Cecr2* expression throughout development. Loss of *Epha7* in mice results in exencephaly in 24% of mutant embryos on a mixed 129X1/SvJ * C57BL/6 background due to an overgrowth of neural progenitors and a loss of apoptotic cell culling (Depaepe et al., 2005). Mutants of *Epha7* are not known to show renal, otic, gonadal, or anterior craniofacial defects, but these structures may not have been examined. Other than neural closure, *Epha7* does not appear to have a broad functional overlap with *Cecr2* during development.

The disruption of *Epha7* by *Cecr2* mutation is affected solely on the NTD-susceptible BALB/c strain. However, it is still considered among the candidate genes due to its phenotypic association with exencephaly. The *Cecr2*^{Gt45Bic} BALB/c microarray shows a -1.33-fold reduction, which was confirmed by qRT-PCR in *Cecr2*^{tm1.1Hemc} BALB/c at a -1.41-fold reduction. No significant fold-change in *Epha7* appears between *Cecr2*^{Gt45Bic} FVB/N and the FVB/N reference samples. The reduction in *Epha7*, specific to *Cecr2*^{Gt45Bic} BALB/c, in addition to other candidates may cross a threshold effect resulting in exencephaly. *Epha7* could then be a key differential factor between the BALB/c and FVB/N strains during the neural closure in *Cecr2* mutants, but its regulation is unlikely to be the primary function of CECR2 remodeling activity based on expression overlap and mutant phenotype comparisons.

Cecr2^{tm1.1Hemc} FVB/N homozygous pups with exencephaly could be tested by qRT-PCR to confirm whether *Epha7* correlates with the appearance of NTDs in the new mutation. If it does not show a disruption by qRT-PCR, *Epha7* could be eliminated as a candidate in *Cecr2* mutant neural tube defects. If *Epha7* does show a *Cecr2*^{tm1.1Hemc} FVB/N homozygous effect, then *Epha7* could be further examined by generating *Cecr2*^{Gt45Bic}/*Cecr2*^{Gt45Bic}; *Epha7*^{tm1.1Jf}/*Epha7*⁺ double mutants bred onto the FVB/N background. The disruption of *Epha7* would be expected to result in higher incidence of neural tube defects compared to either *Cecr2*^{Gt45Bic} homozygotes or *Epha7*^{tm1.1Jf} heterozygotes in FVB/N. Follow-up questions could focus on why *Epha7* is specifically altered in the BALB/c strain? This line of inquiry could tie directly into the NTD strain modifier project as reported by Davidson et al. (2007) and Kooistra et al. (2011). *Epha7* could represent a tipping point or threshold effect in NTD manifestation, or may be an early secondary consequence of neurulation failure. *Epha7* gene is not located within one of the currently identifies enriched target regions, and the expression and associated phenotypes do not generally match *Cecr2*. For these reasons, this researcher predicts it to be a secondary effect.

Met

Mesenchyme Epithelial Transition factor (MET) acts as a receptor for hepatocyte growth factor as part of a signaling cascade in tissues undergoing mesenchymal-epithelial and epithelial-mesenchymal transitions (Bladt et al., 1995; Sonnenberg et al., 1993). The microarray data of *Cecr2*^{Gt45Bic} mutants show a *Met* reduction averaging -1.36-fold. The phenotypes and functions associated with a reduction in *Met* include roles in craniofacial and renal defects (Bladt et al., 1995). Although *Met* mutations are not known to directly induce neural tube defects on its own, a genetic interaction between *Met* mutations and neural tube defect associated mutation *Pax3/Splootch* (Relaix et al., 2003) shows that *Met* can influence neural closure. *Met* is also associated with a variety of renal processes including planar cell polarity-like defects (Qin et al., 2010). The MET signaling cascade can interact with WNT signaling (Birchmeier et al., 2003; Monga et al., 2002). The renal roles of MET and its signaling in the early metanephric kidney are necessary for mesenchymal survival, mesenchymal-epithelial transitions during nephron development, and the branching of the ureteric bud (Woolf et al., 1995). The heterozygous *Met* mouse mutations go on to develop hydronephrosis, although the cause is not known (Graveel et al., 2004). MET signaling is active in the developing renal system in the invading ureteric bud and the forming metanephros undergoing mesenchymal-epithelial transitions (Sonnenberg et al., 1993; Woolf et al., 1995).

Unfortunately, *Met* was initially overlooked as a candidate and absent from the qRT-PCR confirmation experiments. Thus qRT-PCR confirmation of a *Met* misregulation should be tested in future projects examining *Cecr2* neural closure or renal development. The reported developmental roles and expression of *Met* resembles *Cecr2*-related neural and renal processes now identified (Bladt et al., 1995; Woolf et al., 1995; Relaix et al., 2003; Graveel et al., 2004; Qin et al., 2010). The similarities, along with its chromosomal position within the Chr6A enrichment region, suggest CECR2 may directly regulate *Met*.

Alx1

Within the *Cecr2*^{Gt45Bic} microarray, *Alx1* was reduced an average of -1.82 fold, and was confirmed by *Cecr2*^{tm1.1Hemc} cranial qRT-PCR at a -2.32 fold-reduction. The ALX1 homeobox transcription factor is an early marker of mesenchyme cell lineage (Ettensohn et al., 2003), chondrocyte development, as well as branchial arch and forebrain mesenchyme development (Zhao et al., 1994). Mouse mutants of *Alx1* develop exencephaly with variable strain penetrance (Zhao et al., 1994) and *Alx1/Alx4* show evidence of genetic compensation as the double homozygous mutants further present with midline clefts (Qu et al., 1999). The phenotypic comparison between published *Alx1* defects and those found in *Cecr2* mutants show clear similarities in the embryonic head.

Zhou et al. (1994) suggest that loss of forebrain mesenchyme is sufficient to drive a cranial neural tube defect. Whereas a case can be made for an *Alx1* involvement in *Cecr2* neural defects, a comprehensive argument cannot be made

for *Alx1* in all tissues showing *Cecr2* expression or defect. Furthermore, a 2-fold reduction in *Alx1*, as confirmed in *Cecr2* homozygotes, would be equivalent to *Alx1* heterozygote levels, which are not reported to have neural fold defects (Qu et al., 1999). Further testing of *Alx1* mouse mutant heterozygotes could be tested on the sensitized BALB/c strain to directly confirm whether a 2-fold reduction is sufficient to develop exencephaly. A reduction of *Alx1* likely adds to a complex interaction of multiple gene disruption leading to the defect manifestation.

Dlx5

Dlx5 is the second favoured candidate positioned within the enriched chromosomal region Chr6A. *Dlx5* is predicted to be directly regulated by *CECR2*. Early neural expression of *Dlx5* includes the ventral cephalic epithelium, otic/olfactory placodes, and along the boundary of the neural plate (Acampora et al., 1999). The microarray analyses show a *Dlx5* reduction averaging -1.28-fold, which was confirmed by qRT-PCR in the *Cecr2^{tm1.1Hemc}* BALB/c at a -1.42-fold reduction. *Dlx5* also appears within the branchial arches and forebrain mesenchyme (Acampora et al., 1999), which overlaps with *Alx1* expression (Zhao et al., 1994). The cranial morphology of *Dlx5* with exencephaly resembles the neural tube defects found in *Cecr2* mutant embryos (Acampora et al., 1999). *Dlx5* expression is consistently downregulated in all *Cecr2* mutant microarrays. The *Dlx5* mouse mutants also show cleft palates and abnormal morphology in their inner and middle ear (Acampora et al., 1999; Depew et al., 1999). Misregulation of *Dlx5* is implicated in some ovarian tumors (Tan et al., 2010), although this is due to an upregulation of *Dlx5* and so likely unrelated to the *Cecr2^{Gt45Bic}* FVB/N ovarian cancers. A role for *Dlx5* in renal development is not established, although the *Cecr2^{tm1.1Hemc}* FVB/N qRT-PCR could detect *Dlx5* transcripts in TS24 renal samples.

During *Drosophila* development, the homologous *distal-less* (*Dll/Dlx*) targets and regulates *aristal-less*, which is the homologue of the vertebrate *Alx* genes (Campbell and Tomilison, 1998). Both the *Dlx* and *Alx* families have expanded to multiple genes in mice. Mutations of *Dlx5/6* genes are known to disrupt *Alx4* expression (Depew et al., 2002). This suggests the regulation of *Alx* by *Dlx* is conserved in some combinations. A direct interaction of *Dlx5*->*Alx1* has not been shown in mice, but a developmental pathway of *Cecr2*->*Dlx5*->*Alx1* may be present in the craniofacial and neural tube defects of *Cecr2* mutations. Biologically, the interaction might not be a simple linear relationship and the disruption of both might act in concert, or with any number of other candidates or modifiers to bring about the defects.

Gene interactions and pathways identified by the embryonic culture experiments proposed could also be tested with mutant mouse lines when available. *Dlx5* and *Alx1* mouse mutations exist, and *Dlx5* mutant homozygous embryos could be tested for a reduction in *Alx1* to establish whether regulation is conserved. Likewise, *Alx1^{+/-}*; *Dlx5^{+/-}* double heterozygous mutations could be analyzed to test whether the dual reduction as seen in *Cecr2* mutations is sufficient to manifest exencephaly or midline clefts. However, such crosses are

limited by the availability of mouse lines and the background genetic strain must be considered. In the case of *Alx1*^{+/-}; *Dlx5*^{+/-} double heterozygotes, they would be expected to show exencephaly and midline clefts in a BALB/c background if the pathway is confirmed, with perhaps a much-reduced penetrance in FVB/N.

4.5: *Cecr2* mutations manifest congenital abnormalities of the kidney and urinary tract, but whether the same candidates identified during neurulation are targeted in renal organogenesis remains unclear

The presented work seeks to establish *Cecr2* as a CAKUT-associated gene with roles in renal development. The particular set of renal defects appearing together is unique to *Cecr2* mutants, but resembles other CAKUT models. Over 280 mouse mutations present with small kidneys (Mouse Genome Informatics (MGI), <http://www.informatics.jax.org>, 2012). Likewise, over a hundred gene-disruptions are associated with unilateral agenesis and an overlapping list of over a hundred genes are associated with hydronephrosis (MGI, <http://www.informatics.jax.org>, 2012). The sheer volume makes direct comparisons cumbersome. The most selective list was found when looking at causes of multiple ureter and duplex kidney phenotypes. Only a handful of genes are known to induce multiple or bifid ureteric buds. Genes with mutations manifesting UB defects include *Slit2* (Grieshammer et al., 2004), *Bmp4* (Miyazaki et al., 2000), *Dlg1* (Iizuka-Kogo et al., 2007), *Foxc1* (Kume et al., 2000), *Spry1* (Basson et al., 2005), and *Ret* (Jain et al., 2006). Multiple ureters and duplex kidneys are likewise quite rare in mouse models. A subset of the genes with multiple ureter defects consisting of *Fat4/Fjx1* (Saburi et al., 2008), *Lim1* (Pedersen et al., 2005), *Mks1* (Cui et al., 2011), *Nfia* (Weining et al., 2007), and *Ptprf/Ptprs* (Uetani et al., 2009) mutations also manifest duplex kidneys. Even within this limited list, many have secondary defects such as tubule cysts not consistent with traits found in *Cecr2* mutants. *Cecr2* mutant renal defects are found with double ureters, duplex kidneys, hydronephrosis, smaller embryonic kidneys, reduced glomeruli numbers, and unilateral agenesis.

The closest phenotypic match among the previously discussed list is *Foxc1*^{tm1Blh}, which possesses renal defects, but also open neural tube, craniofacial and gonad developmental defects. However, the particular types of defects in *Foxc1*^{tm1Blh} do not directly resemble *Cecr2* mutant phenotypes. Whereas *Foxc1* mutants show the relevant duplex kidneys, extra ureters, and hydronephrosis, *Foxc1* disruption is not known to induce smaller embryonic kidneys, apoptosis, or renal agenesis. Conversely, *Eya1* mutants show mesenchyme apoptosis, smaller kidneys, and agenesis from a lack of ureteric budding. No single identified candidate gene covers the entirety of *Cecr2* renal phenotypes. From the comparisons, an oddity in the *Cecr2* condition is that both multiple ureteric buds (duplex kidneys) and a loss of ureteric budding (agenesis) present both from the same mutation. These phenotypes are generally regarded as resulting from opposing effects (Pedersen et al., 2005). The combination of *Foxc1* and *Eya1* both downregulated in the *Cecr2* mutant kidneys may bring about the combined set of phenotypic manifestations. This cross has not been reported in the literature, but I

propose that the resulting double-heterozygotes in the FVB/N background would develop duplex kidneys or agenesis similar to *Cecr2*-like CAKUT defects in the NTD sensitive BALB/c genetic background.

Ideally, a second microarray of a *Cecr2*^{Gt45Bic} homozygous vs wildtype dataset during metanephric development would allow for the most robust comparison of targets/changes. As this resource was not available, predictions of potentially conserved candidates were drawn from the neural closure microarray dataset and individually tested by qRT-PCR during metanephric development. As to whether the transcriptional targets of CECR2 are conserved between renal and neural development, the interpretation of the data remains ambiguous. The transcripts tested in the maturing metanephric kidneys by qRT-PCR did not show changes consistent with the neural microarrays in the majority of samples tested. This may indicate that the original hypothesis was incorrect, and that the TS24 renal function of CECR2 is distinct from the TS14 embryonic effects. There has not yet been a study of ISWI remodeling or transcriptional targets throughout development, nor is there a clear understanding of how ISWI is recruited to, or even affects, target regions. BPTF and the NURF complex were found to bind to and regulate the *Engrailed* genes (Deuring et al., 2000; Badenhurst et al., 2002; Barak et al., 2003) in neurons, yet *En1/En2* were not reported to be targeted or disrupted in the ES lines of *Bptf* mutant microarray by Landry et al (2008). The discrepancy between the reports may further support the idea that ISWI targeting changes depending on the cell line tested.

Alternatively, in the *Cecr2* studies it may be that key candidates were overlooked and not yet tested in the renal samples. *Eya1* primers from the previous neurulation arrays failed to amplify target regions during the renal runs in both wildtype and mutant samples, despite *in situ* hybridization confirming the presence of *Eya1* transcript. *Met* was not yet considered a prime candidate at the time of the qRT-PCR studies and so was not tested. As the enriched regions of Chr6A, F-G, and 12B are proposed to be direct targets, a larger number of genes from these regions could be selected for further testing in renal samples. Until a ChIP-seq database or similar approach is carried out to distinguish direct targets versus secondary transcriptional changes we cannot be sure which genes are critical to answer the question of conserved targeting.

Cecr2 now bolsters a small cohort of mouse mutations capable of modeling defects of ureteric bud induction. Establishing *Cecr2* mutants as CAKUT developmental models signifies a major addition to *Cecr2* research projects. This increases both the breadth of the *Cecr2* project as well as the impact of *Cecr2* research to the new community of CAKUT researchers. Following the established trend of this thesis work, the renal defect found do not match those of known PCP-defects and do not develop the archetypical polycystic kidney disease of PCP misregulation or mutation.

4.5.1: A proposed role for *Cecr2* in renal development

The phenotypic and molecular data suggest four distinct stages involving *Cecr2* in renal development:

Stage 1: *Cecr2* expression is detected within the Wolffian duct, mesonephric tubules, and the region of the presumptive future metanephric mesenchyme preceding metanephric induction. No morphological defects have been found among the *Cecr2* mutant lines within mesonephric structures. A detailed cellular examination was not done beyond *in situ* hybridization of standard developmental markers. The mesonephric tubules and surrounding mesenchyme express wildtype equivalent levels and patterns of the tested markers.

Stage 2: The duplex kidneys with double ureter phenotype arise from ureteric bud induction during Theiler stage 15 (by 25 somites). Theiler stage 13-14 *Cecr2*^{Gt45Bic} FVB/N mutant embryos show a disruption in overall levels of *Slit2*, *Foxc1*, *Eya1/Six1*, and *Met*. As the array data came from whole embryos, changes in expression may not represent changes specifically in the forming kidney despite these genes being present in the appropriate tissues. At TS13-14, mesonephric development is underway, with the intermediate mesenchyme and nephrogenic cord both present. SLIT2 acts as a secreted ligand for ROBO receptors. In the intermediate mesenchyme, SLIT/ROBO signaling restricts future development of the metanephric mesenchyme (Wilm et al., 2004). The *Foxc1* and *Eya1* genes are early metanephric mesenchyme transcription factors, but generally show a counterbalancing expression wherein FOXC1 in regions of SLIT2 signaling restricts the fate of the *Eya1* (Kume et al., 2000). FOXC1 defines regions outside of the presumptive future kidney, while EYA1 specifies tissue fated for the metanephric kidney. MET is necessary for the survival of early mesenchyme, the transition of the mesenchymal into epithelial tissue during nephrogenesis, and is involved in the branching of the early uterine bud (Woolf et al., 1995). The disruption of these key regulatory genes in *Cecr2* mutants suggests CECR2 is necessary for early ureteric bud induction.

The loss of *Foxc1* results in fewer limitations controlling the expansion of ureteric bud sites and gives rise to multiple ureters (Kume et al., 2000). The loss of *Eya1* prevents ureteric bud formation and results in complete absence of budding or kidney formation (Xu et al., 1999). Both phenotypes are present in *Cecr2* mutant animals on the FVB/N background. If *Cecr2* loss results in the reduction, but not loss, of both fates within the early metanephric blastema, this could destabilize the ureteric bud induction. With fewer signals to restrict exogenous sites, but less activity driving individual site induction, the embryo may become sensitized to ureteric defects through the removal of the upper and lower thresholds controlling bud formation. The particular factors driving one fate over the other in the *Cecr2* mutants FVB/N animals are unknown, but appears to favour multiple ureters as this phenotype is more common than kidney absence.

Stage 3: The branching metanephric kidney shows additional defects. The reduction in mature glomeruli numbers and smaller kidney volume suggests the disruption of *Cecr2* either reduces nephron differentiation, leads to a loss of

nephron structures, or delays nephron development. The qRT-PCR and *in situ* hybridization evidence for the embryonic metanephric kidneys suggests that many key cellular identifiers of the nephron stages are not disrupted. Once initiated, the nephron development cascade proceeds. The kidneys of animals surviving to adulthood show the ability to induce hypertrophic compensation and on average achieve a comparable size and weight to wildtype kidneys.

Stage 4: A third of neonatal *Cecr2*^{tm1.1Hemc} pups die within 36 hours of birth with no noted neural tube defects and both kidneys present. The kidneys of pups found dead show a range of apoptosis levels all above wildtype states and the presence of renal hemorrhages. Some showed complete apoptosis of all renal tissue. Apoptosis of the majority of renal cells, or severe hemorrhage, could result in complete renal failure and offers a potential pathological explanation for neonatal death. CECR2 may then act as a survival factor for late-stage renal development, or its loss results in a cascade effect culminating into mass renal apoptosis. One important caveat of this study is that the apoptotic samples were collected from pups found dead, and does not control for the amount of time between death and discovery. Necrotic cells can trigger TUNEL signals (Grasl-Kraupp et al., 1995; Unal-Cevik et al., 2004), and although the wildtype sample was also from a pup found dead, it could have been a comparatively recent death. The apoptosis study should be repeated in TS26 embryos.

Taken together, the data collectively point toward a disruption of renal mesenchyme and its ability to undergo mesenchymal-epithelial transitions. Early disruption of the intermediate and metanephric mesenchyme through the misregulation of *Eya1* and *Foxc1* could explain the ureteric bud defects. However, these transcriptional changes may not be a direct effect of CECR2, as later developmental stages do not show these disruptions. The early misregulation of *Eya/Six/Dach* and *Foxc1/Slit* genes could arise from the mesenchymal loss/disruption and not from direct regulation of CECR2 remodeling. No singular disruption of a given candidate gene identified thus far can explain the entire cascade of events leading to renal defects of the *Cecr2* homozygous FVB/N animals. A number of candidates were tested, but many others were not, and it may be that relevant genes were overlooked.

Alternatively, the renal function of CECR2 may be altogether distinct and separate from the candidates and regions identified during neurulation. The phenotypic comparison of *Cecr2* homozygous FVB/N could suggest a number of potential new candidates to further test by qRT-PCR. This would start with genes known to manifest duplex kidneys. However, if restarting the search for disrupted pathways or genes in *Cecr2* homozygous FVB/N renal development, a microarray approach could be considered.

4.5.2: Proposed future directions to determine whether the targets of CECR2 are consistent throughout development

The earliest stages of ureteric bud induction could be analyzed by comparing microarray data from the *Cecr2* homozygotes to wildtype along with direct binding assays by chromatin immunoprecipitation. The budding

ureter is quite a small structure and surrounded by mesonephric and urogenital regions, which poses the risk of tissue heterogeneity during dissections. Flow cytometry could be considered to isolate a pure population of renal epithelial and metanephric mesenchymal cells for RNA extraction (Plotkin et al., 2006; Metsuyanin et al., 2009; Potter et al., 2010). These isolates would also be useful as purified samples for RNA work, co-immunoprecipitation of the functional complex, and chromatin immunoprecipitation of renal CECR2 and CERF.

Direct binding assays such as ChIP-seq have been suggested throughout this text as the necessary next step towards determining the targets of CECR2 remodeling. Comparing ChIP-seq datasets of CECR2 targets during neurulation to those during metanephric development would be the most direct and comprehensive method to test whether sites of CECR2 binding changes between neural and renal development. However, as at least two CECR2 complexes have been discovered (Banting et al., 2005; Thompson et al., 2011) they may have different targets. Co-immunoprecipitation of CECR2 binding partners should also be confirmed from both neural and renal samples to confirm whether both have the same CERF complex active. Banting et al. (2005) identified a human CECR2-SNF2L complex in HEK and Thompson et al. (2011) confirmed a mouse CECR2-SNF2H complex in adult testis. Neither study identified additional cofactors beyond the core CECR2-ISWI. Thompson et al. (2011) noted the 1 MDa complex found in the testes could contain other co-factors, as the size was larger than expected, but was unable to identify the other components. It is unknown which complex is active in a given cell type during development, whether the activities differ, or whether other components are present in these complexes. The presence of multiple CECR2 complexes signifies that the *Cecr2* mouse lines should not be treated as a single, simplistic knockout model. Multiple complexes may be affected with a single mutation, each with distinct developmental roles.

Lazarro and Picketts (2001) suggested the transition between SNF2H and SNF2L complexes may represent a progression between proliferative (SNF2H) and terminally differentiated (SNF2L) tissue based on expression analysis. Testing whether this is the case with the two currently identified CECR2 complexes could begin with *in situ* hybridization or immunohistochemistry of *Snf2l* and *Snf2h* in the closing neural tube and surrounding mesenchyme, as well as in the developing metanephric kidney to look for overlap with *Cecr2*. Lazarro and Picketts (2001) reported antibodies for identifying the SNF2L and SNF2H components. A confirmed CECR2 antibody is now available (Niri, personal communications, 2012). Another option to identify cell types expressing CECR2 would be to use an anti-B-gal in a two- or three-colour immunohistochemistry analysis of *Cecr2*^{Gt45Bic} heterozygotes. Identifying where in the forming neural tube, the early metanephric kidney, or other organs such as the adult testis *Cecr2* overlaps with either *Snf2l* or *Snf2h* at various developmental stages would help to focus study in the given organ system onto the relevant ISWI complex.

A next step would be to follow up on the work of Thompson et al. (2011) with co-immunoprecipitation of the various complexes from each of the tissues of interest. SNF2H and SNF2L exist in many functional complexes and expression

overlap alone is not sufficient to determine functional complexes. Banting et al. (2005) used a nucleosome-shift assay to test CERF activity, and this could be used to confirm CERF-H activity, but it may have little physiological relevance. ChIP-seq databases could be obtained from each identified CERF member. The common regions between CECR2 and SNF2L would identify the functional targets of CERF, while those in common between CECR2 and SNF2H indicate functional targets of CERF-H. As additional co-factors are identified, their ChIP-seq can be added to the target-matrix to further refine regions of interest.

Future CECR2 research should also address the claims put forward in Liu et al. (2002) and Liu and McKeehan (2002). These papers demonstrated yeast-two-hybrid associations, with partial confirmation by immunoprecipitation and subcellular localization that CECR2 binds with LRPPRC. However, I question the interpretation of the results of Liu et al. (2002) or Liu and McKeehan (2002). Their proposal that CECR2 is involved with mitochondrial function and vesicular trafficking is not supported by subsequent studies. They suggest that the CECR2 protein, tethered to LRPPRC, is involved in an unconfirmed mechanism by which apoptotic chromosomes are transported out into the cytoplasm to mitochondria, where mitochondrial apoptotic cascades could then act directly on the chromatin. Yet, the evidence provided (Liu et al., 2002) showed CECR2 to be confined to the nucleus, which is consistent with the subcellular studies of Tate et al. (1998). This unfounded model was based nearly entirely on theoretical interactions between protein domains identified by Liu et al. (2002) and Liu and McKeehan (2002). Their analyses of CECR2 reported two bromodomains, an AT-hook, a strong similarity to a guanylate binding protein, a region similar to a PAP-specific phosphatase, and a C-terminus of poly (A)-binding domain. Other than a single bromodomain and the AT-hook, their report was inconsistent with the domain analysis of Banting et al. (2005). Moreover, my attempts to replicate their results using the reference sequence and prediction programs cited were unsuccessful in generating the same domain architecture. There appears to be an error in the domain analysis of Liu et al. (2002) and Liu and McKeehan (2002), which cumulated in an unfounded model based upon theoretical interactions of these erroneous domains.

However, the original yeast-two-hybrid association of LRPPRC to CECR2 (Liu and McKeehan, 2002) may still be correct and relevant. Future work on the CERF complexes should test whether LRPPRC is a member of CERF or CERF-H through co-immunoprecipitation and Western blotting. The original yeast-two-hybrid (Liu and McKeehan, 2002) could not indicate what tissues may be expressing both CECR2 and LRPPRC, but a new *Lrpprc* tagged mouse line should allow sites of overlap to be identified (Xu et al., 2012).

4.5.3: Proposed future directions of CECR2 CAKUT research

The discovery of so many *Cecr2* renal defects presents a number of new questions regarding their causal connections or characteristics. Are the duplex kidneys of *Cecr2* mutants due to multiple budding events, or a later bifid split of the ureteric bud? Answering this will establish the earliest stage showing *Cecr2*

related defects. This would direct future qRT-PCR or microarray experiments to the appropriate stage just preceding defect manifestation in order to test the most direct transcriptional changes of *Cecr2* metanephric disruption. It is now proposed that the duplex state predisposes affected kidneys to the rare manifestation of hydronephrosis, but a direct association has yet to be found. Do the *Cecr2* homozygous FVB/N hydronephrotic kidneys always appear in duplex kidneys, or is there a secondary blockage event? Both of these possibilities could be addressed through increased sample collection and serial histology of the ureters from hydronephrotic kidneys. The limitation is the rarity of phenotypic penetrance.

This author predicts the reduced size of the kidneys to be caused by abnormal renal apoptosis throughout development. Apoptotic loss of cells is noted in neonates, but TS16-26 metanephric kidneys could be tested by TUNEL using the same methods as presented for the *Cecr2^{tm1.1Hemc}* FVB/N neonates. Apoptotic remodeling is an active part of renal development (Kim et al., 1996), and so a large sample size of both mutant and wildtype samples should be compared for abnormal apoptotic patterns. Alternatively, a reduction in ureteric branching is linked to reduced renal size in other gene mutations (Cain and Bertram, 2006), and the wholemount immunostaining methods presented in such papers could be applied to the *Cecr2* homozygous samples in order to visualize potential branching defects. There is an apoptotic pattern difference between most *Cecr2^{tm1.1Hemc}* FVB/N homozygous samples and those showing hemorrhage. Does the unusual apoptotic pattern precede the hemorrhaging or is it a secondary effect? There may be an undiscovered defect in angiogenesis. Gene ontology GOEAST analysis of the *Cecr2* microarray candidate shortlist identified an overabundance of candidate genes involved in blood vessel development, including *Hand2*, *Sox17*, *Prrx1*, *Slit2*, and *Arhgap24*. *Pecam1* markers did not show a change in metanephric renal vessel expression, but perhaps further *in situ* analysis of the five candidates identified by GOEAST or 3D imaging of the vessels (Walker et al., 2011), would reveal an underlying blood vessel defect.

Finally, the strain-specific nature of *Cecr2* mutant neural tube defects lead to the mapping and identification of modifier regions affecting *Cecr2* manifestation (Davidson et al., 2007; Kooistra et al., 2011). The FVB/N strain confers a dominant resistance to the neural defects (Davidson et al., 2007). The renal defects of *Cecr2* homozygous mutants appear to show an inverse relationship of FVB/N sensitivity or BALB/c resistance. However, the BALB/c penetrance must first be confirmed through increased sampling and histology of homozygous *Cecr2^{Gt45Bic}* BALB/c and *Cecr2^{tm1.1Hemc}* BALB/c TS26 embryonic kidneys. If confirmed, this would offer the possibility to future projects of mapping the modifier regions of the renal phenotypes using the same methods established by Davidson et al. (2007). The modifier regions affecting the renal defects may be unique and separate from those discovered by Davidson et al. (2007). If this is the case, then CECR2 may be showing a variety of complex interactions with the inherent differences between strains. Should the renal modifier region map to the same Chr19 segment identified by Davidson et al.

(2007), the modifier(s) would also need to be expressed and active in renal development as well as neural closure. The cross-reference of both requirements may allow candidates in the region to be further narrowed to the critical gene(s) of interest.

4.6: Re-exploring *Cecr2* as a Cat Eye Syndrome gene candidate

A yet unaddressed aspect to the *Cecr2* function lies within the naming and location of the *Cecr2* gene. Cat Eye Chromosomal Region gene candidate 2 (*Cecr2*) is located within a genomic region which in humans is identified as the causative region duplicated in Cat Eye Syndrome (CES). With the advances provided in this text we now have a much broader phenotypic and molecular understanding of *Cecr2* and its relation to CES should be re-explored. CES patients are identified by the presence of an additional bisatellited, dicentric, or ring chromosome 22(pter --> q11.2::q11.2 --> pter). Phenotypically, the CES spectrum is highly variable. CES is associated with bilateral ocular coloboma of iris, preauricular skin tags and pits, a variety of heart defects, downslanting palpebral fissures, anal atresia, microcephaly, bilateral total absence of the external ears, hypertelorism, micrognathia, cleft palate, scoliosis or skeletal defects, short stature, mental retardation, spina bifida, vaginal atresia, and renal defects including absent, ectopic or underdeveloped kidneys and hydronephrosis (Reviewed in Denavit et al., 2004; Berends et al., 2001; Rosias et al., 2001; OMIM entry #115470).

Cecr2^{Gt45Bic} and *Cecr2*^{tm1.1Hemc} mouse mutations both represent reductions in *Cecr2* activity whereas CES is caused by a duplication and likely overexpression of candidate genes. Cleft palate and hypertelorism could be structurally analogous to the milder cases of mid-line clefts found in *Cecr2*^{tm1.1Hemc} FVB pups, although both are heterogeneous defects. *Cecr2* shows strong staining within the developing eye and mouse mutants may possess abnormally placed and sized pupils, but did not show CES-like colobomas (Lehmann, personal communications 2009). *Cecr2* mutant renal defects show absent or underdeveloped kidneys and are associated with hydronephrosis on the FVB/N background. Dawe et al. (2011) found vaginal atresia and spina bifida among *Cecr2* mutants when combined with *Vangl2* mutants. Although these comparisons are by no means definitive, they do push *Cecr2* again to the forefront of CES candidates. A notable exception is that *Cecr2* is absent from developing cardiac tissue (Banting et al., 2005; Dawe et al., 2011). If *Cecr2* is involved in some of the CES phenotypes it likely represents a polygenic amalgamation of defects. The causal region of at least the renal, anal, and preauricular defects associated with CES was recently refined to only a 600 kbp region in humans (Knijnenburg et al., 2012). Only *CECR2*, *SLC25A18* and *ATP6V1E1* remain as candidates causing those traits of the syndrome.

Further placing *Cecr2* among the premier CES candidate genes is the speculation of a possible auto-regulatory role of *CECR2* as identified by the microarray studies. The largest cluster of affected transcripts surrounds the mouse CES chromosomal region. The syntenic mouse CES chromosomal region

spanning from 1L17RA to USP18, and including the *CECR* genes, maps to mouse chromosome 6F. The region of mouse chromosome 6F-G surrounding the CES chromosomal region is syntenic to human chromosomes 10 and 12. Working under the model that ISWI remodelers are not single-gene transcription factors, rather affecting larger regions of chromatin spanning clusters of genes, the location of *Cecr2* within one of its own affected clusters suggests CECR2 can affect its own transcription. If CECR2 is involved in directly regulating the CES region it could be amplifying, or countering, the dosage sensitivity of the region through auto-regulatory feedback in CES patients.

4.7: Concluding Remarks

Banting et al. (2005) first presented CECR2 as an ISWI-binding protein and the *Cecr2*^{Gt45Bic} mouse mutation with associated defects in neural closure. The presented thesis project prompted the generation of a new *Cecr2*^{tm1.1Hemc} deletion allele, and used both mutations to further characterize *Cecr2*-associated developmental defects. *Cecr2* mutants are now known to manifest exencephaly, open eyelids, midline facial clefts, encephaloceles, reduced adult brain and testes weight, caudal hemivertebrae, stereocilia defects (Dawe et al., 2011), hyperkalemia, ovarian cystic tumours, duplex kidneys, absent kidneys, renal apoptosis, renal hemorrhage, and hydronephrosis.

This work generated the first functional data of CECR2 remodeling; having identified genes disrupted by *Cecr2* mutation during neurulation and potential CECR2 target regions. The data argue against the hypothesis suggested in Dawe et al. (2011) that PCP is the primary defect causing exencephaly in *Cecr2* mutants. The microarray and qRT-PCR data suggest that disruptions in mesenchymal/epithelial transcription factors may cause of the neural tube closure defects exencephaly and midline clefts. The data further indicate potential target regions clustered within chromosome 6A, 6F-G, and 12B.

In almost every aspect, the results demonstrate that the function of CECR2 is complex. No individual target region, or candidate gene, identified is thought to cause all developmental defects associated with *Cecr2* mutations. Even if CECR2 is confirmed to directly regulate the transcription of genes during neurulation, these targets may be transient and change depending on the stage or cells tested. CECR2 appears to be involved in multiple complexes and each complex may have unique functions. A cumulative effect of multiple disruptions likely leads to the defects of *Cecr2* mutant mice.

Bibliography

- Acampora, D., Merlo G. R., Paleari, L., Zerega, B., Postiglione, M. P., Mantero, S., Bober, E., Barbieri, O., Simeone, A., and Levi, G. (1999). Craniofacial, vestibular and bone defects in mice lacking the Distal-less-related gene *Dlx5*. *Development* **126**, 3795–3809.
- Agarwala, S., Sanders, T.A., and Ragsdale, C.W. (2001). Sonic hedgehog control of size and shape in midbrain pattern formation. *Science* **291**, 2147–50.
- Akasaka, T., van Lohuizen, M., van der Lugt, N., Mizutani-Koseki, Y., Kanno, M., Taniguchi, M., Vidal, M., Alkema, M., Berns, A., and Koseki, H. (2001). Mice doubly deficient for the Polycomb Group genes *Mel18* and *Bmi1* reveal synergy and requirement for maintenance but not initiation of Hox gene expression. *Development* **128**, 1587–97.
- Araujo, M., Piedra, M. E., Herrera, M. T., Ros, M. A., and Nieto, M. A. (1998). The expression and regulation of chick *Epha7* suggests roles in limb patterning and innervation. *Development* **125**, 4195–204.
- Badenhorst, P., Voas, M., Rebay, I., and Wu, C. (2002). Biological functions of the ISWI chromatin remodeling complex NURF. *Genes & Dev.* **16**, 3186–3198.
- Badenhorst, P., Xiao, H., Cherbas, L., Kwon, S. Y., Voas, M., Rebay, I., Cherbas, P., and Wu, C. (2005). The Drosophila nucleosome remodeling factor NURF is required for Ecdysteroid signaling and metamorphosis. *Genes Dev.* **19**, 2540–2545.
- Bandyopadhyay, A., Tsuji, K., Cox, K., Harfe, B. D., Rosen, V., and Tabin, C. J. (2006). Genetic analysis of the roles of BMP2, BMP4, and BMP7 in limb patterning and skeletogenesis. *PLOS Genetics* **2**, e216.doi:10.1371/journal.pgen.0020216.
- Banting, G. S., Barak, O., Ames, T. M., Burnham, A. C., Kardel, M. D., Cooch, N. S., Davidson, C. E., Godbout, R., McDermid, H. E., and Shiekhhattar R. (2005). CECR2, a protein involved in neurulation, forms a novel chromatin remodeling complex with SNF2L. *Hum Mol Genet* **14**, 513–524.
- Barak, O., Lazzaro, M. A., Lane, W. S., Speicher, D. W., Picketts, D. J., and Shiekhhattar, R. (2003). Isolation of human NURF: a regulator of Engrailed gene expression. *EMBO J.* **22**, 6089–6100.
- Basson, M.A. Akbulut, S. Watson-Johnson, J. Simon, R. Carroll, T.J. Shakya, R. Gross, I. Martin, G.R. Lufkin, T. McMahon, A.P. Wilson, P. D., Costantini F. D., Mason, I. J., and Licht J. D. (2005). Sproutyl is a critical regulator of GDNF/RET-mediated kidney induction. *Dev Cell* **8**, 229–239.
- Belikov, S., Gelius, B., Almouzni, G., and Wrangé, Ö. (2000). Hormone activation induces nucleosome positioning in vivo. *EMBO J.*, **19**, 1023–1033.
- Bera, T.K., Liu, X. F., Yamada, M., Gavrilova, O., Mezey, E., Tessarollo, L., Anver, M., Hahn, Y., Lee, B., and Pastan, I. (2008). A model for obesity and gigantism due to disruption of the *Ankrd26* gene. *Proc Natl Acad Sci USA* **105**, 270–5.

- Berends, M. J., Tan-Sindhunata, G., Leegte, B., and Van Essen, A. J. (2001). Phenotypic variability of cat-eye syndrome. *Genet Couns.* **12**, 23-34.
- Berk, M., Desai, S. Y., Heyman, H. C., and Colmenares, C. (1997). Mice lacking the ski proto-oncogene have defects in neurulation, craniofacial patterning, and skeletal muscle development. *Genes & Dev.* **11**, 2029-2039.
- Beverdam, A., Brouwer, A., Reijnen, M., Korving, J., and Meijlink, F. (2001). Severe nasal clefting and abnormal embryonic apoptosis in Alx3/Alx4 double mutant mice. *Development* **128**, 3975-3986.
- Birchmeier, C., Birchmeier, W., Gherardi, E., and Vande Woude, G. F. (2003). Met, metastasis, motility and more. *Nat Rev Mol Cell Biol* **4**, 915-925.
- Bladt, F., Riethmacher, D., Isenmann, S., Aguzzi, A. and Birchmeier, C. (1995). Essential role for the c-met receptor in the migration of myogenic precursor cells into the limb bud. *Nature* **376**, 768-771.
- Bochar, D. A., Savard, J., Wang, W., Lafleur, D. W., Moore, P., Côté, J., and Shiekhatter, R. (2000) A family of chromatin remodeling factors related to Williams syndrome transcription factor. *Proc Natl Acad Sci USA* **97**, 1038–1043.
- Boyer, L.A., Langer, M.R., Crowley, K.A., Tan, S., Denu, J.M. and Peterson, C.L. (2002). Essential role for the SANT domain in the functioning of multiple chromatin remodeling enzymes. *Mol. Cell* **10**, 935–942.
- Boyer, L.A., Latek, R. R., and Peterson, C. L. (2004). The SANT domain: a unique histone-tail-binding module? *Nat. Rev. Mol. Cell Biol.* **5**, 158–163.
- Bozhenok, L., Wade, P.A. and Varga-Weisz, P. (2002). WSTF–ISWI chromatin remodeling complex targets heterochromatic replication foci. *EMBO J.* **21**, 2231–2241.
- Bronner-Fraser, M., Wolf, J. J. and Murray, B. A. (1992). Effects of antibodies against N-cadherin and N-CAM on the cranial neural crest and neural tube. *Dev. Biol.* **153**, 291-301.
- Buehler, B.A., Rao, V., and Finnell, R.H. (1994). Biochemical and molecular teratology of fetal hydantoin syndrome. *Neurol Clin.* **12**, 741–748.
- Bultman, S., Gebuhr, T., Yee, D., La Mantia, C., Nicholson, J., Gilliam, A., Randazzo, F., Metzger, D., Chambon, P., Crabtree, G., and Magnuson, T. (2000). A Brg1 null mutation in the mouse reveals functional differences among mammalian SWI/SNF complexes. *Mol. Cell* **6**, 1287-1295.
- Cain, J. E., and Bertram, J. F. (2006). Ureteric branching morphogenesis in BMP4 heterozygous mutant mice. *J Anat.* **209**, 745–755.
- Cairns, B. R., Lorch, Y., Li, Y., Lacomis, L., Erdjument-Bromage, H., Tempst, P., Laurent, B., and Kornberg, R. D. (1996). RSC, an abundant and essential chromatin remodeling complex. *Cell* **87**, 1249– 1260.
- Campbell, G., and Tomlinson, A. (1998). The roles of the homeobox genes *aristaless* and *Distal-less* in patterning the legs and wings of *Drosophila*. *Development* **125**, 4483–4493.

- Caubit, X., Lye, C. M., Martin, E., Core, N., Long, D. A., Vola, C., Jenkins, D., Garratt, A. N., Skaer, H., Woolf, A. S., and Fasano, L. (2008). Teashirt 3 is necessary for ureteral smooth muscle differentiation downstream of SHH and BMP4. *Development* **135**, 3301-10.
- Centers for Disease Control and Prevention. (1991). Use of folic acid for prevention of spina bifida and other neural tube defects: 1983–1991. *MMWR*. **40**, 513–516.
- Ching, Y. P., Qi, Z., and Wang, J.H. (2000). Cloning of three novel neuronal Cdk5 activator binding proteins. *Gene* **242**, 285-294.
- Collins, N., Poot, R. A., Kukimoto, I., Garcia-Jimenez, C., Dellaire, G., and Varga-Weisz, P. D. (2002). An ACF1-ISWI chromatin-remodeling complex is required for DNA replication through heterochromatin. *Nat Genet*. **32**, 627–632.
- Colmenares, C., Heilstedt, H.A., Shaffer, L.G., Schwartz, S., Berk, M., Murray, J.C., and Stavnezer, E. (2002). Loss of the SKI proto-oncogene in individuals affected with 1p36 deletion syndrome is predicted by strain-dependent defects in Ski-/- mice. *Nat. Genet*. **30**, 106–109.
- Copp, A.J., Greene, N.D., and Murdoch, J.N. (2003). The genetic basis of mammalian neurulation. *Nat Rev Genet* **4**, 784–793.
- Cui, C., Chatterjee, B., Francis, D., Yu, Q., SanAgustin, J. T., Francis, R., Tansey, T., Henry, C., Wang, B., Lemley, B., Pazour G. J., and Lo CW. (2011). Disruption of Mks1 localization to the mother centriole causes cilia defects and developmental malformations in Meckel-Gruber syndrome. *Dis. Model Mech*. **4**, 43-56.
- Davidson, C.E., Li, Q., Churchill, G. A., Osborne, L. R., and McDermid, H. E. (2007). Modifier locus for exencephaly in Cc2r mutant mice is syntenic to the 10q25.3 region associated with neural tube defects in humans. *Physiol Genomics* **31**, 244-251.
- Dawe, C. E., Kooistra, M. K., Fairbridge, N. A., Pisio, A. C., and McDermid, H. E. (2011). Role of chromatin remodeling gene Cc2r in neurulation and inner ear development. *Developmental Dynamics* **240**, 372-383.
- De Marco, P., Merello, E., Mascelli, S., and Capra, V. (2006). Current perspectives on the genetic causes of neural tube defects. *Neurogenetics* **7**, 201-221.
- Denavit, T. M., Malan, V., Grillon, C., Saniaville, D., Ardaian, A., Jacquemont, M. L., Burgien, L., Tailemite, J. L., and Portnoi, M. F. (2004). A new case of a severe clinical phenotype of the cat-eye syndrome. *J Genet Couns* **15**, 443–448.
- Denis, G. V., Nikolajczyk, B. S., and Schnitzler, G. R. (2010). An emerging role for bromodomain-containing proteins in chromatin regulation and transcriptional control of adipogenesis. *FEBS Lett* **584**, 3260-3268.
- Depaepe, V., Suarez-Gonzalez, N., Dufour, A., Passante, L., Gorski, J. A., Jones, K. R., Ledent, C., and Vanderhaeghen, P. (2005). Ephrin signalling controls brain size by regulating apoptosis of neural progenitors. *Nature* **435**, 1244-50.

- Depew, M. J., Liu, J. K., Long, J. E., Presley, R., Meneses, J. J., Pedersen, R. A. and Rubenstein, J. L. (1999). Dlx5 regulates regional development of the branchial arches and sensory capsules. *Development* **126**, 3831-3846.
- Depew, M.J., Lufkin, T., and Rubenstein, J.L. (2002). Specification of jaw subdivisions by Dlx genes. *Science* **298**, 381-385.
- Deuring, R., Fanti, L., Armstrong, J. A., Sarte, M., Papoulas, O., Prestel, M., Daubresse, G., Verardo, M., Moseley, S. L., Berloco, M., Tsukiyama, T., Wu, C., Pimpinelli, S., and Tamkun, J. W. (2000). The ISWI chromatin-remodeling protein is required for gene expression and the maintenance of higher order chromatin structure in vivo. *Mol Cell*, **5**, 355–365.
- DeWals, P., Tairou, F., Van Allen M.I., Uh, S.H., Lowry, R.B., and Sibbald, B. (2007). Reduction in neural-tube defects after folic acid fortification in Canada. *N Engl J Med* **357**, 135–42.
- Doerks, T., Copley, R., and Bork, P. (2001). DDT -- a novel domain in different transcription and chromosome remodeling factors. *Trends Biochem. Sci.* **26**, 145-6.
- Dressler, G. R. (2006). The cellular basis of kidney development. *Annu. Rev. Cell Dev. Biol.* **22**, 509-529.
- Eberharder, A., Ferrari, S., Langst, G., Straub, T., Imhof, A., Varga-Weisz, P., Wilm, M., and Becker, P. B. (2001) Acf1, the largest subunit of CHRAC, regulates ISWI-induced nucleosome remodelling. *EMBO J* **20**, 3781–3788.
- Egelhofer, T. A., Minoda, A., Klugman, S., Lee, K., Kolasinska-Zwierz, P., Alekseyenko, A. A., Cheung, M., Day, D. S., Gadel, S., Gorchakov, A. A., Gu, T., Kharchenko, P. V., Kuan, S., Latorre, I., Linder-Basso, D., Luu, Y., Ngo, Q., Perry, M., Rechtsteiner, A., Riddle, N. C., Schwartz, Y. B., Shanower, G. A., Vielle, A., Ahringer, J., Elgin S. C. R., et al. (2011). An assessment of histone-modification antibody quality. *Nature Structural & Molecular Biology* **18**, 91–93.
- Egger, G., Liang, G., and Aparicio, A. (2004). Epigenetics in human disease and prospects for epigenetic therapy. *Nature* **429**, 457-63.
- Elfring, L. K., Deuring, R., McCallum, C. M., Peterson, C. L., and Tamkun, J. W. (1994). Identification and characterization of Drosophila relatives of the yeast transcriptional activator SNF2/SWI2. *Mol Cell Biol* **14**, 2225–2234.
- Eriksson, U.J., Cederberg, J., and Wentzel, P. (2003). Congenital malformations in offspring of diabetic mothers--animal and human studies. *Rev Endocr Metab Disord.* **4**, 79-93.
- Ettensohn, C. A., Illies, M. R., Oliveri, P., and DeJong, D. L. (2003). Alx 1, a member of the Cart1/Alx3/Alx4 subfamily of paired-class homeodomain proteins, is an essential component of the gene network controlling skeletogenic fate specification in the sea urchin embryo. *Development* **130**, 2917–2928.
- Farley, F. A., Hall, J., and Goldstein, S. A. (2006). Characteristics of congenital scoliosis in a mouse model. *J Pediatr Orthop.* **26**, 341–6.

- Farley, F. A., Loder, R. T., Nolan, B. T., Dillon, M. T., Frankenburg, E. P., Kaciroti, N. A., Miller, J. D., Goldstein, S. A., and Hensinger, R. N. (2001). Mouse model for thoracic congenital scoliosis. *J Pediatr Orthop* **21**, 537-40.
- Fleming, A., and Copp, A.J. (1998). Embryonic folate metabolism and mouse neural tube defects. *Science* **280**, 2107-9.
- Fleming, A. and Copp, A. J. (2000). A genetic risk factor for mouse neural tube defects: defining the embryonic basis. *Hum. Mol. Genet.* **9**, 575-581.
- Fyodorov, D. V., and Kadonaga, J. T. (2002). Binding of Acf1 to DNA involves a WAC motif and is important for ACF-mediated chromatin assembly. *Molecular and Cellular Biology* **22**, 6344-6353.
- Goodrich L. V. (2008). The Plane Facts of PCP in the CNS. *Neuron* **60**, 9-16.
- Grasl-Kraupp B, Ruttkay-Nedecky B, Koudelka H, Bukowska K, Bursch W, Schulte-Hermann R. (1995). *In situ* detection of fragmented DNA (TUNEL assay) fails to discriminate among apoptosis, necrosis, and autolytic cell death: a cautionary note. *Hepatology* **21**, 1465-8.
- Graveel, C., Su, Y., Koeman, J., Wang, L., Tessarollo, L., Fiscella, M., Birchmeier, C., Swiatek, P., Bronson, R., and Woude, G. V. (2004). Activating Met mutations produce unique tumor profiles in mice with selective duplication of the mutant allele. *PNAS* **101**, 17198-17203.
- Gray, R. S., Roszko, I., and Solnica-Krezel, L. (2011). Planar Cell Polarity: Coordinating Morphogenetic Cell Behaviors with Embryonic Polarity. *Dev Cell* **21**, 120-133.
- Greene, N. D. E., and Copp, A.J. (2009). Development of the vertebrate central nervous system: formation of the neural tube. *Prenatal Diagnosis* **29**, 303 - 311.
- Grieshammer, U., Le, M., Plump, A. S., Wang, F., Tessier-Lavigne, M., and Martin, G. R. (2004). SLIT2-mediated ROBO2 signaling restricts kidney induction to a single site. *Dev Cell* **6**, 709–717.
- Grosse, S.D., Waitzman, N.J., Romano, P.S., and Mulinare, J. (2005). Reevaluating the Benefits of Folic Acid Fortification in the United States: Economic Analysis, Regulation, and Public Health. *Am J Public Health* **95**, 1917-1922.
- Grüne, T., Brzeski, J., Eberharder, A., Clapier, C. R., Corona, D. F., Becker, P. B., and Müller, C. W. (2003) Crystal structure and functional analysis of the nucleosome recognition module of the remodeling factor ISWI. *Mol Cell* **12**, 449–460.
- Guyot, M. C., Bosoi, C. M., Kharfallah, F., Reynolds, A., Drapeau, P., Justice, M., Gros, P., and Kibar, Z. (2011). A novel hypomorphic Looptail allele at the planar cell polarity Vangl2 gene. *Developmental Dynamics* **240**, 839-849.
- Hahn, H. (2010). Genetics of kidney development: pathogenesis of renal anomalies. *Korean J Pediatr* **53**, 729-734.

- Haigo, S. L., Hildebrand, J. D., Harland, R. M., and Wallingford, J. B. (2003). Shroom induces apical constriction and is required for hinge point formation during neural tube closure. *Curr. Biol.* **13**, 2125-2137.
- Hakimi, M.A., Bochar, D.A., Schmiesing, J.A., Dong, Y., Barak, O.G., Speicher, D.W., Yokomori, K. and Shiekhata, R. (2002) A chromatin remodelling complex that loads cohesin onto human chromosomes. *Nature* **418**, 994–998.
- Hall, J.G., Solehdin, F. (1999). Genetics of neural tube defects. *Ment Retard Dev Disabil.* **4**, 269–281
- Hamblet, N. S., Lijam, N., Ruiz-Lozano, P., Wang, J., Yang, Y., Luo, Z., Mei, L., Chien, K. R., Sussman, D. J., and Wynshaw-Boris, A. (2002). Dishevelled 2 is essential for cardiac outflow tract development, somite segmentation and neural tube closure. *Development* **129**, 5827–5838.
- Handrigan, G.R. (2003). Concordia discors: duality in the origin of the vertebrate tail. *J Anat.* **202**, 255–267.
- Harris, M. J., and Juriloff, D. M. (1999). Mini-review: toward understanding mechanisms of genetic neural tube defects in mice. *Teratology* **60**, 292–305.
- Harris, M. J., and Juriloff, D. M. (2007). Mouse mutants with neural tube closure defects and their role in understanding human neural tube defects. *Birth Defects Res. A Clin Mol Teratol.* **79**, 187-210.
- Harris, M. J., and Juriloff, D. M. (2010). An update to the list of mouse mutants with neural tube closure defects and advance toward a complete genetic perspective of neural tube closure. *Birth Defects Res. A Clin Mol Teratol.* **88**, 653-69.
- Hatini, V., Huh, S. O., Herzlinger, D., Soares, V. C., and Lai, E. (1996). Essential role of stromal mesenchyme in kidney morphogenesis revealed by targeted disruption of Winged Helix transcription factor BF-2. *Genes Dev.* **10**, 1467–1478.
- Hay, E. D. (2005). The mesenchymal cell, its role in the embryo, and the remarkable signaling mechanisms that create it. *Dev Dyn.* **233**, 706-20.
- He, X., Fan, H. Y., Garlick, J. D., and Kingston, R. E. (2008). Diverse regulation of SNF2h chromatin remodeling by noncatalytic subunits. *Biochemistry.* **47**, 7025–33.
- Hebert, C., and Roest Crollius, H. (2010). Nucleosome rotational setting is associated with transcriptional regulation in promoters of tissue-specific human genes. *Genome Biol* **11**, R51.
- Hebert, J. M., and McConnell, S. K. (2000). Targeting of cre to the Foxg1 (BF-1) locus mediates loxP recombination in the telencephalon and other developing head structures. *Dev Biol* **222**, 296-306.
- Hedlund, G. (2006). Congenital frontonasal masses: developmental anatomy, malformations, and MR imaging. *Pediatr Radiol* **36**, 647-662.
- Hendricks, K.A., Nuno, O.M., Suarez, L., and Larsen, R. (2001). Effects of hyperinsulinemia and obesity on risk of neural tube defects among Mexican Americans. *Epidemiology.* **12**, 630-5.

- Holmberg, J., Clarke, D. L., and Frisen, J. (2000). Regulation of repulsion versus adhesion by different splice forms of an Eph receptor. *Nature* **408**, 203–206.
- Hu, Z., and Corwin, J. T. (2007). Inner ear hair cells produced in vitro by a mesenchymal-to-epithelial transition. *Proc Natl Acad Sci USA* **104**, 16675–16680.
- Hughes, A., (1955). The development of the neural tube of the chick embryo. A study with the ultraviolet microscope. *J. Embryol. Exp. Morph.* **3**, 305-25.
- Huth, J. R., Bewley, C. A., Nissen, M. S., Evans, J. N. S., Reeves, R., Gronenborn, A. M., and Clore, G. M. (1997). The solution structure of an HMG-I(Y)/DNA complex defines a new architectural minor groove binding motif. *Nature Struct Biol* **4**, 657-665.
- Ichi, S., Costa, F.F., Bischof, J.M., Nakazaki, H., Shen, Y.W., Boshnjaku, V., Sharma, S., Mania-Farnell, B., McLone, D.G., Tomita, T., Soares, M.B., and Mayanil, C.S. (2010). Folic acid remodels chromatin on Hes1 and Neurog2 promoters during caudal neural tube development. *J. Biol. Chem.* **285**, 36922-32.
- Iizuka-Kogo, A., Ishida, T., Akiyama, T., and Senda, T. (2007). Abnormal development of urogenital organs in Dlg1-deficient mice. *Development* **134**, 1799–1807.
- Ikeda, K., Watanabe, Y., Ohto, H., and Kawakami, K. (2002). Molecular Interaction and Synergistic Activation of a Promoter by Six, Eya, and Dach Proteins Mediated through CREB Binding Protein. *Mol. Cell. Biol.* **22**, 6759-6766.
- Ito, T., Bulger, M., Pazin, M. J., Kobayashi, R., and Kadonaga, J. T. (1997) ACF, an ISWI-containing and ATP-utilizing chromatin assembly and remodeling factor. *Cell* **90**, 145–155.
- Jain, S. (2009). The many faces of RET dysfunction in kidney. *Organogenesis* **5**, 95-108.
- Janse, M. J., and A. L. Wit. (1989). Electrophysiological mechanisms of ventricular arrhythmias resulting from myocardial ischemia and infarction. *Physiol. Rev.* **69**, 1049–1169.
- Jenkins, D., Caubit, X., Dimovski, A., Matevska, N., Lye, C. M., Cabuk, F., Gucev, Z., Tasic, V., Fasano, L., Woolf, A. S. (2010). Analysis of TSHZ2 and TSHZ3 genes in congenital pelvi-ureteric junction obstruction. *Nephrol. Dial. Transplant.* **25**, 54-60.
- Jeong, Y., and Epstein, D.J. (2003). Distinct regulators of Shh transcription in the floor plate and notochord indicate separate origins for these tissues in the mouse node. *Development* **130**, 3891-3902.
- Jones, M.H., Hamana, N., Nezu, J., and Shimane, M. (2000) A novel family of bromodomain genes. *Genomics* **63**, 40–45.
- Juriloff, D. M., Harris, M. J., Dewell, S. L., Brown C. J., Mager, D. L., Gagnier, L., and Mah, D. G. (2005). Investigations of the genomic region that contains the clf1 mutation, a causal gene in multifactorial cleft lip and palate in mice. *Birth Defects Research (Part A)* **73**, 103-113.

- Juriloff, D. M., Harris, M. J., Tom, C., and MacDonald, K. B. (1991). Normal mouse strains differ in the site of initiation of closure of the cranial neural tube *Teratology* **44**, 225-233.
- Kalatzis, V., Sahly, I., El Amraoui, A., and Petit, C. (1998). Eya1 expression in the developing ear and kidney: towards the understanding of the pathogenesis of Branchio-Oto-Renal (BOR) syndrome. *Developmental Dynamics* **213**, 486-499.
- Kawakami, M., Umeda, M., Nakagata, N., Takeo, T., and Yamamura, K. (2011). Novel migrating mouse neural crest cell assay system utilizing P0-Cre/EGFP fluorescent time-lapse imaging. *BMC Developmental Biology* **11**, 68.
- Kibar, Z., Capra, V., and Gros, P. (2007). Toward understanding the genetic basis of neural tube defects. *Clin Genet.* **71**, 295–310.
- Kibar, Z., Vogan, K. J., Groulx, N., Justice, M. J., Underhill, D. A., and Gros, P. (2001). Ltap, a mammalian homolog of Drosophila Strabismus/Van Gogh, is altered in the mouse neural tube defect mutant Loop-tail. *Nat Genet.* **28**, 251–255.
- Kim, H. G., Herrick, S. R., Lemyre, E., Kishikawa, S., Salisz, J. A., Seminara, S., MacDonald, M. E., Bruns, G. A. P., Morton, C. C., Quade, B. J., Gusella, J. F. (2005). Hypogonadotropic hypogonadism and cleft lip and palate caused by a balanced translocation producing haploinsufficiency for FGFR1. *J Med Genet* **42**, 666-72.
- Kim, J.K., Huh, S.O., Choi, H., Lee, K.S., Shin, D., Lee, C., Nam, J.S., Kim, H., Chung, H., Lee, H.W., Park, S.D., and Seong, R.H. (2001). Srg3, a mouse homolog of yeast SWI3, is essential for early embryogenesis and involved in brain development. *Mol Cell Biol.* **21**, 7787-95.
- Kim, J., Lee, G. S., Tisher, C. C., and Madsen, K. M. (1996). Role of apoptosis in development of the ascending thin limb of the loop of Henle in rat kidney. *AJP - Renal Physiol* **271**, F831-F845.
- Kirke, P.N., Molloy, A.M., Daly, L.E., Burke, H., Weir, D.G., and Scott, J.M. (1993). Maternal plasma folate and vitamin B12 are independent risk factors for neural tube defects. *Q J Med.* **86**, 703-8.
- Kitagawa, H., Fujiki, R., Yoshimura, K., Mezaki, Y., Uematsu, Y., Matsui, D., Ogawa, S., Unno, K., Okubo, M., Tokita, A., Nakagawa, T., Ito, T., Ishimi, Y., Nagasawa, H., Matsumoto, T., Yanagisawa, J., and Kato, S. (2003). The chromatin-remodeling complex WINAC targets a nuclear receptor to promoters and is impaired in Williams syndrome. *Cell* **113**, 905–917.
- Klootwijk, R., Franke, B., van der Zee, C. E. E. M., de Boer, R. T., Wilms, W., Hol, F. A., and Mariman, E. C. M. (2000). A deletion encompassing Zic3 in Bent tail, a mouse model for X-linked neural tube defects. *Human Molecular Genetics* **9**, 1615-22.

- Knijnenburg, J., van Bever, Y., Hulsman, L. O. M., van Kempen, C. A. P., Bolman, G. M., van Loon, R. L. E., Beverloo, H. B., and van Zutven, L. J. C. M. (2012). A 600 kb triplication in the cat eye syndrome critical region causes anorectal, renal and preauricular anomalies in a three-generation family. *European Journal of Human Genetics* doi:10.1038/ejhg.2012.43.
- Kohut, R., and Rusen, I.D. (2002). Congenital Anomalies in Canada – A Perinatal Health Report. *Minister of Public Works and Government Services Canada*.
- Kooistra, M. K., Leduc, R. Y., Dawe, C. E., Fairbridge, N. A., Rasmussen, J. D., Man, J. H., Bujold, M., Juriloff, D. M., King-Jones, K., and McDermid, H. E. (2011). Strain-specific modifier genes of *Cecr2*-associated exencephaly in mice: genetic analysis and identification of differentially expressed candidate genes. *Physiol Genomics* **44**, 35-46.
- Kume, T., Deng, K., and Hogan, B. L. M. (2000). Minimal phenotype of mice homozygous for a null mutation in the forkhead/winged helix gene, *Mf2*. *Mol. Cell. Biol.* **20**, 1419–1425.
- Landry, J. W., Banerjee, S., Taylor, B., Aplan, B. D., Singer, A., and Wu, C. (2011). Chromatin remodeling complex NURF regulates thymocyte maturation. *Genes & Dev.* **25**, 275-286.
- Landry, J., Sharov, A. A., Piao, Y., Sharova, L. V., Xiao, H., Southon, E., Matta, J., Tessarollo, L., Zhang, Y. E., and Ko, M. S. (2008). Essential role of chromatin remodeling protein Bptf in early mouse embryos and embryonic stem cells. *PLoS Genet* **4**, e1000241. doi: 10.1371/journal.pgen.1000241
- Lawrence, P. A., and Shelton, P. M. J. (1975). The determination of polarity in the developing insect retina. *J Embryol. Exp Morphol* **33**, 471-486
- Lazzaro, M. A., and Picketts, D. J. (2001). Cloning and characterization of the murine Imitation Switch (ISWI) genes: differential expression patterns suggest distinct developmental roles for *Snf2h* and *Snf2l*. *J Neurochem* **77**, 1145-1156.
- Lazzaro, M. A., Pépin, D., Pescador, N., Murphy, B. D., Vanderhyden, B. C., and Picketts, D. J. (2006). The imitation switch protein SNF2L regulates steroidogenic acute regulatory protein expression during terminal differentiation of ovarian granulosa cells. *Molecular Endocrinology* **20**, 2406-17.
- Lazzaro, M. A., Todd, M. A. M., Lavigne, P., Vallee, D., De Maria, A., and Picketts, D. (2008). Characterization of novel isoforms and evaluation of SNF2L/SMARCA1 as a candidate gene for X-linked mental retardation in 12 families linked to Xq25-26. *BMC Med Genet* **9**, 11.
- Lee, C., Scherr, H. M., and Wallingford, J. B. (2007). Shroom family proteins regulate gamma-tubulin distribution and microtubule architecture during epithelial cell shape change. *Development* **134**, 1431-1441.
- Lee, S. K., Park, E. J., Lee, H. S., Lee, Y. S., and Kwon, J. (2012). Genome-wide screen of human bromodomain-containing proteins identifies *Cecr2* as a novel DNA damage response protein. *Mol Cells.* **34**, 85-91.

- LeRoy, G., Loyola, A., Lane, W. S., and Reinberg, D. (2000). Purification and characterization of a human factor that assembles and remodels chromatin. *J Biol Chem* **275**, 14787–14790.
- LeRoy, G., Orphanides, G., Lane, W. S., and Reinberg, D. (1998) Requirement of RSF and FACT for transcription of chromatin templates in vitro. *Science* **282**, 1900–1904.
- Li, H., Ilin, S., Wang, W., Duncan, E. M., Wysocka, J., Allis, C. D., and Patel, D. J. (2006). Molecular basis for site-specific read-out of histone H3K4me3 by the BPTF PHD finger of NURF. *Nature* **442**, 91-95.
- Lipschutz, J. H. (1998). Molecular development of the kidney: A review of the results of gene disruption studies. *Am. J. Kidney Dis.* **31**, 383–397.
- Liu, L., Amy, V., Lui, G., and McKeehan, W. L. (2002). Novel complex integrating mitochondria and the microtubular cytoskeleton with chromosome remodeling and tumor suppressor RASSF1 deduced by in silico homology analysis, interaction cloning in yeast, and colocalization in cultured cells. *In Vitro Cell. Dev. Biol. Anim.* **38**, 582-594
- Liu, L., and McKeehan, W. L. (2002). Sequence analysis of LRPPRC and its SEC1 domain interaction partners suggests roles in cytoskeletal organization, vesicular trafficking, nucleocytosolic shuttling and chromosome activity. *Genomics* **79**, 124-136.
- Lowery, L.A., and Sive, H. (2004). Strategies of vertebrate neurulation and a re-evaluation of teleost neural tube formation. *Mechanisms of Development* **12**, 1189-1197.
- Lowary, P. T., and J. Widom. (1997). Nucleosome packaging and nucleosome positioning of genomic DNA. *Proc. Natl. Acad. Sci. USA* **94**, 1183-1188.
- Lu, X., Le Noble, F., Yuan, L., Jiang, Q., De Lafarge, B., Sugiyama, D., Breant, C., Claes, F., De Smet, F., Thomas, J. L., Autiero, M., Carmeliet, P., Tessier-lavinge, M., and Eichmann, A. (2004). The netrin receptor UNC5B mediates guidance events controlling morphogenesis of the vasculature system. *Nature* **432**, 179-86.
- Luger, K., and Richmond, T. J. (1998). DNA binding within the nucleosome core. *Curr Opin Struct Biol* **8**, 33–40.
- Mackie, G. G., and Stephens, F. D. (1975). Duplex kidneys: a correlation of renal dysplasia with position of the ureteral orifice. *J. Urol.* **114**, 274-280.
- Maclean, J. A., Chen, M. A., Wayne, C. M., Bruce, S. R., Rao, M., Meistrich, M. L., Macleod, C., and Wilkinson, M. F. (2005). Rhox: a new homeobox gene cluster. *Cell* **120**, 369–382.
- Mahler, J. F., Stokes, W., Mann, P. C., Takaoka, M., and Robert R. (1996). Spontaneous Lesions in Aging FVB/N Mice. *Maronpot Toxicol Pathol* **24**, 710.
- Majumdar, A., Vainio, S., Kispert, A., McMahon, J., and McMahon, A. P. (2003). Wnt11 and Ret/Gdnf pathways cooperate in regulating ureteric branching during metanephric kidney development. *Development* **130**, 3175-85.

- Mannon, R., Croxtall, J. D., Getting, S. J., Roviezzo, F., Yona, S., Paul-Clark, M. J., Gavins, F. N., Perretti, M., Morris, J. F., Buckingham, J. C., and Flower, R. J. (2003). Aberrant inflammation and resistance to glucocorticoids in annexin 1-/- mouse. *FASEB J* **17**, 253-5.
- Mao, Y., Kukuk, B., Irvine, K. D. (2009). Drosophila lowfat, a novel modulator of Fat signaling. *Development* **136**, 3223-33.
- Marasas, W.F., Riley, R.T., Hendricks, K.A., Stevens, V.L., Sadler, T.W., and Gelineau-van Waes, J. (2004). Fumonisin disrupt sphingolipid metabolism, folate transport and neural tube development in embryo culture and in vivo: a potential risk factor for human neural tube defects among populations consuming fumonisin-contaminated maize. *J Nutr.* **134**, 711–716.
- Martens, J. A., and Winston, F. (2003). Recent advances in understanding chromatin remodeling by Swi/Snf complexes. *Curr. Opin. Genet. Dev.* **13**, 136–42.
- Martin, J. F., Bradley, A., and Olson, E. N. (1995). The paired-like homeo box gene MHOX is required for early events of skeletogenesis in multiple lineages. *Genes Dev.* **9**, 1237-49.
- Matsumoto, A., Hatta, T., Moriyama, K., and Otani, H. (2002). Sequential observations of exencephaly and subsequent morphological changes by mouse exo utero development system: analysis of the mechanism of transformation from exencephaly to anencephaly. *Anat Embryol* **205**, 7-18.
- Matsuura, T., Narama, I., Ozaki, K., Nishimura, M., Imagawa, T., Kitagawa, H., and Uehara, M. (1998). Developmental study on reduction and kinks of the tail in a new mutant knotty-tail mouse. *Anatomy and Embryology* **198**, 91-99.
- Matthew D. Plotkin and Michael S. Goligorsky (2006). Mesenchymal cells from adult kidney support angiogenesis and differentiate into multiple interstitial cell types including erythropoietin-producing fibroblasts. *AJP - Renal Physiol* **291**, F902-912.
- Mavrich, T. N., Jiang, C., Ioshikhes, I. P., Li, X., Venters, B. J., Zanton, S. J., Tomsho, L. P., Qi, J., Glaser, R. L., Schuster, S. C., Gilmour, D. S., Albert, I., and Pugh, B. F. (2008). Nucleosome organization in the Drosophila genome. *Nature* **453**, 358–362.
- McNairn, A. J., and Gilbert, D. M. (2003). Epigenomic replication: linking epigenetics to DNA replication. *BioEssays* **25**, 647–656.
- McNeil, H. (2009). Planar cell polarity and the kidney. *J Am Soc Nephrol* **20**, 2104-11.
- Mendelsohn, C., Batourina, E., Fung, S., Gilbert, T., and Dodd, J. (1999). Stromal cells mediate retinoid-dependent functions essential for renal development. *Development* **126**, 1139-1148.
- Merte, J., Jensen, D., Wright, K., Sarsfield, S., Wang, Y., Schekman, R., and Ginty, D. D. (2010). Sec24b selectively sorts Vangl2 to regulate planar cell polarity during neural tube closure. *Nat Cell Biol.* **41**, 1-8.

- Metsuyanin, S., Harari-Steinberg, O., Buzhor, E., Omer, D., Pode-Shakked, N., et al. (2009) Expression of Stem Cell Markers in the Human Fetal Kidney. *PLoS ONE* **4**, e6709. doi:10.1371/journal.pone.0006709.
- Miyazaki, Y., and Ichikawa, I. (2003). Ontogeny of congenital anomalies of the kidney and urinary track, CAKUT. *Pediatr Int* **45**, 598-604.
- Miyazaki, Y., Oshima, K., Fogo, A., Hogan, B. L., and Ichikawa, I. (2000). Bone morphogenetic protein 4 regulates the budding site and elongation of the mouse ureter. *J Clin Invest*. **105**, 863–873.
- Moase, C.E., and Trasler, D. G. (1991). N-CAM alterations in splotch neural tube defect mouse embryos. *Development* **113**, 1049-1058.
- Monga, S. P., Mars, W. M., Pediaditakis, P., Bell, A., Mulé, K., Bowen, W. C., Wang, X., Zarnegar, R., and Michalopoulos, G. K. (2002). Hepatocyte growth factor induces Wnt-independent nuclear translocation of beta-catenin after Met-beta-catenin dissociation in hepatocytes. *Cancer Res* **7**, 2064–71.
- Monier, S., Jolivet, F., Janoueic-Lerosey, I., Johannes, L., and Goud, B. (2002). Characterization of novel Rab6-interacting proteins involved in endosome-to-TGN transport. *Traffic* **3**, 289-297.
- Montcouquiol, M., Rachel, R. A., Lanford, P. J., Copeland, N. G., Jenkins, N. A., and Kelley, M. W. (2003). Identification of *Vangl2* and *Scrb1* as planar polarity genes in mammals. *Nature* **423**, 173-177.
- Naf, D., Wilson, L. A., Bergstrom, R. A., Smith, R. S., Goodwin, N. C., Verkerk, A., van Ommen, G. J., Ackerman, S. L., Frankel, W. N., and Schimenti, J. C. (2001). Mouse models for the Wolf-Hirschhorn deletion syndrome. *Human Molecular Genetics* **10**, 91-8.
- Nagasu, H., Satoh, M., Kidokoro, K., Nishi, Y., Channon, K. M., Sasaki, T., and Kashiwara, N. (2012). Endothelial dysfunction promotes the transition from compensatory renal hypertrophy to kidney injury after unilateral nephrectomy in mice. *Am J Physiol Renal Physiol*. **302**, F1402-8.
- Nakanishi, K., and Yoshikawa, N. (2003). Genetic disorders of human congenital anomalies of the kidney and urinary tract (CAKUT). *Pediatrics International* **45**, 610-616.
- Narlis, M., Grote, D., Gaitan, Y., Boualia, S. K., and Bouchard, M. (2007). Pax2 and Pax8 Regulate Branching Morphogenesis and Nephron Differentiation in the Developing Kidney. *JASN* **18**, 1121-1129.
- Neugeborn, L., and Carlson, M. (1984). Genes affecting the regulation of SUC2 gene expression by glucose repression in *Saccharomyces cerevisiae*. *Genetics* **108**, 845-858.
- Nishida, H., Suzuki, T., Tomaru, Y., and Hayashizaki, Y. (2005). A novel replication-independent histone H2a gene in mouse. *BMC Genet*. **6**, 10.
- Patthey, C., and Gunhaga, L. (2011). Specification and regionalisation of the neural plate border. *Eur J Neurosci*. **34**, 1516-28.

- Pauler, F. M., Sloane, M. A., Huang, R., Regha, K., Koerner, M. V., Tamir, I., Sommer, A., Aszodi, A., Jenuwein, T., and Barlow, D. P. (2009). H3K27me3 forms BLOCs over silent genes and intergenic regions and specifies a histone banding pattern on a mouse autosomal chromosome. *Genome Res.* **19**, 221–233.
- Pedersen, A., Skjong, C., and Shawlot, W. (2005). Lim1 is required for nephric duct extension and ureteric bud morphogenesis. *Dev. Biol.* **288**, 571–581.
- Petryk, A., Anderson, R. M., Jarcho, M. P., Leaf, I., Carlson, C. S., Klingensmith, J., Shawlot, W., and O'Connor, M. B. (2004). The mammalian twisted gastrulation gene functions in foregut and craniofacial development. *Developmental Biology* **267**, 374–386.
- Pfaffl, M.W. (2001). A new mathematical model for relative quantification in real-time RT-PCR. *Nucleic Acids Res* **29**: e45.
- Plisov, S. Y., Ivanov, S. V., Yoshino, K., Dove, L. F., Plisova, T. M., Higinbotham, K. G., Karavanova, I., Lerman, M., and Perantoni, A. O. (2000). Mesenchymal-epithelial transition in the developing metanephric kidney: gene expression study by differential display. *Genesis* **27**, 22–31.
- Pohl, M., Stuart, R. O., Sakurai, H. and Nigam, S. K. (2000). Branching morphogenesis during kidney development. *Annu. Rev. Physiol.* **62**, 595–620.
- Poot, R. A., Dellaire, G., Hulsman, B. B., Grimaldi, M. A., Corona, D. F., Becker, P. B., Bickmore, W. A. and Varga-Weisz, P. D. (2000). HuCHRAc, a human ISWI chromatin remodelling complex contains hACF1 and two novel histone-fold proteins. *EMBO J.* **19**, 3377–3387.
- Pope, J.C.T., Brock III, J.W., Adams, M.C., Stephens, F.D., and Ichikawa, I. (1999). How they begin and how they end: Classic and new theories for the development and deterioration of congenital anomalies of the kidney and urinary tract, CAKUT. *J. Am. Soc. Nephrol.* **10**, 2018–2028.
- Potter, S., Brunskill, E. W., and Patterson, L. T. (2010). Microdissection of the gene expression codes driving nephrogenesis. *Organogenesis* **6**, 263–269.
- Pufulete, M., Al-Ghnaniem, R., Khushal, A., Appleby, P., Harris, N., Gout, S., Emery, P.W., and Sanders, T.A.B.. (2005). Effect of folic acid supplementation on genomic DNA methylation in patients with colorectal adenoma. *Gut* **54**, 648–653.
- Qian, D., Jones, C., Rzdzińska, A., Mark, S., Zhang, X., Steel, K. P., Dai, X., and Chen, P. (2007). Wnt5a functions in planar cell polarity regulation in mice. *Dev Biol* **306**, 121–133.
- Qiao, J., Cohen, D., and Herzlinger, D. (1995). The metanephric blastema differentiates into collecting system and nephron epithelia in vitro. *Development* **121**, 3207–14.
- Qin, S., Taglienti, M., Nauli, S. M., Contrino, L., Takakura, A., Zhou, J., and Kriedberg, J. A. (2010). Failure to ubiquitinate c-Met leads to hyperactivation of mTOR signaling in a mouse model of autosomal dominant polycystic kidney disease. *J Clin Invest* **120**, 3617–3628.

- Qu, S., Tucker, S. C., Zhao, Q., deCrombrughe, B. and Wisdom, R. (1999). Physical and genetic interactions between *Alx4* and *Cart1*. *Development* **126**, 359 -369.
- Reeves, R. (2000). Structure and function of the HMGI(Y) family of architecturaltranscription factors. *Environ Health Perspect* **108**, 803-809.
- Relaix, F., Polimeni, M., Rocancourt, D., Ponzetto, C., Schafer, B.W., and Buckingham, M. (2003). The transcriptional activator PAX3–FKHR rescues the defects of Pax3 mutant mice but induces a myogenic gain-of-function phenotype with ligand-independent activation of Met signaling in vivo. *Genes & Dev.* **17**, 2950–2965.
- Reyes, J. C., Barra, J., Muchardt, C., Camus, A., Babinet, C., and Yaniv, M. (1998). Altered control of cellular proliferation in the absence of mammalian brahma (SNF2alpha). *EMBO J.* **17**, 6979-6991.
- Rippe, K., Schrader, A., Riede, P., Strohnner, R., Lehmann, E., and Längst, G. (2007). DNA sequence- and conformation-directed positioning of nucleosomes by chromatin-remodeling complexes. *PNAS* **104**, 15635-15640.
- Robledo, R. F., Rajan, L., Li, X., and Lufkin, T. (2002). The *Dlx5* and *Dlx6* homeobox genes are essential for craniofacial, axial, and appendicular skeletal development. *Genes Dev.* **16**, 1089-101.
- Rosias, P., Sijstermans, J., Theunissen, P., Pulles-Heintzberger, C., De Die-Smulders, C. E. M., Engelen, J., and Van Der Meer, S. (2001). Phenotypic variability of the cat eye syndrome: case report and review of the literature. *Genet Couns* **12**, 273–282.
- Saburi, S., Hester, I., Fischer, E., Pontoglio, M., Eremina, V., Gessler, M., Quaggin, S. E., Harrison, R., Mount, R. and McNeill, H. (2008). Loss of *Fat4* disrupts PCP signaling and oriented cell division and leads to cystic kidney disease. *Nat. Genet.* **40**, 1010-1015.
- Sajan, S. A., Rubenstein, J. L., Warchol, M. E., and Lovett, M. (2011). Identificatoin of direct downstream targets of *Dlx5* during early inner ear development. *Hum Mol Genet.* **20**, 1262-73
- Santoro, R., Li, J., and Grummt, I. (2002) The nucleolar remodeling complex NoRC mediates heterochromatin formation and silencing of ribosomal gene transcription. *Nat Genet* **32**, 393–396.
- Sartini, B. L., Wang, H., Wang, W., Millette, C. F., and Kilpatrick, D. L. (2007). Pre-messenger RNA cleavage factor 1 (CF1m): potential role in alternative polyadenylation during spermatogenesis. *Biology of Reproduction* **78**, 472-482.
- Schaeper, U., Vogel, R., Chmielowiec, J., Huelsken, J., Rosario, M., and Birchmeier, W. (2007). Distinct requirements for *Gab1* in Met and EGF receptor signaling in vivo. *Proc Natl Acad Sci USA* **104**, 15376-81.
- Schlosser, G. (2007). How old genes make a new head: redeployment of *Six* and *Eya* genes during the evolution of the cranial placodes. *Int Comp Biol* **47**, 343–359. doi: 10.1093/icb/icm031.

- Schoenwolf, G. C. (1983). The Chick epiblast: A model for examining epithelial morphogenesis. *Scanning Electron Microsc.* **3**, 1371-1985.
- Serbedzija, G. N., Bronner-Fraser, M., and Fraser, S. E. (1992). Vital dye analysis of cranial neural crest cell migration in the mouse embryo. *Development* **116**, 297-307.
- Sharova, L. V., Sharov, A. A., Piao, Y., Shaik, N., Sullivan, T., Stewart, C. L., Hogan, B. L. M., and Ko, M. S. H. (2007). Global gene expression profiling reveals similarities and differences among mouse pluripotent stem cells of different origins and strains. *Dev Biol.* **307**, 446-459.
- Shekar, P. C., Goel, S., Rani, S. D. S., Sarathi, D. P., Alex, J. L., Singh, S., and Kuma, S. (2006). K-Casein-deficient mice fail to lactate. *Proc Nat Acad Sci USA* **103**, 8000-8005.
- Sif, S., Saurin, A.J., Imbalzano, A.N., and Kingston, R.E. (2001). Purification and characterization of mSin3A-containing Brg1 and hBrm chromatin remodeling complexes. *Genes Dev.* **15**, 603-18.
- Singh, A. P., Castranio, T., Scott, G., Guo, D., Harris, M. A., Ray, M., Harris, S. E., and Mishina, Y. (2008). Influences of reduced expression of maternal bone morphogenetic protein 2 on mouse embryonic development. *Sex Dev.* **2**, 134-141.
- Smithells, R.W., Sheppard, S., and Schorah, C.J. (1976). Vitamin deficiencies and neural tube defects. *Arch Dis Child.* **51**, 944-50.
- Song, H., Spichiger-Hausermann, C., and Basler, K. (2009). The ISWI-containing NURF complex regulates the output of the canonical Wntless pathway. *EMBO Rep* **10**, 1140-1146.
- Song, R., and Yosypiv, I. V. (2011). (Pro)renin receptor in kidney development and disease. *International Journal of Nephrology* doi:10.4061/2011/247048.
- Sonnenberg, E., Meyer, D., Weidner, K. M. and Birchmeier, C. (1993). Scatter factor/hepatocyte growth factor and its receptor, the c-met tyrosine kinase, can mediate a signal exchange between mesenchyme and epithelia during mouse development. *J. Cell Biol.* **123**, 223-235.
- Stahl, D.A., Koul, H.K., Chacko, J.K. and Mingin, G.C. (2005). Congenital anomalies of the kidney and urinary tract (CAKUT): a current review of cell signalling processes in ureteral development. *Journal of Pediatric Urology Company* **2**, 2-9.
- Star, R. A. (1998). Treatment of acute renal failure. *Kidney Int* **54**, 1817-1831.
- Stern, M., Jensen, R., and Herskowitz, I. (1984). Five SWI genes are required for reexpression of the HO gene in yeast. *J.Mol.Biol.* **178**, 853-868.
- Stopka, T., and Skoultschi, A.I. (2003). The ISWI ATPase Snf2h is required for early mouse development. *Proc. Natl. Acad. Sci. USA* **100**, 14097-14102.
- Strohner, R., Nemeth, A., Jansa, P., Hofmann-Rohrer, U., Santoro, R., Langst, G. and Grummt, I. (2001) NoRC—a novel member of mammalian ISWI-containing chromatin remodeling machines. *EMBO J.* **20**, 4892-4900.

- Strohner, R., Németh, A., Nightingale, K.P., Grummt, I., Becker, P.B. and Längst, G. (2004) Recruitment of the nucleolar remodeling complex NoRC establishes ribosomal DNA silencing in chromatin. *Mol Cell Biol* **24**, 1791-1798.
- Strong, L. C. and Hollander, W. F. (1949). Hereditary loop-tail in the house mouse accompanied by inperforate vagina and with lethal craniorachischisis when homozygous. *J. Hered.* **40**, 329 -334.
- Suarez, L., Ramadhani, T., Felkner, M., Canfield, M.A., Brender, J.D., and Romitti, P.A. (2011). Maternal smoking, passive tobacco smoke and neural tube defects. *Birth Defects Res A Clin Mol Teratol.* **91**, 29–33.
- Sudo, K., Maekawa, M., Shioya, M., Ikeda, K., Takahashi, N., Isogai, Y., Li, S. S., Kanno, T., Machida, K., and Toriumi, J. (1992). Molecular analysis of genetic mutation in electrophoretic variant of human lactate dehydrogenase-A(M) subunit. *Biochem Int* **27**, 1051-7.
- Susztak, K., Bitzer, M., Meyer, T. W., and Hostetter, T. H. (2008). Animal models of renal disease. *Kidney International* **73**, 526-528
- Suzuki-Inoue, K., Kato, Y., Inoue, O., Kaneko, M. K., Mishima, K., Yatomi, Y., Yamazaki, Y., Narimatsu, H., and Ozaki, Y. (2007). Involvement of snake toxin receptor CLEC-2, in podoplanin-mediated platelet activation, by cancer cells. *J Biol Chem* **282**, 25993-6001.
- Tan, Y., Cheung, M., Pei, J., Menges, C. W., Godwin, A. K., and Testa, J. R. (2010). Upregulation of DLX5 promotes ovarian cancer cell proliferation by enhancing IRS-2-AKT signaling. *Cancer Res* doi: 10.1158/0008-5472.CAN-10-1568.
- Taneja, R., Thisse, B., Rijli, F. M., Thisse, C., Bouillet, P., Dolle, P., and Chambon, P. (1996). The expression pattern of the mouse receptor tyrosine kinase gene MDK1 is conserved through evolution and requires Hoxa-2 for rhombomere-specific expression in mouse embryos. *Dev Biol.* **177**, 397-412.
- Tang, L., Nogales, E., and Ciferri, C. (2010). Structure and function of SWI/SNF chromatin remodeling complexes and mechanistic implications for transcription. *Prog Biophy Mol Biol* **102**, 122-128.
- Tate, P., Lee, M., Tweedie, S., Skarnes, W. C., and Bickmore, W. A. (1998) Capturing novel mouse genes encoding chromosomal and other nuclear proteins. *J Cell Sci* **111**, 2575–2585.
- Terzian, T., Wang, Y., Van Pelt, S. C., Box, N. F., Travis, E. L., and Lozano, G. (2007). Haploinsufficiency of MDM2 and MDM4 in tumorigenesis and development. *Mol Cell Biol* **27**, 5479–5485.
- Tessier, P. (1976). Anatomical Classification of Facial, Cranio-Facial and Latero-Facial Clefts. *Journal of Maxillofacial Surgery* **4**, 69-92.
- Thompson, P. J., Norton, K. A., Niri, F. H., Dawe, C. E., and McDermid HE. (2012). CECR2 is involved in spermatogenesis and forms a complex with SNF2H in the testis. *J Mol Biol* **415**, 793-806.

- Timmer, J.R., Wang, C., and Niswander, L. (2002). BMP signaling patterns the dorsal and intermediate neural tube via regulation of homeobox and helix–loop–helix transcription factors. *Development* **129**, 2459–2472.
- Ting, S. B., Wilanowski, T., Auden, A., Hall, M., Voss, A. K., Thomas, T., Parekh, V., Cunningham, J. M., and Jane, S. M. (2003). Inositol- and folate-resistant neural tube defects in mice lacking the epithelial-specific factor Grhl-3. *Nat Med* **9**, 1513–9.
- Torban, E., Patenaude, A. M., Leclerc, S., Rakowiecki, S., Gauthier, S., and Andelfinger, G. (2008). Genetic interaction between members of the Vangl family causes neural tube defects in mice. *PNAS* **105**, 3449–3454.
- Traslavina, R. P., King, E. J., Loar, A. S., Riedel, E. R., Garvey, M. S., Ricart-Arbona, R., Wolf, F. R., and Couto, S. S. (2010). Euthanasia by CO₂ inhalation affects potassium levels in mice. *J Am Assoc Lab Anim Sci* **49**, 316–322.
- Tsukiyama, T., and Wu, C. (1995). Purification and properties of an ATP-dependent nucleosome remodeling factor. *Cell* **83**, 1011–1020.
- Uetani, N., Bertozzi, K., Chagnon, M. J., Hendriks, W., Tremblay, M. L., and Bouchard, M. (2009). Maturation of ureter-bladder connection in mice is controlled by LAR family receptor protein tyrosine phosphatases. *J. Clin. Invest.* **119**, 924–935.
- Ünal-Çevik, I., Kılınç, M., Can, A., Gürsoy-Özdemir, Y., and Dalkara, T. (2004). Apoptotic and necrotic death mechanisms are concomitantly activated in the same cell after cerebral ischemia. *Stroke* **35**, 2189–2194.
- Uz, E., Alanay, Y., Aktas, D., Vargel, I., Gucer, S., Tuncbilek, G., von Eggeling, F., Yilmaz, E., Deren, O., Posorski, N., Ozdag, H., Liehr, T., Balci, S., Alikasifoglu, M., Wollnik, B., and Akarsu, N. A. (2010). Disruption of Alx1 causes extreme microphthalmia and severe facial clefting: expanding the spectrum of autosomal-recessive Alx-related frontonasal dysplasia. *Am J Hum Genet* **86**, 789–796.
- Van de Putte, T., Maruhashi, M., Francis, A., Nelles, L., Kondoh, H., Huylebroeck, D., and Higashi, Y. (2003). Mice lacking ZFHX1B, the gene that codes for Smad-interacting protein-1, reveal a role for multiple crest cell defects in the etiology of Hirschsprung disease-mental retardation syndrome. *Am. J. Hum. Genet.* **72**, 465–470.
- VanAllen, M. I., Kalousek, D. K., Chernoff, G. F., Jurilof, D., Harris, M., McGillivray, B. C., Yong, S. L., Langois, S., MacLeod, P. M., Chitayat, D., Friedman, J. M., Wilson, R. D., McFadden, D., Pantzar, J., Ritchie, S., and Hall, J. G. (1993). Evidence for multi-site closure of the neuraltube in humans. *Am J Med Genet* **47**, 723–743.
- Walker, E. J., Shen, F., Young, W. L., and Su, H. (2011). Cerebrovascular casting of the adult mouse for 3D imaging and morphological analysis. *J. Vis. Exp.* **57**, e2958, DOI: 10.3791/2958.

- Wang, Y., Thekdi, N., Smallwood, P. M., Macke, J.P., and Nathans, J. (2002). Frizzled-3 is required for the development of major fiber tracts in the rostral CNS. *J Neurosci* **22**, 8563–8573.
- Weining, L., Quintero-Rivera, F., Fan, Y., Alkuraya, F. S., Donovan, D. J., Xi, Q., Turbe-Doan, A., Li, Q. G., Campbell, C. G., Shanske, A. L., Sherr, E. H., Ahmad, A., Peters, R., Rilliet, B., Parvex, P., Bassuk, A. G., Harris, D. J., Ferguson, H., Kelly, C., Walsh, C. A., Gronostajski, R. M., Devriendt, K., Higgins, A., Ligon, A. H., Quade, B. J., Morton, C. C., Gusella, J. F., and Maas, R. L. (2007). NFIA haploinsufficiency is associated with CNS malformation syndrome and urinary tract defects. *PLoS Genetics* **3**, e80. doi:10.1371/journal.pgen.0030080.
- Wellik, D. M., Hawkes, P. J. and Capecchi, M. R. (2002). Hox11 paralogous genes are essential for metanephric kidney induction. *Genes Dev.* **16**, 1423-1432.
- Wiggan, O., Fadel, M. P., and Hamel, P. A. (2002). Pax3 induces cell aggregation and regulates phenotypic mesenchymal-epithelial interconversion. *Journal of Cell Science* **115**, 517-529.
- Willecke, R., Heuberger, J., Grossmann, K., Michosb, O., Schmidt-Otta, K., Walentina, K., Costantinib, F., and Birchmeiera, W. (2011). The tyrosine phosphatase Shp2 acts downstream of GDNF/Ret in branching morphogenesis of the developing mouse kidney. *Developmental Biology* **360**, 310-317.
- Williamson, M. P. (1994). The structure and function of proline-rich regions in proteins. *Biochem J* **297**, 249-260.
- Wilm, B., James, R. G., Schultheiss, T.M., Hogan, B. L. (2004). The forkhead genes, Foxc1 and Foxc2, regulate paraxial versus intermediate mesoderm cell fate. *Dev Biol.* **271**, 176-89.
- Wilson, D. B., and Center, E. M. (1977). Differences in cerebral morphology in 2 stocks of mutant mice heterozygous for the loop-tail (Lp)-gene. *Experientia* **33**, 1502-3.
- Winston, F., and Carlson, M. (1992). Yeast SWI/SNF transcriptional activators and the SPT/SIN chromatin connection. *Trends Genet.* **8**, 387–391.
- Wolffe, A.P., and Hayes, J.J.(1999). Chromatin disruption and modification. *Nucleic Acids Res.* **27**, 711–720.
- Woolf, A. S., Kolatsi-Joannou, M., Hardman, P., Andermarcher, E., Moorby, C., Fine, L. G., Jat, P. S., Noble, M. D., and Gherardi, E. (1995). Roles of hepatocyte growth factor/scatter factor and the met receptor in the early development of the metanephros. *J Cell Biol* **128**, 171-84.
- Xu, F., Addis, J. B., Cameron, J. M., and Robinson, B. H. (2012). LRPPRC mutation suppresses cytochrome oxidase activity by altering mitochondrial RNA transcript stability in a mouse model. *Biochem J.* **441**, 275-83.
- Xu, P. X., Adams, J., Peters, H., Brown, M. C., Heaney, S., and Maas, R. (1999). Eya1-deficient mice lack ears and kidneys and show abnormal apoptosis of organ primordia. *Nat. Genet.* **23**, 113–117.

- Yazdy, M.M., Liu, S., Mitchell, A.A., and Werler, M.M. (2010). Maternal dietary glycemic intake and the risk of neural tube defects. *Am J Epidemiol.* **171**, 407-14.
- Yip, D. J., Corcoran, C. P., Alvarez-Saavedra, M., DeMaria, A., Rennick, S., Mears, A. J., Rudnicki, M. A., Messier, C., and Picketts, D. J. (2012). Snf2l regulates Foxg1-dependent progenitor cell expansion in the developing brain. *Dev Cell.* **22**, 871-8.
- Yoshimura, K., Kitagawa, H., Fujiki, R., Tanabe, M., Takezawa, S., Takada, I., Yamaoka, I., Yonezawa, M., Kondo, T., Furutani, Y., Yagi, H., Yoshinaga, S., Masuda, T., Fukuda, T., Yamamoto, Y., Ebihara, K., Li, D. Y., Matsuoka, R., Takeuchi, J. K., Matsumoto, T., and Kato, S. (2009). Distinct function of 2 chromatin remodeling complexes that share a common subunit, Williams syndrome transcription factor (WSTF). *Proc Natl Acad Sci USA* **106**, 9280–9285.
- Zawadzki, K. A., Morozov, A. V., and Broach, J. R. (2009). Chromatin-dependent transcription factor accessibility rather than nucleosome remodeling predominates during global transcriptional restructuring in *Saccharomyces cerevisiae*. *Mol Biol Cell.* **20**, 3503–3513.
- Zeng, L., and Zhou, M. M. (2002). Bromodomain: an acetyl-lysine binding domain. *FEBS Lett* **513**, 124–128.
- Zhao, G. Q., Eberspaecher, H., Seldin, M. F., and de Crombrughe, B. (1994). The gene for the homeodomain-containing protein Cart-1 is expressed in cells that have a chondrogenic potential during embryonic development. *Mech. Dev.* **48**, 245–254.
- Zhao, Q., Behringer, R. R., and de Crombrughe, B. (1996). Prenatal folic acid treatment suppresses acrania and meroanencephaly in mice mutant for the Cart1 homeobox gene. *Nat. Genet.* **13**, 275–83.
- Zheng, Q., and Wang, X. J. (2008). GOEAST: a web-based software toolkit for Gene Ontology enrichment analysis. *Nucleic Acids Res.* **36**, W358-63.
- Zou, D., Erickson, C., Kim, E. H., Jin, D., Frittsch, B., and Xu, P. X. (2008). Eya1 gene dosage critically affects the development of sensory epithelia in the mammalian inner ear. *Hum. Mol. Genet.* **17**, 3340–3356.
- Zou, D., Silvius D., Rodrigo-Blomqvist S., Enerback S., and Xu P.X. (2006). Eya1 regulates the growth of otic epithelium and interacts with Pax2 during the development of all sensory areas in the inner ear. *Dev Biol* **298**, 430-41.

Appendix 1: Primer master lists		
Name	Sequence	Use
NHENHEKZCECR2F1	5PHOS-GCTAGCGCTAGCCACCATGTGCCCGGAGGAAGGC	CECR2 CLONING
SALSALNESTOPCECR2R19	5PHOS-GTCGACGTGACCCCGAGCTCTGAGGAAGGCTTGATTC	CECR2 CLONING
SNF2LINTRON6 3REV	GTATGGACAAGTGTGTGAAGCC	SNF2L GENOTYPE
SNF2LEXON6 REV	CCATGTGGGTCCAGGAATG	SNF2L GENOTYPE
SNF2LINTRON5 2FOR	CCTGGGCTGGAACCATGATC	SNF2L GENOTYPE
PAX6CRE-F	ATGCTTCTGTCCGTTTGCCG	SNF2L DEL
PAX6CRE-R	CCTGTTTGCACGTTTCAACCG	SNF2L DEL
LOXCECR2 DEL1R	ACCACAACGGTCAGACTTCC	INGDEL GENOTYPE
LOXCECR2 DEL2R	ACTCAACCTGCCAACCAATC	INGDEL GENOTYPE
LOXCECR2 DEL3R	AATGTGGCGAAATCAACTC	INGDEL GENOTYPE
CREIMR0042	CTAGGCCACAGAATTGAAAGATCT	CRE GENOTYPING
CREIMR0043	GTAGGTGGAAATCTAGCATCATCC	CRE GENOTYPING
CREIMR0567	ACCAGCCAGCTATCAACTCG	CRE GENOTYPING
CREIMR0568	TTACATTGGTCCAGCCACC	CRE GENOTYPING
INGENIOUS A2	AAGATTGAGCCTGGGAAAGAGGAG	INGDEL GENOTYPE
INGENIOUS LAN1	CCAGAGGCCACTTGTGTAGC	INGDEL GENOTYPE
INGENIOUS UNI	AGCGCATCGCCTTCTATCGCCTTC	INGDEL GENOTYPE
INGENIOUS LOX1	TTAGAATAGGTGAGGGAGGAG	INGDEL GENOTYPE
INGENIOUS SDL2	GTAGCGCCTATTGTATTGGTCA	INGDEL GENOTYPE
CRET INSITU FOR	ATTCCTATGTGAAGAAAAGCAAGG	IN SITU PROBE
CRET INSITU REV	TTGAAAACCTGCAAGACTTCAAAAAG	IN SITU PROBE
CRET INSITU NEST	GAAATTAATACGACTCACTATAGGAAAAGCATCAATGAGGAGATTAG	IN SITU PROBE
LIM1 INSITU FOR	CTTCTCCTTTTACGGAGATTACCA	IN SITU PROBE
LIM1 INSITU REV	TGAAGAGGTGATGTTCAAGTCATT	IN SITU PROBE
LIM1 INSITU NEST	GAAATTAATACGACTCACTATAGGAAACAAATCAAAAACCCAGAGAGA	IN SITU PROBE
GDNF INSITU FOR	GTGCTCACAATAACAAAGGTGAC	IN SITU PROBE
GDNF INSITU REV	GGAAGGGGAAAGGATACCTAGTAA	IN SITU PROBE

Appendix 1: Primer master lists		
Name	Sequence	Use
GDNF INSITU NEST	GAATTAATACGACTCACTATAGGAGGACTCAAGGCTCTAACATAGG	IN SITU PROBE
WT1 INSITU FOR	TTTAAGCTGTCCCACTTACAGATG	IN SITU PROBE
WT1 INSITU REV	AACATCATTTCTTAAGAGCCCAAGT	IN SITU PROBE
WT1 INSITU NEST	GAATTAATACGACTCACTATAGGGAAGGCTCCTCTCTGTCTCTAACTA	IN SITU PROBE
DLX5 5' INSITU	CAGAAGAGTCCCAAGCATCC	IN SITU PROBE
DLX5 3' INSITU	CTGGTGACTGTGGCGAGTTA	IN SITU PROBE
DLX5 NST INSITU	GGTAATACGACTCACTATAGGCGACCTGTGTTTGGCTCAGTC	IN SITU PROBE
NUDT21 5' INSITU	AGCTCTGTTGCAGCCAGATT	IN SITU PROBE
NUDT21 3' INSITU	AACACTGCCACATGTTTCCA	IN SITU PROBE
NUDT21 NST INSITU	GGTAATACGACTCACTATAGGGGTGGCAATTTAGGGAACAA	IN SITU PROBE
(FAT4) FOX4 1 FOR UNIV	GCAAGATCATTTAAGTTTAGCCAAC	QRT
(FAT4) FOX4 1 REV UNIV	AAATGTGCAGCCTTTCATCC	QRT
(FAT4) FOX4 2 FOR UNIV	TGCAGACAGCACCCCTGAA	QRT
(FAT4) FOX4 2 REV UNIV	CAAAAGTTGTCCCAGTTGAA	QRT
FJX1 1 FOR UNIV	TTCAGGACTAGTTATAAGCAGAGTCAA	QRT
FJX1 1 REV UNIV	ATCATCATTGTCAATTTTGGTCA	QRT
FJX1 2 FOR UNIV	GTGGAGATTGGATCCGAAGA	QRT
FJX1 2 REV UNIV	CTCCCAAAGAGGACTGCCATT	QRT
VANGL1 1 FOR UNIV	CGATGGCTCTCGACACAGT	QRT
VANGL1 1 REV UNIV	CATCCCCTAACCCGTTTGT	QRT
VANGL1 2 FOR UNIV	GTGAAGAAGCGGAGAGCAAG	QRT
VANGL1 2 REV UNIV	GGGTCCATCACCTCTCCAG	QRT
WNT5B FWD CODING1	CCTGCAGCCTCAAGACCT	QRT
WNT5B RVS CODING1	CAAACGGTCCCCAACCTT	QRT
WNT5A FWD CODING1	TGAAGCAGGCCGTAGGAC	QRT
WNT5A RVS CODING1	AGCCAGCACGTCTTGAGG	QRT
PAX6 FWD1	CAAGATTGGCCATGGATTTAAGA	QRT

Appendix 1: Primer master lists		
Name	Sequence	Use
PAX6 REV1	ACAACTTGGAAACATCAGTCCA	QRT
NUDT21 FWD1	TGACAACTGTGGCCCTCTTAAA	QRT
NUDT21 REV1	GCTGGACTCTGTTACATAAACTACTGG	QRT
PAX2 FWD2	CAGTTTGGGAAGCACCT	QRT
PAX2 REV2	GAAGGACGCTCAAGACTCG	QRT
DACH1 FWD1	CAAACTCCACTACAGAGGGTGA	QRT
DACH1 REV1	TTTTGTTTTTCAGCAACATTAAACAT	QRT
ELAV4 1 FWD	TCACCATGACCAACTACGATG	QRT
ELAV4 1 REV	CCAGGCGATAGCCATTGA	QRT
HEY2 1 FWD	GGGAGAGGGTGTTCATTT	QRT
HEY2 1 REV	CATTATGTAGCTTTTCCCTTCCA	QRT
HOXD1 1 FWD	TGCTCCCCACCTTTGAATAG	QRT
HOXD1 1 REV	TCCGTATTAAATTTCTACCCATGC	QRT
PRRX1 1 FWD	GGGAGGCAGAGCTGGTATTT	QRT
PRRX1 1 REV	CACCAGGAAATGCCAAAG	QRT
TSHZ3 1 FWD	TGACCCCTTTCTTCTTGCAATTA	QRT
TSHZ3 1 REV	GGAATATACACTATACAGAGCATGG	QRT
CECR2 ANTISENSE PROBE	GTGTCCTAGGGTCCAGCTATCTACAGCCTGGG - 3DIGOXN	IN SITU PROBE
CECR2 EXON1 ANTISENSE PROBE	CTCGTCACTCGCTCTCGCTCGCTCGTCTCGGACTC - 3DIGOXN	IN SITU PROBE
PAX1 3' ANTISENSE PROBE	CCAGTCCCAACACCAGTCCCGCATCTCTTTCTCC - 3DIGOXN	IN SITU PROBE
CART1 INSITU FOR1	GCGAGAAAGTTTGCCCTGA	IN SITU PROBE
CART1 INSITU REV1	AAATGCGTGTCCGTTGGT	IN SITU PROBE
CART1 INSITU NESTED T7 1	GAATTAATACGACTCACTATAGGCTGAACTGATTCTGGTG	IN SITU PROBE
CECR2 INSITU FOR 1	TTGCTGAGGACCCAGAG	IN SITU PROBE
CECR2 INSITU REV 1	CCTGGAAGAGAAAGTGCTGGA	IN SITU PROBE
CECR2 NESTED T7 1	GAATTAATACGACTCACTATAGGAAGTGCTGGAAGCAGAAAAGG	IN SITU PROBE
EYA1 INSITU FOR 1	GTCCACCAATGCCACTTACC	IN SITU PROBE

Appendix 1: Primer master lists		
Name	Sequence	Use
EYA1 INSITU REV 1	CAGACCTCCACGTTGTTTT	IN SITU PROBE
EYA1 INSITU NESTED T7 1	GAAATTAATACGACTCACTATAGGACCTCCACGTTGTTTT	IN SITU PROBE
EPHA7 INSITU FOR 1	ATGAGGCTTAAGACTGCAGGAG	IN SITU PROBE
EPHA7 INSITU REV 1	CAGACGAAGCTCAGCCTTTTAT	IN SITU PROBE
EPHA7 INSITU NESTED T7 1	GAAATTAATACGACTCACTATAGGTACCTGCCAATCAGCAAACA	IN SITU PROBE
CD5KRAP1 INSITU FOR 1	AGGAGGGCTTCGTTTTCTC	IN SITU PROBE
CD5KRAP1 INSITU REV 1	GAGCTGGCAGAGGTGATCTT	IN SITU PROBE
CDK5RAP1 INSITU NESTED T7 1	GAAATTAATACGACTCACTATAGGAGCACATAGTCCCCCAGGTTG	IN SITU PROBE
SIX1 INSITU FOR 1	CTCGGTCCTTCTGCTCCA	IN SITU PROBE
SIX1 INSITU REV 1	TCGCTGCTACCCCTAACCG	IN SITU PROBE
SIX1 INSITU NESTED T7 1	GAAATTAATACGACTCACTATAGGACCTTGTTCCTTCCCTTGCT	IN SITU PROBE
CDK5RAP1 1 FOR UNIV	CAACCTGGGGACTATGTGCT	QRT
CDK5RAP1 1 REV UNIV	TGTGTCTTTCAGGGTCTGAG	QRT
CDK5RAP1 2 FOR UNIV	TCAAGAAATCGATCCTGAAATGA	QRT
CDK5RAP1 2 REV UNIV	TCACGAATCAGCTGAAGAACC	QRT
WNT5A 1456976 LEFT 1	TCCTGCTTTGCTTTGATTGA	QRT
WNT5A 1456976 RIGHT 1	GGGTTTTAGTTTTAAAGGGCTT	QRT
WNT7B 1420892 LEFT 1	GACCCCTTGTTTGCCCTTG	QRT
WNT7B 1420892 RIGHT 1	GGCTTGAACATCCTGACAT	QRT
FZD1 1437284 LEFT 1	TGTACACAATCAACAATACACTTTGC	QRT
FZD1 1437284 RIGHT 1	CGGGGGTGTGACTGTTTCT	QRT
FZD10 1455689 LEFT 1	TGCCTGCAGATCCCTTAAAA	QRT
FZD10 1455689 RIGHT 1	TGTTGGGAGAAACATGGCTA	QRT
FZD2 1428533 LEFT 1	CGTATACCTGTTTCATCGGTACATC	QRT
FZD2 1428533 RIGHT 1	ATCGGGAAGAGTGACACGA	QRT
FZD5 1455604 LEFT 1	CCGTGCAGTAAGAATCACCA	QRT
FZD5 1455604 RIGHT 1	GATCAAGCTGATTGTCTACAAATAAA	QRT
FZD7 1450044 LEFT 1	TGCAATGTTCTTCAGTTTCTCAG	QRT
FZD7 1450044 RIGHT 1	GTAATCTGTCTCTCCCGACAATC	QRT

Appendix 1: Primer master lists		
Name	Sequence	Use
EYA1 LEFT 1	TTGCCATAAAATTACCCCTTTGG	QRT
EYA1 RIGHT 1	TTTTCTGCTACTCTGGGTCAA	QRT
SIX1 LEFT 1	AACAAGAAACCTTCAGTGTGAGG	QRT
SIX1 RIGHT 1	AAAAACAGCTGTGATTATAGTTTTCT	QRT
TFPI LEFT 1	CCTCTGGGTGCCCATTAACA	QRT
TFPI RIGHT 1	GCCTATAAACCTAAAGTGAGTTAGGG	QRT
DLX5 LEFT 1	CTGGAGAACTCGGCTTCCT	QRT
DLX5 RIGHT 1	TGGCAGGTGGGAATTGAT	QRT
EPHA7 LEFT 1	CAAAAAGGGAATTTAGGATCCAC	QRT
EPHA7 RIGHT 1	ACTTTGTTTATTGTCCTGCTGTGTT	QRT
GSK3B LEFT 1	AGTCCGTTGCTCCGTTGT	QRT
GSK3B RIGHT 1	CCCTTATGTACTGGCTGTCA	QRT
PRICKLE1 LEFT 1	AAGCTATCTGGCGCTCTTC	QRT
PRICKLE1 RIGHT 1	AGCTCATCGCGTGGACAT	QRT
VANGL2 LEFT 1	ACCTGTGGCCTCGTCTCTTA	QRT
VANGL2 RIGHT 1	TTAAGGCAGGGGATGAGAAG	QRT
CELSR2 LEFT 1	AGGACTCCTCTGGCTCTGAAT	QRT
CELSR2 RIGHT 1	AGGGACGGAAGGAACACC	QRT
INTU 1444272_AT LEFT 1	GGTCAGGTCCTGGTTGGTAA	QRT
INTU 1444272_AT RIGHT 1	CCTTAACCATGTACCTCAGCAA	QRT
FGFR1 1425911_A_AT LEFT 1	TCGACTACTACAAGAAAACCA	QRT
FGFR1 1425911_A_AT RIGHT 1	CCACAAGAGCACTCCAAA	QRT
HEY2 1418106_AT LEFT 1	GGAGAGGGTGTTCATTCT	QRT
HEY2 1418106_AT RIGHT 1	AACCTGACCAGGGCATTTACA	QRT
CUX1 1424667_A_AT LEFT 1	AGCTGCCAGGAGCTCAGAT	QRT

Appendix 1: Primer master lists		
Name	Sequence	Use
CUX1 1424667_A_AT RIGHT 1	TGTTGAACCTTTAGGGCTCCA	QRT
WNT5B ANTISENSE 3' PROBE	TCATCAGAAAGGCAGAGCCAGGGTCCAGGGAGGCC - 3DIGOXN	IN SITU PROBE
FRZB ANTISENSE 3' PROBE	CCGCGGTACGATGGCCTCAGGAGACATGCACACG - 3DIGOXN	IN SITU PROBE
ALX1 1 ANTISENSE 3' PROBE	CACTTGAATGTGACAGGGGGAAGGAGTAGAAGG - 3DIGOXN	IN SITU PROBE
TSHZ3 ANTISENSE 3' PROBE	AGAGTGTGTACGGTGTCTGTGTGTTACATGCC - 3DIGOXN	IN SITU PROBE
VANGL2 1 FOR UNIV	ACCTGTGGCCTCGTCTCTTA	QRT
VANGL2 1 REV UNIV	TTAAGGCAGGGGATGAGAAG	QRT
VANGL2 2 FOR UNIV	GCAGCAATCTGAACGAATCT	QRT
VANGL2 2 REV UNIV	TGAAAATATCCATTAGAGGGTTAGTG	QRT
FOXC1 INSITU F	GGCCAGAGCTCCCTCTACA	IN SITU PROBE
FOXC1 INSITU R	ACGTGCGGTACAGAGACTGA	IN SITU PROBE
FOXC1 INSITU NST	GAAATTAATACGACTCACTATAGGAGAGACTGACTGGCAGGGAAA	IN SITU PROBE
PAX3 INSITU F	GCCTCAGACCGACTATGCTC	IN SITU PROBE
PAX3 INSITU R	AAGGAAACACACGCAGCTTT	IN SITU PROBE
PAX3 INSITU NST	GAAATTAATACGACTCACTATAGGTCATGCTGGGACAATTC	IN SITU PROBE
CRIM1 INSITU F	TCAGGCACATGTCTGTCCAT	IN SITU PROBE
CRIM1 INSITU R	TCAATATCCCACCGTTCCTC	IN SITU PROBE
CRIM1 INSITU NST	GAAATTAATACGACTCACTATAGGAACACTGGCCTTTCCTCAAA	IN SITU PROBE
ZFP9 INSITU F	CAGAAGCCACACCTCACAGA	IN SITU PROBE
ZFP9 INSITU R	CACTCCTGGCACTCATAGGG	IN SITU PROBE
ZFP INSITU NST	GAAATTAATACGACTCACTATAGGCTGGCACTCATAGGGCTTCT	IN SITU PROBE
PECAM1 INSITU F	CGGATTCAAATTGCAGGAGT	IN SITU PROBE
PECAM1 INSITU R	ATGGGTGCAGTTCATTTC	IN SITU PROBE
PECAM1 INSITU NST	GAAATTAATACGACTCACTATAGGTAAGTGGGCTTCGAGAGCAATT	IN SITU PROBE

Appendix 2: *Cecr2*^{Gt45Bic} BALB/c versus BALB/c microarrays

Gene	PROBE ID	gcRMA		Arraystar		dCHIP	
		Fold	p-value	Fold	p-value	Fold	p-value
Cecr2	1457039_at	-14.52	5.27E-08	-5.14	1.33E-06	-5.75	3.00E-06
Cecr2	1431014_at	-11.35	8.63E-09	-5.23	4.03E-04	-7.73	3.00E-06
Nudt21	1455966_s_at	-6.25	1.27E-02	-4.16	1.41E-02	-3.90	4.85E-02
Nudt21	1437213_at	-5.06	1.42E-02	-3.72	1.49E-02	-3.59	4.71E-02
Zfp9	1456483_at	-3.66	1.54E-04	-2.52	4.56E-04	-2.72	1.13E-03
Csn3	1419735_at	-3.01	1.43E-05	-2.14	3.44E-05	-1.84	7.21E-04
Alx1	1435022_at	-2.33	1.11E-05	-1.78	2.13E-04	-1.72	5.79E-03
Wnt5b	1439373_x_at	-1.59	4.16E-03	-1.38	2.20E-02	-2.50	4.90E-05
Anxa1	1448213_at	-2.13	1.66E-02	-1.51	1.78E-02	-1.29	4.27E-02
Cd36	1450883_a_at	-1.86	1.01E-04	-1.60	2.40E-03	-1.46	2.84E-02
1810014B01Rik	1430991_at	-1.67	4.95E-02	-1.53	4.94E-02	-1.62	2.85E-02
Tax1bp1	1420175_at	-1.50	1.00E-02	-1.58	2.03E-02	-1.66	4.37E-02
Mnx1	1460299_at	-1.28	7.67E-03	-1.62	2.91E-03	-1.74	1.36E-02
Nol7	1420487_at	-1.75	1.61E-02	-1.43	1.74E-02	-1.46	2.68E-02
Gm715	1445503_at	-1.75	1.26E-03	-1.48	3.13E-03	-1.38	2.30E-02
AW551984	1433434_at	-1.67	1.54E-03	-1.46	6.28E-04	-1.46	1.16E-02
Prrx1	1439774_at	-1.54	3.53E-02	-1.51	3.18E-02	-1.43	3.69E-02
Hoxd1	1420573_at	-1.64	1.25E-03	-1.40	9.73E-03	-1.40	2.50E-02
Perp	1416271_at	-1.68	2.18E-03	-1.49	8.01E-03	-1.27	1.88E-02
Asb4	1423422_at	-1.54	4.33E-02	-1.43	3.55E-02	-1.45	2.93E-02
Cpa2	1454623_at	-1.57	8.96E-03	-1.36	4.51E-03	-1.42	2.36E-03
Hey2	1418106_at	-1.65	2.05E-03	-1.42	3.40E-03	-1.28	1.36E-03
Pm20d1	1438980_x_at	-1.54	6.47E-03	-1.36	5.39E-03	-1.43	3.42E-02
Grb14	1417673_at	-1.53	2.71E-03	-1.42	1.32E-03	-1.36	1.22E-02
Nkx1-2	1422050_at	-1.50	2.24E-02	-1.43	3.62E-02	-1.35	1.81E-02
Tshz3	1435337_at	-1.59	5.46E-03	-1.31	1.08E-03	-1.36	3.14E-02
Spin2	1455297_at	-1.47	1.44E-02	-1.36	1.96E-02	-1.40	2.53E-02
Thbs4	1449388_at	-1.47	1.10E-02	-1.37	9.21E-03	-1.38	4.25E-02
Lix1	1421180_at	-1.55	3.33E-04	-1.28	6.20E-05	-1.38	4.19E-03
Frzb	1448424_at	-1.50	9.88E-03	-1.31	3.58E-03	-1.35	2.04E-02
Sema3e	1419717_at	-1.39	8.69E-03	-1.40	7.08E-03	-1.36	1.96E-02
Met	1434447_at	-1.42	1.51E-03	-1.36	1.21E-03	-1.36	2.85E-03
Dlx2	1448877_at	-1.48	1.33E-02	-1.31	2.46E-02	-1.31	3.77E-02
Gliplr1	1449746_s_at	-1.43	2.62E-02	-1.36	3.11E-02	-1.32	3.39E-02
Mbnl3	1422836_at	-1.46	4.02E-02	-1.30	3.63E-02	-1.34	2.24E-02
Slc38a4	1428111_at	-1.44	2.08E-02	-1.36	1.82E-02	-1.26	2.48E-02
Tmem56	1434553_at	-1.38	2.49E-02	-1.32	2.92E-02	-1.35	3.53E-02
Plp1	1425468_at	-1.44	1.68E-02	-1.26	1.20E-02	-1.35	3.70E-02
Dsp	1435493_at	-1.43	1.53E-02	-1.38	9.55E-03	-1.23	1.83E-02
Sox17	1429177_x_at	-1.42	1.82E-02	-1.29	2.69E-02	-1.33	7.56E-03
Dynl1	1440278_at	-1.29	2.29E-02	-1.38	1.05E-02	-1.33	2.55E-02
Zfhx4	1437556_at	-1.38	2.76E-04	-1.33	7.23E-04	-1.29	4.91E-03
Grasp	1441894_s_at	-1.65	1.19E-02	-1.16	2.07E-02	-1.19	1.42E-02
Adams20	1456901_at	-1.35	6.91E-03	-1.31	1.51E-03	-1.34	5.39E-03
Synpo2l	1447657_s_at	-1.44	8.07E-03	-1.30	1.52E-02	-1.26	3.44E-02
Unc5b	1453269_at	-1.49	4.30E-02	-1.26	1.23E-02	-1.25	4.15E-02
Epha7	1451991_at	-1.33	2.28E-03	-1.33	1.81E-03	-1.32	1.41E-02
Rspo3	1455607_at	-1.36	2.18E-03	-1.30	1.35E-03	-1.31	9.71E-03
---	1457041_at	-1.37	1.15E-02	-1.19	1.41E-02	-1.41	3.54E-02
LOC100046086	1436041_at	-1.40	1.40E-03	-1.29	4.51E-03	-1.27	2.80E-03
Hsd17b7	1457248_x_at	-1.36	3.97E-02	-1.30	4.08E-03	-1.30	2.02E-02
Foxg1	1418357_at	-1.35	1.23E-02	-1.32	1.06E-02	-1.28	3.69E-02
Etv2	1421773_at	-1.38	2.93E-02	-1.24	2.80E-02	-1.33	2.72E-02
Frzb	1416658_at	-1.37	3.10E-02	-1.24	2.12E-02	-1.32	1.20E-02
Dlx5	1449863_a_at	-1.32	3.50E-03	-1.30	2.50E-05	-1.30	7.85E-03
Scd1	1415965_at	-1.29	1.08E-02	-1.32	1.33E-02	-1.30	7.81E-03
St8sia4	1419186_a_at	-1.36	1.01E-02	-1.28	1.98E-02	-1.27	1.49E-02
Amph	1427044_a_at	-1.37	9.02E-03	-1.21	1.51E-02	-1.31	6.44E-03
Klhl4	1439078_at	-1.35	4.20E-02	-1.35	4.25E-03	-1.19	4.89E-02
Cck	1419473_a_at	-1.47	7.69E-03	-1.17	2.30E-02	-1.24	3.38E-02
Gap43	1423537_at	-1.34	5.72E-05	-1.27	5.73E-04	-1.28	3.33E-03
Noc4l	1443794_x_at	-1.32	4.45E-03	-1.27	5.15E-03	-1.27	7.10E-03
E430028B21Rik	1443869_at	-1.36	5.30E-03	-1.26	1.06E-03	-1.23	1.02E-02
Sema3a	1449865_at	-1.34	5.11E-03	-1.25	8.73E-03	-1.25	1.43E-02
Foxa1	1418496_at	-1.34	1.30E-02	-1.27	1.14E-02	-1.23	4.40E-02
Nebi	1439897_at	-1.36	2.36E-02	-1.26	1.57E-02	-1.22	2.71E-02

Appendix 2: *Cecr2*^{Gt45Bic} BALB/c versus BALB/c microarrays

Gene	PROBE ID	gcRMA		Arraystar		dCHIP	
		Fold	p-value	Fold	p-value	Fold	p-value
Six1	1427277_at	-1.36	5.94E-03	-1.23	5.99E-03	-1.25	2.60E-02
Ifrd1	1416067_at	-1.30	2.48E-02	-1.28	2.07E-02	-1.25	1.52E-02
Cdkn2aip	1438300_at	-1.41	2.99E-03	-1.20	1.52E-02	-1.22	3.01E-02
Cd38	1433741_at	-1.34	1.47E-02	-1.30	1.06E-02	-1.20	3.95E-02
Vegfc	1440739_at	-1.31	1.63E-02	-1.27	9.60E-03	-1.25	2.65E-02
A730089K16Rik	1437263_at	-1.23	4.58E-03	-1.18	1.32E-02	-1.42	1.02E-02
A730017C20Rik	1437528_x_at	-1.31	9.00E-03	-1.30	2.53E-03	-1.21	2.41E-02
Tshz1	1427233_at	-1.29	6.34E-03	-1.29	1.79E-03	-1.24	2.93E-02
C030045D06Rik	1436569_at	-1.27	9.04E-03	-1.28	4.77E-03	-1.27	8.78E-03
Vegfc	1439766_x_at	-1.31	3.06E-02	-1.28	2.18E-02	-1.22	4.60E-02
Noc4l	1438095_x_at	-1.34	7.21E-03	-1.25	5.84E-03	-1.22	9.72E-03
Eya1	1457424_at	-1.28	5.10E-03	-1.28	4.20E-04	-1.25	6.28E-03
Kbtbd4	1417922_at	-1.30	1.25E-02	-1.18	1.09E-02	-1.32	1.68E-02
Cbx4	1419583_at	-1.25	9.65E-03	-1.19	4.13E-03	-1.37	6.29E-03
Ripk4	1418488_s_at	-1.26	3.52E-02	-1.28	4.62E-02	-1.26	4.17E-02
Chordc1	1435574_at	-1.31	1.29E-02	-1.29	2.32E-03	-1.18	3.45E-02
LOC100044968	1434283_at	-1.30	6.36E-03	-1.20	6.73E-03	-1.28	6.54E-03
Pkp2	1449799_s_at	-1.31	1.78E-02	-1.25	2.03E-02	-1.21	3.64E-02
Dtwd2	1428901_at	-1.29	5.44E-03	-1.24	5.27E-03	-1.24	2.44E-02
Steap1	1424938_at	-1.32	3.23E-02	-1.23	1.37E-02	-1.21	4.58E-02
Ccdc101	1451166_a_at	-1.31	7.26E-03	-1.24	4.35E-03	-1.21	1.13E-02
Coq10b	1428487_s_at	-1.29	6.15E-03	-1.28	6.52E-03	-1.19	1.80E-02
Arhgap24	1424842_a_at	-1.29	2.69E-03	-1.23	9.15E-03	-1.24	2.73E-02
Mib1	1433853_at	-1.27	3.53E-02	-1.23	3.83E-02	-1.25	6.33E-03
Sifn9	1436472_at	-1.27	1.23E-02	-1.19	5.79E-04	-1.29	2.40E-02
Colec11	1458345_s_at	-1.21	3.90E-02	-1.18	4.24E-02	-1.35	2.45E-02
Hdh2	1428507_at	-1.29	2.66E-02	-1.20	2.51E-02	-1.25	1.79E-02
---	1437967_at	-1.28	5.77E-03	-1.22	4.80E-03	-1.23	8.42E-03
Defcr-rs7	1422934_x_at	-1.22	9.34E-03	-1.18	4.73E-02	-1.33	3.88E-02
Klhl6	1437886_at	-1.32	2.36E-02	-1.24	2.45E-02	-1.17	4.02E-02
Ube2v2	1417984_at	-1.30	5.22E-03	-1.21	1.39E-02	-1.22	1.87E-02
Mapre2	1451989_a_at	-1.27	2.35E-02	-1.24	2.43E-02	-1.21	3.05E-02
---	1437766_at	-1.31	3.59E-03	-1.20	1.26E-02	-1.21	3.19E-02
Uap1	1456516_x_at	-1.26	1.39E-02	-1.24	1.25E-02	-1.22	3.68E-02
Dsp	1435494_s_at	-1.29	1.02E-02	-1.25	1.50E-02	-1.18	2.40E-02
Zfp69	1458274_at	-1.38	8.66E-03	-1.17	9.08E-03	-1.16	3.96E-02
Golt1b	1460583_at	-1.29	8.41E-03	-1.19	4.26E-03	-1.23	7.56E-03
Ccdc101	1437592_x_at	-1.34	4.99E-03	-1.19	5.72E-04	-1.18	8.94E-03
Grwd1	1455841_s_at	-1.26	5.07E-03	-1.23	1.23E-02	-1.22	1.86E-02
Polr3a	1437525_a_at	-1.25	3.37E-02	-1.26	1.34E-02	-1.20	2.76E-02
Nubp2	1459842_x_at	-1.28	3.16E-04	-1.21	5.43E-03	-1.22	1.44E-02
9330118A15Rik	1456798_at	-1.33	4.56E-03	-1.20	1.94E-02	-1.17	2.80E-02
Cops7a	1429078_a_at	-1.24	5.29E-05	-1.21	1.05E-04	-1.25	7.63E-04
Tmem158	1428074_at	-1.24	1.55E-02	-1.21	1.93E-02	-1.25	1.08E-02
Capn6	1450429_at	-1.27	7.41E-03	-1.20	8.94E-03	-1.22	1.02E-02
Mtf1	1429170_a_at	-1.28	2.75E-02	-1.19	2.01E-02	-1.21	3.22E-02
Fbxo33	1426870_at	-1.29	5.86E-04	-1.22	3.96E-04	-1.18	3.12E-02
Mpp6	1449348_at	-1.27	1.65E-02	-1.22	2.24E-02	-1.19	3.08E-02
Steap1	1451532_s_at	-1.22	2.16E-02	-1.19	5.94E-03	-1.27	1.07E-02
Fdft1	1438322_x_at	-1.25	7.57E-03	-1.22	1.38E-02	-1.20	4.91E-02
Tmem164	1433854_at	-1.26	4.76E-03	-1.20	7.45E-03	-1.21	4.94E-02
Cisd1	1443822_s_at	-1.24	1.14E-02	-1.19	3.19E-03	-1.24	6.07E-03
Cyp20a1	1430452_at	-1.23	2.01E-02	-1.21	1.35E-02	-1.22	3.81E-02
---	1434848_at	-1.26	1.76E-02	-1.24	9.66E-03	-1.16	1.60E-02
Ccnc	1417861_at	-1.33	1.78E-03	-1.17	1.92E-03	-1.16	4.41E-02
Lrrc28	1433858_at	-1.23	2.91E-02	-1.21	5.53E-03	-1.21	5.04E-02
Minpp1	1423265_at	-1.24	5.02E-03	-1.21	3.46E-03	-1.21	4.37E-02
Lrp11	1433536_at	-1.25	3.41E-02	-1.19	2.68E-02	-1.22	4.16E-02
---	1460125_at	-1.29	3.47E-02	-1.14	3.80E-02	-1.22	3.65E-02
Cldn9	1439427_at	-1.22	6.13E-03	-1.22	2.49E-02	-1.21	4.62E-02
Nr2f6	1460647_a_at	-1.26	5.15E-03	-1.20	2.90E-03	-1.18	2.77E-02
Dhps	1434003_a_at	-1.26	3.54E-02	-1.19	2.82E-02	-1.20	3.69E-02
Sgpp1	1420822_s_at	-1.28	2.24E-02	-1.19	1.39E-02	-1.17	3.40E-02
Pcm1	1422665_a_at	-1.23	3.66E-02	-1.22	1.43E-02	-1.19	1.56E-02
Kitl	1415855_at	-1.26	8.78E-03	-1.19	2.01E-02	-1.19	3.93E-02
Prkcm	1447623_s_at	-1.24	2.92E-02	-1.22	2.38E-02	-1.18	1.78E-02

Appendix 2: *Cecr2*^{Gt45Bic} BALB/c versus BALB/c microarrays

Gene	PROBE ID	gcRMA		Arraystar		dCHIP	
		Fold	p-value	Fold	p-value	Fold	p-value
Six1	1427277_at	-1.36	5.94E-03	-1.23	5.99E-03	-1.25	2.60E-02
Ifrd1	1416067_at	-1.30	2.48E-02	-1.28	2.07E-02	-1.25	1.52E-02
Cdkn2aip	1438300_at	-1.41	2.99E-03	-1.20	1.52E-02	-1.22	3.01E-02
Cd38	1433741_at	-1.34	1.47E-02	-1.30	1.06E-02	-1.20	3.95E-02
Vegfc	1440739_at	-1.31	1.63E-02	-1.27	9.60E-03	-1.25	2.65E-02
A730089K16Rik	1437263_at	-1.23	4.58E-03	-1.18	1.32E-02	-1.42	1.02E-02
A730017C20Rik	1437528_x_at	-1.31	9.00E-03	-1.30	2.53E-03	-1.21	2.41E-02
Tshz1	1427233_at	-1.29	6.34E-03	-1.29	1.79E-03	-1.24	2.93E-02
C030045D06Rik	1436569_at	-1.27	9.04E-03	-1.28	4.77E-03	-1.27	8.78E-03
Vegfc	1439766_x_at	-1.31	3.06E-02	-1.28	2.18E-02	-1.22	4.60E-02
Noc4l	1438095_x_at	-1.34	7.21E-03	-1.25	5.84E-03	-1.22	9.72E-03
Eya1	1457424_at	-1.28	5.10E-03	-1.28	4.20E-04	-1.25	6.28E-03
Kbtbd4	1417922_at	-1.30	1.25E-02	-1.18	1.09E-02	-1.32	1.68E-02
Cbx4	1419583_at	-1.25	9.65E-03	-1.19	4.13E-03	-1.37	6.29E-03
Ripk4	1418488_s_at	-1.26	3.52E-02	-1.28	4.62E-02	-1.26	4.17E-02
Chordc1	1435574_at	-1.31	1.29E-02	-1.29	2.32E-03	-1.18	3.45E-02
LOC100044968	1434283_at	-1.30	6.36E-03	-1.20	6.73E-03	-1.28	6.54E-03
Pkp2	1449799_s_at	-1.31	1.78E-02	-1.25	2.03E-02	-1.21	3.64E-02
Dtwd2	1428901_at	-1.29	5.44E-03	-1.24	5.27E-03	-1.24	2.44E-02
Steap1	1424938_at	-1.32	3.23E-02	-1.23	1.37E-02	-1.21	4.58E-02
Ccdc101	1451166_a_at	-1.31	7.26E-03	-1.24	4.35E-03	-1.21	1.13E-02
Coq10b	1428487_s_at	-1.29	6.15E-03	-1.28	6.52E-03	-1.19	1.80E-02
Arhgap24	1424842_a_at	-1.29	2.69E-03	-1.23	9.15E-03	-1.24	2.73E-02
Mib1	1433853_at	-1.27	3.53E-02	-1.23	3.83E-02	-1.25	6.33E-03
Sifn9	1436472_at	-1.27	1.23E-02	-1.19	5.79E-04	-1.29	2.40E-02
Colec11	1458345_s_at	-1.21	3.90E-02	-1.18	4.24E-02	-1.35	2.45E-02
Hdh2	1428507_at	-1.29	2.66E-02	-1.20	2.51E-02	-1.25	1.79E-02
---	1437967_at	-1.28	5.77E-03	-1.22	4.80E-03	-1.23	8.42E-03
Defcr-rs7	1422934_x_at	-1.22	9.34E-03	-1.18	4.73E-02	-1.33	3.88E-02
Klhl6	1437886_at	-1.32	2.36E-02	-1.24	2.45E-02	-1.17	4.02E-02
Ube2v2	1417984_at	-1.30	5.22E-03	-1.21	1.39E-02	-1.22	1.87E-02
Mapre2	1451989_a_at	-1.27	2.35E-02	-1.24	2.43E-02	-1.21	3.05E-02
---	1437766_at	-1.31	3.59E-03	-1.20	1.26E-02	-1.21	3.19E-02
Uap1	1456516_x_at	-1.26	1.39E-02	-1.24	1.25E-02	-1.22	3.68E-02
Dsp	1435494_s_at	-1.29	1.02E-02	-1.25	1.50E-02	-1.18	2.40E-02
Zfp69	1458274_at	-1.38	8.66E-03	-1.17	9.08E-03	-1.16	3.96E-02
Golt1b	1460583_at	-1.29	8.41E-03	-1.19	4.26E-03	-1.23	7.56E-03
Ccdc101	1437592_x_at	-1.34	4.99E-03	-1.19	5.72E-04	-1.18	8.94E-03
Grwd1	1455841_s_at	-1.26	5.07E-03	-1.23	1.23E-02	-1.22	1.86E-02
Polr3a	1437525_a_at	-1.25	3.37E-02	-1.26	1.34E-02	-1.20	2.76E-02
Nubp2	1459842_x_at	-1.28	3.16E-04	-1.21	5.43E-03	-1.22	1.44E-02
9330118A15Rik	1456798_at	-1.33	4.56E-03	-1.20	1.94E-02	-1.17	2.80E-02
Cops7a	1429078_a_at	-1.24	5.29E-05	-1.21	1.05E-04	-1.25	7.63E-04
Tmem158	1428074_at	-1.24	1.55E-02	-1.21	1.93E-02	-1.25	1.08E-02
Capn6	1450429_at	-1.27	7.41E-03	-1.20	8.94E-03	-1.22	1.02E-02
Mtf1	1429170_a_at	-1.28	2.75E-02	-1.19	2.01E-02	-1.21	3.22E-02
Fbxo33	1426870_at	-1.29	5.86E-04	-1.22	3.96E-04	-1.18	3.12E-02
Mpp6	1449348_at	-1.27	1.65E-02	-1.22	2.24E-02	-1.19	3.08E-02
Steap1	1451532_s_at	-1.22	2.16E-02	-1.19	5.94E-03	-1.27	1.07E-02
Fdft1	1438322_x_at	-1.25	7.57E-03	-1.22	1.38E-02	-1.20	4.91E-02
Tmem164	1433854_at	-1.26	4.76E-03	-1.20	7.45E-03	-1.21	4.94E-02
Cisd1	1443822_s_at	-1.24	1.14E-02	-1.19	3.19E-03	-1.24	6.07E-03
Cyp20a1	1430452_at	-1.23	2.01E-02	-1.21	1.35E-02	-1.22	3.81E-02
---	1434848_at	-1.26	1.76E-02	-1.24	9.66E-03	-1.16	1.60E-02
Ccnc	1417861_at	-1.33	1.78E-03	-1.17	1.92E-03	-1.16	4.41E-02
Lrrc28	1433858_at	-1.23	2.91E-02	-1.21	5.53E-03	-1.21	5.04E-02
Minpp1	1423265_at	-1.24	5.02E-03	-1.21	3.46E-03	-1.21	4.37E-02
Lrp11	1433536_at	-1.25	3.41E-02	-1.19	2.68E-02	-1.22	4.16E-02
---	1460125_at	-1.29	3.47E-02	-1.14	3.80E-02	-1.22	3.65E-02
Cldn9	1439427_at	-1.22	6.13E-03	-1.22	2.49E-02	-1.21	4.62E-02
Nr2f6	1460647_a_at	-1.26	5.15E-03	-1.20	2.90E-03	-1.18	2.77E-02
Dhps	1434003_a_at	-1.26	3.54E-02	-1.19	2.82E-02	-1.20	3.69E-02
Sgpp1	1420822_s_at	-1.28	2.24E-02	-1.19	1.39E-02	-1.17	3.40E-02
Pcm1	1422665_a_at	-1.23	3.66E-02	-1.22	1.43E-02	-1.19	1.56E-02
Kitl	1415855_at	-1.26	8.78E-03	-1.19	2.01E-02	-1.19	3.93E-02
Prkcm	1447623_s_at	-1.24	2.92E-02	-1.22	2.38E-02	-1.18	1.78E-02

Appendix 2: *Cecr2*^{Gt45Bic} BALB/c versus BALB/c microarrays

Gene	PROBE ID	gcRMA		Arraystar		dCHIP	
		Fold	p-value	Fold	p-value	Fold	p-value
Cugbp2	1451154_a_at	-1.20	9.99E-03	-1.21	5.34E-03	-1.13	3.28E-02
Pdlim5	1427475_a_at	-1.23	7.09E-04	-1.14	3.32E-03	-1.17	8.36E-03
Pctk1	1438625_s_at	-1.22	1.83E-02	-1.17	2.74E-02	-1.14	4.30E-02
D530033C11Rik	1447704_s_at	-1.23	7.29E-03	-1.18	2.06E-02	-1.13	2.85E-02
Mum1l1	1455238_at	-1.22	1.12E-02	-1.16	3.90E-03	-1.15	2.23E-02
Tsga14	1434576_at	-1.22	4.49E-02	-1.14	3.84E-02	-1.16	2.89E-02
Car3	1449434_at	-1.19	2.00E-02	-1.18	6.50E-03	-1.15	3.49E-02
Hoxb5	1418415_at	-1.18	2.10E-02	-1.11	2.91E-02	-1.24	1.53E-02
2610030H06Rik	1452607_at	-1.22	2.76E-03	-1.14	2.19E-03	-1.16	2.10E-02
Gpsm1	1436917_s_at	-1.20	6.19E-03	-1.22	6.67E-03	-1.11	2.92E-02
Ung	1425753_a_at	-1.22	1.37E-02	-1.17	2.10E-02	-1.13	3.44E-02
Tulp4	1448548_at	-1.20	5.48E-03	-1.16	7.52E-03	-1.16	4.19E-02
Vamp7	1452007_at	-1.19	1.19E-02	-1.18	1.97E-02	-1.15	2.25E-02
4930453N24Rik	1449718_s_at	-1.18	2.92E-02	-1.16	6.67E-03	-1.17	2.48E-02
Elavl2	1421883_at	-1.17	1.59E-02	-1.16	1.27E-02	-1.19	7.19E-03
Ccdc56	1423840_at	-1.21	2.60E-03	-1.15	6.98E-03	-1.15	4.31E-02
Hoxa9	1455626_at	-1.20	7.28E-03	-1.16	1.22E-02	-1.15	2.53E-02
Recql	1439047_s_at	-1.20	7.12E-03	-1.15	1.82E-02	-1.16	3.60E-02
Ddx31	1438962_s_at	-1.19	4.42E-03	-1.14	3.01E-03	-1.18	1.35E-02
1110004E09Rik	1437682_x_at	-1.12	1.99E-02	-1.22	2.88E-02	-1.15	4.30E-02
Scoc	1430999_a_at	-1.20	4.93E-03	-1.16	7.67E-03	-1.14	1.73E-02
Prpf6	1454789_x_at	-1.20	1.46E-02	-1.15	1.05E-02	-1.14	4.48E-02
Lamb1-1	1424113_at	-1.18	4.18E-02	-1.15	3.83E-02	-1.16	3.67E-02
D16Ert472e	1436125_at	-1.19	7.40E-03	-1.18	1.44E-02	-1.12	4.09E-02
Exoc4	1422685_at	-1.19	5.73E-03	-1.14	3.02E-02	-1.16	3.77E-02
LOC100040608	1435834_at	-1.18	1.83E-02	-1.14	1.54E-02	-1.17	1.91E-02
Kctd6	1428186_at	-1.20	2.90E-04	-1.13	1.36E-03	-1.15	1.64E-02
Tjp2	1434600_at	-1.21	1.72E-02	-1.16	1.82E-02	-1.12	3.85E-02
Pgm2l1	1452841_at	-1.13	2.61E-02	-1.16	1.39E-02	-1.20	6.40E-03
Thg1l	1432393_a_at	-1.14	2.03E-02	-1.17	1.96E-02	-1.17	3.77E-02
6030443O07Rik	1438233_at	-1.17	3.08E-02	-1.15	2.68E-02	-1.16	4.72E-02
Lrba	1449099_at	-1.19	2.91E-02	-1.15	2.12E-03	-1.14	2.81E-02
Vcpip1	1434706_at	-1.18	4.23E-02	-1.16	2.04E-02	-1.14	2.70E-02
Nsg1	1423055_at	-1.19	7.65E-05	-1.15	6.21E-03	-1.14	4.06E-02
4933439C20Rik	1436944_x_at	-1.10	3.86E-03	-1.17	2.81E-03	-1.20	3.26E-03
Tnfrsf1	1448863_a_at	-1.18	2.11E-03	-1.16	1.27E-03	-1.14	5.91E-03
Sdcbp	1450941_at	-1.19	7.39E-03	-1.15	6.22E-03	-1.14	3.50E-02
Ints12	1428985_at	-1.19	1.30E-02	-1.13	1.94E-02	-1.15	3.36E-02
Nipa1	1434864_at	-1.18	1.24E-03	-1.15	1.01E-02	-1.14	4.19E-02
Ddx54	1438853_x_at	-1.20	2.58E-03	-1.16	1.14E-02	-1.11	1.27E-02
Tex10	1434317_s_at	-1.19	1.98E-02	-1.16	3.35E-02	-1.12	2.84E-02
Ugp2	1426461_at	-1.19	2.64E-02	-1.12	1.61E-02	-1.15	3.97E-02
Ndn	1435383_x_at	-1.19	5.33E-03	-1.18	1.16E-03	-1.09	4.75E-02
Itgb5	1456195_x_at	-1.17	1.83E-02	-1.14	2.54E-02	-1.15	2.46E-02
Map2k5	1455941_s_at	-1.18	1.52E-02	-1.11	4.51E-02	-1.18	1.41E-02
Yipf6	1455111_at	-1.17	1.66E-02	-1.13	2.69E-02	-1.16	4.70E-02
Trim8	1418577_at	-1.16	6.37E-03	-1.14	6.34E-03	-1.16	4.90E-02
Lrrc57	1428312_at	-1.18	3.19E-02	-1.12	4.33E-03	-1.16	3.24E-02
LOC100048397	1455349_at	-1.19	2.16E-02	-1.15	1.87E-02	-1.12	4.78E-02
Dhrs4	1419382_a_at	-1.18	2.91E-03	-1.15	2.08E-03	-1.13	3.05E-02
Araf	1428607_at	-1.19	3.17E-02	-1.16	1.40E-02	-1.11	4.91E-02
Rabep2	1440795_x_at	-1.17	7.12E-03	-1.14	3.99E-03	-1.14	1.58E-02
---	1434919_at	-1.15	4.09E-02	-1.14	1.36E-02	-1.16	4.58E-02
Prkar2b	1456475_s_at	-1.17	1.56E-02	-1.17	2.34E-02	-1.12	2.86E-02
Dhrs4	1451559_a_at	-1.16	8.71E-03	-1.15	5.57E-03	-1.14	3.47E-02
2310011J03Rik	1452043_at	-1.17	1.74E-03	-1.14	4.36E-04	-1.14	3.64E-02
4933439C20Rik	1426387_x_at	-1.14	1.22E-02	-1.14	5.77E-03	-1.17	4.44E-02
Mrps23	1421874_a_at	-1.17	4.79E-03	-1.15	3.11E-03	-1.12	2.04E-02
Ror2	1423428_at	-1.19	9.12E-04	-1.15	8.56E-03	-1.11	3.15E-02
Ndn	1437853_x_at	-1.17	2.93E-03	-1.14	6.46E-04	-1.13	2.69E-03
3200002M19Rik	1424328_s_at	-1.15	2.34E-02	-1.16	7.43E-03	-1.13	2.40E-02
Zxdb	1455817_x_at	-1.18	8.06E-03	-1.12	1.50E-02	-1.14	4.66E-02
Cugbp2	1450069_a_at	-1.17	2.93E-02	-1.13	2.95E-02	-1.14	4.61E-02
Klfl	1425860_x_at	-1.17	1.07E-02	-1.13	9.66E-03	-1.14	2.27E-02
Polr3k	1422753_a_at	-1.17	6.69E-03	-1.13	9.76E-03	-1.14	4.63E-02
Kctd3	1455816_a_at	-1.16	4.73E-02	-1.15	2.94E-02	-1.12	5.07E-02

Appendix 2: *Cecr2*^{Gt45Bic} BALB/c versus BALB/c microarrays

Gene	PROBE ID	gcRMA		Arraystar		dCHIP	
		Fold	p-value	Fold	p-value	Fold	p-value
Zfp364	1437009_a_at	-1.18	1.22E-02	-1.15	6.28E-03	-1.11	2.37E-02
Zcchc9	1424557_at	-1.17	9.93E-04	-1.14	3.07E-04	-1.12	1.38E-02
Lmo2	1454086_a_at	-1.16	1.44E-02	-1.13	3.76E-02	-1.14	2.71E-02
4933428G09Rik	1426253_at	-1.12	2.98E-02	-1.17	1.12E-03	-1.14	3.03E-02
---	1460085_at	-1.20	9.12E-03	-1.10	3.58E-03	-1.13	4.72E-02
Ppp2r1b	1428265_at	-1.18	1.03E-03	-1.14	2.71E-03	-1.11	4.41E-03
Ugp2	1434486_x_at	-1.16	8.57E-04	-1.13	1.47E-04	-1.14	9.79E-03
Acyp2	1427943_at	-1.14	3.10E-02	-1.10	2.40E-02	-1.19	1.92E-02
Gmcl1	1417113_at	-1.19	3.58E-04	-1.13	1.39E-03	-1.11	3.03E-02
Dmxl2	1428749_at	-1.15	5.13E-04	-1.13	1.37E-03	-1.14	3.55E-02
Cpsf2	1431089_at	-1.17	1.45E-02	-1.14	2.67E-02	-1.11	2.68E-02
Csnk1g3	1429384_at	-1.17	5.09E-03	-1.15	3.04E-03	-1.10	2.81E-02
Tmed2	1436452_x_at	-1.17	2.14E-02	-1.15	1.28E-02	-1.10	1.12E-02
Rps19bp1	1455174_at	-1.17	6.30E-04	-1.14	1.35E-03	-1.12	8.99E-03
Poldip3	1437837_x_at	-1.14	3.10E-02	-1.17	1.41E-02	-1.11	4.66E-02
Rfc3	1423700_at	-1.17	1.11E-02	-1.14	8.67E-03	-1.11	2.65E-02
Pmvk	1427893_a_at	-1.15	8.31E-03	-1.13	6.14E-03	-1.14	4.86E-02
Pkig	1434820_s_at	-1.18	2.48E-03	-1.15	8.77E-03	-1.09	3.15E-02
1700040I03Rik	1429122_a_at	-1.12	2.77E-02	-1.13	1.05E-03	-1.17	3.07E-02
Smad1	1423956_at	-1.14	4.20E-02	-1.13	2.63E-02	-1.14	1.86E-02
Krt10	1452166_a_at	-1.20	2.03E-03	-1.12	2.79E-04	-1.09	4.27E-02
Tirap	1457676_at	-1.16	2.75E-02	-1.14	8.82E-03	-1.11	3.37E-02
Gins3	1429149_at	-1.15	2.33E-03	-1.11	6.27E-05	-1.16	8.42E-03
Insig2	1417981_at	-1.17	1.77E-02	-1.11	1.35E-02	-1.13	2.74E-02
Rexo4	1434113_a_at	-1.15	5.64E-03	-1.14	5.89E-03	-1.12	1.37E-02
Has2	1449169_at	-1.14	3.87E-03	-1.15	2.00E-03	-1.11	4.95E-02
2310005N01Rik	1432447_a_at	-1.17	9.09E-03	-1.14	2.49E-02	-1.10	4.43E-02
5730494M16Rik	1441960_x_at	-1.13	4.23E-02	-1.13	4.09E-02	-1.14	3.86E-02
Pih1d1	1447750_x_at	-1.18	3.30E-03	-1.15	5.39E-03	-1.07	3.13E-02
Nek3	1418947_at	-1.13	2.13E-02	-1.13	1.20E-02	-1.13	2.25E-02
Eif4e2	1435803_a_at	-1.17	1.98E-02	-1.12	3.08E-02	-1.11	2.55E-02
Eya3	1420933_a_at	-1.17	1.10E-02	-1.12	1.71E-02	-1.11	4.87E-02
Zfand3	1441948_x_at	-1.15	1.98E-02	-1.15	1.49E-02	-1.10	3.14E-02
Ube2i	1422714_at	-1.16	3.91E-02	-1.13	4.13E-02	-1.10	4.87E-02
23100061F22Rik	1439387_x_at	-1.14	3.43E-02	-1.14	1.36E-02	-1.11	4.91E-02
BC052040	1434577_at	-1.15	8.04E-03	-1.13	4.37E-03	-1.11	2.67E-02
Drg1	1434688_x_at	-1.17	1.99E-02	-1.12	1.22E-02	-1.10	2.21E-02
Acpl2	1456735_x_at	-1.13	6.39E-04	-1.15	4.42E-04	-1.11	2.50E-02
Tox4	1416574_at	-1.14	3.30E-02	-1.12	2.45E-02	-1.13	1.63E-02
Ssh1	1455854_a_at	-1.13	3.17E-02	-1.12	1.30E-02	-1.13	3.45E-02
Phf8	1460398_at	-1.16	1.66E-02	-1.11	5.05E-02	-1.12	4.06E-02
LOC100036521	1428603_at	-1.16	1.10E-02	-1.13	2.45E-02	-1.10	4.43E-02
Pfdn5	1415736_at	-1.15	2.86E-02	-1.14	1.16E-02	-1.10	2.69E-02
Mcl1	1456243_x_at	-1.13	1.89E-02	-1.14	1.47E-02	-1.11	2.25E-02
Ugp2	1434485_a_at	-1.15	5.92E-03	-1.13	1.58E-03	-1.10	3.23E-02
Sh3rf1	1455149_at	-1.12	3.02E-02	-1.13	1.55E-02	-1.13	1.24E-02
2610209A20Rik	1423357_at	-1.11	1.49E-02	-1.13	1.17E-03	-1.14	1.29E-02
Vamp7	1426269_at	-1.16	3.99E-03	-1.14	7.13E-03	-1.08	3.28E-02
Zfp289	1439460_a_at	-1.14	1.58E-02	-1.13	1.70E-02	-1.11	1.98E-02
Usp39	1437007_x_at	-1.16	1.30E-02	-1.11	1.82E-02	-1.10	2.20E-02
Smadcb1	1435856_x_at	-1.10	5.53E-03	-1.14	3.58E-03	-1.13	3.04E-02
Stk4	1436015_s_at	-1.14	3.56E-02	-1.12	3.96E-02	-1.11	2.61E-02
9130011J15Rik	1426646_at	-1.14	4.31E-03	-1.14	2.74E-04	-1.09	3.20E-02
Tmed2	1436451_a_at	-1.14	1.40E-02	-1.12	1.06E-02	-1.11	4.21E-02
Parl	1433478_at	-1.15	5.46E-03	-1.12	1.08E-02	-1.10	2.25E-02
Zfp451	1456415_at	-1.12	3.05E-03	-1.12	1.83E-02	-1.13	2.08E-02
Ints8	1431096_at	-1.12	1.45E-02	-1.13	1.43E-02	-1.12	1.14E-02
Gart	1424436_at	-1.16	1.92E-02	-1.11	9.27E-03	-1.10	1.53E-02
Pphln1	1435766_at	-1.15	4.19E-03	-1.11	2.78E-02	-1.11	4.91E-02
Calm2	1422414_a_at	-1.15	1.97E-02	-1.13	2.18E-02	-1.09	3.94E-02
Rfc3	1432538_a_at	-1.14	8.22E-03	-1.13	7.66E-03	-1.10	2.04E-02
Lrwd1	1437194_x_at	-1.15	1.29E-02	-1.12	1.89E-02	-1.10	2.03E-02
Ubl4	1424538_at	-1.15	1.22E-02	-1.12	1.46E-02	-1.10	1.48E-02
Nans	1417773_at	-1.13	1.40E-02	-1.10	1.68E-02	-1.13	1.55E-02
Hspa14	1448586_at	-1.15	1.27E-03	-1.13	1.61E-03	-1.09	5.92E-03
Rbm13	1426426_at	-1.15	2.38E-02	-1.12	2.02E-02	-1.10	2.03E-02

Appendix 2: <i>Cecr2</i> ^{Gt45Bic} BALB/c versus BALB/c microarrays							
Gene	PROBE ID	gcRMA		Arraystar		dCHIP	
		Fold	p-value	Fold	p-value	Fold	p-value
Srpkl	1454042_a_at	-1.13	2.62E-02	-1.11	6.07E-03	-1.12	2.46E-02
Trap1	1437379_x_at	-1.14	1.03E-02	-1.10	2.24E-02	-1.12	2.82E-02
Mrpl48	1437997_x_at	-1.09	3.36E-02	-1.13	2.39E-03	-1.14	3.18E-02
Nexn	1435649_at	-1.09	1.92E-02	-1.12	9.02E-03	-1.15	3.74E-02
Rrs1	1456865_x_at	-1.14	3.74E-02	-1.12	3.05E-02	-1.09	4.16E-02
Crim1	1452253_at	-1.14	2.03E-02	-1.09	2.14E-02	-1.13	2.60E-02
Secisbp2	1428496_at	-1.14	3.13E-02	-1.10	4.35E-02	-1.12	3.62E-02
Serinc5	1433571_at	-1.09	3.55E-02	-1.09	7.60E-03	-1.17	3.13E-02
2410022L05Rik	1420113_s_at	-1.13	1.17E-02	-1.12	1.16E-02	-1.11	2.78E-02
Fchs2	1434260_at	-1.15	1.58E-02	-1.09	3.77E-02	-1.11	4.98E-02
Ipo9	1424466_at	-1.13	1.36E-03	-1.09	1.63E-03	-1.13	3.16E-02
Apip	1418254_at	-1.10	4.95E-02	-1.12	1.35E-04	-1.13	3.26E-02
Bysl	1422767_at	-1.13	8.74E-03	-1.11	3.10E-02	-1.10	3.45E-02
Tmem134	1455752_a_at	-1.16	1.25E-02	-1.08	3.59E-02	-1.11	3.19E-02
2410004B18Rik	1419174_at	-1.13	1.64E-03	-1.12	3.56E-03	-1.09	2.52E-02
Uba5	1435247_at	-1.13	1.55E-02	-1.12	4.70E-03	-1.09	5.07E-02
1110007L15Rik	1428528_at	-1.16	3.19E-02	-1.09	2.96E-02	-1.08	2.95E-02
Nelf	1436959_x_at	-1.13	5.91E-04	-1.11	4.40E-03	-1.10	9.79E-03
Ppp1r7	1448888_at	-1.13	8.46E-03	-1.13	1.48E-02	-1.08	3.43E-02
Pdcd2l	1426845_at	-1.13	1.16E-02	-1.10	2.59E-02	-1.10	4.34E-02
Ssr2	1449930_a_at	-1.15	1.35E-02	-1.12	6.79E-03	-1.07	2.42E-02
Taf11	1451995_at	-1.12	8.49E-03	-1.11	4.40E-02	-1.11	4.31E-02
Enoph1	1437327_x_at	-1.14	2.40E-02	-1.11	2.37E-02	-1.09	3.48E-02
Smardc2	1448400_a_at	-1.12	1.72E-02	-1.11	1.79E-02	-1.10	4.01E-02
Ubl4	1424539_at	-1.13	2.45E-02	-1.10	3.53E-02	-1.10	3.36E-02
Igf2bp3	1453957_a_at	-1.14	3.71E-03	-1.11	5.55E-03	-1.08	4.41E-02
Eif1ad	1428542_at	-1.12	5.25E-03	-1.10	6.65E-03	-1.11	1.21E-02
Impa1	1423127_at	-1.13	1.77E-02	-1.11	2.00E-02	-1.09	4.85E-02
Ap4s1	1451665_a_at	-1.15	5.50E-03	-1.10	6.61E-03	-1.08	4.73E-02
2410001C21Rik	1460362_at	-1.12	3.13E-04	-1.10	2.69E-03	-1.10	2.58E-02
Kcnmb4	1449471_at	-1.08	2.89E-02	-1.05	1.93E-02	-1.19	2.06E-02
Dohh	1417322_at	-1.12	1.06E-03	-1.07	1.06E-02	-1.13	4.72E-02
Lyar	1417511_at	-1.13	4.79E-03	-1.10	3.81E-03	-1.09	1.61E-02
Rce1	1418779_at	-1.12	7.88E-03	-1.07	5.85E-03	-1.12	3.87E-02
Gps1	1415699_a_at	-1.13	8.09E-03	-1.10	1.10E-02	-1.08	2.89E-02
Ppp2r5c	1427003_at	-1.13	1.89E-03	-1.07	2.35E-02	-1.11	4.50E-02
Grk6	1437436_s_at	-1.13	1.41E-02	-1.10	3.74E-02	-1.08	1.80E-02
Mrpl39	1448909_a_at	-1.11	1.20E-02	-1.10	1.08E-02	-1.09	2.16E-02
Slc39a6	1424674_at	-1.13	1.57E-03	-1.12	1.18E-03	-1.06	2.12E-02
Tiparp	1426721_s_at	-1.13	1.90E-03	-1.08	2.73E-03	-1.10	2.86E-02
Gosr1	1416215_at	-1.05	1.60E-02	-1.09	2.33E-02	-1.17	1.82E-02
Rbm14	1456566_x_at	-1.12	3.17E-02	-1.12	2.19E-02	-1.07	2.29E-02
Gdi2	1431645_a_at	-1.13	1.66E-04	-1.09	1.57E-04	-1.08	1.29E-02
Dis3	1426609_at	-1.12	3.82E-03	-1.10	2.07E-02	-1.07	4.28E-02
1110059E24Rik	1416841_at	-1.11	2.03E-02	-1.09	3.23E-02	-1.09	1.80E-02
Wipi2	1428882_at	-1.10	1.99E-04	-1.09	1.05E-04	-1.11	3.24E-02
Tmem161a	1426212_s_at	-1.11	2.43E-03	-1.09	2.61E-03	-1.10	1.57E-02
Uchl3 /// Uchl4	1449855_s_at	-1.12	7.08E-03	-1.11	5.53E-03	-1.06	1.13E-02
5330431N19Rik	1452603_at	-1.10	3.17E-02	-1.09	3.97E-03	-1.10	3.24E-02
Zfp105	1460252_s_at	-1.11	1.39E-02	-1.10	5.29E-03	-1.08	5.00E-02
Katna1	1450949_at	-1.08	2.55E-02	-1.13	1.83E-03	-1.08	2.78E-02
Clptm11	1423730_at	-1.12	1.85E-02	-1.10	3.21E-02	-1.07	2.67E-02
Trip13	1429295_s_at	-1.11	4.26E-02	-1.10	3.44E-02	-1.07	4.48E-02
Ttll1	1436833_x_at	-1.10	8.95E-03	-1.09	1.99E-03	-1.09	3.58E-02
Pgrmc1	1423451_at	-1.11	1.52E-02	-1.10	2.19E-02	-1.08	4.96E-02
Clns1a	1427548_a_at	-1.12	4.40E-04	-1.08	1.42E-02	-1.08	2.27E-02
Prkaca	1447720_x_at	-1.10	1.64E-02	-1.09	6.83E-03	-1.08	4.91E-02
Eif3j	1452052_s_at	-1.10	2.79E-02	-1.09	1.95E-02	-1.08	2.23E-02
Ing1	1416860_s_at	-1.09	4.40E-02	-1.09	2.88E-02	-1.09	4.87E-02
Ergic1	1437908_a_at	-1.08	2.30E-02	-1.09	1.64E-02	-1.09	3.90E-02
Exosc9	1418462_at	-1.11	5.88E-04	-1.09	9.62E-04	-1.06	3.45E-02
Anapc10	1429376_s_at	-1.10	9.19E-03	-1.08	2.00E-02	-1.08	4.83E-02
Rgs19	1417786_a_at	-1.10	1.91E-02	-1.07	3.03E-02	-1.09	3.61E-02
2410022L05Rik	1448971_at	-1.07	3.66E-02	-1.09	1.29E-02	-1.09	2.56E-02
Tmtc4	1428113_at	-1.09	1.69E-02	-1.08	1.56E-02	-1.08	2.18E-02
Hnrnpa1	1423531_a_at	-1.11	8.84E-03	-1.08	2.28E-02	-1.06	1.88E-02

Appendix 2: *Cecr2*^{Gt45Bic} BALB/c versus BALB/c microarrays

Gene	PROBE ID	gcRMA		Arraystar		dCHIP	
		Fold	p-value	Fold	p-value	Fold	p-value
4732418C07Rik	Bud31 1433611_s_at	-1.10	8.07E-03	-1.09	7.73E-03	-1.06	4.44E-02
	1433875_at	-1.08	3.17E-02	-1.05	4.66E-02	-1.11	2.81E-02
	F2r 1437308_s_at	-1.10	4.19E-03	-1.08	3.96E-03	-1.06	2.23E-02
	Med8 1431423_a_at	-1.10	7.58E-03	-1.09	1.28E-02	-1.05	1.79E-02
	Sfrs3 1416150_a_at	-1.09	4.61E-02	-1.08	3.51E-02	-1.07	2.61E-02
	Psmc2 1435859_x_at	-1.10	3.26E-02	-1.08	4.79E-02	-1.06	4.78E-02
	Impdh2 1415851_a_at	-1.12	2.09E-02	-1.07	4.92E-02	-1.05	4.60E-02
	Nmt1 1415683_at	-1.09	1.45E-02	-1.07	3.20E-02	-1.07	2.18E-02
	Snrbp 1437193_s_at	-1.09	5.21E-03	-1.06	1.75E-02	-1.07	3.50E-02
	Psmc6 1437144_x_at	-1.09	1.38E-02	-1.08	1.66E-02	-1.05	2.46E-02
	Pgd 1437380_x_at	-1.07	4.65E-02	-1.09	2.82E-02	-1.06	3.81E-02
	Fbxl10 1459861_s_at	-1.08	2.32E-02	-1.08	6.91E-03	-1.05	4.82E-02
3230401D17Rik	1416856_at	-1.08	7.17E-03	-1.07	1.73E-02	-1.06	3.47E-02
	Bud31 1439466_s_at	-1.08	1.08E-03	-1.08	3.34E-03	-1.05	2.72E-02
	Mrms7 1453725_a_at	-1.06	4.01E-02	-1.07	2.59E-02	-1.07	3.99E-02
	Psmc14 1421751_a_at	-1.08	5.35E-03	-1.06	6.59E-03	-1.04	4.38E-02
	Ahey 1417125_at	-1.07	4.32E-02	-1.06	3.47E-02	-1.05	2.45E-02
	Eif4a3 1417242_at	-1.08	3.51E-03	-1.05	3.88E-02	-1.05	1.87E-02
	Clns1a 1436935_x_at	-1.08	3.56E-03	-1.05	1.40E-02	-1.04	3.32E-02
	Eif4h 1438554_x_at	-1.06	4.16E-02	-1.05	3.14E-02	-1.05	2.72E-02
	Eif2s1 1452662_a_at	-1.06	2.71E-02	-1.05	3.78E-02	-1.05	3.21E-02
	Ppp1cc 1450149_a_at	-1.05	3.64E-02	-1.05	2.33E-02	-1.05	2.26E-02
	App 1427442_a_at	1.07	2.97E-02	1.06	3.88E-02	1.07	4.03E-02
	Bub1b 1447363_s_at	1.06	3.78E-02	1.06	3.92E-02	1.09	3.09E-02
	Ndufb4 1428075_at	1.07	1.85E-02	1.07	1.90E-02	1.09	1.60E-02
	Slc2a3 1437052_s_at	1.09	3.46E-02	1.08	1.61E-02	1.07	2.86E-02
2010109N14Rik	1447896_s_at	1.08	4.39E-02	1.09	3.31E-02	1.10	2.47E-02
	Fth1 1448771_a_at	1.12	1.07E-02	1.09	2.25E-02	1.09	4.77E-02
	Rrm1 1448127_at	1.11	2.12E-02	1.11	1.13E-02	1.10	4.51E-02
	Gpi1 1420997_a_at	1.11	1.36E-02	1.10	1.43E-02	1.10	2.57E-02
	Peg3 1433924_at	1.12	6.83E-03	1.09	2.37E-02	1.10	4.05E-02
2610024B07Rik	1429556_at	1.13	3.39E-03	1.10	1.83E-02	1.10	4.80E-02
	Alg10b 1454917_at	1.09	1.29E-02	1.10	2.77E-02	1.14	4.57E-02
	Add1 1420954_a_at	1.10	3.48E-02	1.08	2.40E-02	1.15	7.50E-03
2310005N03Rik	1428619_at	1.13	4.13E-03	1.10	1.40E-02	1.12	1.34E-02
	Nrtn 1449281_at	1.08	3.19E-02	1.11	4.82E-02	1.17	3.63E-02
	39699 1426801_at	1.12	2.31E-02	1.09	6.24E-03	1.15	8.64E-03
	Belaf1 1428845_at	1.13	8.47E-03	1.10	2.59E-02	1.13	1.53E-02
	Hnrpul1 1451984_at	1.17	2.66E-02	1.10	2.14E-02	1.10	3.62E-02
	Usp34 1434393_at	1.12	5.02E-03	1.11	1.53E-02	1.14	2.29E-02
	Arl13b 1437021_at	1.16	1.68E-02	1.11	1.26E-02	1.15	3.97E-02
	Prkacb 1420611_at	1.15	1.30E-03	1.13	1.19E-03	1.14	4.12E-02
	Podxl 1448688_at	1.14	1.17E-02	1.13	6.42E-03	1.16	4.77E-03
	Cotl1 1425801_x_at	1.12	3.20E-02	1.15	3.99E-03	1.17	3.21E-02
	Igfbp5 1452114_s_at	1.16	2.72E-02	1.14	4.60E-02	1.14	2.38E-02
	Myo5a 1436051_at	1.17	9.62E-03	1.12	3.47E-02	1.15	3.58E-02
	Bmi1 1448733_at	1.18	1.73E-02	1.13	9.47E-03	1.14	3.35E-02
	Jarid2 1422698_s_at	1.15	7.93E-03	1.13	1.60E-02	1.17	1.58E-02
	Bub1b 1416961_at	1.17	3.43E-03	1.13	8.01E-03	1.15	2.47E-02
	Hdac6 1448928_at	1.19	3.53E-03	1.12	9.74E-03	1.15	2.38E-02
1600014C10Rik	1424444_a_at	1.18	2.19E-02	1.08	5.70E-04	1.21	4.54E-02
EG622782	1423071_x_at	1.19	3.18E-02	1.15	4.69E-02	1.14	3.62E-02
LOC100045753	1434478_at	1.19	2.01E-02	1.14	1.29E-02	1.15	1.81E-02
	Bnip3l 1448525_a_at	1.18	4.40E-02	1.14	4.85E-02	1.18	4.24E-02
	Cotl1 1436838_x_at	1.17	4.08E-02	1.17	2.95E-02	1.17	2.60E-02
	Peg3 1417356_at	1.17	3.24E-02	1.15	2.33E-02	1.18	4.60E-02
	Col4a1 1426348_at	1.22	4.08E-03	1.19	5.64E-03	1.10	3.93E-02
	Flna 1426677_at	1.18	1.91E-02	1.15	2.69E-02	1.19	4.73E-02
	Stox2 1429401_at	1.19	9.32E-03	1.17	1.58E-02	1.16	3.64E-02
	Trim68 1455124_at	1.20	2.03E-02	1.10	2.26E-02	1.24	3.57E-02
	Ahnak 1452217_at	1.18	5.51E-03	1.16	1.75E-02	1.22	5.86E-03
	Flywhc1 1426982_at	1.23	3.60E-02	1.17	3.52E-02	1.16	4.72E-02
	Mdm2 1423605_a_at	1.24	6.34E-03	1.14	3.77E-02	1.19	5.05E-02
	Pgm2 1451149_at	1.23	8.88E-03	1.17	5.10E-03	1.18	3.46E-02
	Mil5 1427236_a_at	1.20	3.47E-02	1.17	2.50E-02	1.21	3.52E-02
	Cent1 1419313_at	1.20	2.39E-02	1.16	4.81E-02	1.23	4.58E-02

Appendix 2: *Cecr2*^{Gt45Bic} BALB/c versus BALB/c microarrays

Gene	PROBE ID	gcRMA		Arraystar		dCHIP	
		Fold	p-value	Fold	p-value	Fold	p-value
Foxo1	1416981_at	1.20	2.45E-02	1.17	7.46E-03	1.22	3.80E-02
Myh9	1417472_at	1.26	2.03E-02	1.13	1.57E-02	1.21	3.10E-02
Sox10	1424985_a_at	1.15	4.41E-02	1.19	1.60E-02	1.27	1.13E-02
Zfp248	1436473_at	1.28	2.60E-02	1.16	3.16E-02	1.17	4.11E-02
Pfkfb	1416069_at	1.21	4.32E-02	1.20	1.66E-02	1.21	1.77E-02
Irx5	1421072_at	1.24	2.57E-02	1.17	4.21E-02	1.21	2.37E-02
LOC100047292	1434889_at	1.30	1.32E-02	1.13	3.71E-02	1.20	4.90E-02
Senp1	1451319_at	1.28	2.45E-02	1.15	4.05E-02	1.20	4.93E-02
Atp1a1	1423653_at	1.25	1.18E-02	1.16	2.49E-02	1.22	1.42E-02
---	1459138_at	1.07	4.54E-02	1.17	3.44E-02	1.40	3.43E-02
Baz2a	1438192_s_at	1.22	8.39E-03	1.20	3.34E-03	1.24	4.71E-02
Stom	1438910_a_at	1.34	5.90E-03	1.15	2.37E-02	1.18	3.11E-02
Pdk1	1435836_at	1.28	5.68E-03	1.19	2.51E-02	1.23	1.15E-02
Klf3	1429360_at	1.26	3.40E-02	1.21	1.56E-02	1.24	4.48E-02
Mdm4	1460542_s_at	1.26	9.72E-03	1.23	1.16E-02	1.22	3.51E-02
Cbx5	1454636_at	1.26	2.19E-02	1.23	2.04E-02	1.23	3.45E-02
Foxp4	1429719_at	1.28	2.73E-02	1.18	2.86E-02	1.26	2.02E-02
Foxo1	1416982_at	1.35	4.38E-02	1.19	1.13E-02	1.18	3.88E-02
Nek6	1423596_at	1.27	2.12E-02	1.22	3.60E-02	1.24	3.90E-02
3930401B19Rik	1453238_s_at	1.26	3.96E-02	1.23	2.90E-02	1.25	2.58E-02
Stx3	1434559_at	1.27	5.55E-03	1.18	3.90E-02	1.30	1.49E-02
Bptf	1427310_at	1.28	1.10E-02	1.21	1.91E-02	1.27	1.46E-02
E2f5	1447625_at	1.29	2.90E-02	1.24	2.84E-02	1.23	1.56E-02
Bmi1	1417493_at	1.28	1.77E-02	1.23	1.76E-02	1.26	9.31E-03
Jarid1b	1427143_at	1.30	8.04E-03	1.22	6.39E-03	1.27	2.96E-02
Stox2	1436166_at	1.31	7.41E-03	1.22	5.54E-03	1.27	2.50E-02
B430119L13Rik	1435648_at	1.31	8.29E-04	1.24	1.93E-03	1.25	6.66E-03
Pgrmc2	1428714_at	1.28	1.78E-02	1.22	2.52E-02	1.31	4.84E-02
Col4a1	1452035_at	1.28	1.56E-02	1.24	8.72E-03	1.29	1.73E-03
Rspol	1449319_at	1.34	3.54E-02	1.26	2.66E-02	1.22	4.18E-02
Tug1	1456398_at	1.31	2.95E-02	1.25	3.75E-02	1.26	2.55E-02
Jhdm1d	1427359_at	1.35	6.48E-03	1.20	4.94E-02	1.28	4.29E-02
---	1444971_at	1.27	1.71E-02	1.22	2.49E-02	1.36	3.73E-02
Igflr	1452982_at	1.33	2.37E-02	1.26	2.94E-02	1.27	4.46E-02
Npm3	1423522_at	1.35	8.40E-03	1.19	1.98E-02	1.33	2.74E-02
Sox10	1451689_a_at	1.36	1.16E-02	1.21	7.29E-03	1.29	1.58E-02
Zfp644	1436985_at	1.36	2.05E-02	1.25	3.97E-02	1.26	3.82E-02
Plod2	1416686_at	1.34	1.55E-02	1.25	2.56E-02	1.29	1.59E-02
Ngfr	1454903_at	1.34	8.56E-03	1.27	8.20E-03	1.28	3.05E-02
Zfp608	1442050_at	1.41	9.60E-03	1.23	1.46E-02	1.28	4.22E-02
Rnf11	1452058_a_at	1.37	2.22E-02	1.29	2.62E-02	1.27	4.36E-02
Bnip3	1422470_at	1.35	2.26E-02	1.28	2.58E-02	1.33	3.02E-02
Ahdcl	1424956_at	1.38	6.54E-03	1.28	2.86E-02	1.33	2.31E-02
---	1426061_x_at	1.40	2.06E-02	1.25	4.35E-02	1.35	1.48E-02
Arl4c	1454788_at	1.44	3.30E-03	1.27	1.02E-02	1.33	1.27E-02
---	1457338_at	1.03	5.04E-02	1.17	2.99E-02	1.86	1.99E-02
Itga5	1423267_s_at	1.42	2.05E-02	1.30	1.26E-02	1.36	4.57E-02
Ankrd11	1437633_at	1.47	1.58E-02	1.30	2.02E-02	1.33	2.82E-02
Galnt2	1426756_at	1.46	1.75E-02	1.31	3.30E-02	1.37	2.82E-02
Gpr56	1421118_a_at	1.53	3.39E-02	1.27	1.03E-02	1.35	3.77E-02
Igfbp2	1454159_a_at	1.42	1.06E-03	1.37	1.19E-03	1.37	5.77E-03
Ankrd26	1436071_at	1.45	3.19E-03	1.29	3.53E-03	1.43	3.27E-03
---	1457175_at	1.53	2.41E-02	1.40	1.70E-02	1.31	3.06E-02
Rbm5	1456262_at	1.74	3.97E-02	1.28	1.38E-02	1.36	3.20E-02
Cdca3	1452040_a_at	1.57	7.47E-06	1.45	1.11E-05	1.40	1.38E-03
---	1445008_at	1.59	1.28E-02	1.40	6.74E-03	1.49	3.25E-02
AI467606	1433466_at	1.08	4.89E-02	1.22	2.66E-03	2.20	3.00E-02
Trim62	1452650_at	1.72	1.68E-03	1.46	1.21E-02	1.35	2.25E-02
---	1436637_at	1.72	2.26E-02	1.39	3.11E-02	1.47	2.26E-02
Etnk1	1439972_at	1.63	1.60E-02	1.43	4.45E-02	1.58	4.93E-02
Mdfr	1420713_a_at	1.87	1.52E-03	1.36	5.22E-04	1.59	4.40E-02
---	1458382_a_at	1.90	3.10E-02	1.52	2.71E-02	1.74	2.57E-02
---	1458282_at	1.99	1.54E-02	1.60	3.39E-02	1.61	3.51E-02
Ncapd2	1423847_at	2.32	4.84E-07	2.05	1.23E-06	1.87	5.00E-06

Appendix 3: <i>Cecr2</i> ^{G45Bic} FVB/N versus FVB/N microarrays							
Gene	PROBE ID	gcRMA		Arraystar		dCHIP	
		Fold	p-value	Fold	p-value	Fold	p-value
Cdk5rap1	1448626_at	-30.15	1.78E-07	-10.69	1.05E-07	-25.15	6.70E-05
Cecr2	1431014_at	-13.32	1.58E-05	-7.77	2.87E-05	-7.21	4.00E-06
Cecr2	1457039_at	-12.73	1.00E-08	-4.01	1.34E-06	-4.54	1.00E-06
Ldhb	1434499_a_at	-3.28	1.41E-05	-2.75	1.49E-05	-2.75	3.20E-04
Ldhb	1455235_x_at	-2.97	2.61E-04	-2.56	8.68E-05	-2.17	3.40E-04
2700089E24Rik	1453208_at	-1.79	9.97E-05	-1.63	2.22E-05	-4.02	1.07E-04
Ldhb	1448237_x_at	-2.86	7.13E-04	-2.19	1.66E-04	-2.37	2.72E-04
Prdm8	1455925_at	-2.50	1.47E-02	-1.96	9.74E-04	-2.87	2.57E-03
3110021A11Rik	1430158_at	-3.42	2.19E-03	-2.11	9.95E-04	-1.69	1.11E-02
3110021A11Rik	1445708_x_at	-3.19	2.88E-05	-1.77	5.34E-05	-1.88	4.37E-04
Csn3	1419735_at	-3.31	4.04E-04	-1.76	2.45E-04	-1.64	7.74E-03
Nrk	1450079_at	-2.53	3.88E-02	-2.16	4.32E-02	-1.98	1.12E-02
Anub1l	1429642_at	-2.56	8.73E-05	-2.07	7.00E-04	-1.87	3.15E-03
Ldhb	1416183_a_at	-2.50	2.53E-04	-2.21	1.08E-04	-1.77	4.92E-04
Wnk1	1436746_at	-2.35	2.30E-02	-2.07	2.07E-02	-1.93	2.72E-02
Prkg1	1449876_at	-3.02	6.45E-03	-1.61	3.24E-03	-1.60	2.42E-02
Dnajb14	1430561_at	-2.48	1.71E-04	-1.92	6.02E-04	-1.70	1.29E-02
3110001I20Rik	1456120_at	-2.59	2.84E-02	-1.75	1.88E-02	-1.69	2.38E-02
Crim1	1426951_at	-2.30	4.91E-03	-1.79	1.05E-02	-1.70	1.40E-02
2610507B11Rik	1455905_at	-2.48	1.21E-02	-1.61	4.04E-03	-1.63	4.69E-03
Emp1	1416529_at	-2.09	3.41E-06	-1.85	5.45E-04	-1.77	1.65E-04
Tle1	1422751_at	-2.06	6.36E-03	-1.82	4.84E-03	-1.81	2.10E-02
Cenpf	1458447_at	-2.25	1.70E-02	-1.66	1.17E-02	-1.71	1.77E-02
Gbf1	1438207_at	-2.48	2.44E-02	-1.58	1.83E-02	-1.48	2.90E-02
Foxp2	1438231_at	-2.08	4.78E-03	-1.70	4.31E-03	-1.71	1.01E-02
Elf2	1428045_a_at	-2.51	1.44E-02	-1.53	5.41E-03	-1.45	3.02E-02
Kctd12b	1442368_at	-2.02	3.87E-04	-1.80	1.74E-04	-1.65	8.72E-03
Asxl3	1442095_at	-2.15	3.91E-02	-1.65	2.14E-02	-1.63	2.21E-02
Mtap1b	1450397_at	-2.11	3.15E-02	-1.52	3.85E-02	-1.80	5.03E-02
Gm715	1445503_at	-2.16	1.55E-02	-1.69	1.64E-02	-1.56	1.83E-02
Aldh1a7	1418601_at	-1.84	3.78E-03	-1.68	3.08E-04	-1.88	7.16E-03
Etnk1	1439972_at	-1.96	2.78E-02	-1.63	6.18E-03	-1.77	9.57E-03
Bach1	1449311_at	-1.89	4.79E-02	-1.62	2.92E-02	-1.76	3.57E-02
Mbd4	1449490_at	-2.06	2.10E-03	-1.61	8.21E-05	-1.55	2.00E-03
Peg10	1427550_at	-1.95	7.77E-03	-1.69	1.22E-02	-1.57	1.62E-02
Ankrd11	1437633_at	-1.92	1.56E-02	-1.63	2.50E-02	-1.65	3.07E-02
Chd4	1436343_at	-1.87	9.36E-03	-1.60	1.02E-02	-1.70	7.48E-03
Prrx1	1425526_a_at	-2.08	1.75E-02	-1.58	3.22E-03	-1.50	2.36E-02
---	1446155_at	-1.45	1.04E-02	-1.61	2.74E-04	-2.07	2.97E-02
Wasl	1426777_a_at	-1.90	2.73E-02	-1.57	3.91E-02	-1.66	3.40E-02
Casc5	1438833_at	-1.91	1.61E-02	-1.56	2.98E-02	-1.66	2.55E-02
Alx1	1435022_at	-1.91	1.05E-03	-1.57	9.58E-04	-1.62	1.81E-03
Eif4ebp2	1417084_at	-1.76	9.33E-03	-1.63	5.80E-03	-1.70	2.99E-02
Gsk3b	1437001_at	-1.78	2.39E-02	-1.60	2.78E-02	-1.65	3.49E-02
Tpr	1456112_at	-1.78	1.21E-02	-1.63	1.24E-02	-1.62	1.88E-02
Mia3	1459984_at	-1.88	4.19E-03	-1.66	5.57E-04	-1.44	2.62E-03
Cenpe	1439040_at	-1.83	2.65E-02	-1.64	1.83E-02	-1.51	3.96E-02
Pcdh17	1453070_at	-1.70	1.42E-05	-1.62	8.22E-06	-1.63	5.00E-04
Erdr1	1452406_x_at	-1.74	8.44E-04	-1.62	9.05E-04	-1.58	9.61E-04
Atrx	1420947_at	-1.66	1.62E-02	-1.61	8.73E-03	-1.64	2.52E-02

Appendix 3: <i>Cecr2</i> ^{G45Bic} FVB/N versus FVB/N microarrays							
Gene	PROBE ID	gcRMA		Arraystar		dCHIP	
		Fold	p-value	Fold	p-value	Fold	p-value
Epha4	1456863_at	-1.30	9.63E-03	-1.51	4.61E-03	-2.09	1.54E-02
Pdap1	1434020_at	-1.72	6.67E-03	-1.56	8.86E-03	-1.60	1.19E-02
Bbx	1422741_a_at	-1.76	1.11E-02	-1.50	5.20E-03	-1.62	1.45E-02
Sostdc1	1460250_at	-2.00	4.44E-04	-1.49	6.33E-04	-1.37	2.39E-02
2810474O19Rik	1437110_at	-1.73	3.05E-02	-1.57	3.44E-02	-1.56	3.86E-02
Trove2	1436533_at	-1.69	1.61E-03	-1.66	1.25E-03	-1.50	7.85E-03
Aspm	1441520_at	-1.87	2.38E-02	-1.52	1.13E-02	-1.46	1.18E-02
Luzp1	1448352_at	-1.70	1.21E-02	-1.48	3.25E-02	-1.67	1.03E-02
---	1439200_x_at	-1.69	3.88E-04	-1.53	8.16E-04	-1.63	5.53E-03
Eif2c2	1426366_at	-1.68	4.19E-02	-1.54	4.49E-02	-1.58	4.43E-02
Pip4k2a	1419280_at	-1.76	1.37E-02	-1.52	6.25E-03	-1.52	8.32E-03
Bbx	1425835_a_at	-1.95	1.96E-02	-1.43	8.10E-03	-1.41	1.17E-02
Aldh1a3	1448789_at	-1.81	1.36E-02	-1.47	1.45E-03	-1.50	2.04E-02
A430093A21Rik	1439180_at	-1.72	1.56E-02	-1.44	2.41E-02	-1.62	2.04E-02
Heatr6	1424687_at	-1.87	6.66E-03	-1.46	1.59E-02	-1.44	2.40E-02
Atrx	1450051_at	-1.71	3.07E-02	-1.54	4.32E-02	-1.50	1.47E-02
Csnk2a1	1419038_a_at	-1.66	3.00E-02	-1.54	3.19E-02	-1.54	4.59E-02
Asb4	1423422_at	-1.62	1.39E-02	-1.53	1.19E-02	-1.59	8.16E-03
Col23a1	1429210_at	-1.71	1.87E-02	-1.51	1.39E-02	-1.51	3.73E-02
Bat2d	1429432_at	-1.68	4.25E-02	-1.51	2.29E-02	-1.54	4.64E-02
Ddx6	1439122_at	-1.71	2.58E-02	-1.51	3.46E-02	-1.50	4.59E-02
Ccdc59	1449446_at	-1.56	1.66E-02	-1.59	4.36E-03	-1.56	2.03E-02
---	1427820_at	-1.56	3.76E-02	-1.54	3.89E-02	-1.61	3.01E-02
Fbxo32	1448747_at	-1.89	1.61E-03	-1.40	1.91E-02	-1.41	2.36E-02
Glg1	1417087_at	-1.68	1.86E-02	-1.50	3.69E-02	-1.51	2.64E-02
5830417I10Rik	1430680_a_at	-1.78	2.02E-02	-1.39	4.18E-02	-1.51	3.85E-02
Frk	1426569_a_at	-1.73	2.41E-02	-1.53	3.05E-02	-1.41	3.64E-02
Clip1	1425060_s_at	-1.55	2.56E-03	-1.51	1.63E-03	-1.59	8.57E-03
Nrip1	1418469_at	-1.60	8.16E-03	-1.52	4.20E-03	-1.53	1.39E-02
Pknox1	1450172_at	-1.67	6.53E-03	-1.52	1.44E-03	-1.45	1.64E-02
Nup214	1456503_at	-1.72	1.16E-02	-1.42	1.41E-02	-1.49	2.28E-02
Recql	1436371_at	-1.65	1.62E-02	-1.38	7.56E-03	-1.59	4.80E-03
Sim1	1449967_at	-1.49	2.53E-02	-1.53	1.89E-02	-1.60	1.20E-02
Cand2	1429622_at	-2.02	1.71E-02	-1.40	2.63E-03	-1.20	3.75E-03
Asb4	1433919_at	-1.61	9.82E-03	-1.51	2.06E-02	-1.50	1.42E-02
---	1438059_at	-1.67	3.36E-02	-1.42	7.04E-04	-1.53	2.04E-02
4932438A13Rik	1458401_at	-1.46	3.65E-02	-1.58	4.04E-03	-1.57	1.42E-02
Msi2	1435521_at	-1.47	2.97E-03	-1.58	1.14E-02	-1.56	9.98E-03
Ube2i	1453189_at	-1.69	2.84E-02	-1.43	3.50E-02	-1.49	2.29E-02
Cul5	1452722_a_at	-1.62	1.77E-02	-1.49	1.66E-02	-1.49	2.28E-02
Gatad2b	1425075_at	-1.62	2.23E-02	-1.44	2.04E-02	-1.54	1.60E-02
Smc6	1422910_s_at	-1.57	9.13E-03	-1.51	8.23E-03	-1.51	9.65E-03
Gtf3c1	1438425_at	-1.73	1.75E-02	-1.28	1.02E-02	-1.58	2.13E-03
Six6	1419408_at	-1.63	1.68E-02	-1.41	1.91E-02	-1.55	1.60E-02
Iqgap2	1459894_at	-1.68	1.41E-03	-1.46	9.55E-03	-1.44	9.12E-03
Utx	1445198_at	-1.70	3.06E-02	-1.33	1.10E-02	-1.56	1.17E-02
Sgpp2	1457867_at	-1.74	8.95E-04	-1.41	2.08E-03	-1.43	1.01E-02
Tshz1	1427233_at	-1.59	4.51E-03	-1.51	4.90E-03	-1.48	9.98E-03
Foxa2	1422833_at	-1.60	1.20E-03	-1.48	2.33E-03	-1.50	5.67E-03
Klf6	1427742_a_at	-1.70	1.08E-02	-1.39	1.16E-02	-1.48	1.10E-02

Appendix 3: <i>Cecr2</i> ^{G45Bic} FVB/N versus FVB/N microarrays							
Gene	PROBE ID	gcRMA		Arraystar		dCHIP	
		Fold	p-value	Fold	p-value	Fold	p-value
4930402E16Rik	1434480_at	-1.62	3.55E-03	-1.44	4.30E-03	-1.50	6.42E-03
Xrn1	1450308_a_at	-1.74	1.61E-02	-1.32	2.90E-03	-1.50	1.36E-02
Jarid1a	1452360_a_at	-1.56	5.25E-03	-1.51	4.43E-03	-1.48	1.93E-02
Foxa1	1418496_at	-1.58	1.94E-03	-1.48	3.75E-03	-1.49	2.06E-03
Chd4	1438476_a_at	-1.77	2.22E-02	-1.31	5.10E-03	-1.46	1.70E-02
Neurog1	1438551_at	-1.55	1.31E-02	-1.46	4.46E-03	-1.52	1.32E-02
5133401H06Rik	1428663_at	-1.57	4.92E-04	-1.46	3.43E-03	-1.51	1.74E-02
Prdm2	1453068_at	-1.60	2.82E-03	-1.46	2.25E-03	-1.47	4.49E-03
Rest	1425565_at	-1.63	2.50E-03	-1.44	3.06E-03	-1.45	2.51E-02
Elavl4	1450258_a_at	-1.67	3.26E-02	-1.43	9.68E-03	-1.42	2.33E-02
Gas2l3	1455980_a_at	-1.53	1.33E-04	-1.50	7.92E-04	-1.49	2.87E-03
B430201A12Rik	1455033_at	-1.59	3.27E-03	-1.48	2.27E-03	-1.44	5.75E-03
Baz2b	1440984_at	-1.62	1.22E-02	-1.45	1.64E-02	-1.42	3.13E-02
6430547I21Rik	1455537_at	-1.58	2.71E-02	-1.46	1.47E-02	-1.45	2.64E-02
Cul5	1456102_a_at	-1.52	2.06E-02	-1.46	1.34E-02	-1.50	1.37E-02
Dmrta2	1441107_at	-1.63	4.87E-03	-1.43	3.91E-03	-1.43	1.95E-02
Mbnl3	1442549_at	-1.47	4.28E-02	-1.47	3.55E-02	-1.54	1.43E-02
Cad	1440857_at	-1.65	1.63E-02	-1.37	8.47E-03	-1.46	4.57E-02
Rad23b	1456822_at	-1.77	9.78E-03	-1.27	3.63E-02	-1.44	3.69E-02
Nab1	1417624_at	-1.57	8.05E-06	-1.47	1.46E-05	-1.43	1.81E-03
Nrip1	1449089_at	-1.57	7.27E-03	-1.45	9.16E-03	-1.44	2.01E-02
Smad1	1416081_at	-1.63	2.79E-03	-1.42	3.08E-03	-1.41	7.05E-03
Gsg2	1450886_at	-1.55	1.99E-02	-1.48	2.19E-02	-1.43	3.08E-02
Dcc	1441572_at	-1.36	2.81E-02	-1.41	4.15E-02	-1.67	1.84E-02
Brd4	1424922_a_at	-1.54	1.99E-02	-1.42	2.62E-02	-1.48	2.48E-02
Gas2l3	1437244_at	-1.52	5.11E-04	-1.42	6.30E-04	-1.50	1.54E-03
Elavl4	1428741_at	-1.38	8.21E-03	-1.49	1.74E-03	-1.56	1.75E-02
Anxa1	1448213_at	-1.86	3.33E-04	-1.33	6.31E-04	-1.25	4.13E-02
Elavl4	1452894_at	-1.49	3.18E-03	-1.52	1.28E-02	-1.41	2.34E-02
Rbm25	1425522_at	-1.57	1.74E-02	-1.41	2.48E-02	-1.44	4.77E-02
Sod1	1440222_at	-1.63	1.45E-02	-1.45	5.24E-03	-1.33	4.24E-02
Nipbl	1430309_at	-1.49	3.61E-02	-1.44	2.57E-02	-1.48	3.09E-02
Abcf1	1452236_at	-1.57	3.58E-03	-1.40	7.37E-03	-1.44	1.72E-02
Ddi2 /// Rsc1a1	1429093_at	-1.50	3.73E-02	-1.40	2.19E-02	-1.49	3.82E-02
Gsk3b	1451020_at	-1.55	4.16E-03	-1.40	4.53E-03	-1.43	4.83E-03
Srpk2	1417136_s_at	-1.49	1.23E-02	-1.46	1.53E-02	-1.44	3.50E-02
Bbx	1430820_a_at	-1.53	7.56E-03	-1.47	4.81E-03	-1.39	1.32E-02
Ece1	1434177_at	-1.51	2.26E-02	-1.41	4.11E-03	-1.46	3.26E-02
Cldn8	1449091_at	-1.55	3.70E-04	-1.50	2.09E-04	-1.33	1.01E-02
Tfpi2	1418547_at	-1.33	8.71E-03	-1.51	3.74E-03	-1.54	3.60E-02
Map3k12	1456565_s_at	-1.50	1.30E-02	-1.41	3.09E-03	-1.47	1.58E-02
Cbx4	1419583_at	-1.47	3.13E-04	-1.36	1.38E-03	-1.53	2.60E-03
Il17d	1435714_x_at	-1.50	1.10E-02	-1.29	2.81E-02	-1.56	2.92E-02
Dzip3	1444058_at	-1.49	1.89E-02	-1.45	1.44E-02	-1.41	3.74E-02
Nup188	1442314_at	-1.57	5.09E-03	-1.37	8.76E-03	-1.40	1.03E-02
2700049A03Rik	1437248_at	-1.47	8.27E-03	-1.40	8.49E-03	-1.47	3.08E-02
4631422O05Rik	1428861_at	-1.53	1.70E-03	-1.45	1.66E-03	-1.36	1.60E-02
Prkar1b	1434325_x_at	-1.60	2.02E-02	-1.33	1.24E-03	-1.40	2.92E-02
Dach2	1449823_at	-1.51	7.08E-03	-1.45	2.39E-03	-1.37	4.50E-02
Aspm	1458560_at	-1.49	1.11E-02	-1.45	4.82E-03	-1.39	7.57E-03

Appendix 3: <i>Cecr2</i> ^{Gt45Bic} FVB/N versus FVB/N microarrays							
Gene	PROBE ID	gcRMA		Arraystar		dCHIP	
		Fold	p-value	Fold	p-value	Fold	p-value
Rpo1-4	1460215_at	-1.57	6.67E-04	-1.39	3.05E-03	-1.37	5.27E-03
Eif4g1	1438686_at	-1.53	3.48E-02	-1.41	3.03E-02	-1.38	3.61E-02
Tcfap2b	1423340_at	-1.54	6.71E-04	-1.38	5.20E-04	-1.40	5.37E-03
Golga4	1448803_at	-1.50	2.05E-03	-1.37	5.01E-03	-1.45	2.79E-03
Lpgat1	1424349_a_at	-1.47	4.46E-04	-1.42	8.80E-04	-1.43	1.37E-03
Centg2	1435433_at	-1.56	3.65E-02	-1.41	3.23E-02	-1.34	2.66E-02
Rbm5	1438069_a_at	-1.42	3.96E-02	-1.48	1.36E-02	-1.41	1.71E-02
LOC100044968	1434283_at	-1.56	6.25E-04	-1.35	2.50E-03	-1.40	4.82E-03
Dmn	1457275_at	-1.51	4.46E-02	-1.40	7.81E-03	-1.39	3.54E-02
Ebf1	1416301_a_at	-1.43	1.05E-02	-1.41	1.09E-02	-1.46	3.79E-02
Gclc	1424296_at	-1.51	3.88E-03	-1.40	5.56E-03	-1.38	1.29E-02
Lox12	1452436_at	-1.51	7.44E-03	-1.35	1.30E-02	-1.42	1.30E-02
4930402E16Rik	1459869_x_at	-1.51	3.32E-03	-1.39	5.19E-03	-1.38	1.66E-02
Pax3	1430335_a_at	-1.55	1.29E-02	-1.33	9.21E-03	-1.40	2.52E-02
Setd5	1439515_at	-1.55	6.47E-04	-1.33	1.70E-02	-1.39	8.16E-03
Prrx1	1425528_at	-1.52	3.63E-03	-1.37	3.28E-03	-1.38	4.96E-03
Dmrt3	1440707_at	-1.62	1.90E-02	-1.27	5.73E-03	-1.37	2.21E-02
Cadm1	1417377_at	-1.43	1.08E-03	-1.39	9.25E-04	-1.44	8.73E-04
Trim2	1459860_x_at	-1.46	1.29E-03	-1.41	1.97E-03	-1.39	3.55E-03
Rnf168	1455586_at	-1.50	1.75E-03	-1.39	1.31E-02	-1.36	1.51E-02
Rgs2	1419247_at	-1.50	3.74E-04	-1.41	2.15E-05	-1.34	4.74E-03
Mpz12	1416237_at	-1.71	1.64E-03	-1.24	8.10E-03	-1.30	3.63E-02
Fgf18	1449545_at	-1.46	1.96E-02	-1.31	1.37E-02	-1.48	4.22E-02
Foxp2	1438232_at	-1.54	2.89E-02	-1.30	2.57E-02	-1.40	1.64E-02
---	1436633_at	-1.53	3.01E-03	-1.37	1.86E-03	-1.34	7.70E-03
Wwc2	1417198_at	-1.51	7.29E-04	-1.31	6.22E-03	-1.42	1.42E-02
Sox5	1423500_a_at	-1.49	6.26E-03	-1.33	3.82E-03	-1.42	1.10E-02
Fktn	1446624_at	-1.44	7.87E-03	-1.35	1.43E-02	-1.44	1.01E-02
Qk	1425597_a_at	-1.51	1.78E-02	-1.34	2.09E-03	-1.38	1.63E-02
4921509J17Rik	1429106_at	-1.57	1.07E-02	-1.33	1.32E-02	-1.33	3.31E-02
Galnt3	1417588_at	-1.57	4.55E-03	-1.28	9.26E-03	-1.38	3.11E-02
Tnks	1459910_at	-1.55	2.26E-02	-1.33	4.78E-04	-1.34	1.33E-02
Srpk2	1417135_at	-1.43	1.50E-02	-1.48	2.84E-02	-1.31	3.85E-02
Dgkd	1454655_at	-1.46	5.91E-03	-1.36	1.42E-02	-1.39	4.60E-03
---	1460118_at	-1.55	5.50E-03	-1.39	5.82E-04	-1.27	4.23E-02
Ubn1	1438401_at	-1.48	1.50E-02	-1.37	1.09E-02	-1.36	2.18E-02
Reep3	1424778_at	-1.46	9.13E-03	-1.38	1.08E-02	-1.37	1.22E-02
Wdr51b	1453110_at	-1.51	4.60E-03	-1.35	1.47E-03	-1.35	9.90E-03
Prrx1	1439774_at	-1.41	4.68E-03	-1.45	1.04E-02	-1.35	1.88E-02
Fzd4	1419301_at	-1.51	1.18E-02	-1.34	1.07E-02	-1.36	1.83E-02
Gpd2	1452741_s_at	-1.42	1.69E-03	-1.36	6.63E-03	-1.42	5.01E-03
Mizf	1437757_at	-1.41	3.15E-03	-1.38	1.07E-03	-1.41	1.86E-02
Pknox1	1421233_at	-1.42	3.48E-03	-1.39	1.14E-03	-1.39	9.33E-03
Bcr	1452368_at	-1.58	8.93E-04	-1.29	9.76E-03	-1.33	1.26E-02
Rapgef5	1455840_at	-1.49	1.69E-04	-1.33	1.02E-04	-1.37	4.22E-03
Rnf169	1434208_at	-1.45	2.54E-02	-1.38	1.79E-02	-1.35	2.70E-02
Gabra4	1433707_at	-1.40	2.28E-02	-1.36	1.33E-02	-1.41	4.00E-02
Atf7ip	1449192_at	-1.44	6.66E-03	-1.38	1.87E-02	-1.36	1.04E-02
Ndr1	1423413_at	-1.34	1.67E-02	-1.42	3.88E-05	-1.42	1.71E-02
Sox5	1432189_a_at	-1.45	7.98E-04	-1.31	9.09E-04	-1.41	1.60E-02

Appendix 3: <i>Cecr2</i> ^{Gt45Bic} FVB/N versus FVB/N microarrays							
Gene	PROBE ID	gcRMA		Arraystar		dCHIP	
		Fold	p-value	Fold	p-value	Fold	p-value
Rhou	1449028_at	-1.39	3.19E-04	-1.32	1.07E-03	-1.45	1.39E-03
Kcnk6	1435342_at	-1.65	3.74E-02	-1.27	9.68E-03	-1.22	2.57E-02
Eny2	1429410_at	-1.44	4.88E-03	-1.37	3.53E-03	-1.34	3.25E-02
Ap3s2	1444413_at	-1.57	1.26E-02	-1.22	2.65E-02	-1.35	2.50E-02
Tbl1x	1434643_at	-1.42	2.03E-02	-1.35	2.18E-02	-1.37	3.64E-02
Klf12	1439847_s_at	-1.45	3.55E-02	-1.35	3.19E-02	-1.34	3.30E-02
Baz1b	1450068_at	-1.41	1.62E-02	-1.25	2.10E-02	-1.47	1.97E-02
Spsb1	1420150_at	-1.34	3.52E-02	-1.34	1.47E-02	-1.45	1.95E-02
Alkbh8	1429521_at	-1.42	3.15E-02	-1.36	1.76E-02	-1.34	2.09E-02
Pum1	1456054_a_at	-1.43	3.21E-02	-1.37	4.33E-02	-1.32	4.73E-02
Cpsf6	1437372_at	-1.37	4.22E-02	-1.35	3.24E-02	-1.39	4.82E-02
Ndst1	1422044_at	-1.23	4.79E-02	-1.36	1.11E-02	-1.53	4.08E-02
Rspry1	1424134_at	-1.42	4.26E-03	-1.34	3.12E-03	-1.34	1.69E-02
---	1439609_at	-1.38	5.68E-03	-1.33	4.89E-03	-1.39	1.31E-02
Mbnl2	1436858_at	-1.42	1.46E-03	-1.30	6.77E-04	-1.37	2.09E-03
Cpm	1429413_at	-1.42	4.28E-02	-1.33	2.97E-02	-1.34	3.76E-02
Evi5	1417513_at	-1.41	8.12E-04	-1.32	6.68E-04	-1.36	5.07E-03
BC017647	1424663_at	-1.46	3.77E-03	-1.33	3.79E-03	-1.29	1.53E-02
Ulk2	1417846_at	-1.53	3.24E-02	-1.29	2.56E-02	-1.26	1.70E-02
Zeb2	1422748_at	-1.40	2.37E-02	-1.34	3.71E-02	-1.34	4.82E-02
Slc38a1	1415903_at	-1.42	9.76E-03	-1.31	1.55E-02	-1.35	9.58E-03
Cbx2	1422059_at	-1.54	2.60E-03	-1.27	1.76E-03	-1.26	1.86E-02
Pum1	1423117_at	-1.39	2.31E-02	-1.33	2.47E-02	-1.35	3.60E-02
Rab6	1448304_a_at	-1.38	8.57E-03	-1.32	6.46E-03	-1.35	1.62E-02
Nlk	1419112_at	-1.44	5.94E-03	-1.32	9.04E-03	-1.30	1.07E-02
LOC100044322	1448009_at	-1.53	4.87E-03	-1.31	2.96E-02	-1.22	1.81E-02
Ogdh	1445632_at	-1.58	1.12E-03	-1.22	8.03E-03	-1.26	2.90E-02
Homer2	1424367_a_at	-1.38	1.00E-03	-1.29	1.64E-03	-1.38	6.15E-03
Pdlim5	1422862_at	-1.32	3.67E-02	-1.38	7.95E-03	-1.35	1.89E-02
---	1434025_at	-1.41	1.72E-02	-1.31	4.77E-03	-1.33	4.35E-02
Lman1	1428130_at	-1.41	3.94E-03	-1.30	2.47E-03	-1.34	6.48E-03
Pknox1	1437470_at	-1.47	1.19E-03	-1.35	6.02E-04	-1.23	3.54E-02
BC025076	1451583_a_at	-1.40	4.84E-04	-1.31	2.35E-04	-1.34	9.04E-03
Epha4	1439757_s_at	-1.36	5.94E-03	-1.38	3.23E-03	-1.30	4.63E-03
Pou3f2	1453478_at	-1.30	1.64E-03	-1.40	8.17E-03	-1.33	4.47E-02
Met	1434447_at	-1.36	1.79E-02	-1.35	2.06E-02	-1.32	6.44E-03
Etv6	1434880_at	-1.45	3.24E-04	-1.32	2.46E-04	-1.26	2.52E-02
Bcl2l11	1426334_a_at	-1.38	8.66E-03	-1.34	5.38E-03	-1.31	1.91E-02
Mef2c	1451506_at	-1.37	1.55E-02	-1.27	5.38E-03	-1.39	1.59E-02
Hdlbp	1449615_s_at	-1.41	2.23E-02	-1.30	2.09E-02	-1.32	2.59E-02
Timp2	1433662_s_at	-1.46	1.41E-02	-1.26	3.26E-02	-1.31	3.57E-02
Synj1	1436334_at	-1.41	2.74E-04	-1.28	2.53E-04	-1.33	5.58E-03
Jarid1a	1437106_at	-1.29	5.26E-04	-1.31	2.29E-03	-1.42	1.32E-02
Pkp4	1438677_at	-1.42	2.43E-02	-1.27	4.48E-02	-1.33	3.38E-02
Acbd3	1456316_a_at	-1.40	7.31E-03	-1.30	1.84E-02	-1.32	2.43E-02
Nat8l	1435842_at	-1.39	3.15E-02	-1.26	3.77E-02	-1.36	2.12E-02
Glg1	1448580_at	-1.40	1.43E-03	-1.28	7.58E-04	-1.33	7.70E-03
Sostdc1	1449340_at	-1.45	2.32E-03	-1.23	1.34E-02	-1.33	1.16E-02
Osblp6	1456495_s_at	-1.47	6.24E-03	-1.22	3.24E-02	-1.31	3.98E-02
Zfp318	1425346_at	-1.42	2.16E-02	-1.31	1.66E-02	-1.28	4.14E-02

Appendix 3: <i>Cecr2</i> ^{Gt45Bic} FVB/N versus FVB/N microarrays							
Gene	PROBE ID	gcRMA		Arraystar		dCHIP	
		Fold	p-value	Fold	p-value	Fold	p-value
3321401G04Rik	1428541_at	-1.36	1.28E-02	-1.31	1.77E-02	-1.33	3.93E-02
Zfp644	1436985_at	-1.39	3.65E-02	-1.29	1.76E-02	-1.31	4.78E-02
Atp6v0a2	1449870_a_at	-1.37	3.15E-04	-1.31	8.58E-05	-1.31	1.76E-03
Sltm	1429624_at	-1.36	1.59E-02	-1.31	1.72E-02	-1.32	2.17E-02
Upp1	1448562_at	-1.36	9.13E-04	-1.28	3.96E-03	-1.35	1.20E-03
Pdpk1	1416501_at	-1.38	1.03E-03	-1.31	3.86E-03	-1.30	7.59E-03
Six1	1427277_at	-1.33	8.77E-03	-1.35	3.80E-03	-1.30	1.58E-02
5730508B09Rik	1447100_s_at	-1.26	2.53E-02	-1.30	2.46E-02	-1.42	8.41E-03
Cald1	1424768_at	-1.37	1.16E-02	-1.31	8.05E-03	-1.31	5.45E-03
Trim2	1417029_a_at	-1.38	5.94E-03	-1.29	7.72E-04	-1.31	2.62E-02
Hdlbp	1415988_at	-1.36	3.00E-02	-1.29	2.51E-02	-1.34	1.51E-02
Nol8	1428951_at	-1.35	3.40E-02	-1.30	2.26E-02	-1.33	4.01E-02
Rcor1	1437545_at	-1.37	2.52E-02	-1.29	3.73E-02	-1.33	3.44E-02
1700020I14Rik	1437774_at	-1.39	1.56E-02	-1.30	9.36E-03	-1.30	3.64E-02
Ptar1	1431073_at	-1.34	1.66E-02	-1.29	5.20E-03	-1.35	4.97E-02
Pdgfc	1419123_a_at	-1.36	9.37E-03	-1.31	8.10E-03	-1.31	2.28E-02
Erc1	1451279_at	-1.42	2.88E-03	-1.16	1.73E-02	-1.40	1.84E-02
Cald1	1424770_at	-1.37	1.09E-03	-1.28	2.60E-03	-1.33	8.73E-03
Gm266	1436115_at	-1.39	3.73E-03	-1.30	3.62E-03	-1.28	1.99E-03
Mtdh	1455129_at	-1.37	4.83E-03	-1.31	8.20E-03	-1.30	7.17E-03
Kbtbd11	1435465_at	-1.37	2.61E-02	-1.29	3.29E-02	-1.31	3.63E-02
Cdx1	1449582_at	-1.36	4.10E-02	-1.24	6.67E-03	-1.37	2.28E-02
Ikbkap	1424142_at	-1.38	9.17E-04	-1.26	2.54E-04	-1.33	5.77E-03
Ing1	1448496_a_at	-1.38	1.10E-02	-1.30	2.15E-02	-1.29	1.45E-02
Efnb1	1418285_at	-1.26	3.00E-02	-1.32	1.80E-02	-1.38	6.11E-03
Dnm2	1432004_a_at	-1.37	6.05E-04	-1.32	2.96E-05	-1.27	2.10E-03
Sfrs2ip	1452885_at	-1.38	9.54E-03	-1.28	1.07E-02	-1.30	1.54E-02
Lpgat1	1424350_s_at	-1.36	2.61E-03	-1.26	1.41E-02	-1.33	1.68E-02
Tgs1	1421905_at	-1.33	7.65E-03	-1.27	1.01E-02	-1.35	9.29E-03
AI314180	1456255_at	-1.42	2.31E-02	-1.26	3.55E-03	-1.27	9.77E-03
Klf7	1419356_at	-1.45	3.44E-02	-1.25	3.94E-02	-1.25	4.65E-02
Sumf1	1424603_at	-1.29	3.97E-02	-1.33	1.65E-02	-1.32	3.17E-02
Gap43	1423537_at	-1.36	1.51E-03	-1.27	4.00E-03	-1.32	1.01E-02
Col1a2	1450857_a_at	-1.37	2.37E-02	-1.28	2.89E-02	-1.29	3.58E-02
Mbtps1	1431385_a_at	-1.35	4.04E-02	-1.30	2.94E-02	-1.29	2.77E-02
Brd3	1460328_at	-1.37	1.18E-02	-1.22	2.43E-02	-1.35	2.40E-02
Cpsf2	1420937_at	-1.35	2.05E-03	-1.29	7.29E-03	-1.30	1.04E-02
Keap1	1450747_at	-1.39	7.86E-03	-1.22	1.04E-02	-1.33	1.64E-02
---	1434848_at	-1.31	1.39E-02	-1.32	1.08E-02	-1.30	5.72E-03
Scamp2	1448404_at	-1.34	6.78E-03	-1.26	1.76E-03	-1.33	3.09E-03
Iqgap1	1417379_at	-1.36	1.82E-03	-1.29	2.82E-03	-1.28	5.61E-03
Lypla3	1422341_s_at	-1.44	5.74E-03	-1.19	1.16E-02	-1.29	3.78E-02
Ubx4	1425019_at	-1.35	1.12E-02	-1.26	2.33E-02	-1.31	4.36E-02
Nbeal1	1442027_at	-1.36	8.55E-03	-1.27	1.45E-02	-1.29	1.12E-02
Nefl	1426255_at	-1.37	1.21E-02	-1.25	3.20E-02	-1.30	4.49E-02
Dnaja2	1457233_at	-1.35	2.36E-02	-1.24	2.89E-02	-1.33	1.35E-02
Pard6g	1420851_at	-1.38	7.36E-03	-1.25	1.67E-02	-1.29	1.63E-02
Rab6	1447776_x_at	-1.30	1.61E-03	-1.32	6.87E-03	-1.29	7.91E-03
Dbt	1449118_at	-1.36	3.95E-03	-1.26	1.01E-02	-1.29	1.18E-02
Eif4e3	1417978_at	-1.27	4.98E-04	-1.29	1.74E-02	-1.35	9.40E-03

Appendix 3: <i>Cecr2</i> ^{Gt45Bic} FVB/N versus FVB/N microarrays							
Gene	PROBE ID	gcRMA		Arraystar		dCHIP	
		Fold	p-value	Fold	p-value	Fold	p-value
Dhx36	1424398_at	-1.33	1.76E-02	-1.29	1.43E-02	-1.29	2.17E-02
Ppp2r5e	1452788_at	-1.35	3.52E-03	-1.29	6.16E-03	-1.27	1.03E-02
Dhx29	1439076_at	-1.37	2.81E-03	-1.23	1.13E-03	-1.31	2.27E-02
Cd44	1423760_at	-1.32	1.03E-02	-1.30	5.27E-03	-1.28	4.53E-02
Rdh11	1418760_at	-1.33	4.52E-02	-1.28	3.15E-02	-1.29	2.88E-02
Foxc1	1419485_at	-1.31	1.61E-02	-1.29	2.87E-02	-1.30	4.40E-02
Fndc3b	1452783_at	-1.35	7.10E-03	-1.25	3.30E-03	-1.30	1.36E-02
Ccnd2	1448229_s_at	-1.35	4.62E-02	-1.22	3.98E-02	-1.33	3.91E-02
Zbtb45	1435802_at	-1.41	1.40E-03	-1.23	6.95E-03	-1.25	2.04E-02
Gemin5	1436311_at	-1.35	2.17E-02	-1.25	1.04E-02	-1.30	7.58E-03
Cln5	1429400_at	-1.31	3.61E-03	-1.26	2.88E-03	-1.32	1.48E-03
LOC100046086	1436041_at	-1.34	8.40E-03	-1.29	8.02E-03	-1.26	2.04E-02
Mef2c	1421027_a_at	-1.33	2.40E-02	-1.24	2.58E-02	-1.32	1.83E-02
Bicc1	1441137_at	-1.30	3.84E-04	-1.29	4.34E-03	-1.30	7.17E-03
Ralbp1	1417248_at	-1.36	1.66E-02	-1.27	2.83E-02	-1.26	3.47E-02
Ints5	1417887_at	-1.35	8.64E-03	-1.26	2.35E-02	-1.28	2.74E-02
Iqgap1	1417380_at	-1.31	3.32E-03	-1.29	2.99E-03	-1.29	1.03E-02
Cxxc1	1454106_a_at	-1.33	2.59E-02	-1.26	1.52E-02	-1.30	2.78E-02
Slfn9	1436472_at	-1.32	4.11E-03	-1.29	1.81E-03	-1.27	1.18E-02
---	1459021_at	-1.35	1.77E-02	-1.21	7.81E-04	-1.32	2.08E-02
Eif4g1	1427037_at	-1.34	3.39E-02	-1.26	3.43E-02	-1.27	3.32E-02
Pex11a	1449442_at	-1.43	1.58E-03	-1.24	5.55E-03	-1.21	2.67E-02
Dnajc1	1420500_at	-1.32	4.88E-03	-1.28	8.33E-03	-1.28	1.23E-02
Epm2aip1	1434106_at	-1.32	1.18E-02	-1.25	1.59E-02	-1.31	2.04E-02
Pard3	1436764_at	-1.34	2.29E-03	-1.25	3.39E-03	-1.28	9.53E-03
Wdr51b	1429325_at	-1.35	1.21E-03	-1.24	1.47E-03	-1.28	4.00E-03
Mef2c	1421028_a_at	-1.45	1.60E-02	-1.18	3.22E-02	-1.24	4.74E-02
Atp2b1	1428936_at	-1.30	7.88E-03	-1.28	6.78E-03	-1.29	1.04E-02
Bptf	1427310_at	-1.31	1.57E-02	-1.27	2.34E-02	-1.28	2.01E-02
E130308A19Rik	1438277_at	-1.36	1.61E-02	-1.25	2.51E-02	-1.25	1.85E-02
Pcyt1a	1421957_a_at	-1.37	2.89E-03	-1.24	3.67E-03	-1.25	1.12E-02
Rgs2	1419248_at	-1.31	1.52E-03	-1.27	1.49E-03	-1.27	2.57E-03
Lima1	1450629_at	-1.28	1.03E-02	-1.27	3.49E-03	-1.30	2.09E-03
Sertad2	1417209_at	-1.38	6.20E-04	-1.25	9.49E-03	-1.23	3.08E-02
Herc1	1440437_at	-1.13	2.60E-02	-1.34	7.62E-03	-1.38	3.91E-02
Ncor1	1423201_at	-1.29	3.64E-02	-1.28	4.30E-02	-1.28	2.82E-02
Jak1	1433804_at	-1.29	2.59E-02	-1.27	9.76E-03	-1.29	1.48E-02
Rbm14	1452003_at	-1.33	1.61E-03	-1.26	1.40E-03	-1.26	4.92E-02
Slit2	1424659_at	-1.27	9.95E-04	-1.27	8.11E-03	-1.30	1.39E-02
Eif3c	1415859_at	-1.32	2.14E-03	-1.26	2.10E-03	-1.27	8.15E-03
Sypl	1422882_at	-1.32	2.12E-02	-1.29	1.54E-02	-1.24	4.73E-02
Stat3	1426587_a_at	-1.44	2.40E-03	-1.21	6.56E-03	-1.20	4.43E-02
Laspl	1448207_at	-1.38	3.03E-02	-1.18	4.35E-02	-1.27	3.46E-02
Tm7sf3	1452664_a_at	-1.37	1.46E-02	-1.24	1.43E-02	-1.23	4.41E-02
Sox17	1429177_x_at	-1.31	4.65E-03	-1.27	7.67E-03	-1.26	1.11E-02
Slc25a44	1436909_at	-1.31	1.78E-02	-1.22	4.51E-03	-1.31	8.85E-03
Rnf6	1427899_at	-1.37	9.98E-03	-1.23	1.96E-02	-1.23	1.51E-02
Zfhx3	1453267_at	-1.25	1.43E-02	-1.30	1.61E-02	-1.28	2.98E-02
Ripply3	1420459_at	-1.33	7.25E-03	-1.21	1.15E-02	-1.29	2.95E-02
Smc1a	1417832_at	-1.38	2.87E-02	-1.20	4.11E-02	-1.25	2.83E-02

Appendix 3: <i>Cecr2</i> ^{Gt45Bic} FVB/N versus FVB/N microarrays							
Gene	PROBE ID	gcRMA		Arraystar		dCHIP	
		Fold	p-value	Fold	p-value	Fold	p-value
Zc3h15	1427877_at	-1.30	2.46E-03	-1.26	2.23E-03	-1.27	7.44E-03
Bmp2	1423635_at	-1.30	1.73E-02	-1.29	1.99E-02	-1.23	3.58E-02
Epha4	1421929_at	-1.32	7.96E-03	-1.26	1.86E-03	-1.24	2.66E-02
5830417C01Rik	1451621_at	-1.33	2.54E-03	-1.26	1.73E-03	-1.23	5.25E-03
Pdgfc	1449351_s_at	-1.36	1.62E-02	-1.25	3.00E-02	-1.21	3.10E-02
Flt1	1451756_at	-1.36	4.09E-02	-1.18	2.01E-02	-1.28	3.40E-02
Gm944	1436827_at	-1.28	3.09E-02	-1.27	3.54E-02	-1.26	3.62E-02
Sypl	1435082_at	-1.28	1.30E-02	-1.29	2.44E-03	-1.24	1.59E-02
Trim2	1417028_a_at	-1.29	2.61E-03	-1.24	1.35E-03	-1.27	4.54E-03
Zfhx4	1437556_at	-1.29	9.52E-05	-1.28	1.77E-03	-1.24	3.32E-02
Tagln2	1439407_x_at	-1.30	1.45E-03	-1.24	4.16E-03	-1.26	3.32E-03
Vldlr	1434465_x_at	-1.29	4.54E-02	-1.29	2.36E-02	-1.23	3.08E-02
Vegfc	1419417_at	-1.27	1.40E-02	-1.29	2.29E-02	-1.24	3.88E-02
Fryl	1427199_at	-1.33	4.01E-03	-1.19	1.26E-02	-1.28	1.64E-02
Id2	1453596_at	-1.35	2.00E-02	-1.25	7.55E-03	-1.20	4.86E-02
Sbk1	1423978_at	-1.31	1.10E-02	-1.23	1.55E-02	-1.26	2.52E-02
4631416L12Rik	1429185_at	-1.29	1.10E-03	-1.22	2.72E-03	-1.29	4.26E-03
Cdc42ep3	1450700_at	-1.30	4.59E-03	-1.24	9.70E-03	-1.26	1.68E-02
Bbx	1458602_at	-1.24	1.27E-03	-1.30	9.72E-04	-1.26	1.71E-02
Cbll1	1437203_at	-1.29	1.45E-02	-1.22	1.46E-02	-1.28	1.40E-02
AW061290	1438036_x_at	-1.24	1.11E-02	-1.30	8.22E-03	-1.25	2.18E-02
Sf3b1	1418562_at	-1.30	1.95E-04	-1.25	5.59E-04	-1.24	8.09E-04
Usp1	1423674_at	-1.30	1.28E-02	-1.24	1.56E-02	-1.25	1.82E-02
Sema3a	1449865_at	-1.28	2.05E-02	-1.29	1.57E-02	-1.21	4.32E-02
Auts2	1438680_at	-1.25	8.89E-03	-1.23	1.13E-02	-1.30	3.77E-02
Zc3h13	1445499_at	-1.31	4.24E-02	-1.19	1.28E-02	-1.28	3.00E-02
Rmnd5a	1431068_at	-1.31	2.71E-03	-1.24	1.36E-03	-1.23	3.42E-02
Dlx5	1449863_a_at	-1.27	5.33E-03	-1.23	1.38E-02	-1.28	2.55E-02
Med1	1450402_at	-1.27	3.10E-03	-1.20	3.66E-02	-1.31	2.85E-02
H2-D1	1451683_x_at	-1.31	2.42E-02	-1.23	1.49E-02	-1.23	9.29E-03
E130309F12Rik	1436733_at	-1.24	5.26E-03	-1.31	4.08E-03	-1.23	3.91E-02
Lims1	1418230_a_at	-1.28	1.40E-02	-1.23	1.15E-02	-1.26	8.85E-03
Mphosph9	1438063_at	-1.30	1.95E-02	-1.22	4.18E-02	-1.25	6.39E-03
Il6st	1437303_at	-1.29	2.22E-03	-1.24	3.73E-03	-1.24	4.06E-03
Slitrk5	1429718_at	-1.21	1.03E-02	-1.27	1.93E-02	-1.28	1.55E-02
Thap2	1421177_at	-1.28	3.35E-02	-1.20	3.16E-02	-1.29	4.38E-02
Slc35f2	1429154_at	-1.26	3.54E-02	-1.23	8.41E-03	-1.27	4.39E-02
Nfatc3	1452497_a_at	-1.27	2.82E-02	-1.28	1.23E-02	-1.21	4.37E-02
Zfp148	1449069_at	-1.32	6.77E-04	-1.23	1.47E-03	-1.21	1.76E-02
Baiap211	1424951_at	-1.29	2.70E-04	-1.23	2.90E-04	-1.24	3.81E-03
Rbm9	1418246_at	-1.19	1.88E-02	-1.19	1.09E-02	-1.38	3.50E-02
Zfa /// Zfx	1428047_s_at	-1.23	6.90E-03	-1.26	1.10E-03	-1.26	3.41E-02
Sox7	1416564_at	-1.31	2.84E-02	-1.23	3.03E-02	-1.21	3.08E-02
Ankhd1	1419867_a_at	-1.28	1.51E-03	-1.23	5.46E-03	-1.24	1.22E-02
Csnk1g1	1438246_at	-1.26	4.22E-02	-1.22	2.00E-02	-1.27	1.52E-02
Aebp2	1434080_at	-1.27	3.06E-04	-1.21	2.01E-03	-1.27	1.07E-03
Trim2	1448551_a_at	-1.27	1.77E-03	-1.26	9.73E-04	-1.22	2.71E-03
Rassf8	1452283_at	-1.28	8.38E-03	-1.17	4.36E-02	-1.30	3.25E-03
Dera	1424047_at	-1.27	1.42E-03	-1.24	2.03E-03	-1.24	1.29E-03
Thoc2	1444004_at	-1.28	2.64E-02	-1.22	3.05E-02	-1.24	4.17E-02

Appendix 3: <i>Cecr2</i> ^{G45Bic} FVB/N versus FVB/N microarrays							
Gene	PROBE ID	gcRMA		Arraystar		dCHIP	
		Fold	p-value	Fold	p-value	Fold	p-value
Raet1	1420603_s_at	-1.21	2.98E-02	-1.21	3.75E-02	-1.32	1.06E-02
Tfb2m	1423441_at	-1.28	1.34E-02	-1.22	1.56E-02	-1.24	1.68E-02
Senp1	1451319_at	-1.31	1.20E-02	-1.22	1.39E-02	-1.22	3.91E-02
Arl5b	1437884_at	-1.25	1.24E-02	-1.25	4.46E-03	-1.24	1.41E-02
Flt1	1419300_at	-1.29	5.16E-03	-1.26	1.60E-02	-1.18	1.32E-02
2310047D13Rik	1435076_at	-1.32	2.22E-03	-1.18	2.89E-03	-1.24	1.15E-02
A230046K03Rik	1439450_x_at	-1.27	2.53E-02	-1.24	8.13E-03	-1.22	4.17E-02
March9	1427409_at	-1.30	2.13E-02	-1.12	2.45E-02	-1.31	3.99E-02
Sgtb	1451529_at	-1.31	2.23E-02	-1.21	3.32E-03	-1.22	2.98E-02
Klhl28	1428721_at	-1.31	5.24E-04	-1.22	5.18E-05	-1.20	1.59E-02
Rell1	1452359_at	-1.25	2.88E-03	-1.24	3.31E-04	-1.24	4.88E-03
Hhip	1437933_at	-1.28	3.39E-03	-1.26	1.29E-03	-1.18	1.19E-02
Phip	1443522_s_at	-1.31	4.07E-02	-1.18	3.22E-02	-1.23	4.22E-02
Sfrs18	1453185_at	-1.23	4.25E-02	-1.19	3.29E-02	-1.30	2.08E-02
Cyba	1454268_a_at	-1.25	1.96E-02	-1.22	2.83E-02	-1.25	4.34E-02
Ankrd12	1443867_at	-1.15	2.04E-02	-1.21	2.13E-03	-1.36	1.51E-02
1110057K04Rik	1436519_a_at	-1.27	9.06E-03	-1.23	5.74E-03	-1.22	2.41E-02
Setd8	1426406_at	-1.26	1.16E-02	-1.21	1.48E-02	-1.25	2.26E-02
Bms1	1447679_s_at	-1.27	8.25E-03	-1.22	9.56E-03	-1.23	1.45E-02
Ubx2	1426485_at	-1.28	5.44E-03	-1.22	3.52E-03	-1.22	1.44E-02
Fgd1	1416865_at	-1.28	1.21E-03	-1.24	2.37E-03	-1.20	1.78E-02
Fbxo42	1427071_at	-1.30	5.77E-03	-1.19	4.27E-02	-1.23	2.48E-02
3222402P14Rik	1444612_at	-1.25	3.10E-02	-1.24	1.19E-02	-1.23	4.03E-02
Utx	1427672_a_at	-1.27	2.09E-02	-1.20	2.21E-02	-1.25	2.90E-02
Wwtr1	1437155_a_at	-1.23	2.78E-02	-1.22	1.01E-02	-1.27	3.36E-02
Zdhc2	1452656_at	-1.28	3.10E-02	-1.24	1.37E-02	-1.19	4.89E-02
Ncor1	1423202_a_at	-1.30	3.72E-03	-1.22	3.54E-03	-1.20	2.17E-02
Prdm1	1420425_at	-1.31	3.05E-02	-1.19	1.31E-02	-1.21	4.66E-02
---	1434569_at	-1.28	7.26E-03	-1.20	3.36E-02	-1.23	1.76E-02
Ldb2	1421101_a_at	-1.25	3.01E-02	-1.22	2.42E-02	-1.24	2.24E-02
St3gal5	1460241_a_at	-1.28	3.81E-02	-1.21	2.96E-02	-1.22	4.16E-02
LOC100047693	1421133_at	-1.06	3.71E-02	-1.28	1.49E-02	-1.37	4.54E-02
Etv6	1423401_at	-1.25	1.12E-02	-1.18	1.28E-02	-1.27	1.90E-02
Kif5b	1418431_at	-1.27	1.49E-02	-1.25	1.42E-02	-1.19	9.34E-03
Slc25a30	1450018_s_at	-1.24	3.16E-02	-1.20	1.05E-02	-1.26	1.40E-02
Tspyl3	1433826_at	-1.27	2.68E-02	-1.23	4.05E-03	-1.20	3.16E-02
Purb	1419642_at	-1.27	6.32E-03	-1.20	1.21E-02	-1.23	1.56E-02
Pja2	1424442_a_at	-1.23	2.15E-02	-1.22	1.67E-02	-1.25	3.40E-02
Xpnpep3	1437926_at	-1.26	8.71E-03	-1.23	3.99E-03	-1.20	1.37E-02
Gpd2	1417434_at	-1.26	2.08E-02	-1.22	1.67E-02	-1.22	4.56E-02
Rasgrp3	1438031_at	-1.17	9.40E-03	-1.22	1.33E-02	-1.31	1.60E-02
Atxn2	1419866_s_at	-1.25	1.71E-02	-1.22	1.30E-02	-1.23	1.34E-02
Trp53rk	1444453_at	-1.06	2.54E-02	-1.24	4.24E-03	-1.40	4.19E-02
Smc2	1458479_at	-1.23	4.71E-02	-1.25	8.08E-03	-1.21	2.50E-02
Pon2	1429019_s_at	-1.27	1.38E-02	-1.23	3.32E-02	-1.19	3.36E-02
A930037G23Rik	1454628_at	-1.20	1.08E-02	-1.20	2.04E-02	-1.29	1.88E-02
Smad4	1422485_at	-1.28	2.81E-03	-1.25	1.83E-03	-1.17	9.43E-03
Wac	1451494_at	-1.24	5.19E-03	-1.23	3.36E-03	-1.22	1.25E-02
Pmm2	1431464_a_at	-1.21	1.28E-02	-1.21	3.15E-02	-1.27	7.86E-03
Ube2h	1438971_x_at	-1.26	2.81E-02	-1.22	3.78E-02	-1.20	4.98E-02

Appendix 3: <i>Cecr2</i> ^{Gt45Bic} FVB/N versus FVB/N microarrays							
Gene	PROBE ID	gcRMA		Arraystar		dCHIP	
		Fold	p-value	Fold	p-value	Fold	p-value
Frzb	1416658_at	-1.26	1.37E-03	-1.19	1.34E-02	-1.23	3.78E-02
Ppp2r5e	1428463_a_at	-1.24	2.86E-02	-1.22	2.35E-02	-1.22	2.64E-02
Nek7	1448474_at	-1.25	2.20E-03	-1.21	1.54E-04	-1.23	2.20E-03
Baz1a	1447930_at	-1.27	2.44E-03	-1.19	5.08E-03	-1.23	1.78E-02
Nsd1	1440972_at	-1.23	1.04E-03	-1.25	9.38E-04	-1.20	1.58E-02
Wdr26	1451188_at	-1.25	3.40E-03	-1.21	9.96E-03	-1.22	1.59E-02
LOC100047339	1431004_at	-1.29	3.90E-02	-1.24	2.07E-02	-1.15	4.02E-02
Cited2	1452207_at	-1.24	5.08E-03	-1.22	2.71E-03	-1.22	6.22E-03
Evi1	1438325_at	-1.22	3.48E-02	-1.22	3.42E-02	-1.24	3.10E-02
Sel1l	1430692_a_at	-1.26	1.63E-02	-1.23	1.32E-02	-1.18	1.59E-02
Vgll4	1455992_at	-1.27	6.27E-03	-1.20	2.08E-03	-1.21	3.17E-03
1110014N23Rik	1429834_a_at	-1.24	6.04E-03	-1.23	5.56E-03	-1.21	3.77E-02
Zc3h15	1453684_s_at	-1.23	1.38E-03	-1.21	2.28E-03	-1.23	3.96E-03
Synj1	1436333_a_at	-1.20	3.83E-02	-1.25	1.59E-03	-1.22	2.02E-02
Gas2l1	1434928_at	-1.26	1.88E-02	-1.19	2.77E-02	-1.23	4.81E-02
5730559C18Rik	1436345_at	-1.29	1.49E-02	-1.18	4.07E-03	-1.21	1.83E-02
Pex26	1451393_at	-1.24	2.26E-02	-1.20	1.25E-02	-1.23	2.10E-02
Zcchc6	1441986_at	-1.23	5.04E-02	-1.23	1.78E-02	-1.22	4.24E-02
Zfp292	1449515_at	-1.26	1.11E-02	-1.21	2.95E-03	-1.21	1.96E-02
Ccrn4l	1425837_a_at	-1.27	7.97E-03	-1.21	7.45E-03	-1.20	4.23E-02
Igf2bp2	1437103_at	-1.26	1.55E-02	-1.20	2.30E-02	-1.21	3.99E-02
Topors	1417754_at	-1.22	9.36E-03	-1.21	3.19E-03	-1.24	2.73E-02
1810011O10Rik	1451415_at	-1.19	3.54E-03	-1.22	1.42E-02	-1.26	1.62E-02
Shmt2	1455084_x_at	-1.25	3.55E-02	-1.21	3.62E-02	-1.21	3.85E-02
Sp1	1418180_at	-1.25	1.47E-02	-1.21	2.14E-02	-1.20	3.76E-02
Atp7a	1418774_a_at	-1.21	3.01E-02	-1.23	9.16E-03	-1.23	3.38E-02
Nat12	1431026_at	-1.22	1.52E-02	-1.21	3.11E-02	-1.24	2.36E-02
Plxna2	1453286_at	-1.23	4.12E-02	-1.22	2.05E-02	-1.20	3.76E-02
Arhgap24	1424842_a_at	-1.23	1.71E-02	-1.20	4.26E-03	-1.23	4.45E-02
Mbnl2	1455827_at	-1.25	2.00E-02	-1.22	1.08E-02	-1.18	2.76E-02
Trove2	1436535_at	-1.24	1.34E-02	-1.23	1.10E-03	-1.18	1.68E-02
Sec61a1	1416191_at	-1.27	6.33E-03	-1.16	1.99E-02	-1.21	6.95E-03
Reep3	1424779_at	-1.22	1.57E-02	-1.21	9.40E-03	-1.22	4.17E-02
2610207I05Rik	1455657_at	-1.20	3.16E-02	-1.19	1.76E-02	-1.25	1.67E-02
Ppp1r11	1417060_at	-1.25	4.58E-03	-1.19	1.56E-03	-1.20	1.16E-02
F730014I05Rik	1455756_at	-1.25	1.12E-02	-1.15	2.05E-02	-1.24	4.90E-02
Atp2b1	1428937_at	-1.22	4.80E-03	-1.18	9.07E-03	-1.23	2.73E-03
Opa3	1455131_at	-1.21	2.56E-02	-1.19	1.26E-02	-1.23	2.93E-02
Dgcr2	1435276_a_at	-1.24	9.13E-03	-1.15	4.20E-02	-1.24	2.28E-02
Sgms1	1436499_at	-1.22	6.11E-03	-1.23	3.86E-02	-1.18	2.60E-02
Sel1l	1425187_at	-1.25	1.66E-03	-1.18	3.48E-03	-1.21	7.22E-03
Mllt1	1421060_at	-1.22	1.83E-02	-1.20	8.94E-04	-1.21	4.51E-02
Bicc1	1423484_at	-1.25	4.69E-02	-1.17	2.96E-02	-1.21	4.64E-02
Nol9	1429338_a_at	-1.23	2.76E-02	-1.22	1.60E-02	-1.18	4.01E-02
A930041I02Rik	1456357_at	-1.20	2.50E-02	-1.17	3.27E-02	-1.26	1.99E-02
Kdr	1449379_at	-1.26	8.53E-03	-1.18	7.71E-03	-1.18	7.81E-03
G3bp2	1421323_a_at	-1.25	3.13E-03	-1.23	2.30E-03	-1.15	1.60E-02
Plxna2	1451753_at	-1.23	2.22E-02	-1.17	1.20E-02	-1.23	1.74E-02
Ctdspl	1422510_at	-1.21	2.66E-02	-1.17	3.70E-02	-1.25	8.16E-03
Llgl2	1423938_at	-1.29	3.17E-02	-1.14	2.96E-02	-1.19	2.04E-02

Appendix 3: <i>Cecr2</i> ^{Gt45Bic} FVB/N versus FVB/N microarrays							
Gene	PROBE ID	gcRMA		Arraystar		dCHIP	
		Fold	p-value	Fold	p-value	Fold	p-value
Khdrbs1	1418628_at	-1.20	9.84E-03	-1.16	1.52E-02	-1.25	3.98E-03
Slc39a6	1424675_at	-1.28	4.54E-02	-1.15	5.77E-03	-1.18	4.64E-02
4931406P16Rik	1433994_at	-1.18	2.79E-02	-1.25	2.39E-03	-1.19	1.08E-02
BC062127	1445274_at	-1.21	1.88E-03	-1.21	3.99E-03	-1.19	4.49E-02
4632434I11Rik	1429734_at	-1.23	1.24E-02	-1.18	6.81E-03	-1.20	1.60E-02
Snrk	1425678_a_at	-1.25	2.05E-03	-1.18	1.78E-02	-1.17	1.26E-02
Sf3a2	1455546_s_at	-1.22	4.07E-02	-1.18	3.21E-02	-1.20	4.21E-02
Sec24d	1426972_at	-1.22	1.54E-02	-1.19	4.19E-02	-1.20	1.99E-02
BC003331	1426089_a_at	-1.22	1.02E-03	-1.17	1.44E-03	-1.21	1.11E-02
D15Wsu75e	1460278_a_at	-1.25	3.58E-03	-1.18	8.37E-03	-1.18	3.60E-03
Fndc3b	1433833_at	-1.23	2.06E-02	-1.17	2.09E-02	-1.20	2.81E-02
Dsp	1435494_s_at	-1.22	2.31E-02	-1.20	2.48E-02	-1.18	3.39E-02
Xrn2	1422842_at	-1.23	5.30E-03	-1.18	9.41E-04	-1.19	6.70E-03
Pard3b	1427169_at	-1.10	4.50E-02	-1.24	2.36E-02	-1.26	4.05E-02
Snx24	1428822_a_at	-1.20	1.14E-02	-1.17	1.92E-03	-1.22	1.81E-02
Sbno1	1426559_at	-1.22	1.69E-03	-1.17	1.64E-03	-1.20	1.20E-02
Cops7a	1429078_a_at	-1.21	9.83E-04	-1.17	5.47E-03	-1.21	9.11E-03
Mier3	1460614_at	-1.20	2.67E-02	-1.19	1.56E-02	-1.20	1.56E-02
Hbegf	1418350_at	-1.22	4.75E-02	-1.17	4.38E-03	-1.20	4.08E-02
LOC100044766	1444241_at	-1.23	3.50E-02	-1.15	4.51E-02	-1.21	4.62E-02
Mfsd11	1455487_at	-1.23	1.82E-02	-1.16	2.79E-02	-1.20	3.34E-02
Fem1b	1418323_at	-1.14	2.35E-02	-1.20	1.09E-02	-1.24	1.85E-02
Rbm16	1455310_at	-1.19	2.84E-02	-1.18	8.97E-03	-1.21	2.51E-02
Nr4a2	1450750_a_at	-1.17	3.23E-02	-1.14	3.39E-02	-1.27	4.57E-02
Rfxdc2	1460567_at	-1.20	1.12E-02	-1.18	1.45E-02	-1.20	1.92E-02
Cdc25a	1417131_at	-1.21	1.23E-02	-1.17	8.11E-03	-1.20	2.82E-02
Rpl23	1422859_a_at	-1.21	1.63E-02	-1.20	8.31E-03	-1.17	3.86E-02
Edg2	1448606_at	-1.21	2.37E-02	-1.18	2.52E-02	-1.19	1.75E-02
Rhoj	1418892_at	-1.20	4.59E-02	-1.18	3.47E-02	-1.19	2.80E-02
Zfp445	1427254_at	-1.24	1.20E-02	-1.14	4.29E-02	-1.19	3.65E-02
Ttf1	1426610_a_at	-1.25	6.95E-03	-1.13	6.09E-03	-1.19	2.94E-02
Twistnb	1428634_at	-1.21	1.29E-02	-1.16	8.59E-03	-1.20	2.33E-02
Sdc1	1415944_at	-1.25	8.15E-03	-1.13	3.44E-03	-1.19	2.20E-02
Ankhd1	1448008_at	-1.21	4.91E-02	-1.17	3.81E-02	-1.18	3.97E-02
D11Wsu99e	1449258_at	-1.21	8.06E-04	-1.16	1.73E-03	-1.19	2.27E-03
Dag1	1456131_x_at	-1.23	4.23E-02	-1.15	3.47E-02	-1.18	4.13E-02
Sec61a1	1416190_a_at	-1.19	3.36E-03	-1.16	1.99E-03	-1.21	1.07E-02
Impad1	1437289_at	-1.20	1.28E-02	-1.18	7.07E-03	-1.17	3.60E-02
Tfdp2	1437174_at	-1.25	3.13E-02	-1.12	4.97E-02	-1.18	2.90E-02
Npnt	1452107_s_at	-1.17	1.03E-02	-1.18	1.94E-02	-1.20	3.11E-02
Pcbp2	1435881_at	-1.18	2.75E-02	-1.14	3.11E-02	-1.22	1.83E-02
E2f7	1437187_at	-1.19	1.68E-02	-1.16	1.59E-02	-1.19	2.69E-02
Ripk3	1448449_at	-1.19	3.11E-02	-1.16	4.12E-02	-1.20	2.75E-02
Timp2	1460287_at	-1.21	2.48E-03	-1.14	3.41E-03	-1.20	7.32E-03
Tmem2	1451458_at	-1.20	5.08E-04	-1.17	3.07E-04	-1.17	8.46E-03
Mrpl45	1423492_at	-1.19	1.47E-03	-1.17	3.09E-04	-1.18	6.77E-03
Ctdsp2	1423661_s_at	-1.16	2.22E-02	-1.17	1.69E-02	-1.21	1.88E-02
Slc25a30	1420836_at	-1.21	1.36E-02	-1.15	4.02E-02	-1.17	4.04E-02
Gltpt	1419027_s_at	-1.16	4.92E-03	-1.17	2.22E-02	-1.20	2.77E-03
Med16	1438416_at	-1.22	7.86E-03	-1.14	1.78E-02	-1.17	3.94E-02

Appendix 3: <i>Cecr2</i> ^{Gt45Bic} FVB/N versus FVB/N microarrays							
Gene	PROBE ID	gcRMA		Arraystar		dCHIP	
		Fold	p-value	Fold	p-value	Fold	p-value
Zfp618	1436190_at	-1.10	4.05E-02	-1.16	4.67E-02	-1.27	5.06E-03
Skp2	1460247_a_at	-1.20	1.13E-02	-1.16	1.24E-02	-1.16	2.01E-02
BC046404	1436195_at	-1.16	2.37E-02	-1.17	4.23E-02	-1.20	4.95E-02
Cdv3	1451100_a_at	-1.16	4.62E-03	-1.15	3.52E-02	-1.21	5.14E-03
Larp4	1437177_at	-1.17	1.71E-02	-1.16	1.37E-02	-1.19	8.90E-03
Akap2	1449168_a_at	-1.16	4.00E-03	-1.15	1.86E-02	-1.20	2.30E-02
Igsf3	1431322_at	-1.17	2.34E-03	-1.15	4.49E-03	-1.19	2.00E-02
Gapvd1	1453146_at	-1.20	7.13E-03	-1.16	6.30E-03	-1.15	3.52E-02
Mia3	1455066_s_at	-1.20	1.95E-02	-1.15	3.93E-02	-1.16	4.08E-02
Myo1c	1419649_s_at	-1.22	1.12E-02	-1.13	8.54E-03	-1.16	9.90E-03
---	1460632_at	-1.18	4.32E-03	-1.15	1.49E-03	-1.18	1.43E-02
Papola	1427544_a_at	-1.15	4.19E-02	-1.17	6.74E-03	-1.19	1.08E-02
Epn2	1427225_at	-1.16	5.01E-02	-1.14	1.41E-02	-1.21	2.70E-02
Ctdsp2	1423660_at	-1.17	2.11E-02	-1.12	3.08E-02	-1.22	3.73E-03
Gnai2	1419449_a_at	-1.17	1.15E-02	-1.15	1.29E-02	-1.19	6.38E-03
---	1426049_a_at	-1.20	8.62E-03	-1.11	9.99E-03	-1.20	2.81E-02
Ap3b1	1450915_at	-1.19	6.39E-03	-1.15	6.03E-03	-1.17	3.45E-03
Brd3	1436960_at	-1.18	7.86E-03	-1.15	5.76E-03	-1.17	2.85E-02
Rdh10	1426968_a_at	-1.19	1.06E-03	-1.14	5.64E-04	-1.17	1.67E-03
Dnaje5	1448850_a_at	-1.18	2.10E-02	-1.12	2.76E-02	-1.20	1.72E-02
Pip5k1a	1418144_a_at	-1.20	3.10E-03	-1.16	4.87E-04	-1.14	2.49E-02
LOC100047863	1433455_at	-1.17	1.24E-03	-1.15	3.20E-02	-1.18	2.41E-02
Ppp1r12a	1429487_at	-1.18	8.05E-03	-1.15	9.28E-03	-1.17	2.12E-02
---	1455961_at	-1.16	2.06E-02	-1.16	9.67E-03	-1.18	1.29E-02
Nr6a1	1428825_at	-1.17	1.33E-02	-1.15	1.87E-02	-1.18	2.72E-02
Zfp704	1417849_at	-1.14	2.14E-02	-1.11	3.03E-02	-1.25	7.69E-03
Gtf2h1	1453169_a_at	-1.17	1.40E-02	-1.13	1.37E-02	-1.19	1.27E-02
2310022B05Rik	1428910_at	-1.16	1.65E-02	-1.14	1.56E-02	-1.19	3.75E-02
2310061I04Rik	1434155_a_at	-1.22	2.32E-02	-1.13	4.21E-02	-1.14	4.59E-02
Dag1	1426779_x_at	-1.13	4.37E-02	-1.15	3.44E-02	-1.21	1.21E-02
Dnab4	1451177_at	-1.16	2.74E-02	-1.17	1.73E-02	-1.16	1.97E-02
Gys1	1450196_s_at	-1.14	8.32E-03	-1.14	1.83E-02	-1.21	1.19E-02
Arhgef1	1421164_a_at	-1.17	3.68E-02	-1.13	4.77E-02	-1.19	4.33E-02
Hsd11	1454996_at	-1.20	9.68E-03	-1.15	2.83E-02	-1.14	4.06E-02
Pvrl2	1417703_at	-1.20	7.96E-05	-1.14	1.59E-05	-1.15	3.46E-02
Srp72	1428877_at	-1.17	2.96E-02	-1.15	1.92E-02	-1.17	1.00E-02
Nipal	1434864_at	-1.16	2.57E-02	-1.16	4.36E-02	-1.17	4.46E-02
39515	1428385_at	-1.14	3.06E-02	-1.14	3.66E-02	-1.20	1.73E-02
AI597468	1433897_at	-1.16	4.84E-03	-1.16	6.19E-03	-1.16	5.61E-03
Pphln1	1435766_at	-1.16	2.94E-03	-1.15	8.17E-03	-1.17	6.97E-03
Pax3	1441743_at	-1.15	3.07E-02	-1.14	4.21E-02	-1.19	3.61E-02
Rbx1	1416578_at	-1.18	7.75E-03	-1.15	1.76E-03	-1.15	3.00E-02
Snape2	1436703_x_at	-1.18	3.48E-02	-1.13	3.27E-02	-1.17	4.38E-02
Dsg2	1449740_s_at	-1.16	3.12E-02	-1.15	3.51E-02	-1.17	9.57E-03
Cugbp2	1451154_a_at	-1.19	5.77E-03	-1.14	3.43E-02	-1.15	2.87E-02
Rab14	1419243_at	-1.19	3.21E-02	-1.17	1.04E-02	-1.11	2.48E-02
5930434B04Rik	1435018_at	-1.16	2.55E-03	-1.14	5.52E-03	-1.17	1.71E-02
Wdr32	1438727_at	-1.12	4.88E-02	-1.17	9.36E-03	-1.19	8.05E-03
Topors	1417755_at	-1.17	1.17E-02	-1.13	2.11E-02	-1.17	3.29E-02
Stard4	1429240_at	-1.17	1.12E-02	-1.14	2.06E-02	-1.16	1.26E-02

Appendix 3: <i>Cecr2</i> ^{Gt45Bic} FVB/N versus FVB/N microarrays							
Gene	PROBE ID	gcRMA		Arraystar		dCHIP	
		Fold	p-value	Fold	p-value	Fold	p-value
Agl	1431032_at	-1.17	1.31E-02	-1.16	3.78E-03	-1.15	1.95E-02
Ndn	1455792_x_at	-1.16	5.08E-03	-1.15	4.39E-03	-1.16	1.68E-02
Pa2g4	1423060_at	-1.17	3.45E-03	-1.15	6.82E-03	-1.15	4.47E-03
Leprel1	1436178_at	-1.13	1.46E-04	-1.15	3.79E-03	-1.19	2.18E-02
Arpc2	1437148_at	-1.17	1.03E-02	-1.16	1.37E-02	-1.14	3.03E-02
Plod2	1416687_at	-1.18	2.51E-02	-1.13	3.44E-02	-1.16	2.97E-02
Mak10	1429720_at	-1.18	1.15E-02	-1.16	7.54E-03	-1.13	4.49E-02
Herpud2	1415981_at	-1.12	1.72E-02	-1.21	4.20E-03	-1.13	2.51E-02
Ccdc80	1424186_at	-1.18	4.55E-02	-1.14	4.05E-02	-1.15	4.63E-02
Cnot4	1436645_a_at	-1.16	3.85E-02	-1.16	2.68E-02	-1.14	3.00E-02
Pip4k2a	1419279_at	-1.17	2.82E-02	-1.11	4.92E-02	-1.18	3.07E-02
Mboat5	1423960_at	-1.15	1.17E-02	-1.13	6.75E-03	-1.18	1.15E-02
Cox15	1452146_a_at	-1.15	3.57E-02	-1.14	4.55E-02	-1.16	4.01E-02
Phf20l1	1456871_a_at	-1.18	1.11E-02	-1.11	1.72E-02	-1.16	3.98E-02
Nubp1	1418906_at	-1.16	2.13E-02	-1.13	3.59E-03	-1.15	2.35E-02
Snx9	1423077_at	-1.17	6.14E-03	-1.14	1.26E-02	-1.14	1.43E-02
Cops7a	1423245_at	-1.14	1.92E-02	-1.16	4.49E-03	-1.14	2.31E-02
Dap	1451112_s_at	-1.18	1.30E-02	-1.12	2.87E-02	-1.14	2.97E-02
2810432L12Rik	1423679_at	-1.16	9.46E-03	-1.11	4.37E-02	-1.16	4.27E-02
Gphn	1430038_at	-1.11	3.16E-02	-1.16	3.75E-02	-1.17	2.61E-02
Ogfr	1422512_a_at	-1.14	1.93E-02	-1.15	1.10E-02	-1.14	1.66E-02
Cand2	1429621_at	-1.15	2.88E-02	-1.14	1.54E-02	-1.15	3.87E-02
Kif5b	1418430_at	-1.15	2.74E-02	-1.13	1.73E-02	-1.15	3.58E-02
Tcf3	1434318_a_at	-1.18	3.89E-02	-1.08	3.70E-02	-1.16	4.41E-02
2610206B13Rik	1428498_at	-1.14	1.60E-02	-1.13	1.55E-02	-1.16	6.47E-03
Nus1	1434304_s_at	-1.16	1.27E-02	-1.12	3.42E-02	-1.14	1.39E-02
Wbscr16	1416622_at	-1.19	2.52E-03	-1.12	1.58E-02	-1.11	1.98E-02
2610002M06Rik	1419690_at	-1.14	9.85E-03	-1.13	2.77E-05	-1.15	2.40E-02
Thoc2	1438736_at	-1.15	1.98E-02	-1.13	2.00E-02	-1.14	3.91E-02
Ap1m1	1459832_s_at	-1.16	1.11E-03	-1.13	1.57E-03	-1.12	6.55E-03
Gtlf3b	1417477_at	-1.18	1.90E-02	-1.12	2.43E-02	-1.12	4.86E-02
Lysmd3	1460335_at	-1.11	2.31E-02	-1.13	1.46E-03	-1.18	5.39E-03
Cars	1452394_at	-1.15	2.90E-02	-1.13	2.85E-02	-1.13	1.05E-02
Spire1	1454962_at	-1.15	3.66E-02	-1.12	2.12E-02	-1.14	4.18E-02
Arf2	1438661_a_at	-1.12	2.91E-02	-1.16	1.45E-02	-1.13	3.88E-02
Sap18	1419443_at	-1.14	6.71E-03	-1.13	3.05E-04	-1.14	1.88E-02
Spin1	1460164_at	-1.13	1.73E-02	-1.13	2.29E-02	-1.15	3.43E-02
St3gal5	1449198_a_at	-1.19	6.92E-03	-1.08	3.13E-02	-1.14	4.76E-02
Ckap4	1455019_x_at	-1.14	6.43E-03	-1.11	1.40E-02	-1.15	2.67E-02
Ndn	1435382_at	-1.14	6.59E-03	-1.13	2.34E-02	-1.13	2.62E-02
Nus1	1460563_at	-1.13	2.27E-02	-1.13	3.02E-02	-1.14	3.72E-02
rp9	1418277_at	-1.11	2.20E-02	-1.10	3.53E-02	-1.19	1.54E-02
D10Bwg1364e	1442883_s_at	-1.13	4.35E-03	-1.13	3.36E-04	-1.13	3.36E-02
Cyb5r3	1425329_a_at	-1.14	1.92E-02	-1.12	1.50E-02	-1.13	2.47E-02
Bag4	1449186_at	-1.16	5.84E-05	-1.12	2.45E-03	-1.11	4.10E-02
D10Bwg1364e	1415753_at	-1.13	2.72E-03	-1.12	2.74E-03	-1.14	1.61E-02
0610007L01Rik	1433900_at	-1.14	2.31E-02	-1.12	2.03E-02	-1.12	2.83E-02
Prpf4	1429724_at	-1.16	4.83E-03	-1.11	2.05E-02	-1.11	3.51E-02
Ehd1	1448175_at	-1.12	2.10E-02	-1.11	2.04E-02	-1.14	1.64E-02
Ankrd13a	1460428_at	-1.15	1.18E-02	-1.11	1.36E-02	-1.11	3.22E-02

Appendix 3: <i>Cecr2</i> ^{G45Bic} FVB/N versus FVB/N microarrays							
Gene	PROBE ID	gcRMA		Arraystar		dCHIP	
		Fold	p-value	Fold	p-value	Fold	p-value
Ndn	1435383_x_at	-1.13	1.22E-02	-1.11	1.34E-02	-1.14	2.85E-02
Nubp1	1418905_at	-1.14	1.86E-04	-1.10	2.80E-04	-1.13	1.64E-02
Arhgap28	1434809_at	-1.11	2.64E-02	-1.14	1.55E-02	-1.13	3.36E-02
Lrrc59	1416235_at	-1.14	2.29E-03	-1.12	5.40E-03	-1.12	8.79E-03
Terf2	1455651_at	-1.13	1.71E-02	-1.12	1.91E-02	-1.12	4.87E-02
Esf1	1434942_at	-1.14	1.71E-03	-1.12	5.45E-03	-1.11	2.12E-02
Phf20	1452259_at	-1.12	1.78E-02	-1.11	2.95E-03	-1.13	1.79E-02
Appbp2	1451251_at	-1.13	1.56E-02	-1.11	2.31E-02	-1.12	2.28E-02
Cdc42se1	1428131_a_at	-1.14	1.30E-02	-1.09	4.64E-02	-1.13	1.35E-02
Sfrs12	1427135_at	-1.08	4.17E-02	-1.13	3.49E-02	-1.14	4.10E-02
4933407N01Rik	1451449_at	-1.12	6.90E-03	-1.10	3.30E-02	-1.14	3.35E-02
Vkorc1l1	1429092_at	-1.09	2.37E-02	-1.14	3.14E-02	-1.12	1.18E-02
Arih1	1427188_at	-1.12	1.50E-02	-1.13	9.50E-03	-1.10	2.99E-02
Plp2	1453572_a_at	-1.12	4.04E-02	-1.09	4.26E-02	-1.14	2.29E-02
Tpm3	1427260_a_at	-1.13	1.03E-03	-1.11	4.91E-03	-1.11	4.80E-02
Zcrb1	1428489_at	-1.13	4.49E-03	-1.11	8.22E-03	-1.11	5.01E-02
Ccar1	1436157_at	-1.11	1.64E-02	-1.10	1.12E-02	-1.13	1.19E-02
Gna11	1434254_at	-1.09	5.98E-03	-1.08	2.29E-02	-1.18	1.48E-02
Ide	1423120_at	-1.12	1.61E-02	-1.11	5.74E-03	-1.11	3.23E-02
Ythdf2	1451317_at	-1.12	4.00E-03	-1.11	9.32E-03	-1.11	3.73E-02
Ppp1r7	1417919_at	-1.13	2.69E-02	-1.10	2.75E-02	-1.11	4.33E-02
Gnb1l	1419316_s_at	-1.08	2.53E-02	-1.11	6.59E-03	-1.14	9.31E-03
1700025G04Rik	1455732_at	-1.14	2.01E-02	-1.08	4.67E-02	-1.12	4.71E-02
Ehd1	1416011_x_at	-1.10	9.86E-04	-1.10	5.03E-04	-1.13	1.38E-03
Noc4l	1423827_s_at	-1.12	4.29E-02	-1.09	9.69E-03	-1.13	2.40E-02
Insig2	1417982_at	-1.11	2.28E-02	-1.09	1.45E-02	-1.13	2.74E-02
Prr13	1423686_a_at	-1.10	3.74E-02	-1.10	2.83E-03	-1.13	1.27E-02
Ndn	1437853_x_at	-1.09	3.03E-03	-1.09	4.41E-03	-1.14	4.51E-03
Parl	1433478_at	-1.11	2.75E-02	-1.10	1.71E-02	-1.11	1.32E-02
Ankib1	1429193_at	-1.10	2.52E-02	-1.10	2.71E-02	-1.12	1.70E-02
Zfyve21	1424670_s_at	-1.11	3.09E-02	-1.09	3.76E-02	-1.11	3.12E-02
Ppa2	1424488_a_at	-1.10	5.70E-03	-1.10	1.70E-03	-1.11	7.46E-03
Dnttip1	1417666_at	-1.10	1.66E-03	-1.09	6.17E-04	-1.12	2.38E-02
Bms1	1433636_at	-1.11	2.54E-02	-1.08	2.88E-02	-1.13	2.24E-02
2510003E04Rik	1452874_at	-1.10	1.06E-02	-1.10	5.20E-03	-1.11	3.57E-02
Psen1	1421853_at	-1.12	1.22E-04	-1.07	1.01E-03	-1.12	1.39E-02
---	1435129_at	-1.11	8.22E-03	-1.10	1.25E-02	-1.10	3.77E-02
Mtpn	1420474_at	-1.10	2.74E-02	-1.09	2.27E-02	-1.12	2.56E-02
Atp6v0c	1435732_x_at	-1.10	2.43E-02	-1.10	1.62E-02	-1.11	1.65E-02
Narg1l	1429057_at	-1.09	4.99E-02	-1.11	1.11E-02	-1.11	4.62E-02
Yap1	1416487_a_at	-1.11	1.47E-04	-1.07	3.31E-03	-1.12	2.98E-02
Styx	1421664_a_at	-1.10	3.28E-03	-1.09	1.52E-02	-1.11	6.73E-03
Mgrn1	1454645_at	-1.09	9.49E-03	-1.08	3.22E-02	-1.13	1.86E-02
LOC100040608	1435834_at	-1.07	3.71E-02	-1.11	3.55E-04	-1.12	2.95E-02
Odc1	1427364_a_at	-1.11	4.33E-02	-1.09	3.72E-02	-1.09	2.42E-02
Tor1aip2	1435526_at	-1.11	1.09E-03	-1.10	4.15E-02	-1.08	4.66E-02
Ube2a	1448772_at	-1.10	2.10E-02	-1.10	2.96E-02	-1.09	4.47E-02
Sod2	1448610_a_at	-1.10	3.80E-02	-1.09	1.93E-02	-1.09	2.62E-02
Map3k7	1425795_a_at	-1.11	3.62E-02	-1.07	4.13E-02	-1.10	4.82E-02
Atp6v1c1	1419545_a_at	-1.10	2.91E-02	-1.08	4.27E-02	-1.10	3.13E-02

Appendix 3: <i>Cecr2</i> ^{Gt45Bic} FVB/N versus FVB/N microarrays							
Gene	PROBE ID	gcRMA		Arraystar		dCHIP	
		Fold	p-value	Fold	p-value	Fold	p-value
Donson	1426739_at	-1.09	3.85E-02	-1.08	1.84E-02	-1.11	4.70E-02
Dgcr2	1421810_at	-1.10	1.95E-02	-1.07	3.58E-02	-1.11	1.71E-02
Gorasp2	1460460_a_at	-1.09	3.40E-03	-1.09	5.97E-03	-1.09	1.86E-02
3110001A13Rik	1416892_s_at	-1.10	5.24E-04	-1.08	5.62E-03	-1.09	1.63E-02
Fkbp1a	1416036_at	-1.09	2.90E-02	-1.07	4.19E-02	-1.11	3.21E-02
Sdc1	1415943_at	-1.09	1.09E-02	-1.07	8.01E-03	-1.10	2.27E-02
Rab7	1415734_at	-1.11	1.51E-02	-1.08	1.71E-02	-1.08	4.21E-02
Lrrc59	1416234_at	-1.09	1.53E-02	-1.07	8.22E-03	-1.10	2.80E-02
Rpo1-3	1459657_s_at	-1.09	1.47E-02	-1.08	6.87E-03	-1.09	3.94E-02
Rab34	1416590_a_at	-1.08	4.33E-02	-1.08	4.61E-02	-1.10	2.66E-02
Pccb	1450969_at	-1.10	6.21E-06	-1.07	2.00E-02	-1.08	3.05E-02
Ubap1	1450893_a_at	-1.09	4.45E-04	-1.07	2.19E-03	-1.09	4.65E-02
Psmc7	1451056_at	-1.09	9.14E-03	-1.07	1.96E-03	-1.09	3.36E-02
Tmem41a	1424191_a_at	-1.08	3.75E-03	-1.06	3.73E-02	-1.11	1.55E-02
Txndc17	1423035_s_at	-1.09	2.10E-02	-1.07	2.56E-02	-1.09	4.87E-02
Calr	1417606_a_at	-1.10	5.03E-03	-1.07	1.51E-02	-1.08	1.90E-02
P2ry5	1428615_at	-1.09	2.15E-02	-1.07	2.07E-02	-1.08	1.71E-02
Chuc1	1425455_a_at	-1.06	7.30E-03	-1.09	6.22E-04	-1.08	2.27E-02
Map1lc3b	1415928_a_at	-1.07	7.09E-03	-1.06	5.02E-02	-1.09	8.70E-03
BC043118	1434410_at	-1.03	4.61E-02	-1.07	2.52E-02	-1.13	4.01E-02
Rpo1-3	1447320_x_at	-1.06	1.10E-02	-1.08	6.90E-03	-1.08	1.87E-02
Eif4e2	1421985_a_at	-1.07	3.05E-02	-1.07	1.38E-02	-1.08	1.07E-02
Srpr	1423670_a_at	-1.07	2.48E-02	-1.04	4.31E-02	-1.10	1.35E-02
LOC100043257	1422660_at	-1.08	1.88E-02	-1.07	8.68E-03	-1.06	1.49E-02
Gorasp2	1424710_a_at	-1.07	2.42E-02	-1.05	2.16E-02	-1.09	2.17E-02
Sar1a	1423720_a_at	-1.07	3.90E-02	-1.06	6.29E-03	-1.08	3.85E-02
Map2k1	1416351_at	-1.07	6.16E-03	-1.06	8.18E-03	-1.08	1.70E-02
Rfwd2	1426912_at	-1.06	4.82E-03	-1.06	3.28E-02	-1.07	4.85E-02
Cox4i1	1448322_a_at	-1.06	2.45E-02	-1.06	2.25E-02	-1.06	4.70E-02
Ube2l3	1448879_at	-1.06	9.21E-03	-1.05	1.87E-02	-1.06	1.07E-02
Phb	1417053_at	1.08	4.51E-03	1.06	4.34E-02	1.06	3.69E-02
Bola2	1434544_at	1.07	3.09E-02	1.08	5.98E-03	1.08	2.68E-02
Xpo7	1415682_at	1.09	1.67E-02	1.06	1.10E-02	1.08	4.34E-02
Pfdn5	1460637_s_at	1.09	1.45E-02	1.06	5.02E-02	1.08	1.81E-02
Bsg	1456616_a_at	1.09	9.69E-03	1.08	6.61E-04	1.07	2.69E-02
Osgp	1418529_at	1.10	3.54E-02	1.09	9.72E-03	1.07	4.49E-02
Mrpl11	1417918_at	1.10	4.23E-02	1.08	2.75E-02	1.08	4.84E-02
Kars	1416068_at	1.10	1.81E-02	1.09	2.38E-02	1.07	2.89E-02
Rrm1	1415878_at	1.11	1.00E-02	1.09	1.01E-02	1.06	4.92E-02
Cdc27	1454739_at	1.12	5.73E-03	1.09	2.44E-02	1.06	2.44E-02
Sfrs3	1454993_a_at	1.11	1.73E-02	1.10	8.59E-03	1.06	3.94E-02
C330023M02Rik	1439027_at	1.13	7.38E-03	1.10	2.89E-03	1.06	2.91E-02
Mgea5	1422902_s_at	1.12	5.41E-03	1.09	9.46E-03	1.09	3.49E-02
Uqcrh	1453229_s_at	1.13	1.82E-02	1.09	2.96E-02	1.08	4.62E-02
Ndufa7	1436567_a_at	1.11	1.60E-02	1.09	1.84E-02	1.10	5.73E-03
Phip	1429004_at	1.12	1.39E-03	1.10	3.18E-04	1.09	2.85E-02
Txndc10	1419925_s_at	1.14	2.94E-03	1.10	2.06E-03	1.08	4.71E-02
Pfdn4	1454888_at	1.13	9.85E-03	1.11	8.63E-03	1.09	3.27E-02
Commd2	1433594_at	1.12	3.79E-03	1.10	3.11E-02	1.11	2.96E-02
Ppp1cb	1433540_x_at	1.14	5.32E-03	1.12	1.76E-03	1.08	1.36E-02

Appendix 3: <i>Cecr2</i> ^{G45Bic} FVB/N versus FVB/N microarrays							
Gene	PROBE ID	gcRMA		Arraystar		dCHIP	
		Fold	p-value	Fold	p-value	Fold	p-value
Rnaseh2c	1417427_at	1.13	8.33E-03	1.10	1.39E-02	1.11	5.03E-02
Supt16h	1419741_at	1.13	4.67E-03	1.12	5.74E-03	1.10	1.28E-02
Prpf38a	1433565_at	1.14	2.86E-02	1.11	2.13E-02	1.10	3.00E-02
Ogt	1425516_at	1.12	7.95E-04	1.14	4.84E-04	1.09	3.02E-02
Sephs1	1433974_at	1.14	3.62E-03	1.10	1.07E-02	1.11	3.15E-02
Timm8a1	1416346_at	1.15	1.90E-03	1.11	5.01E-03	1.10	4.67E-02
Eif4e	1450908_at	1.14	4.95E-03	1.10	7.34E-03	1.12	1.14E-02
Acp6	1448445_at	1.13	3.16E-02	1.10	1.69E-02	1.13	3.38E-02
AI848100	1460573_at	1.15	3.73E-03	1.11	3.52E-02	1.10	3.56E-02
Usp1	1423675_at	1.15	1.17E-02	1.11	1.39E-02	1.11	2.00E-02
1110005A23Rik	1456626_a_at	1.15	7.86E-03	1.12	2.02E-02	1.11	6.34E-03
Rps4y2	1452730_at	1.14	2.95E-02	1.12	4.31E-02	1.12	5.03E-02
Mcts2	1451058_at	1.15	3.30E-02	1.12	1.12E-02	1.13	1.34E-02
Mphosph10	1429080_at	1.18	5.19E-03	1.13	4.71E-03	1.08	1.64E-02
Nol5a	1426533_at	1.16	1.28E-03	1.12	1.82E-04	1.11	2.32E-03
Aasdhppt	1428756_at	1.16	1.52E-02	1.13	1.48E-02	1.11	5.01E-02
Anapc1	1434443_at	1.18	1.96E-03	1.12	5.30E-03	1.10	2.88E-02
---	1434294_at	1.16	1.23E-02	1.14	2.76E-02	1.11	1.65E-02
Thoc2	1437634_at	1.14	3.46E-02	1.14	1.08E-02	1.13	4.10E-02
Eef1e1	1449044_at	1.19	8.07E-03	1.15	9.34E-03	1.07	2.39E-02
Atp5j2	1416269_at	1.16	9.49E-05	1.13	4.93E-04	1.12	2.40E-03
Csdel	1423997_at	1.18	1.67E-03	1.16	5.55E-03	1.08	2.55E-02
Mak10	1460544_at	1.17	5.19E-03	1.11	6.90E-03	1.14	4.28E-02
2610029I01Rik	1428897_at	1.19	1.91E-02	1.14	3.65E-02	1.10	5.01E-02
Rraga	1428905_at	1.19	1.34E-03	1.11	3.03E-02	1.13	3.62E-02
Ywhaz	1448219_a_at	1.15	1.74E-03	1.16	1.19E-03	1.12	1.38E-02
Snhg1	1433675_at	1.16	1.08E-02	1.13	2.73E-02	1.14	9.10E-03
Kdelc1	1450422_a_at	1.18	2.37E-02	1.13	3.42E-02	1.13	3.67E-02
Nola3	1423211_at	1.18	7.10E-04	1.14	7.27E-04	1.12	1.78E-02
Idh1	1422433_s_at	1.18	3.62E-03	1.14	3.93E-03	1.12	1.47E-02
Tomm7	1434732_x_at	1.18	3.44E-02	1.14	3.34E-02	1.13	3.67E-02
Snhg1	1433674_a_at	1.18	2.19E-03	1.15	4.19E-03	1.12	1.58E-02
Hnrnpa2b1	1433830_at	1.18	8.32E-04	1.15	1.75E-03	1.12	1.59E-02
---	1447881_x_at	1.11	2.36E-02	1.23	1.87E-02	1.13	1.57E-02
Pten	1450655_at	1.17	1.69E-03	1.14	8.93E-04	1.15	1.80E-02
Khdrbs3	1453317_a_at	1.21	1.06E-03	1.13	2.65E-03	1.13	1.15E-02
Ywhaz	1416102_at	1.18	8.91E-04	1.15	4.76E-03	1.14	2.64E-02
Coro1c	1449660_s_at	1.18	1.44E-02	1.15	3.04E-02	1.14	3.55E-02
Pnrc2	1416187_s_at	1.20	2.34E-03	1.15	1.12E-03	1.13	4.29E-03
Wdr1	1423054_at	1.21	1.93E-03	1.12	4.89E-03	1.15	1.51E-02
Depdc1a	1424292_at	1.19	2.85E-03	1.15	4.28E-03	1.14	2.89E-02
Gtf2h3	1454092_a_at	1.20	1.11E-02	1.14	1.60E-02	1.15	5.04E-02
Ivns1abp	1425718_a_at	1.21	8.69E-04	1.17	5.18E-04	1.12	2.46E-02
Mdm4	1460542_s_at	1.22	1.99E-02	1.16	2.40E-02	1.15	1.67E-02
Gtpbp10	1436543_at	1.22	2.00E-02	1.16	4.73E-02	1.16	4.88E-02
Ppp1r12a	1437734_at	1.23	8.44E-04	1.15	9.88E-03	1.15	6.61E-03
Nmr1l	1430530_s_at	1.22	3.27E-02	1.17	3.43E-02	1.15	4.76E-02
Trpm7	1431355_s_at	1.27	9.58E-04	1.13	4.27E-02	1.14	3.91E-02
Thumpd1	1436007_a_at	1.17	1.20E-03	1.20	2.59E-05	1.17	9.98E-03
Sin3a	1419101_at	1.24	6.16E-03	1.15	2.05E-02	1.15	3.12E-02

Appendix 3: <i>Cecr2</i> ^{G45Bic} FVB/N versus FVB/N microarrays							
Gene	PROBE ID	gcRMA		Arraystar		dCHIP	
		Fold	p-value	Fold	p-value	Fold	p-value
Glo1	1424109_at	1.22	4.49E-03	1.15	1.95E-02	1.17	1.59E-02
Gatad2a	1445239_at	1.21	1.52E-02	1.15	1.12E-02	1.21	4.13E-02
Cmas	1426662_at	1.25	5.59E-05	1.20	1.61E-04	1.13	1.79E-02
---	1446510_at	1.24	3.24E-03	1.16	1.01E-02	1.18	1.13E-02
EG666684	1428301_at	1.21	2.34E-02	1.20	1.08E-02	1.17	5.00E-02
Tera	1448126_at	1.26	7.05E-03	1.24	8.63E-03	1.08	3.97E-02
Mapk8	1437045_at	1.23	1.71E-04	1.18	9.04E-05	1.18	4.51E-03
Trpm7	1416800_at	1.23	2.15E-02	1.16	2.95E-02	1.21	1.40E-02
Mtm1	1454904_at	1.24	1.43E-03	1.20	1.50E-03	1.16	6.99E-03
D130023J23Rik	1440985_at	1.30	4.11E-02	1.14	5.89E-03	1.16	3.17E-02
Rfc1	1449050_at	1.24	3.81E-03	1.19	3.21E-03	1.17	2.39E-02
Bmi1	1417493_at	1.24	9.96E-05	1.20	3.16E-04	1.17	2.08E-03
Narg1	1418022_at	1.25	7.37E-04	1.22	1.57E-03	1.15	6.87E-03
---	1440579_at	1.24	1.48E-02	1.18	1.60E-02	1.20	2.70E-02
Bmi1	1448733_at	1.26	2.30E-04	1.20	1.18E-03	1.17	6.59E-03
---	1446440_at	1.10	4.68E-02	1.20	9.21E-04	1.33	3.93E-02
C030046I01Rik	1433931_at	1.31	1.11E-02	1.15	2.78E-02	1.18	1.70E-02
Peg3	1417356_at	1.25	4.13E-03	1.21	5.68E-03	1.18	2.16E-02
EG666684	1452731_x_at	1.26	5.17E-03	1.21	1.27E-02	1.17	4.77E-02
C030043A13Rik	1454532_at	1.26	1.40E-04	1.18	3.29E-04	1.22	2.82E-02
---	1458525_at	1.16	1.70E-02	1.22	6.93E-03	1.28	6.23E-03
Ints6	1443128_at	1.29	4.10E-02	1.19	1.89E-02	1.19	2.88E-02
Serpinh1	1450843_a_at	1.27	1.15E-02	1.21	1.48E-02	1.19	2.07E-02
---	1442473_at	1.27	3.67E-02	1.15	1.56E-02	1.25	4.91E-02
Cfl1	1448346_at	1.28	9.64E-03	1.23	2.07E-02	1.17	2.76E-02
Sfrs1	1430982_at	1.27	4.82E-03	1.21	6.17E-03	1.21	1.54E-02
Sms	1428699_at	1.32	2.84E-02	1.21	1.27E-02	1.17	5.03E-02
Mtm1	1434278_at	1.30	1.09E-03	1.23	9.29E-04	1.18	1.08E-02
---	1446022_at	1.16	3.46E-02	1.22	2.81E-02	1.32	2.03E-02
Pbx1	1440037_at	1.28	1.94E-02	1.21	1.41E-02	1.22	2.04E-02
BB070754	1439705_at	1.20	4.14E-02	1.31	2.34E-03	1.21	3.83E-02
Tm7sf3	1428098_a_at	1.32	4.14E-04	1.17	3.67E-03	1.24	2.34E-02
---	1446192_at	1.16	9.57E-04	1.24	8.81E-03	1.33	4.19E-02
---	1441240_at	1.09	4.05E-02	1.14	8.43E-03	1.50	2.74E-02
---	1457842_at	1.29	8.45E-03	1.21	1.53E-02	1.24	3.21E-02
Ilf2	1417949_at	1.30	9.98E-03	1.20	8.23E-03	1.24	1.02E-02
Ogt	1451738_at	1.33	5.05E-03	1.22	1.02E-02	1.20	2.38E-02
AU022855	1458814_at	1.22	1.10E-02	1.19	6.01E-03	1.35	1.62E-02
Tgs1	1439710_at	1.30	1.07E-04	1.22	3.14E-04	1.24	1.84E-02
Stard3nl	1430274_a_at	1.33	7.33E-03	1.22	6.32E-03	1.21	4.83E-02
Tmem48	1424173_at	1.32	7.49E-03	1.22	1.57E-02	1.23	3.32E-02
---	1439305_at	1.33	7.78E-04	1.23	2.31E-03	1.21	3.28E-02
Gspt1	1446550_at	1.35	3.44E-03	1.23	1.26E-02	1.19	2.94E-02
---	1459360_at	1.29	1.85E-03	1.25	1.48E-02	1.23	4.69E-02
C630016I17Rik	1446298_at	1.21	2.70E-02	1.28	1.52E-02	1.29	4.01E-02
Ndufa4	1424085_at	1.31	5.09E-03	1.26	6.87E-03	1.22	1.22E-02
---	1457489_at	1.31	6.20E-03	1.25	2.09E-02	1.22	3.53E-02
---	1447312_at	1.26	1.56E-02	1.30	1.90E-02	1.23	4.19E-02
---	1444459_at	1.33	6.25E-03	1.22	3.49E-03	1.26	4.65E-02
D130007H15Rik	1447567_at	1.33	3.70E-02	1.28	2.27E-02	1.22	5.05E-02

Appendix 3: <i>Cecr2</i> ^{Gt45Bic} FVB/N versus FVB/N microarrays							
Gene	PROBE ID	gcRMA		Arraystar		dCHIP	
		Fold	p-value	Fold	p-value	Fold	p-value
Psmb2	1448262_at	1.33	4.30E-04	1.23	1.84E-04	1.26	1.57E-03
---	1442056_at	1.27	1.42E-02	1.25	2.52E-02	1.32	1.07E-02
---	1447034_at	1.41	1.14E-03	1.25	2.20E-02	1.20	3.23E-02
Myl9	1452670_at	1.35	1.75E-02	1.27	2.22E-02	1.25	1.96E-02
---	1441155_at	1.39	1.27E-03	1.24	3.61E-03	1.24	2.10E-02
8030494B02Rik	1440604_at	1.37	5.15E-03	1.27	8.50E-04	1.23	3.08E-02
Rtn4	1435284_at	1.35	6.98E-03	1.24	3.76E-02	1.28	1.61E-02
---	1446722_at	1.27	1.68E-02	1.27	9.77E-03	1.34	4.00E-02
4933426K21Rik	1435532_at	1.34	3.05E-03	1.25	3.79E-02	1.30	2.69E-02
Evl	1440885_at	1.48	2.21E-06	1.20	4.59E-03	1.22	1.50E-02
Tcf12	1439209_at	1.35	1.30E-02	1.23	2.24E-02	1.32	5.20E-03
Ankrd26	1436071_at	1.36	1.03E-04	1.27	1.11E-03	1.27	5.16E-03
AU041474	1440277_at	1.32	6.42E-03	1.21	6.17E-03	1.37	4.52E-03
Mbtd1	1441100_at	1.35	1.19E-02	1.28	4.62E-03	1.28	3.75E-02
9930031P18Rik	1443088_at	1.37	1.94E-02	1.26	1.14E-02	1.28	3.74E-02
Calm3	1426710_at	1.39	9.15E-03	1.27	1.48E-02	1.25	4.26E-02
D430033H22Rik	1442111_at	1.16	2.08E-02	1.31	3.04E-03	1.44	9.20E-03
---	1452402_at	1.36	5.76E-03	1.29	1.28E-02	1.27	7.96E-03
Pfn1	1449018_at	1.36	1.31E-02	1.29	1.72E-02	1.27	2.36E-02
Wac	1437426_at	1.47	1.06E-03	1.26	4.96E-03	1.19	1.58E-02
8430419L09Rik	1420630_at	1.40	2.09E-02	1.17	4.14E-02	1.36	3.46E-02
---	1438259_at	1.38	5.44E-03	1.28	1.27E-02	1.28	3.32E-03
---	1446921_at	1.35	3.30E-03	1.28	1.65E-03	1.30	3.47E-03
---	1446815_at	1.47	7.84E-04	1.26	1.68E-02	1.21	4.72E-02
---	1446892_at	1.12	4.47E-02	1.24	4.84E-04	1.59	3.46E-02
---	1458575_at	1.30	1.70E-02	1.25	5.82E-05	1.40	7.17E-03
---	1458629_at	1.17	1.06E-02	1.21	1.28E-02	1.58	2.28E-02
B230213L16Rik	1446443_at	1.46	1.01E-02	1.24	1.01E-02	1.26	3.13E-02
---	1444043_at	1.40	3.42E-03	1.28	3.03E-03	1.29	1.37E-02
Hip2	1443148_at	1.31	3.97E-03	1.30	9.11E-03	1.36	9.93E-03
---	1456808_at	1.25	4.85E-02	1.32	5.21E-03	1.41	4.68E-02
Hs2st1	1440905_at	1.39	2.20E-02	1.32	1.38E-02	1.27	2.38E-02
---	1446621_at	1.53	5.89E-04	1.20	6.51E-03	1.26	2.46E-02
---	1440935_at	1.46	4.91E-03	1.26	3.29E-03	1.27	7.92E-03
Rere	1439159_at	1.40	3.71E-03	1.32	2.09E-03	1.29	3.27E-02
8430406H22Rik	1431158_at	1.36	9.83E-03	1.29	6.78E-03	1.36	1.44E-02
Gpc6	1441438_at	1.44	2.39E-02	1.27	4.78E-02	1.31	4.40E-02
---	1443926_at	1.44	4.90E-03	1.29	8.28E-03	1.29	1.62E-02
Hmgb2l1	1453291_at	1.40	1.56E-02	1.32	8.17E-03	1.30	4.20E-02
9030607L02Rik	1432978_at	1.32	2.05E-02	1.35	7.49E-03	1.36	4.02E-02
---	1441230_at	1.33	5.09E-03	1.36	1.65E-03	1.34	5.24E-03
Recql	1418339_at	1.40	1.88E-04	1.32	1.75E-04	1.32	3.75E-04
Aebp2	1437743_at	1.37	4.83E-03	1.26	1.32E-02	1.41	1.04E-02
C78692	1446288_at	1.44	1.14E-02	1.23	7.72E-03	1.39	2.16E-02
---	1446240_at	1.25	5.50E-03	1.43	2.85E-03	1.38	1.89E-02
---	1458241_at	1.41	8.89E-03	1.25	1.57E-02	1.40	1.14E-02
---	1444349_at	1.41	1.80E-03	1.34	1.56E-02	1.31	1.72E-02
---	1459957_at	1.50	3.28E-04	1.33	1.32E-03	1.24	3.53E-02
2010012C16Rik	1450943_at	1.42	8.03E-04	1.33	1.15E-03	1.33	6.36E-04
---	1440954_at	1.31	3.69E-02	1.35	2.22E-02	1.42	2.95E-02

Appendix 3: <i>Cecr2</i> ^{Gt45Bic} FVB/N versus FVB/N microarrays							
Gene	PROBE ID	gcRMA		Arraystar		dCHIP	
		Fold	p-value	Fold	p-value	Fold	p-value
A130064L14Rik	1444343_at	1.45	1.45E-02	1.33	7.41E-04	1.31	8.77E-03
4631423B10Rik	1440028_at	1.52	8.07E-03	1.23	1.65E-03	1.35	2.12E-02
---	1442181_at	1.47	1.41E-03	1.30	4.17E-04	1.33	2.93E-02
Lpp	1425673_at	1.55	1.69E-02	1.27	5.77E-03	1.29	3.55E-02
9530006C21Rik	1441779_at	1.44	1.31E-02	1.34	2.40E-02	1.33	2.03E-02
Cblb	1458469_at	1.52	3.57E-03	1.29	6.69E-03	1.30	1.64E-02
---	1439572_at	1.49	3.82E-04	1.34	1.28E-02	1.28	4.45E-02
---	1441482_at	1.49	7.71E-03	1.35	1.88E-02	1.28	4.35E-02
Btbd7	1432910_at	1.57	6.08E-03	1.26	8.33E-03	1.29	8.31E-03
---	1447240_at	1.52	6.13E-04	1.30	1.14E-03	1.31	1.21E-02
---	1441556_at	1.51	4.78E-04	1.30	5.94E-03	1.32	4.53E-03
C130015C19	1457464_at	1.53	7.97E-04	1.30	3.02E-03	1.31	2.54E-02
---	1438353_at	1.52	3.59E-03	1.38	3.08E-03	1.24	3.29E-02
---	1441404_at	1.49	2.04E-03	1.31	1.96E-02	1.34	2.07E-02
---	1458586_at	1.49	1.17E-03	1.39	1.61E-02	1.27	2.51E-02
D5Wsu152e	1438788_at	1.51	2.17E-02	1.32	1.73E-02	1.32	4.40E-02
---	1458290_at	1.58	5.45E-03	1.28	3.82E-05	1.29	1.64E-02
5830469G19Rik	1430089_at	1.56	2.80E-04	1.30	2.34E-03	1.30	5.72E-03
---	1445512_at	1.43	1.02E-02	1.46	3.82E-03	1.27	4.69E-02
---	1440011_at	1.38	1.13E-02	1.38	1.31E-03	1.40	1.49E-02
Tm7sf3	1438504_x_at	1.61	1.97E-04	1.30	5.52E-04	1.26	1.12E-02
Meg3	1436713_s_at	1.44	6.81E-05	1.35	1.32E-04	1.38	7.46E-04
2610028L16Rik	1460474_at	1.46	4.11E-03	1.38	1.75E-03	1.33	7.47E-03
LOC553096	1442320_at	1.51	2.50E-02	1.30	5.32E-03	1.37	4.18E-02
Myl3	1428266_at	1.46	2.65E-02	1.35	1.12E-02	1.36	2.75E-02
D3Ertd343e	1442656_at	1.45	1.30E-03	1.39	7.54E-04	1.33	3.03E-02
---	1458432_at	1.44	3.54E-03	1.38	2.15E-02	1.36	3.32E-02
---	1445933_at	1.69	2.28E-02	1.26	8.29E-03	1.23	3.44E-02
---	1439993_at	1.51	1.38E-02	1.30	2.37E-02	1.37	1.35E-02
---	1447147_at	1.55	3.34E-03	1.28	3.24E-03	1.36	1.16E-02
---	1440107_at	1.55	3.33E-02	1.35	1.88E-02	1.30	3.50E-02
9930017N22Rik	1456758_at	1.49	2.12E-03	1.34	5.63E-03	1.37	2.14E-02
Recql	1425798_a_at	1.49	6.91E-04	1.36	6.09E-05	1.35	1.82E-02
Pcdhga12	1458721_at	1.41	4.73E-04	1.36	5.81E-03	1.44	2.99E-02
Tle4	1430384_at	1.57	1.18E-02	1.36	1.47E-02	1.29	2.41E-02
Schip1	1437700_at	1.56	1.50E-02	1.32	4.30E-02	1.35	4.54E-02
Cxcl12	1448823_at	1.60	2.04E-04	1.32	2.85E-03	1.30	1.90E-02
9030411K21Rik	1429846_at	1.45	1.10E-02	1.37	8.18E-03	1.42	2.94E-02
Ephb2	1454022_at	1.49	5.61E-03	1.32	2.29E-03	1.42	1.64E-02
A130022J21Rik	1444764_at	1.62	6.67E-04	1.33	1.80E-02	1.29	3.16E-02
Mab21l2	1418934_at	1.53	8.14E-03	1.39	8.19E-03	1.33	2.12E-02
---	1447951_at	1.60	6.88E-04	1.32	1.98E-02	1.33	2.05E-02
Eps15	1430152_at	1.77	1.63E-03	1.23	1.86E-02	1.25	2.56E-02
D13Ertd666e	1440292_at	1.46	1.14E-04	1.41	4.81E-04	1.39	1.20E-02
Saps3	1439161_at	1.52	5.45E-03	1.40	4.87E-03	1.35	2.26E-02
---	1443201_at	1.60	9.32E-03	1.33	4.97E-03	1.33	1.05E-02
---	1457559_at	1.55	7.94E-04	1.40	3.06E-04	1.31	7.15E-03
---	1445697_at	1.58	4.35E-04	1.41	1.69E-02	1.32	4.34E-02
C130068B02Rik	1440317_at	1.54	1.77E-03	1.35	6.14E-04	1.42	4.97E-03
---	1442163_at	1.72	1.13E-02	1.35	2.72E-03	1.25	4.17E-02

Appendix 3: <i>Cecr2</i> ^{Gt45Bic} FVB/N versus FVB/N microarrays							
Gene	PROBE ID	gcRMA		Arraystar		dCHIP	
		Fold	p-value	Fold	p-value	Fold	p-value
2900011L18Rik	1432757_at	1.68	4.40E-02	1.30	4.58E-02	1.35	2.60E-02
AA415038	1457111_at	1.59	2.03E-02	1.35	8.64E-03	1.39	4.12E-02
Rbm6	1440223_at	1.66	3.34E-04	1.33	1.17E-03	1.36	1.47E-03
---	1445966_at	1.58	6.31E-04	1.33	5.75E-04	1.44	4.49E-03
---	1436933_at	1.65	4.57E-02	1.33	5.28E-03	1.37	2.26E-02
Cutl1	1437431_at	1.71	3.55E-03	1.30	4.36E-03	1.35	1.06E-02
Ctnna1	1436631_at	1.63	4.86E-03	1.39	5.37E-03	1.33	3.94E-02
---	1442535_at	1.55	3.19E-03	1.43	1.40E-03	1.38	1.68E-02
Meis2	1440091_at	1.55	2.72E-02	1.39	4.03E-02	1.43	4.96E-02
6430537K16Rik	1438878_at	1.60	1.61E-02	1.41	2.36E-02	1.37	3.80E-02
---	1441718_at	1.59	2.22E-02	1.47	6.26E-03	1.34	4.34E-02
Cspp1	1440219_at	1.66	5.14E-03	1.39	2.57E-03	1.35	1.15E-02
---	1444788_x_at	1.76	2.05E-03	1.36	4.24E-03	1.29	4.79E-02
---	1456453_at	1.72	5.55E-04	1.27	9.15E-04	1.41	2.01E-02
A730062M13Rik	1446810_at	1.53	3.59E-03	1.43	4.88E-03	1.46	3.93E-02
A430102J17Rik	1438895_at	1.63	7.26E-04	1.41	2.63E-03	1.39	4.45E-03
---	1440637_at	1.66	3.60E-02	1.36	1.50E-02	1.43	1.82E-02
---	1439915_at	1.60	2.02E-02	1.44	1.85E-02	1.42	4.54E-02
Rabgap1	1443535_at	1.70	6.96E-04	1.38	1.25E-05	1.38	1.09E-02
---	1458161_at	1.68	3.52E-04	1.40	8.04E-04	1.38	6.72E-03
---	1444787_at	1.77	1.28E-03	1.32	4.86E-03	1.37	1.89E-02
Cdca3	1452040_a_at	1.62	1.68E-05	1.48	7.63E-05	1.37	6.50E-05
---	1444345_at	1.63	8.28E-05	1.42	2.15E-05	1.41	6.00E-03
---	1457781_at	1.58	3.41E-04	1.46	6.74E-04	1.43	9.03E-03
---	1448018_at	1.61	7.73E-03	1.47	3.61E-04	1.41	1.01E-02
---	1441020_at	1.70	3.41E-04	1.44	2.14E-04	1.35	2.63E-03
---	1441505_at	1.65	4.71E-03	1.44	1.91E-03	1.40	1.07E-02
---	1440078_at	1.68	5.43E-05	1.39	7.80E-05	1.43	1.07E-02
---	1457356_at	1.66	5.28E-06	1.41	1.71E-04	1.45	8.09E-04
---	1459442_at	1.67	4.61E-03	1.44	1.97E-03	1.41	1.69E-02
---	1439136_at	1.64	5.42E-04	1.47	2.68E-03	1.42	2.98E-02
---	1444269_at	1.79	3.98E-02	1.40	1.72E-02	1.34	3.55E-02
A730059M13Rik	1443114_at	1.67	7.71E-03	1.48	1.05E-02	1.38	4.73E-02
---	1446497_at	1.61	5.05E-03	1.48	8.12E-03	1.45	3.95E-02
Atp2a2	1443551_at	1.63	4.29E-02	1.36	5.84E-03	1.55	2.13E-02
---	1441663_at	1.77	7.55E-03	1.25	4.13E-02	1.53	3.57E-02
---	1440690_at	1.59	1.28E-02	1.41	2.55E-02	1.56	4.54E-02
---	1446223_at	1.52	1.48E-02	1.52	4.71E-03	1.52	3.30E-02
---	1443533_at	1.56	7.14E-03	1.47	1.50E-02	1.54	3.29E-02
---	1444333_at	1.69	1.09E-03	1.48	9.18E-03	1.40	1.56E-02
---	1446345_at	1.84	1.74E-03	1.40	1.21E-03	1.34	2.59E-02
---	1457479_at	1.80	7.18E-04	1.43	1.11E-03	1.36	1.52E-02
---	1444130_at	1.73	1.87E-03	1.45	5.03E-03	1.41	2.11E-02
---	1458099_at	1.75	5.68E-03	1.26	3.84E-02	1.58	3.81E-02
Rad18	1443954_at	1.66	4.94E-03	1.47	3.55E-03	1.47	1.88E-02
---	1443649_at	1.66	2.01E-03	1.49	1.94E-03	1.45	3.29E-03
---	1444258_at	2.00	1.69E-03	1.41	2.79E-03	1.21	2.60E-02
Nrf1	1445914_at	1.95	9.04E-03	1.42	1.49E-03	1.27	3.67E-02
2900056M20Rik	1441816_at	1.81	2.36E-03	1.43	1.05E-02	1.40	3.66E-02
---	1458309_at	1.75	5.59E-03	1.37	4.22E-03	1.53	3.27E-02

Appendix 3: <i>Cecr2</i> ^{Gt45Bic} FVB/N versus FVB/N microarrays							
Gene	PROBE ID	gcRMA		Arraystar		dCHIP	
		Fold	p-value	Fold	p-value	Fold	p-value
Tmem164	1460016_at	1.64	5.38E-03	1.39	1.97E-02	1.62	4.86E-02
AA409587	1442358_at	1.81	6.20E-03	1.39	2.55E-03	1.45	2.69E-02
---	1446426_at	1.81	7.12E-04	1.38	9.03E-03	1.47	1.07E-02
---	1441140_at	1.76	2.66E-02	1.46	1.55E-02	1.47	2.03E-02
C530014P21Rik	1441577_at	1.84	6.45E-03	1.49	1.96E-03	1.37	1.34E-02
Vgll3	1430596_s_at	1.84	8.70E-03	1.45	3.72E-02	1.43	2.46E-02
---	1458065_at	1.79	1.02E-02	1.38	2.22E-03	1.56	3.84E-03
---	1446167_at	1.82	2.08E-03	1.53	2.81E-04	1.39	1.75E-02
D230044B12Rik	1441558_at	1.84	7.66E-04	1.40	2.90E-04	1.50	1.18E-03
---	1457944_at	1.77	9.83E-03	1.47	5.13E-03	1.51	2.69E-02
---	1437219_at	1.91	3.42E-03	1.46	9.17E-04	1.42	5.23E-03
6030487A22Rik	1441195_at	1.93	7.62E-03	1.49	5.30E-04	1.38	1.38E-02
---	1443394_at	1.85	1.62E-03	1.49	7.68E-04	1.48	9.31E-04
D230040J21Rik	1439330_at	1.88	1.31E-03	1.47	7.75E-03	1.53	2.05E-02
C230037E05Rik	1458942_at	1.95	8.36E-04	1.49	5.49E-03	1.45	6.68E-03
---	1442704_at	1.76	1.96E-02	1.64	1.76E-02	1.52	4.23E-02
Tsen2	1435118_at	1.78	1.59E-06	1.54	1.84E-06	1.59	2.30E-05
Cutl1	1441956_s_at	1.83	2.47E-03	1.60	6.47E-03	1.50	1.49E-02
5730419I09Rik	1444738_at	1.80	5.32E-03	1.55	1.05E-04	1.60	4.13E-02
---	1444890_at	1.99	4.54E-03	1.44	5.60E-03	1.52	9.82E-03
B430203I24Rik	1440586_at	1.60	3.39E-02	1.70	6.02E-03	1.66	3.81E-02
---	1444785_at	2.05	1.16E-03	1.49	2.69E-04	1.42	2.44E-03
Aebp2	1421021_at	1.14	4.86E-02	1.50	1.39E-02	2.33	3.44E-02
Ncam1	1439556_at	2.01	1.02E-02	1.51	1.29E-02	1.47	3.53E-02
---	1445137_at	2.13	4.10E-03	1.47	9.37E-03	1.40	4.48E-02
---	1440014_at	1.78	3.65E-03	1.52	1.30E-02	1.73	1.07E-02
---	1445641_at	2.06	1.01E-02	1.44	3.67E-03	1.53	2.15E-02
---	1456661_at	1.91	7.43E-04	1.64	2.52E-04	1.49	9.56E-03
Mtss1	1440847_at	1.89	2.23E-03	1.55	3.58E-03	1.61	5.97E-03
---	1456547_at	1.90	2.49E-03	1.58	1.95E-03	1.59	2.90E-02
Mrpl51	1416878_at	2.40	1.44E-02	1.30	1.39E-02	1.40	4.60E-02
---	1452500_at	2.19	2.40E-03	1.53	3.66E-03	1.38	1.51E-02
2210017G18Rik	1433209_at	2.14	4.79E-03	1.46	2.74E-03	1.51	1.34E-02
---	1439301_at	1.85	1.28E-02	1.48	2.30E-03	1.79	2.64E-02
---	1456514_at	2.15	5.32E-03	1.49	1.46E-03	1.53	1.22E-02
---	1441769_at	2.04	1.01E-02	1.51	4.46E-02	1.69	1.83E-02
---	1439123_at	2.02	6.15E-03	1.59	4.55E-04	1.65	7.25E-03
---	1441415_at	2.09	4.68E-03	1.46	6.56E-04	1.71	2.13E-03
---	1442067_at	2.04	6.20E-03	1.63	5.51E-03	1.62	1.24E-02
Air	1456139_at	2.16	1.43E-03	1.51	7.12E-03	1.64	9.48E-03
---	1440892_at	2.41	1.21E-03	1.45	1.69E-03	1.45	6.55E-03
St8sia1	1455695_at	1.55	1.21E-02	1.60	1.94E-03	2.20	1.14E-02
6330417A16Rik	1429996_at	2.31	7.16E-05	1.58	5.95E-04	1.46	7.79E-03
MGC7817	1425424_at	2.02	1.96E-03	1.67	1.05E-03	1.68	2.38E-03
Vgll3	1453593_at	2.18	8.30E-03	1.66	1.64E-02	1.54	4.24E-02
B430316J06Rik	1439933_at	2.21	6.00E-03	1.54	1.63E-02	1.65	8.94E-03
---	1441437_at	2.55	2.62E-03	1.40	2.21E-02	1.46	2.13E-02
Ncapd2	1423847_at	1.99	8.79E-05	1.80	1.58E-04	1.66	6.28E-03
---	1443026_at	2.16	1.22E-02	1.68	3.82E-03	1.65	5.39E-03
---	1458663_at	1.96	1.78E-03	1.55	2.89E-03	2.00	3.85E-03

Appendix 3: <i>Cecr2</i> ^{Gt45Bic} FVB/N versus FVB/N microarrays							
Gene	PROBE ID	gcRMA		Arraystar		dCHIP	
		Fold	p-value	Fold	p-value	Fold	p-value
---	1443430_at	1.46	1.89E-02	1.55	2.35E-03	2.57	7.57E-03
Recql	1439047_s_at	2.32	4.05E-05	1.71	9.43E-06	1.57	2.78E-04
---	1458661_at	2.78	3.71E-03	1.41	4.63E-03	1.42	1.13E-02
---	1443526_at	2.63	2.85E-04	1.57	2.30E-04	1.50	5.98E-03
Vgll3	1455299_at	2.24	1.01E-02	1.74	2.28E-02	1.73	4.50E-02
---	1446001_at	2.74	7.26E-04	1.73	1.41E-04	1.63	1.17E-03
---	1442393_at	2.79	9.17E-03	1.77	1.23E-02	1.76	3.03E-02
Fgfr1op2	1431020_a_at	2.37	1.53E-05	2.01	1.64E-05	1.95	2.81E-03
Klhdc5	1426988_at	3.08	1.82E-03	2.13	4.11E-03	2.97	2.80E-03
H2afj	1440252_at	4.95	5.36E-07	3.15	1.49E-04	2.80	5.25E-03
Clec1b	1421182_at	6.19	5.68E-05	2.82	1.38E-05	2.85	1.24E-04

Appendix 4A: Raw body and organ weight of <i>Cecr2</i> ^{Gt45Bic} adults						
Mouse ID	Weight in grams					
	Body	Brain	Kidney		Testes	
FVB/N 1	21.14	0.44	0.17	0.17	0.08	0.08
FVB/N 2	22.09	0.43	0.18	0.17	0.05	0.08
FVB/N 3	22.58	0.42	0.22	0.17	0.07	0.08
FVB/N 4	22.72	0.45	0.20	0.18	0.08	0.07
FVB/N 5	23.50	0.43	0.20	0.19	0.07	0.07
FVB/N 6	25.87	0.47	0.23	0.23	0.08	0.08
FVB/N 7	25.44	0.42	0.22	0.20	0.08	0.08
FVB/N 8	25.74	0.41	0.22	0.21	0.08	0.07
FVB/N 9	25.37	0.43	0.23	0.19	0.07	0.07
FVB/N 10	22.68	0.43	0.19	0.18	0.07	0.08
FVB/N 11	26.52	0.46	0.25	0.23	0.08	0.09
FVB/N 12	24.33	0.45	0.22	0.23	0.09	0.09
<i>Cecr2</i> ^{Gt45Bic} FVB/N 1	26.44	0.42	0.23	0.21	0.07	0.07
<i>Cecr2</i> ^{Gt45Bic} FVB/N 2	27.00	0.36	0.21	0.13	0.06	0.06
<i>Cecr2</i> ^{Gt45Bic} FVB/N 3	24.93	0.41	0.23	0.14	0.06	0.06
<i>Cecr2</i> ^{Gt45Bic} FVB/N 4	26.55	0.41	0.27	0.15	0.06	0.06
<i>Cecr2</i> ^{Gt45Bic} FVB/N 5	28.02	0.40	0.21	0.20	0.06	0.06
<i>Cecr2</i> ^{Gt45Bic} FVB/N 6	30.08	0.43	0.23	0.20	0.06	0.07
<i>Cecr2</i> ^{Gt45Bic} FVB/N 7	31.42	0.43	0.26	0.20	0.06	0.06
<i>Cecr2</i> ^{Gt45Bic} FVB/N 8	32.18	0.42	0.24	0.20	0.06	0.06
<i>Cecr2</i> ^{Gt45Bic} FVB/N 9	30.34	0.43	0.24	0.14	0.06	0.06
<i>Cecr2</i> ^{Gt45Bic} FVB/N 10	31.72	0.44	0.22	0.22	0.07	0.07
<i>Cecr2</i> ^{Gt45Bic} FVB/N 11	29.06	0.43	0.30	0 - Absent	0.07	0.07
<i>Cecr2</i> ^{Gt45Bic} FVB/N 12	26.36	0.40	0.33	0 - Absent	0.05	0.05
<i>Cecr2</i> ^{Gt45Bic} FVB/N 13	27.58	0.39	0.34	0 - Absent	0.05	0.05

Appendix 4B: Raw body and organ weight of <i>Cecr2</i> ^{Gt45Bic} adults						
Mouse ID	Weight in grams					
	Body	Brain	Kidney		Testes	
BALB/c 1	21.06	0.42	0.24	0.25	0.08	0.07
BALB/c 2	23.37	0.42	0.24	0.27	0.08	0.08
BALB/c 3	25.31	0.43	0.23	0.27	0.08	0.08
BALB/c 4	25.82	0.46	0.25	0.27	0.08	0.09
BALB/c 5	24.77	0.48	0.26	0.25	0.08	0.08
BALB/c 6	24.59	0.44	0.25	0.27	0.07	0.08
<i>Cecr2</i> ^{Gt45Bic} BALB/c 1	19.09	0.39	0.16	0.16	0.04	0.04
<i>Cecr2</i> ^{Gt45Bic} BALB/c 2	22.85	ND	0.23	0.20	0.07	0.08
<i>Cecr2</i> ^{Gt45Bic} BALB/c 3	26.22	0.44	0.26	0.29	0.07	0.06
<i>Cecr2</i> ^{Gt45Bic} BALB/c 4	25.11	0.44	0.27	0.26	0.07	0.07
<i>Cecr2</i> ^{Gt45Bic} BALB/c 5	21.01	0.42	0.20	0.20	0.06	0.06
<i>Cecr2</i> ^{Gt45Bic} BALB/c 6	22.94	0.41	0.22	0.21	0.06	0.05